Developmental neurotoxicity in a human model system

Dissertation zur Erlangung des

akademischen Grades eines Doktors der

Naturwissenschaften (Dr.rer.nat)

vorgelegt von

Stefanie Klima

an der

Mathematisch-Naturwissenschaftliche Sektion

Fachbereich Biologie

Tag der mündlichen Prüfung: 22.03.2021

1. Referent: Prof. Marcel Leist

2. Referent: Prof. Alexander Bürkle

Table of content

List of publications IV

1. Abstract VI

2. Zusammenfassung VIII

3. General introduction 1
   3.1. General neurodevelopment 1
      3.1.1. *In vivo* neurodevelopment 1
      3.1.2. Neurodevelopment can be modeled *in vitro* by pluripotent stem cells model . 4
   3.2. Developmental neurotoxicity (DNT) 5
   3.3. The need of a new testing strategy in toxicology 6
   3.4. New approach methods in DNT 8
      3.4.1. Transcriptome analysis as powerful readout 9
      3.4.2. Epigenetics drive transcriptome changes 10
      3.4.3. Neuronal integrity as endpoint for neurotoxicity testing 12
      3.4.4. Alternatives for neuronal receptors mediated neurotoxicity testing 13
      3.4.5. Combination of NAMs in test batteries 14
   3.5. Implementation of NAMs in regulatory toxicology 15
      3.5.1. Adverse outcome pathways (AOP) 15
      3.5.2. Pathways of toxicity (PoT) 17
      3.5.3. Integrated approaches to testing and assessment (IATA) 18

4. Results 20
   4.1. From transient transcriptome responses to disturbed neurodevelopment: role of histone acetylation and methylation as epigenetic switch between reversible and irreversible drug effects 20
      4.1.1. Abstract 21
      4.1.2. Introduction 21
      4.1.3. Material and methods 23
      4.1.4. Results 27
      4.1.5. Discussion 44
      4.1.6. Acknowledgements 50

4.1.7. Conflict of interests 50
4.1.8. Supplements 50
4.2. Paper 2: Examination of Microcystin Neurotoxicity using Central and Peripheral Human Neurons 60
4.2.1. Abstract 61
4.2.2. Introduction 61
4.2.3. Material and methods 63
4.2.4. Results 67
4.2.5. Conclusion and outlook 72
4.2.6. Acknowledgement 72
4.2.7. Conflict of interest 72
4.2.8. Supplements 73
4.3. Paper 3: A human stem cell-derived test system for agents modifying neuronal N-methyl-D-aspartate-type glutamate receptor Ca^{2+}-signaling 77
4.3.1. Abstract 78
4.3.2. Introduction 78
4.3.3. Material and methods 81
4.3.4. Results 86
4.3.5. Conclusion and outlook 105
4.3.6. Acknowledgements 107
4.3.7. Conflict of interest 107
4.3.8. Supplements 108

5. Concluding discussion and perspectives 118
5.1. Interplay of epigenetics and transcriptional changes in early development 118
5.1.1. Epigenetic marks manifest switch between transient and persistent transcriptome changes 118
5.1.2. Transcriptomics reflect MoA and altered differentiation 119
5.1.3. Challenges in transcriptomics in developing systems 120
5.2. Implementation of new approach methods (NAM) in risk assessment 121
5.3. Human mixed cortical cultures (MCC), an essential building block for *in vitro* test batteries 122
5.4. Technical progress of the applied test systems towards regulatory acceptance 123

5.4.1. Neurodevelopmental stages covered by the applied test systems....124
5.4.2. Throughput of the applied test systems....125
5.4.3. Compound selection....126
5.4.4. Readiness of the applied test systems....126
5.5. Future perspectives....127

6. Danksagung....130

7. Author's contribution....131

8. References....132

List of publications

Publications integrated in this thesis

Results chapter 5.1.:

From transient transcriptome responses to disturbed neurodevelopment: Role of histone acetylation and methylation as epigenetic switch between reversible and irreversible drug effects.

Klima S*, Balmer NV*, Rempel E, Ivanova VN, Kolde R, Weng MK, Meganathan K, Henry M, Sachinidis A, Berthold MR, Hengstler JG, Rahnenführer J, Waldmann T, Leist M (2014) *Arch Toxicol* 88, 1451-1468.

* shared authorship

Results chapter 5.2.:

Examination of microcystin neurotoxicity using central and peripheral human neurons.
Klima S, Suciu I, Hoelting L, Gutbier S, Waldmann T, Dietrich DR, Leist M (2020) *Altex*

Results chapter 5.3.:

A human stem cell-derived test system for agents modifying neuronal N-methyl-D-aspartate-type glutamate receptor Ca^{2+} signaling.

Klima S, Brüll M, Spreng AS, Suciu I, Falt T, Schwamborn JC, Waldmann T, Karreman C, Leist M (2020) submitted to *Arch Toxicol*

Publications not integrated in this thesis

Human neuronal signaling and communication assays to assess functional neurotoxicity.
Loser D, Schaefer J, Danker T, Möller C, Brüll M, Suciu I, Ückert AK, **Klima S**, Leist M*, Kraushaar U* (2020) *Arch Toxicol*

* shared authorship

CaFFEE: A program for evaluating time courses of Ca^{2+} dependent signal changes of complex cells loaded with fluorescent indicator dyes.
Karreman C, **Klima S**, Holzer AK, Leist M (2020) *Altex* 37, 332-336.

Time and space-resolved quantification of plasma membrane sialylation for measurements of cell function and neurotoxicity.
Kranaster P, Karreman C, Dold JEGA, Krebs A, Funke M, Holzer AK, **Klima S**, Nyffeler J, Helfrich S, Wittman C, Leist M (2020) *Arch Toxicol* 94, 449-467.

Development of a neural rosette formation assay (RoFA) to identify neurodevelopmental toxicants and to characterize their transcriptome disturbances.
Dreser N, Madjar K, Holzer AK, Kapitza M, Scholz C, Kranaster P, Gutbier S, **Klima S**, Kolb D, Dietz C, Trefzer T, Meisig J, v Thriel C, Henry M, Berthold MR, Blüthgen N, Sachinidis A, Rahnenführer J, Hengstler JG, Waldmann T, Leist M (2020) *Arch Toxicol* 94, 151-171.

A high-throughput approach to identify specific neurotoxicants/ developmental toxicants in human neuronal cell function assays.
Delp J, Gutbier S, **Klima S**, Hoelting L, Pinto-Gil K, Hsieh JH, Aichem M, Klein K, Schreiber F, Tice RR, Pastor M, Behl M, Leist M (2018) *Altex* 35, 235-253.

Recommendation on test readiness criteria for new approach methods in toxicology: Exemplified for developmental neurotoxicity.
Bal-Price A, Hogberg HT, Crofton KM, Daneshian M, FitzGerald RE, Fritsche E, Heinonen T, Hougaard Bennekou S, **Klima S**, Piersma AH, Sachana M, Shafer TJ, Terron A, Monnet-Tschudi F, Viviani B, Waldmann T, Westerink RHS, Wilks MF, Witters H, Zurich MG, Leist M (2018) *Altex* 35, 306-352.

Stem cell-derived immature human dorsal root ganglia neurons to identify peripheral neurotoxicants.
Hoelting L, **Klima S**, Karreman C, Grinberg M, Meisig J, Henry M, Rotshteyn T, Rahnenführer J, Blüthgen N, Sachinidis A, Waldmann T, Leist M (2016) *Stem Cells Transl Med* 5, 476-487.

Human pluripotent stem cell based developmental toxicity assays for chemical safety screening and systems biology data generation.
Klima S*, Shinde V*, Sureshkumar PS, Meganathan K, Jagtap S, Rempel E, Rahnenführer J, Hengstler JG, Waldmann T, Hescheler J, Leist M*, Sachinidis A* (2015) *J Vis Exp*, e52333.
* shared authorship

1. Abstract

There is an urgent scientific and regulatory need for development and implementation of new approach methods (NAM), such as cell culture test methods. NAM can give information about mechanisms of toxicity and about pathways disturbed after test compound exposure. Such knowledge plays an increasingly larger role in modern toxicology. Particularly, in the field of developmental neurotoxicity (DNT), *in vitro* test methods can model different stages of neurodevelopment and thereby inform on stage-specific toxicities. However, there is not yet a suitable test system available for every stage of neurodevelopment. This thesis addresses this gap in two different ways: first, by investigating mechanisms of neurotoxicity at various stages of neurodevelopment, and second, by establishing new test methods for stages not covered so far. In the first part of this thesis, human pluripotent stem cells (hPSC) were differentiated into neuroepithelial precursors (NEP) to investigate transcriptome changes triggered by the well-known teratogen valproic acid and other histone deacetylase inhibitors (HDACi) during very early neurodevelopment. Short exposures (up to 24 h) altered histone acetylation and the transcriptome only transiently. Transcriptome changes after drug exposure both reflected the mode of action (MoA) of a compound and described an altered differentiation state. Altered differentiation was observed after longer HDACi exposures (at least three days) accompanied by altered histone methylation. This study showed that epigenetic modifications can have neuroteratogenic effects by changing the chromatin state. In the second part of this work, it was examined in how far neurotoxicology of complex toxins could be evaluated with human neuronal cultures. To explore the neurotoxicity hazard of microcystins (MC) in humans, two mature neuronal cell types (LUHMES and peripheral neurons) were exposed to MC-LF. Clear neurotoxic effects were identified at low µM concentrations. In this study, the hazard data obtained *in vitro* were combined with literature exposure data for a general risk assessment. In the final part of this thesis, a novel test system was developed to close an obvious gap in the available neurotoxicity test battery: identification of toxicants interfering with ionotropic glutamate receptors. An hPSC-based differentiation protocol was established yielding a mixed cortical culture (MCC) with about 50% N-methyl-D-aspartate receptor (NMDA-R) expressing neurons. Toxicants known to interfere with glutamate receptors, like ibotenic acid and domoic acid, triggered changes in intracellular free calcium ion concentration which could be inhibited by antagonists like ketamine and

phencyclidine. Hence, MCC contribute to the currently available test systems for investigation of compounds affecting important neuronal receptors. The studies presented in this thesis led to the development of novel *in vitro* test systems that allow the study of mode of action (MoA) of toxicants during different stages of neurodevelopment and the screening of unknown compounds of potential neurotoxicity.

2. Zusammenfassung

Es gibt einen dringenden wissenschaftlichen und regulatorischen Bedarf an Entwicklung und Implementierung von Methoden, die einem neuen Ansatz folgen (NAM), wie auf Zellkulturen basierende Testmethoden. NAM können Aufschluss über Toxizitätsmechanismen und gestörte Prozesse nach Substanzexposition geben. Dieses Wissen spielt in der modernen Toxikologie eine immer größere Rolle. Gerade im Feld der Entwicklungsneurotoxizität (DNT), können in vitro Testmethoden verschiedene Stadien der Neuroentwicklung modellieren und dadurch stadiumspezifische Toxizität aufdecken. Allerdings ist bisher nicht für jedes Neuroentwicklungsstadium ein geeignetes Testsystem verfügbar. Diese Dissertation setzt an diesem Bedarf auf zweierlei Weise an: zum einen durch die Untersuchung von Neurotoxizitätsmechanismen in verschiedenen Neuroentwicklungsstadien und zum anderen durch die Entwicklung neuer Testmethoden für derzeit nicht erfasste Stadien. Im ersten Teil der Doktorarbeit wurden humane pluripotente Stammzellen (hPSC) zu neuroepithelialen Vorläuferzellen (NEP) differenziert, um die Transkriptomveränderungen, ausgelöst durch das bekannte Teratogen Valporinsäure und andere Histondeacetylase Inhibitoren (HDACi), in der frühen Neuroentwicklung zu untersuchen. Kurze Expositionen (bis zu 24 h) verändern die Histonacetylierung und das Transcriptom nur vorübergehend. Eine veränderte Differenzierung wurde nach längerer HDACi Exposition (mindestens 3 Tage) beobachtet und ging mit einer veränderten Histonmethylierung einher. Diese Studie zeigte, dass epigenetische Veränderungen durch eine Änderung des Chromatinstatus neuroteratogene Effekte hervorrufen können. Im zweiten Teil der Dissertation wurde untersucht inwieweit die Neurotoxizität komplexer Toxine mit humanen, neuronalen Kulturen untersucht werden kann. Um die neurotoxikologische Gefahr von Microcystin (MC) im Menschen zu untersuchen, wurden zwei reife, neuronale Zelltypen (LUHMES und periphere Neuronen) MC ausgesetzt. Klare neurotoxische Effekte wurde bei niedrigen µM Konzentrationen identifiziert. In dieser Studie wurden die in vitro erhaltenen Daten mit Expositionsdaten aus der Literatur für eine Risikoabschätzung kombiniert. Im letzten Teil der Dissertation wurde ein neues Testsystem entwickelt, um eine offensichtliche Lücke in der verfügbaren Testbatterie für Neurotoxizität zu schließen: die Identifizierung von Giftstoffen welche mit ionotropischen Glutamatrezeptoren interagieren. Ein hPSC-basiertes Differenzierungsprotokoll, das gemischte kortikale Kulturen (MCC) hervorbringt, welche zu ungefähr 50% N-Methyl-D-Aspartat-Rezeptoren (NMDA-R)

exprimieren, wurde etabliert. Giftstoffe, wie Ibotensäure und Domoinsäure, die bekannterweise mit Glutamatrezeptoren interagieren, lösten Veränderungen in der intrazellulären freien Kalziumionenkonzentration aus. Diese konnten durch Antagonisten wie Ketamin und Phencyclidin inhibiert werden. Deshalb tragen MCC zu den zurzeit verfügbaren Testsystemen zur Untersuchung von Substanzen, die neuronale Rezeptoren beeinflussen, entscheidend bei. Die Studien, welche in dieser Dissertation präsentiert wurden, tragen zur Entwicklung neuer in vitro Testsysteme, mit denen sowohl der Wirkmechanismus von Giftstoffen in verschiedenen Stadien der Neuroentwicklung also auch die Untersuchung unbekannter Stoffe auf ihr neurotoxikologisches Potenzial untersucht werden können, bei.

3. General introduction

Neurodevelopment is very sensitive and therefore needs special attention in risk assessment. It starts early in embryonic development and continues far beyond birth. During the whole process compounds can interfere with the tightly regulated processes involved in neurodevelopment and thereby disturb them with long-lasting consequences. To prevent this, it is crucial to apply robust and reliable test systems with a high predictive power for humans to identify such compounds. In the past, it became more and more questionable, whether animal experiments should be considered the best course of action to address developmental neurotoxicity. Therefore, this thesis points out alternative test systems for certain questions in the field of (developmental) neurotoxicity.

3.1. General neurodevelopment

Neurodevelopment comprises four fundamental processes: proliferation, migration, differentiation and network formation. First, neural stem cells (NSC) as well as different progenitor cells like neuronal progenitors, radial glia cells and glial progenitors are generated in the proliferation phase. These progenitors then migrate to their target sites of the developing nervous system and differentiate into mature cells like neurons (and various subtypes thereof), astrocytes and oligodendrocytes. The cells of the nervous system do not only differentiate, they also form a functional network that transmits signals in an organized manner and thereby transfers, transduces and integrates information. Therefore, synaptogenesis and myelination as well as network formation play a critical role. An overview of the involved processes is given in Fig. 3.1.

3.1.1. *In vivo* neurodevelopment

In more detail, embryonic development starts with the fertilization of the oocyte, resulting in the zygote. The zygote undergoes several cell divisions and cleavages, passing the stadium of the morula followed by further differentiation into the blastocyst. The blastocyst consists of an outer layer developing the placenta (trophoblast) and an inner part the inner cell mass (ICM), which develops into the embryo (Houghton 2006). During gastrulation the gastrula is formed comprising the three germ layers ectoderm, mesoderm and endoderm. Each of the three germ layers gives rise to different tissues and organs in the

embryonic body. While the mesoderm gives rise to muscle cells, bones, and connective tissue, the endoderm gives rise to epithelium of gut and lung, and to liver and pancreas and the ectoderm gives rise to epidermis, nervous system, and neural crest (Elshazzly *et al.* 2020).

The ectoderm can be further subdivided into the non-neural ectoderm, the neural crest and the neural tube (neuroectoderm). The neural tube is formed during neurulation (Gammill *et al.* 2003), which can be roughly divided into four steps. (i) Neural plate formation: Morphological changes of the neuroectoderm give rise to the neural plate. (ii) Shaping of the neural plate: By proliferation the neural plate becomes longer and the cells elongate, resulting in a thicker and narrower neural plate, which starts to bend upwards and form the neural groove. (iii) Bending of the neural plate: during this process furrowing and folding shapes the neural groove into the neural tube. (iv) Neural tube closure: The tips of the neural plate merge and close the neural tube (Nikolopoulou *et al.* 2017). At the neural tube border neural crest cells undergo epithelial-to-mesenchymal transition, migrate to their target sites and differentiate further e.g. into peripheral neurons and melanocytes (Gammill *et al.* 2003). The process of neural tube closure is very susceptible to disruptions, which can be caused by exposure to pharmaceuticals or other chemicals. This can lead to so called neural tube closure defects (Greene *et al.* 2014, Nikolopoulou *et al.* 2017).

After neural tube closure, patterning takes place (Kandel *et al.* 2013). Time-dependent and concentration-dependent exposure to signals, such as growth factors, morphogens and cytokines, determines the activation of specific transcription factors thereby establishing a precise spatial order. The cells of the neural tube undergo patterning along the dorso-ventral axis, mostly driven by sonic hedgehog for ventral patterning and TGFß-signaling for dorsal patterning (Ribes *et al.* 2009). The specific combination of signals along the neural tube leads to neural progenitors of different neuronal classes (Jessell 2000).

Neurogenesis itself occurs in two waves (Agirman *et al.* 2017). In the first and early wave, neuroepithelial progenitors (NEP) form the neural tube and undergo symmetrical divisions, which thereby leads to an increase of the cell layers of the neural tube. During this first phase of neurogenesis only few neurons differentiate by asymmetric division of NEP, the vast majority divides symmetrically and forms more NEP (Kriegstein *et al.* 2009).

The epithelium thickens, the NEPs elongate and convert into radial glia cells (RG). The RG are the main class of neural stem cells in the developing brain (Dimou *et al.* 2014). First, RG also divide symmetrically to enlarge the number of RG and thereby build up a pool of RG. These cells then undergo further asymmetrical divisions and develop directly into neurons or neural intermediate progenitor cells (nIPC), which differentiate into more nIPC and neurons. These multiple rounds of divisions lead to a massive thickening of the brain (Kriegstein *et al.* 2009) and a further elongation of RG provides a migration scaffold for newly derived neurons (Allen *et al.* 2018). The numerous divisions provide also the basis for the enlarged human neocortex. In a later phase of neurodevelopment, RG also generate glial progenitors which differentiate further into oligodendrocytes and astrocytes (Kessaris *et al.* 2006).

In order to transmit information across distances, neurite outgrowth as well as connecting of neurite endings and formation of functional signaling networks is crucial. Synapses are formed during synaptogenesis to transmit signals from one cell to another (Südhof 2018). A synapse is a subcellular structure composed of a presynaptic and a postsynaptic part. In the presynaptical membrane a lot of synaptic vesicles cluster (Südhof 2012) and the postsynaptic membrane is mainly characterized by the presence of ion channels and signal transduction molecules (Sheng *et al.* 2011). Most synapses are formed during embryonic and early postnatal life by an initial contact followed by the expression and assembly of pre- and postsynaptic structures (Südhof 2018). Until the age of twenty years, synapses pruning occurs and the persisting synapses are strengthened (Petanjek *et al.* 2011). The strengthening of synapses is closely associated with learning and on a molecular level with long-term-potentiation, involving the NMDA receptor (Südhof 2018). Stimulation of the NMDA receptor is followed by a Ca^{2+} influx into the postsynaptic cell (Balu 2016). This Ca^{2+} influx triggers a number of secondary signals such as BDNF excretion, which strengthens the synapse (Papadia *et al.* 2007).

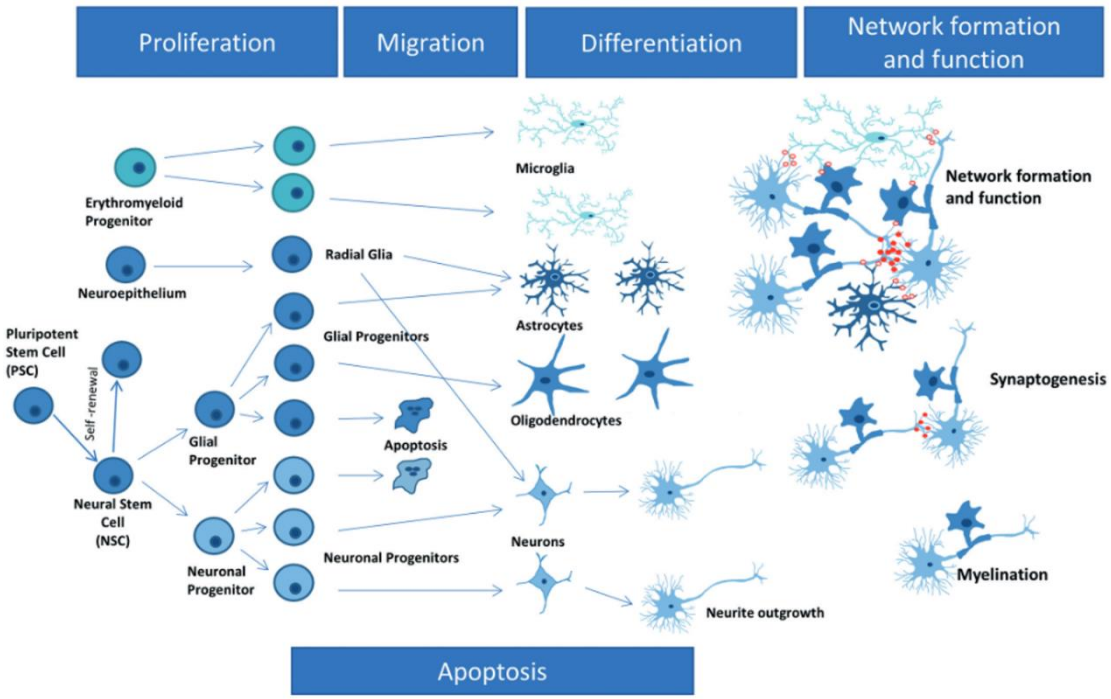

Fig. 3.1: Overview of neurodevelopmental processes

Scheme of the development of a pluripotent stem cell (PSC) passing through different progenitor states, differentiating into specified cells (like neurons, astrocytes and oligodendrocytes) and forming functional. The main processes involved in neurodevelopment are depicted in blue boxes. Figure adopted from Bal-Price *et al.* 2018.

3.1.2. Neurodevelopment can be modeled *in vitro* by pluripotent stem cells model

Stem cells have two major features: First, they are self-renewing and second, they can differentiate into every cell type of the human body. In 1998, the first human embryonic stem cell lines were isolated from the ICM of blastocysts (Thomson *et al.* 1998). This breakthrough changed the research of embryonic development fundamentally. Thus, it was possible to understand and model the very early stages of human development *in vitro*. Also the field of regenerative medicine evolved a lot with the help of this new technique. However, there are also ethical concerns about the use of embryonic material for research. This issue could be circumvented by the discovery of induced pluripotent stem cells (iPSC) (Takahashi *et al.* 2007). With this groundbreaking technique it is possible to reintroduce the pluripotent state in every adult cell of the human body. Therefore, the transcription factors OCT3/4, SOX2, KLF4 and C-MYC are overexpressed in adult differentiated cells. Now, patient derived iPSC cells can be generated and gene corrected, to investigate the underlying mechanisms of disease (Oksanen *et al.* 2017, Guo *et al.* 2019). But also for the field of developmental (neuro)toxicity iPSC are very useful as it is possible

to differentiate iPSC into many different cell types of various developmental stages (Wang *et al.* 2013, Lemoine *et al.* 2017, Nagoshi *et al.* 2018, Zimmer *et al.* 2018) and thereby model development without ethical concerns. This bears a huge potential in many research areas including toxicology.

3.2. Developmental neurotoxicity (DNT)

The development of the nervous system relies on very complex and precisely tuned biological processes. This processes bear a high potential for disturbances e.g. during proliferation, differentiation, apoptosis, neurite outgrowth, migration, patterning, synaptogenesis, myelination and neurotransmitter release (Kadereit *et al.* 2012). Therefore, the term developmental neurotoxicity (DNT) subsumes all long lasting adverse effects linked to exposure to xenobiotics during neurodevelopment resulting in neurobehavioral alterations and malformations (Kuegler *et al.* 2010, van Thriel *et al.* 2012). The effects of DNT result in many different characteristics like motor and mental retardation, learning disabilities, attention-deficit hyperactivity disorder, and spina bifida (Hass 2006).

In the US, about 10 to 15% of all newborns show developmental neurobehavioral disorders with increasing propensity (Grandjean *et al.* 2014). While there are several possible causes, DNT has received the least attention within the field of toxicology (Makris *et al.* 2009, Kadereit *et al.* 2012). As testing for DNT is not mandatory in chemical registration, DNT guideline studies are available only for about 120 substances (Crofton *et al.* 2012, Kadereit *et al.* 2012, Tsuji *et al.* 2012, van Thriel *et al.* 2012). According to the current regulatory guidelines (OECD TG 426 and OECD TG 443), DNT testing is very time, labor and cost intensive and completely relies on rodents. Testing one chemical takes three month, costs approx. $ 1.4 million and needs around 1000 rat pups (Smirnova *et al.* 2014). Even if DNT is assessed, the data interpretation is often demanding and therefore difficult for regulatory use (Beronius *et al.* 2013).

Additionally, for regulatory purposes only reproductive toxicity (reprotox) is included in primary testing but not DNT testing. Testing for adult neurotoxicity (NT) is only required if the compound shows a neurotoxic potential, e.g. organophosphates or pesticides or if structural similarities to known neurotoxicants are observed. Only after the results of the NT studies and the reprotox studies have been assessed, it is decided,

whether a DNT study is required (Smirnova *et al.* 2014). All these factors have contributed to the small number of compounds being tested for DNT. Furthermore, compounds inducing DNT are often neurotoxicants at the same time. Yet, the thresholds which are defined after NT testing are not the same as needed to prevent DNT, because the developing brain is more vulnerable and susceptible to toxicant exposure as the adult brain (Rodier 1995, Bondy *et al.* 2005). The blood brain barrier is not fully established (Leist *et al.* 2008), the embryo has decreased metabolic detoxification abilities, caused by a different expression pattern of cytochrome P450 enzymes, compared to adult organisms (Chazaud *et al.* 2006) and the embryo shows an increased absorption due to the lower bodyweight (Landrigan *et al.* 2004). Therefore, lower doses can already trigger harmful events in a developing organism compared to an adult organism (Hass 2006). Moreover, the degree of reversibility is smaller, e.g. if the network formation is slightly disturbed or even interrupted there might be life-long consequences, as the network was not able to form properly.

3.3. The need of a new testing strategy in toxicology

As the majority of DNT testing is performed in animals, mostly rodents, it is questionable to which degree these data are relevant for human risk assessment. The biology and physiology of animals and humans differ concerning toxicokinetics and toxicodynamics as well as development itself (Hartung 2008). Many questions have to be addressed: Often it remains unknown whether rodents express receptors for chemical absorption and excretion similar to humans. Or whether they have the same enzymes, with the same binding affinity as humans, and thereby produce the same metabolites. It is already known, that human neurodevelopment differs significantly from rodent neurodevelopment. In humans, the neocortex is larger, which results from more radial glia cells. In line with the bigger size, the human neocortex is also much more complex, which results in different neuronal structures and networks. Furthermore, the timing of neurodevelopment is different in rodents and humans (Zhao *et al.* 2018). Another problem with animal based testing becomes obvious when looking at the endpoints in the respective measurements. Not all endpoints relevant for human health and disease, like psychosomatic relationships or higher cognitive functions can be measured in rodents. Furthermore, animal models are used for diseases that have been introduced artificially in animals, as they do not occur in animals naturally (Smirnova *et al.* 2014, Terron *et al.* 2018). However, it is difficult to in-

vestigate the underlying disease mechanisms or the causative chemical exposure of a disease that does not reflect the authentic human situation (Seok *et al.* 2013). Overall, the suitability of animal models is not always verified and in some cases more than questionable. With pharmaceuticals like biologicals entering the market, it becomes more and more difficult to test for the tolerability of new drugs in animals. Furthermore, in guideline studies, the tested dosing is often too high and thereby does not reflect realistic human exposure scenarios (Hartung 2008). These examples show, that predicting human health and disease as well as human risk assessment is not always feasible with data obtained from animals.

With regards to the legal requirements of testing many chemicals for registration and risk assessment it is also important to note that animal-free test methods are less time- and resource-consuming, as they have a higher throughput, than animal based test systems. Albeit ethical concerns are ignored, the number of needed animal testing capabilities exceeds the number of available animal testing capabilities by far (Terron *et al.* 2018). Even more alarming, data produced in line with OECD test guidelines have high variability and low reproducibility and do not provide new insights in mechanistic understanding of underlying effects (Bal-Price *et al.* 2018).

Another aspect of animal testing is more ethical and societal. Already in the late 1950s, Russell and Burch introduced the concept of three R's with respect to ethical aspects of animal testing (Russell *et al.* 1959). In principal, it describes the ideal use of animals in science. The three R's stand for replace, reduce, and refine, which means whenever possible animal experiments should be replaced by animal-free methods or other systems like tissue slices and perfused organs should be considered. If this is not possible, animal numbers must be reduced to the minimal needed number to gain scientific knowledge and the methods must be refined resulting in least pain, stress and suffering for the animals. The three R's concept is not only about banning animal testing, it also provides a basis for better scientific understanding and quality together with improved animal welfare.

Taken together, all these arguments point to the need for new testing strategies in DNT. The consideration of animal-free test methods must become a fundamental part to identify DNT alerts and prioritize substances for further testing.

3.4. New approach methods in DNT

Today many different animal-free alternative test methods are available, including *in silico* approaches, computational models, *in vitro* cell-based test systems and combinations thereof. All these non-animal methods and technologies used to provide information on chemical hazard for risk assessment without using animals are summarized as new approach methodologies (NAMs) (ICCVAM 2018, USEPA 2018). The development and application of these NAMs is driven by different stakeholders like test developers in industry, academic researchers, public institutions, and regulator decision makers, but most of the NAMs have never been validated (Bal-Price *et al.* 2018). In order to implement the developed NAMs in a regulatory context, it is essential that they fulfill certain standards. These standards are compiled and provide an assistance on the performance necessary for *in vitro* test methods to be ready to use for implementation in regulatory toxicity. Therefore, different stakeholders assembled 13 different categories of readiness criteria and validated 17 existing *in vitro* test methods according to these readiness criteria (Bal-Price *et al.* 2018). The number of chemicals not yet assessed on their DNT potential is tremendous (Grandjean *et al.* 2006, Raffaele *et al.* 2010, van Thriel *et al.* 2012, Fritsche *et al.* 2017). Therefore, the *in vitro* test systems with high readiness scores provide a promising opportunity to obtain information on potential hazard and to prioritize chemicals for further testing. The 17 *in vitro* test methods validated there cover most of the neurodevelopmental processes, ranging from test systems investigating neural precursor differentiation (UKN1 (Balmer *et al.* 2012, Dreser *et al.* 2020)), proliferation (NPC1 (Baumann *et al.* 2014)), migration (UKN2 (Nyffeler *et al.* 2017, Nyffeler *et al.* 2017)), oligodendrocyte differentiation (NPC5 (Baumann *et al.* 2014)), neurite outgrowth (UKN4 (Stiegler *et al.* 2011, Delp *et al.* 2018) and UKN5 (Hoelting *et al.* 2016, Delp *et al.* 2018)), 3D astrocyte differentiation and myelination (3Dh (Pamies *et al.* 2017)) synaptogenesis (Syn (Hogberg *et al.* 2011)) to neural network formation and function (Nnff (Strickland *et al.* 2018, Tukker *et al.* 2018)) as depicted in Fig. 3.2. They all have different cellular origins, exposure scenarios and endpoints, but contribute to the gain of information in their specific applicability domain. This set of *in vitro* test methods does by far not include all available *in vitro* test methods. Yet, it is already quite comprehensive and shows that e.g. test methods for neurite outgrowth and neural precursor differentiation are already ready for application in a regulatory context. However, there are also missing parts of neurodevelopment, e.g. the

development of neuronal test systems expressing specific ionotropic receptors or dendrite formation.

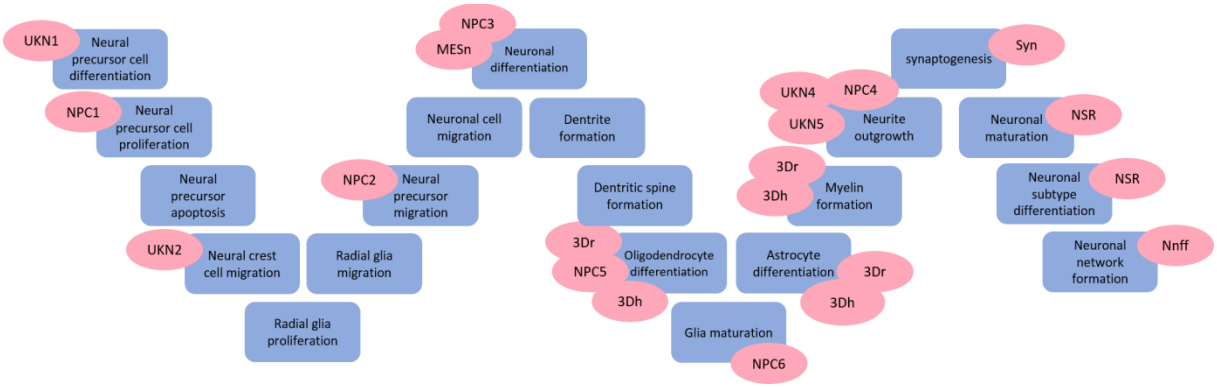

Fig. 3.2: Neurodevelopmental processes and respective available *in vitro* test systems

Some available in vitro test systems (red) for single neurodevelopmental processes (blue) are depicted. The selection of test systems does not include all test systems available, but rather includes test systems examined for their readiness in Bal-Price *et al.* 2018. More detail, about the individual test systems and their readiness is given in the original paper. Abbreviations: UKN1, PSC differentiation into NPC/NSC embryonic phase differentiation; NPC1, hNPC proliferation; NPC2, hNPC migration; NPC3, hNPC neuronal differentiation; NPC4, hNPC differentiated neurons; NPC5, hNPC oligodendrocyte differentiation; NPC6, hNPC oligodendrocyte maturation and TH disruption; UKN2, NCC proliferation and migration; MESn, Morphological ESC to neurons; 3Dr, astrocytes, oligodendrocytes, myelination, microglia in 3D rat; 3Dh, astrocytes, oligodendrocytes, myelination, microglia in 3D human, foetal phase; UKN4 (NeuriTox), neurite outgrowth of central neurons; UKN5 (PeriTox), neurite outgrowth of peripheral neurons; NSR, neuronal subtype ratio, neuronal maturation; Syn, synaptogenesis; Nnff, neuronal network formation and function

3.4.1. Transcriptome analysis as powerful readout

Transcriptomics became an important endpoint in the field of DNT and it is a useful alternative to readouts addressing cell morphological endpoints (Balmer *et al.* 2012, Waldmann *et al.* 2014, Rempel *et al.* 2015, Hoelting *et al.* 2016, Shinde *et al.* 2017, de Leeuw *et al.* 2020, Dreser *et al.* 2020). Transcriptomics data can be used to gain comprehensive information on a molecular level and thereby link the mode of action of compounds to transcriptomic changes (Vojnits *et al.* 2012, Hermsen *et al.* 2013). Information on the molecular level provide the possibility to identify pathways involved in cell biological endpoints, identify modes of action and to understand applicability domains of the underlying test system (Waldmann *et al.* 2017). In the field of DNT, new approaches with a higher throughput than animal testing provides, are needed for better risk assessment. Here, transcriptomics represent a sensitive endpoint allowing to identify different developmental stages and to distinguish between normal and disturbed development. Transcriptomics are also suitable to assess alterations in patterning of a differentiating culture

(Leist *et al.* 2012), as the transcriptome of all cells can be analyzed and thereby reflects the transcriptional state of the whole cell population, which might change its cell composition after drug exposure. The transcriptional state of a culture reveals spatial and temporal information about it, which are similar *in vitro* and *in vivo* (Zimmer *et al.* 2012).

Furthermore, it is possible to identify new biomarkers with the help of transcriptomics data, which can then be further used as a more simplified and cheaper readout for DNT testing (Kuegler *et al.* 2010, Rempel *et al.* 2015).

The change of the fingerprint of a culture is a good indicator for altered (neuronal) differentiation. However, if whole transcriptome analysis is applied in a compound screen, the risk of false negatives might be decreased, as all genes are included in the analysis and not only genes which were defined as maker genes. Unknown compounds might have effects on genes not included in the marker genes set, but also disturb neurodevelopment.

The compounds tested in a screen can also be grouped based to their transcriptome pattern (Rempel *et al.* 2015). Yet, changes in gene expression in a developing test system can originate from to two different reasons: (i) an acute compound effect on a biological process, indicating a pathway of toxicity or (ii) an altered differentiation and thereby a change of the fingerprint of the culture (Leist *et al.* 2012). In (i), the compound interferes with a pathway and thereby induces toxicity, in (ii) the compound changes the differentiation of the culture. Especially in developing systems the investigation of transcriptomics need special consideration and experimental designs. The baseline changes even without a toxic stimulus. Thus, there is no stable baseline. This already results in transcriptional changes, which have to be distinguished from transcriptional changes induced by a compound. As some toxicants only have an effect during a certain time of gene regulation (Zimmer *et al.* 2012), it is crucial to consider the window of sensitivity to choose the right exposure in transcriptomics experiments.

3.4.2. Epigenetics drive transcriptome changes

To answer the question which processes are governing the transcriptome changes in DNT, it is worth including epigenetic endpoints in DNT testing. Epigenetics describe the altera-

tion in gene expression caused by structural chromatin changes (Allis *et al.* 2007). Post-translational histone modifications are one of five epigenetic mechanisms (Dulac 2010). Some of them are clearly associated with one or another chromatin state. Trimethylation of histone H3 at lysine 4 (H3K4me3) is associated with a transcriptionally accessible and open chromatin called euchromatin (Bannister *et al.* 2011). The same is true for the acetylation of histone H3 at lysine 9 (H3K9ac), whereas the trimethylation of histone H3 at lysine 27 (H3K27me3) is associated with a more condensed and transcriptionally silent chromatin called heterochromatin (Bannister *et al.* 2011). Not only the epigenetic marks itself can alter the gene expression, also interference of compounds with the machinery that sets epigenetic marks and the genes coding for them are potential targets for compounds. Thereby, they induce transcriptomic changes (Smirnova *et al.* 2012, Weng *et al.* 2012, Waldmann *et al.* 2013), e.g. for histone deacetylase inhibitors (HDACi) it is known, that they modify epigenetic marks.

As epigenetics are directly interfering with gene expression, it is an important question, whether epigenetic changes are caused by transcriptional changes after compound exposure or whether they are a consequence of the compound exposure itself. Next, epigenetics could be a sensitive measure to investigate the exposure threshold of a compound, which induces an (irreversible) adverse outcome (Bose *et al.* 2012, Senut *et al.* 2012).

The Barker hypothesis claims that the period of gestation has an impact on the health in later life. (Osmond *et al.* 2000) It can also be applied for neurodevelopment and describes that diseases in later life may have a developmental origin. There are some examples like early life pesticide exposure and a linkage to Parkinson's disease (Landrigan *et al.* 2005), developmental lead exposure contributing to Alzheimer's disease (Bihaqi *et al.* 2012), and mice exposed to methyl mercury during pregnancy showing disturbed learning and depressive behavior in the offspring (Onishchenko *et al.* 2007). Here, epigenetic mechanisms could represent the key event, which leads to manifestation of the transcriptional changes during development, and as a consequence the induction of diseases later in life.

3.4.3. Neuronal integrity as endpoint for neurotoxicity testing

Disturbances occur not only during early neurodevelopment but also in later stages and affect e.g. more mature neuronal networks. Therefore, changes in the formation or signaling of neuronal networks should be addressed. This can be performed with more functional endpoints. To this end, the integrity of neuronal networks could serve as an appropriate endpoint. The outgrowth of neurons is a precisely controlled process, which can be modelled very well *in vitro*, and a lot of test systems are available for this neurodevelopmental process (Harrill *et al.* 2010, Krug *et al.* 2013, Hoelting *et al.* 2016, Ryan *et al.* 2016). If the neurite outgrowth is disturbed, the neuronal network is not able to form properly and consequently, the neuronal signaling is disturbed. But even if neuronal network develops properly, it can be impaired afterwards. The corrosion of an intact neuronal network is called degeneration. There are many reasons for network degeneration, e.g. diseases like Alzheimer's (Jeong 2017) or amyotrophic lateral sclerosis (Kiernan *et al.* 2011), but also compounds like rotenone and cisplatin can induce it (Landowski *et al.* 2016, Richardson *et al.* 2019). Therefore, the integrity of a neuronal network is an important endpoint in (D)NT. Neuronal integrity can be measured by high content imaging methods with high throughput. For evaluation, the neuronal network can imaged by an automated microscope and neurite area and viability are determined (Stiegler *et al.* 2011). The comparison of neurite area and viability between treated and untreated networks allows the investigation of neurite integrity and thereby of neurotoxicity. As a consequence, not only neurite outgrowth can be assessed, but also morphological changes in more mature neuronal networks.

Therefore, the use of homogenous and fast developing neuronal cultures, like LUHMES or pluripotent stem cell (pSC) derived neurons is of advantage. LUHMES were isolated from embryonic mesencephalic tissue and can be differentiated within six days into fully mature neurons with typical neuronal structure (Lotharius *et al.* 2005, Scholz *et al.* 2011). Differentiation protocols are also available for pSC derived neurons that generate a homogenous neuronal network suitable for examination of neuronal integrity within seven days (Hoelting *et al.* 2016). As neurotoxic effects of cyanobacterial toxins like microcystin (MC) were found in animal models (Fischer *et al.* 2000, Feurstein *et al.* 2009, Hu *et al.* 2016, Herrera *et al.* 2018, Hinojosa *et al.* 2019), and MC is discussed, to also have neurotoxic effects in humans, the endpoint of neuronal integrity is well suited to test the neurotoxic effects of MC in human neuronal cultures.

Microcystins are small cyclic heptapeptides produced by different cyanobacterial genera (Svirčev *et al.* 2019). The main exposure route is via drinking water and food. MCs are well known to induce severe hepatotoxicity in humans (Carmichael 1992). Therefore, the World Health Organization (WHO) introduced a safe value of 1 µg/l (1 nM) for drinking water and derived from this a tolerable daily intake (TDI) for humans of 0.04 µg MC-$LR_{equivalents}$/kg BW/day (≈ 40 pmol/kg BW/day) (World Health Organization. Water *et al.* 2004).

3.4.4. Alternatives for neuronal receptors mediated neurotoxicity testing

Neuronal integrity is an appropriate endpoint to test for general neurotoxicity, but it is not possible to gain information about the function of neuronal receptors with this endpoint. In drug development and toxicology, test systems with functional neuronal networks allowing studies on glutamate signaling are needed, as glutamate is the main excitatory neurotransmitter in the human brain (Maycox *et al.* 1988, Fukaya *et al.* 2003).

Glutamate receptors can be divided in ionotropic and metabotropic receptors. The ionotropic receptors can be further subdivided in N-methyl-D-aspartate (NMDA) receptors (NMDA-R), AMPA receptors and kainate receptors (Traynelis *et al.* 2010). At the moment, different strategies are followed to identify compounds interfering with glutamate receptors: (i) pharmacological binding assays (Berger *et al.* 2012, Pottel *et al.* 2020) which are uncoupled from a their physiological environment, (ii) cellular and tissue based models (Hondebrink *et al.* 2016, Nehme *et al.* 2018) and (iii) animal testing, in which problems occur regarding target definition, throughput and species correlation. Therefore, it is of advantage to develop test systems modeling the human brain with its cellular variety as close as possible without having the problem of species extrapolation. The NMDA-R is involved in many diseases (DiFiglia 1990, Lipton 1999, Cohen *et al.* 2015, Liu *et al.* 2019), therefore potentially interfering compounds need to be identified as they could be a major health concern. A suitable *in vitro* test system addressing all these issues would be composed of human cells with an endpoint measuring physiological changes of ionotropic glutamate receptors. Therefore, excitatory and inhibitory neurons with different neuronal receptors and glia cells, like astrocytes as important modulators of neuronal signaling, should be included. Especially, test systems containing NMDA-R have been difficult to set up, as NMDA-R activity leads to excitotoxicity (Leist *et al.* 1998, Nicotera *et al.* 1999). Usu-

ally, the systems are inhibited by NMDA-R antagonists which have been washed out before the conduction of the experiments. In these systems, follow-up studies and investigation of downstream targets are not possible. Therefore, the differentiation of pSC into mixed cortical cultures (MCC) is a promising approach.

As endpoint for neurotoxicity, the afore-mentioned Ca^{2+} signaling is well established (Leist *et al.* 1997, Leist *et al.* 1998, Volbracht *et al.* 2006). The effects of agonists and antagonists of NMDA-R can be investigated as a direct response of their administration. Furthermore, pre-incubation with compounds is also possible. The advantage of assessing Ca^{2+} signaling is the possibility to gain information on single cell level, which enables to distinguish between different cell populations within one culture, as it is true for MCC. Another common method is the cultivation of cells on microelectrode arrays (MEA). To measure electric activity of neuronal networks, the extracellular field potential is recorded. This gives a comprehensive picture of the complete neuronal network of the cultured neurons (Hofrichter *et al.* 2017, Strickland *et al.* 2018, Shafer 2019, Nimtz *et al.* 2020). Besides the network information, they also provide the opportunity to follow network formation and performance of cell cultures over long time periods. The cells can be measured multiple times (e.g. every day) in the MEA device or they can even be cultured there. During this time period, the cells can also be manipulated and measured in parallel. Even multiple compound additions and washouts can be performed with increasing concentration, whereby the same well serves as baseline control. These infinite combinations of treatment and washout in different time frames constitute promising opportunities in *in vitro* neurotoxicology. However, the potential of this fascinating technology can only be exploited if a robust cell system composed of excitatory and inhibitory neurons is present, e.g. MCC. These cultures provide the basis for a functional neuronal network which can be manipulated by the addition of agonists and antagonist of e.g. NMDA-R or be used to test the effects of compounds of interest on neuronal networks and specific neuronal receptors.

3.4.5. Combination of NAMs in test batteries

In the sections above, different test systems and cell systems used in this thesis have been described together with their individual endpoints, applicability domains and unique characteristics. Yet, none of these systems is a stand-alone method, covering the whole range of DNT. Therefore, it is beneficial to combine them in a test battery of assays and

thereby capture information across different neurodevelopmental processes (Leist *et al.* 2012, Bal-Price *et al.* 2018). In a DNT test battery, NAMs can be complemented by behavioral studies with alternative species like *C. elegans* or zebrafish, as they have an intact nervous system and add another level of complexity (Leist *et al.* 2012, Bal-Price *et al.* 2018). Also for the implementation of NAMs in regulatory toxicity, the combination of single tests in test batteries has been proposed and included in concepts like adverse outcome pathway or integrated approaches to testing and assessment.

3.5. Implementation of NAMs in regulatory toxicology

Recently, international (regulatory) agencies proposed the integration of NAMs to accelerate their risk assessment (ECHA 2016, USEPA 2018). Still, there are debates of how the integration of NAMs from many different sources with different data structures and readouts can be accomplished. Several approaches, their pitfalls and respective resolutions, are vividly discussed in academia, agencies, industry and research associations (Leist *et al.* 2008, Escher *et al.* 2019, Harrill *et al.* 2019, Avila *et al.* 2020, Fischer *et al.* 2020, Moné *et al.* 2020). In the following section some of the proposed concepts are summarized.

3.5.1. Adverse outcome pathways (AOP)

The concept of adverse outcome pathways (AOP) was initially introduced in 2010 to support risk assessment in ecotoxicology (Ankley *et al.* 2010) and is nowadays also applied to regulatory toxicology. Therefore, AOP integrate the mechanistical knowledge of different biological levels and thereby provide a tool for knowledge management in toxicology and ecotoxicology (Leist *et al.* 2017). The basic structure of an AOP can be described as a molecular initiating event (MIE) followed by a variable amount of measureable key events (KE) with structural, cellular or functional changes finally resulting in a human adverse outcome (AO). All the single components of an AOP are connected by so-called key event relationships (KER) (Villeneuve *et al.* 2014). The anchoring point for every AOP is the AO and each KE is considered regarding its relevance to the AO (Bal-Price *et al.* 2017). The KEs integrate information from different sources like *in vivo* studies, *in vitro* test methods, (Q)SAR and read across and can originate from different biological levels, like molecular, sub-cellular, cellular, organs or organisms (Bal-Price *et al.* 2017). As an example, the AOP "Binding of antagonist to NMDARs impairs cognition" is given in Fig. 3.3 (Sachana *et al.*

2018). It is known, that NMDARs are important for synaptogenesis and synaptic plasticity and binding of antagonists during this processes lead to problems of learning and memory (Traynelis *et al.* 2010). The AOP starts with the MIE "binding of antagonists to NMDAR" followed by six KE connected by KER resulting in the AO "impaired learning and memory". Importantly, every AOP needs to be evaluated concerning its weight of evidence for biological plausibility of the KER and the essentiality of the KE for the AO. For the shown AOP, this was done in great detail in Sachana *et al*. (Sachana *et al.* 2018). AOP are meant to be a pragmatic simplification of complex biological pathways with the intention of applicability for regulatory decision-making (Bal-Price *et al.* 2017). Here, it is important to note that AOP do not represent the mode of action of a specific chemical, nor do they include information about toxicokinetics. Therefore, they cannot be directly used for risk assessment (Villeneuve *et al.* 2014). Nevertheless, they provide a comprehensive tool to describe potential hazard when information about a given specific compound and its relevant concentrations at a target site are known to trigger a MIE (Bal-Price *et al.* 2017). As AOP often do not provide information only on molecular level but also on superordinate processes, it is possible to apply simple and easily accessible test methods to gain confidence in the specific AOP. Especially in the field of (D)NT, it is challenging to develop AOPs as the brain is an extremely complex organ with many specialized neuronal and glial cell types. The function of these cells differ between brain regions and stages of brain development (Rice *et al.* 2000). Furthermore, there is still a lack of understanding molecular and cellular characteristics of the brain and thereby its interaction with potential toxicants. Nevertheless, the AOP concept provides a powerful tool to integrate mechanistical understanding into risk assessment.

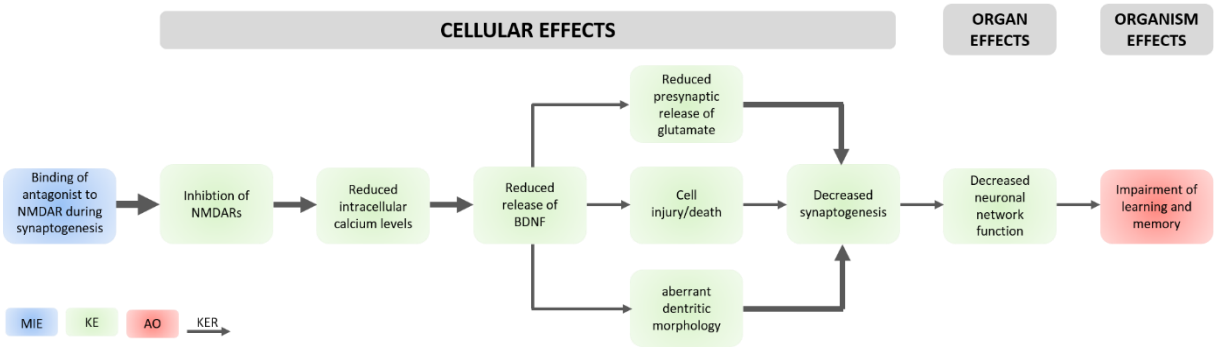

Fig. 3.3: Graphical representation of the AOP "Binding of antagonist to NMDARs impairs cognition"The molecular initiating event (MIE in blue), the key events (KE in green), the adverse outcome (AO in red) and the key event relationships (KER black arrows) are given for AOP number 13 (Sachana *et al.* 2018). The thickness of the KER arrows represent the evidence of the respective KER: thick arrow – strong weight of evidence, middle arrow – strong/mediate weight of evidence, thin arrow – moderate weight of evidence.

3.5.2. Pathways of toxicity (PoT)

Another knowledge-driven approach that relies on the understanding of molecular mechanisms and their integration in a more complex cellular context are pathways of toxicity (PoT). They can be described as "a sequence of intracellular events which regulate normal biology which, when sufficiently perturbed by a xenobiotic, leads to an adverse outcome at the level of the cell, and possibly the whole organism" (Whelan *et al.* 2013). PoT try to depict all changes which are triggered by a chemical in a certain cell. Therefore, it is important to understand the complete biology of a cell with all the signaling pathways, metabolites, genes and processes involved. PoT may help to shift from a "black box" approach of testing a compound in an animal, determining the EC_{50} and extrapolating toxicological thresholds for human exposure towards a system wide understanding by integrating results from high-content high-throughput technologies (Leist *et al.* 2008). An important assumption in the concept of PoT is, that they are finite and once the whole network of PoT is explored and understood toxicity can be assessed very precisely (Kleensang *et al.* 2014). In classical toxicology, an EC_{50} is determined after animal exposure to a limited number of doses and by addition of different security factors and a point of departure (PoD) is determined for different exposure scenarios. In *in vitro* assays, more concentrations can be tested and thereby the PoD can be determined more accurate. PoDs are then extrapolated by *in vitro in vivo* extrapolation depending on the PoT involved (Rotroff *et al.* 2010, Wetmore *et al.* 2012). Thereby, dose and dynamics can be better integrated and safe doses are easier to estimate resulting in fewer uncertainties in decision making (Kleensang *et al.* 2014). It is also possible to determine concentrations were no PoT is triggered. This does not mean that the triggering of a PoT automatically indicates a risk, but a potential hazard. PoT are not only single events connected and resulting in an adverse outcome, they are also interconnected and thereby influence each other in a network of different PoT (Leist *et al.* 2008). Together with the fact that also kinetics and to some extent also quantitative models should be included, this results in a very ambitious

but also comprehensive concept for modern toxicology and will enable a more precise and knowledge based toxicological assessment in the future.

3.5.3. Integrated approaches to testing and assessment (IATA)

One of the most comprehensive approaches in the area of NAMs and regulatory toxicity is the concept of integrated approaches to testing and assessment (IATA). Here, information from different areas of biology, toxicology and computer science are combined in a pragmatic science-based approach for toxicological decision making (OECD 2017, OECD 2017). Therefore, defined questions in a specific regulatory context are addressed in a sequential process. In a first step, existing data from different lines of evidence ((Q)SAR; read-across, *in vivo*, *in vitro*, *in chemico*, *ex vivo*, -omics technologies) are collected and combined. This is followed by a weight of evidence evaluation. In this second step, information gaps are identified, which are, in a third step, filled by a targeted testing strategy that generates new data (Casati 2018). Bal-Price *et al.* developed an IATA for DNT screening and prioritization purposes shown in Fig. 3.4. As data from many different sources are taken into account some rules had to be installed for their integration. For this purpose, so-called defined approaches were introduced: for a fixed set of information sources a fixed data interpretation procedure was established (OECD 2017). Following this, the data interpretation was rule-based and does not require expert knowledge for prediction. This is especially convenient as regulators have to deal with many different chemicals from many different areas and cannot be an expert in every field. Between all tiers mentioned here, decision steps are included (Casati 2018). Therefore, it is possible to always take into account an acceptable level of uncertainty. In traditional regulatory toxicology and classical chemical assessment, the current practice is based on adverse outcomes of animal models. However, it is very unlikely to meet the legislative requirements with this approach, as the number of mandatory chemical assessments increased and at the same time the use of animals and resources shall not increase (Terron *et al.* 2018). Therefore, the integration of NAMs in regulatory toxicology can close the gap between the number of chemicals that need to be assessed and the actually assessed number. To achieve the integration of NAMs in regulatory toxicology, IATA represent a flexible solution as they open the possibility to combine data from different methods, include AOPs and combine them with information from ADME (Sachana *et al.* 2019). Hence, IATA are a chance to turn

the toxicological decision making into a more modern toxicity testing by integrating different individual methods and batteries and thereby enable the assessment of more chemicals.

AOP, PoT, and IATA represent a promising basis for the integration of NAMs into regulatory toxicity and might thereby contribute to the needed paradigm shift from animal based "black box" toxicology towards a knowledge based toxicology, resulting in better risk assessment.

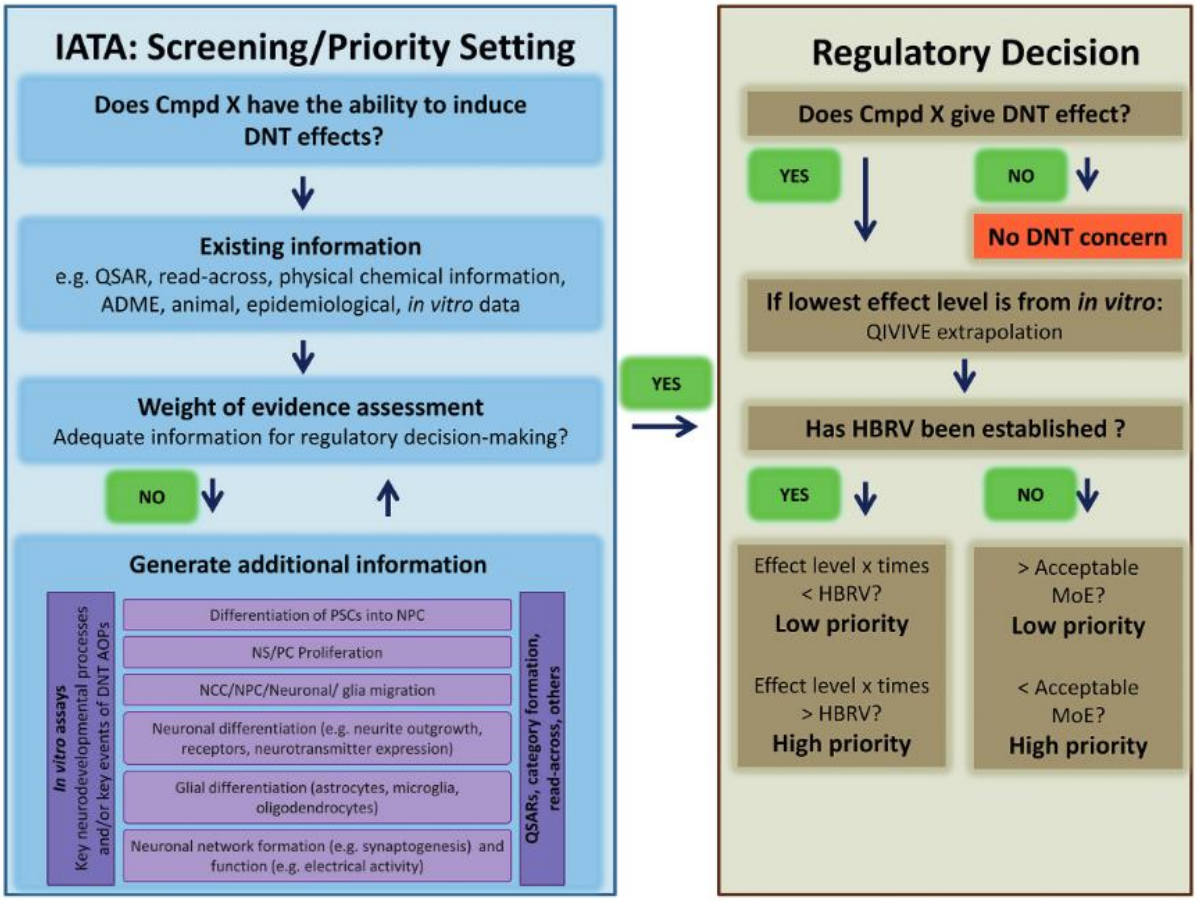

Fig. 3.4: IATA for DNT screening and prioritization purposes

This IATA was developed by Bal-Price *et al.* 2018 to suggest a more efficient way of identifying potential DNT compounds. The IATA integrates information from multiple information sources. It also provides a targeted strategy of in vitro test methods, if new information is required, and the integration of non-testing methods covering key neurodevelopmental processes. Abbreviations: ADME, absorption, distribution, metabolism and excretion; Cmpd, compound; DNT, developmental neurotoxicity; HBRV, health-based reference value; MoE, margin of exposure; QIVIVE, quantitative in vitro in vivo extrapolation; QSAR, quantitative structure activity relationship. Figure adopted from Bal-Price *et al.* 2018.

4. Results

4.1. From transient transcriptome responses to disturbed neurodevelopment: role of histone acetylation and methylation as epigenetic switch between reversible and irreversible drug effects

published in *Arch Toxicol* 88, 1451-1468 (2014)

Stefanie Klima*[1], Nina V. Balmer*[1], Eugen Rempel[2,5], Violeta N. Ivanova[3,4], Raivo Kolde, Matthias K. Weng[1], Kesavan Meganathan[6], Margit Henry[6], Agapios Sachinidis[6], Michael R. Berthold[3, 4], Jan G. Hengstler[7], Jörg Rahnenführer[2], Tanja Waldmann[1], Marcel Leist[1, 4]

* The authors wish it to be known that, in their opinion, the first two authors should be regarded as joint First Authors.

[1] Doerenkamp-Zbinden Chair for In Vitro Toxicology and Biomedicine, University of Konstanz, Box 657, 78457 Constance, Germany

[2] Department of Statistics, TU Dortmund, Dortmund, Germany

[3] Chair for Bioinformatics and Information Mining, University of Konstanz, Constance, Germany

[4] Konstanz Research School Chemical Biology, University of Konstanz, Constance, Germany

[5] OÜ Quretec, 51003 Tartu, Estonia

[6] Institute of Neurophysiology, University of Cologne, 50931 Cologne, Germany

[7] Leibniz Research Centre for Working Environment and Human Factors (IfADo), 44139 Dortmund, Germany

Keywords: valproic acid, embryonic stem cell, histone deacetylase, developmental toxicity, histone modification

4.1.1. Abstract

The superordinate principles governing the transcriptome response of differentiating cells exposed to drugs are still unclear. Often, it is assumed that toxicogenomics data reflect the immediate mode of action (MoA) of drugs. Alternatively, transcriptome changes could describe altered differentiation states as indirect consequence of drug exposure. We used here the developmental toxicants valproate and trichostatin A to address this question. Neurally differentiating human embryonic stem cells were treated for 6 days. Histone acetylation (primary MoA) increased quickly and returned to baseline after 48 h. Histone H3 lysine methylation at the promoter of the neurodevelopmental regulators PAX6 or OTX2 was increasingly altered over time. Methylation changes remained persistent and correlated with neurodevelopmental defects and with effects on PAX6 gene expression, also when the drug was washed out after 3–4 days. We hypothesized that drug exposures altering only acetylation would lead to reversible transcriptome changes (indicating MoA), and challenges that altered methylation would lead to irreversible developmental disturbances. Data from pulse-chase experiments corroborated this assumption. Short drug treatment triggered reversible transcriptome changes; longer exposure disrupted neurodevelopment. The disturbed differentiation was reflected by an altered transcriptome pattern, and the observed changes were similar when the drug was washed out during the last 48 h. We conclude that transcriptome data after prolonged chemical stress of differentiating cells mainly reflect the altered developmental stage of the model system and not the drug MoA. We suggest that brief exposures, followed by immediate analysis, are more suitable for information on immediate drug responses and the toxicity MoA.

4.1.2. Introduction

Toxicogenomics data, systems biology, and the use of human stem cell-based systems are expected to change the ways by which toxicological information will be obtained and interpreted in the future (Waters *et al.* 2004, Wobus *et al.* 2011, Hartung *et al.* 2012, Robinson *et al.* 2012, Robinson *et al.* 2013). This is in line with a 'proposed shift from primarily in vivo animal experimentation to in vitro assays and computational modeling for toxicity assessment,' as suggested by the lead scientists of US national research agencies (Collins *et al.* 2008). It also follows the 'vision for a new toxicology of the twenty-first

century' as promoted by the National Research Council (NRC 2007, Andersen *et al.* 2010). A key assumption for this vision is that it will be possible to define pathways of toxicity, i.e., a drug mode of action (MoA), linking molecular initiating events to a final adverse outcome. This requires an establishment of a 'systems toxicology' that models the pathophysiology of the body with computational tools to understand mechanisms of toxicity, similar to systems biology (Hartung *et al.* 2012).

In the field of developmental toxicology, transcriptome data have been used to infer information on the MoA of chemicals (Colleoni *et al.* 2011, Vojnits *et al.* 2012, Hermsen *et al.* 2013). It is expected that such approaches will lead to major conceptual advances, especially for the use of the emerging technology of differentiating stem cell systems (Zimmer *et al.* 2011, Crofton *et al.* 2012, Theunissen *et al.* 2012). However, more fundamental work is required to understand how experiments need to be designed and interpreted in this field. In contrast to mature tissues or cells, model systems of development do not have a stable baseline, i.e., the transcriptome changes over time, also without toxic stimulus. Moreover, initial exposure to a toxicant may trigger secondary effects even in the absence of the stimulus (Balmer *et al.* 2012). To avoid indirect effects in toxicogenomics measurements, sampling only few hours after compound exposure has been suggested (Jergil *et al.* 2011). However, the sensitivity and response to toxicants of a dynamically differentiating system can be different at different times (van Dartel *et al.* 2009). For instance, in a study of retinoic acid teratogenicity, compound-induced transcriptome changes differed between sampling time points (Robinson *et al.* 2012). Such timing effects of toxicants may be due to interference with specific waves of gene regulation. For instance, neurally differentiating mESC showed several of such waves of gene expression, which determined windows of sensitivity to toxicants (Abranches *et al.* 2009, Zimmer *et al.* 2011).

Alteration of histone deacetylase (HDAC) activity has been associated with several long-term health consequences, ranging from Alzheimer's disease (Gräff *et al.* 2012), over toluene poisoning (Sánchez-Serrano *et al.* 2011) to general teratogenic mechanisms (Menegola *et al.* 2012). Specific, HDAC inhibitor (HDACi) drugs have been particularly well characterized. For instance, the broad-spectrum HDACi valproic acid (VPA), normally used to treat epilepsies, causes the fetal valproate syndrome and has been suspected to trigger autism (Meador *et al.* 2009, Dufour-Rainfray *et al.* 2010, Jentink *et al.* 2010). It triggers gene activation within few hours in several tumor or stem cell lines (Jergil *et al.*

2009, Jergil *et al.* 2011), and it is well recognized that epigenetic modifications are related to the developmental neurotoxicity of the drug. Most studies addressing the latter mechanism have concentrated on transcription activating histone modifications such as acetylation of histone 3 at lysine 9 (H3K9Ac) or methylation of histone 3 at lysine 4 (H3K4me) (Tung *et al.* 2010, Hezroni *et al.* 2011, Marinova *et al.* 2011), and the changes have been found to be reversible after drug withdrawal (Boudadi *et al.* 2013).

In previous work, we established a model of early neural differentiation of hESC that allowed the identification of developmental toxicants (Balmer *et al.* 2012, Krug *et al.* 2013). We found that prolonged exposure to the two HDACi trichostatin A (TSA) or VPA altered the expression of several marker genes in a similar way. However, we also observed that various hESC-based test systems differed strongly in their transcriptome response to VPA (Krug *et al.* 2013). This latter finding triggered the key question of this study: Are the observations on altered transcriptome patterns in developmental toxicity studies indeed a reflection of a compounds primary MoA? As alternative hypothesis, we examined whether the data rather reflect an altered cellular phenotype that would result from disturbed differentiation and that would become independent of the continued presence of drug after some time. This was addressed by transcriptome analysis after pulsed drug exposure. A further key question was how a direct, but reversible effect of short toxicant exposure was switched to a persistent adverse effect, reflected by wrong differentiation after a longer drug exposure. This was addressed by studies of the time dependence of histone modifications. Histone methylations at the promoters of key neurodevelopmental genes were considered as potential persistence detectors responsible for switching a short-term cellular adaptation to permanent toxicity.

4.1.3. Material and methods

Materials

Gelatine, putrescine, selenium, progesterone, apotransferin, glucose, insulin, valproic acid, and trichostatin A were obtained from Sigma (Steinheim, Germany). Accutase was from PAA (Pasching, Austria). FGF-2 (basic fibroblast growth factor), noggin, and sonic hedgehog were obtained from R&D Systems (Minneapolis, MN, USA). Y-27632, SB-43154, and dorsomorphin dihydrochloride were from Tocris Bioscience (Bristol, UK). MatrigelTM was from BD Biosciences (Massachusetts, USA). All cell culture reagents were from Gibco/Invitrogen (Darmstadt, Germany) unless otherwise specified.

Neuroepithelial differentiation

Human embryonic stem cells (hESC) (H9 from WiCells, Madison, WI, USA) were differentiated as described in detail earlier (Chambers *et al.* 2009). Briefly, dual SMAD inhibition was used to prevent BMP and TGF signaling and thus to achieve a highly selective neuroectodermal lineage commitment. For handling details, see supplemental methods of Balmer *et al.* (2012). If not stated otherwise, treatment with trichostatin A (TSA) was done with a concentration of 10 nM and treatment with valproic acid (VPA) was done with a concentration of 600 µM.

Quantitative real-time PCR (qPCR) and microarray analysis

For qPCR analysis, cells were lysed at indicated days of differentiation in TriFast™ (Peqlab, Germany). Total RNA was isolated according to the manufacturer's instruction, and cDNA was produced using the iScript Kit from BioRad (iScript™ Reverse Transcription Supermix for RT-qPCR, BioRad). Quantitative real-time PCR (qPCR) was performed on a BioRad Light Cycler (Biorad, München, Germany), and transcript levels were quantified as described earlier (Balmer *et al.* 2012). The sequences of specific primers are given in Fig. 5.1.S11.

Affymetrix chip-based DNA microarray analysis (Human Genome U133 plus 2.0 arrays) was performed as described earlier (Krug *et al.* 2013). The data were analyzed for differential expression using the Konstanz Information Miner open source software [KNIME; www.knime.org (Berthold *et al.* 2008)]. The raw data were preprocessed using robust multiarray analysis (RMA) (Smyth 2005). Background correction, quantile normalization, and summarization were applied to all expression data samples, using the RMA function from the *affy* package of Bioconductor (Gautier *et al.* 2004, Gentleman *et al.* 2004). The *limma* package (R & Bioconductor) was used to identify differentially expressed genes using indicated groups as control. The moderated *t* statistics was applied in a pairwise fashion (each treatment was compared to its own control) and was used for assessing the raw significance of differentially expressed genes. Then, final *p* values were derived using the Benjamini–Hochberg (BH) method to control the false discovery rate (FDR) (Benjamini *et al.* 1995) due to multiple hypothesis testing. Transcripts with FDR adjusted *p* value of ≤0.05 and fold change values >1.5 or <2/3 were considered significantly regulated, if not stated otherwise in the figure legend. For Fig. 5.1.S5, numbers of PS changed during development (D-genes) were calculated relative to hESC. These data

were obtained from four independent replicates, and they were considered significant if the Benjamini–Yekutieli (BY)-adjusted *p* value was <0.01 and the FC was >1.5 or <2/3. For Figs. 5.1.3, 5.1. 4, 5.1. 5, and 5.1.6, numbers of PS changed by the treatment were calculated relative to untreated controls lysed at the same day as the treated samples (T6h to C6h, T4d to C4d and T6d, early pulse (EP), medium pulse (MP), and late pulse (LP) to C6d). Data were obtained from four independent replicates and chosen if the BH-adjusted *p* value was <0.05 and FC was >1.5 or FC <2/3.

The principal component analysis (PCA) was based on 500 PS with the highest variance.

Western blot

Western blot was performed exactly as previously described (Balmer *et al.* 2012). For quantification, the signal intensity of H3Ac was normalized to total H3, and acetylated α-tubulin was normalized to total α-tubulin for every time point. These normalized values were then displayed relative to untreated controls at the respective time points. Western blots of PAX6 and OTX2 were quantified using ImageJ. Detailed information on used antibodies is given in Fig. 5.1.S12.

Chromatin immunoprecipitation (ChIP)

Chromatin immunoprecipitation (ChIP) assays on native chromatin (N-ChIP) (Fig. 5.1.1) were performed according to established protocols (Umlauf *et al.* 2004). Details and adaptations were exactly as described previously in detail (Balmer *et al.* 2012). ChIP assays on cross-linked chromatin (X-ChIP) (Fig. 5.1.2) were performed according to Kamieniarz and colleagues and adapted to our differentiating cells (Kamieniarz *et al.* 2012). Briefly, cells were trypsinized and resuspended in 1 % formaldehyde in medium. The crosslink was stopped after 10 min by 125 mM Tris, pH 7.5. Cellular suspensions were centrifuged, washed once in PBS and once in L1 buffer (2 mM EDTA, 0.1 % NP-40, 10 % glycerol, 25 mM Tris, pH 8), and finally resuspended in L2 buffer (10 mM EDTA pH 8, 1 % SDS, 50 mM Tris, pH 8) to a final concentration of $2 \times 10_6$ cells/ml. Chromatin was sonicated on a Bioruptor ® sonifier device (Diagenode, Belgium) by 30 steps of 30/30 s ON/OFF cycles to get a fragment size between 300 and 700 bp, and sonication efficiency was checked on agarose gels. Samples were diluted 1:5 in dilution buffer (0.5 % NP-40, 200 mM NaCl, 50 mM Tris, pH 8) and incubated over night at 4 °C with unspecific control antibody, 2 µl anti-H3K4me3 (17–614 Millipore) or 4 µl anti-H3K27me3 (39535 Active Motif) antibodies.

One aliquot, corresponding to 5 % of the input, was stored without antibody treatment. After antibody incubation, the samples were rotated at 4 °C for 3 h with protein A/G Sepharose beads and washed twice in washing buffer (2 mM EDTA, 0.1 % SDS, 0.5 % NP-40, 150 mM NaCl, 20 mM Tris pH 8) and once in final wash buffer (2 mM EDTA, 0.1 % SDS, 0.5 % NP-40, 500 mM NaCl, 20 mM Tris, pH 8). The chromatin was eluted by 2-h incubation and shaking at 65 °C in elution buffer (100 mM $NaHCO_3$, 1 % SDS). The genomic DNA was purified using ChIP DNA Clean and Concentrator (Zymo Research) Kit and analyzed by qPCR, to quantify the amount of DNA from the promoter region of selected genes. For data display, the enrichment factor (EF) was calculated from the qPCR threshold cycle values (Ct) relative to input according to the formula: EF (%IP) = 100 * 2^ − [(Ct(5 % IP) − 4.32) − Ct(specific antibody)]. For Figs. 5.1.1e and 5.1.2a, we wanted to investigate the effects of TSA or VPA in comparison with untreated controls. We compared the ratios of H3K4me3/H3K27me3 of treated cells to the ratios of H3K4me3/H3K27me3 of untreated cells at the respective days of differentiation. Also for transcript levels, the gene expression was presented relative to untreated controls at the respective days. Therefore, H3K4me3/H3K27me3 ratios or gene expression above 1 indicated that TSA or VPA caused an up-regulation compared with untreated control. H3K4me3/H3K27me3 ratios (methylation ratio) or gene expression below 1 indicated that TSA or VPA caused a down-regulation compared with untreated controls. For detailed information on ChIP, primers and antibodies refer to Fig. 5.1.S11 and 5.1.S12.

Statistics and data mining

For statistical analysis of transcript levels and EFs, paired *t* tests were performed using log-transformed expression values relative to hESC, if not stated otherwise in the legend. All data are shown, and all statistics performed refer to biological replicates (=independent experiments).

Over-representation of gene ontologies (GOs) was analyzed using g:profiler (Reimand *et al.* 2011), with *p* values determined via a hypergeometric distribution. Over-represented GOs were selected, if they belonged to the term domain 'biological process' and contained <1,000 genes, and the *p* value was <0.05. For analyses yielding more than 50 GOs, more stringent selection criteria were used: only GOs that had a *p* value <0.001 were selected. For production of the GO word clouds scaling of character size was linearly

proportional to the negative logarithm of the *p* value of the respective GO category. GO terms relating to biological processes (bp) were clustered according to their 'superordinate biological processes' as described earlier. Example of these larger categories were 'neuronal differentiation,' 'non-neuronal differentiation,' or 'migration and adhesion' (Waldmann *et al.* 2014).

Venn diagrams were drawn in order to visualize size relations between the compared groups of genes within one diagram. They do not always represent correct ratios, as this would make visualization difficult in case of big size differences. Numbers in Venn diagrams comparing three groups represent the percentage of the (overlapping or unique) part of the diagram relative to samples lysed at DoD4. The corresponding absolute numbers are indicated in the supplementary files. For Venn diagrams with two circles, absolute numbers of PS and their overlap are presented. The numbers that indicate the percentage of the overlap in two group comparisons are relative to the circle that has the same color as the line under the number.

4.1.4. Results

Time courses of histone acetylation and altered marker gene expression triggered by HDACi during early neurogenesis

A pure population of neuroepithelial cells (NEP) can be generated from human embryonic stem cells (hESC) within 6 days (Chambers *et al.* 2009, Balmer *et al.* 2012, Krug *et al.* 2013). This model system is characterized by up-regulation of the transcription factors PAX6 and OTX2 (Fig. 5.1.1a). We found earlier that continued exposure to TSA and VPA affects the expression of these two genes. In addition, we observed that short drug exposure (for 24 h) showed the expected biochemical effect [increased histone acetylation on day of differentiation 1 (DoD1)]. However, when differentiating hESC, treated for the first 24 h with HDACi, were examined on day of differentiation 6 (DoD6), there was no effect on the expression of the neuroepithelial markers (PAX6 and OTX2) (Chambers *et al.* 2009, Balmer *et al.* 2012, Krug *et al.* 2013). To better understand the relationship of biochemical changes and the expression of differentiation markers, we started this study by examining the time course of key events including gene expression and various histone modifications.

Analysis of mRNA expression of PAX6 during undisturbed differentiation showed that this gene is very little regulated during the first 3 days, while significant OTX2 up-regulation was already detectable after 2 days. Both genes reached high levels (compared to hESC) on DoD6 (Fig. 5.1.1b). Exposure to HDACi (equipotent concentrations of 600 µM VPA or 10 nM TSA) during the entire differentiation process led to a relative down-regulation of both NEP marker genes. Consistent with the time course of developmental up-regulation of the marker genes, the drugs affected OTX2 already from early time points on, while PAX6 levels were only reduced at DoD4–6 (Fig. 5.1.1c).

To examine protein acetylation triggered by drug treatment, we used Western blotting. Histone H3 and α-tubulin were selected as abundant and well-characterized target proteins of HDACs. Exposure to TSA or VPA for the first 6 h of differentiation triggered strong acetylation of histone H3 on the whole-cell level. TSA also increased acetylation of α-tubulin ($p < 0.05$), as expected from the HDAC inhibition profile. VPA effects on this target were not significant, which is consistent with the fact that VPA inhibits specifically HDAC class I enzymes and not the tubulin acetylating class II HDACs (Göttlicher *et al.* 2001, Khan *et al.* 2008, Fass *et al.* 2010). Already after 24 h, the extent of protein acetylation was strongly reduced compared with 6-h drug treatment, and after 48 h, the effect vanished (despite the continued presence of the drugs) (Fig. 5.1.1d).

This was most likely due to cellular counter-regulations, as HDACs and histone acetyl transferases are dynamically regulated during differentiation (Weng *et al.* 2012) and adaptive effects have been described for HDACi drug treatment (Tung *et al.* 2010, Kataoka *et al.* 2013). Nevertheless, we also considered that global analysis of protein acetylation may not be sensitive enough. Therefore, we studied histone H3 acetylation of the lysine 27 residue (H3K27Ac) at four promoter sites of interest (transcription start site of PAX6, OTX2, OCT4, Nanog) using chromatin immunoprecipitation (ChIP). No drug-induced changes in the acetylation levels were observed on DoD1 or any of the following days (Fig. 5.1.S1A). Various control experiments showed that histone acetylation was technically measurable in our cells and that the H3K27 residue can be affected by HDACi (at higher concentrations) at the chosen promoter sites (Fig. 5.1.S1B). These data suggest that the low, human relevant developmental toxicant drug concentrations used here triggered at best very weak, non-measurable promoter acetylation. A more persistent effect on gene regulation and differentiation may thus require another histone modification, such as methylation.

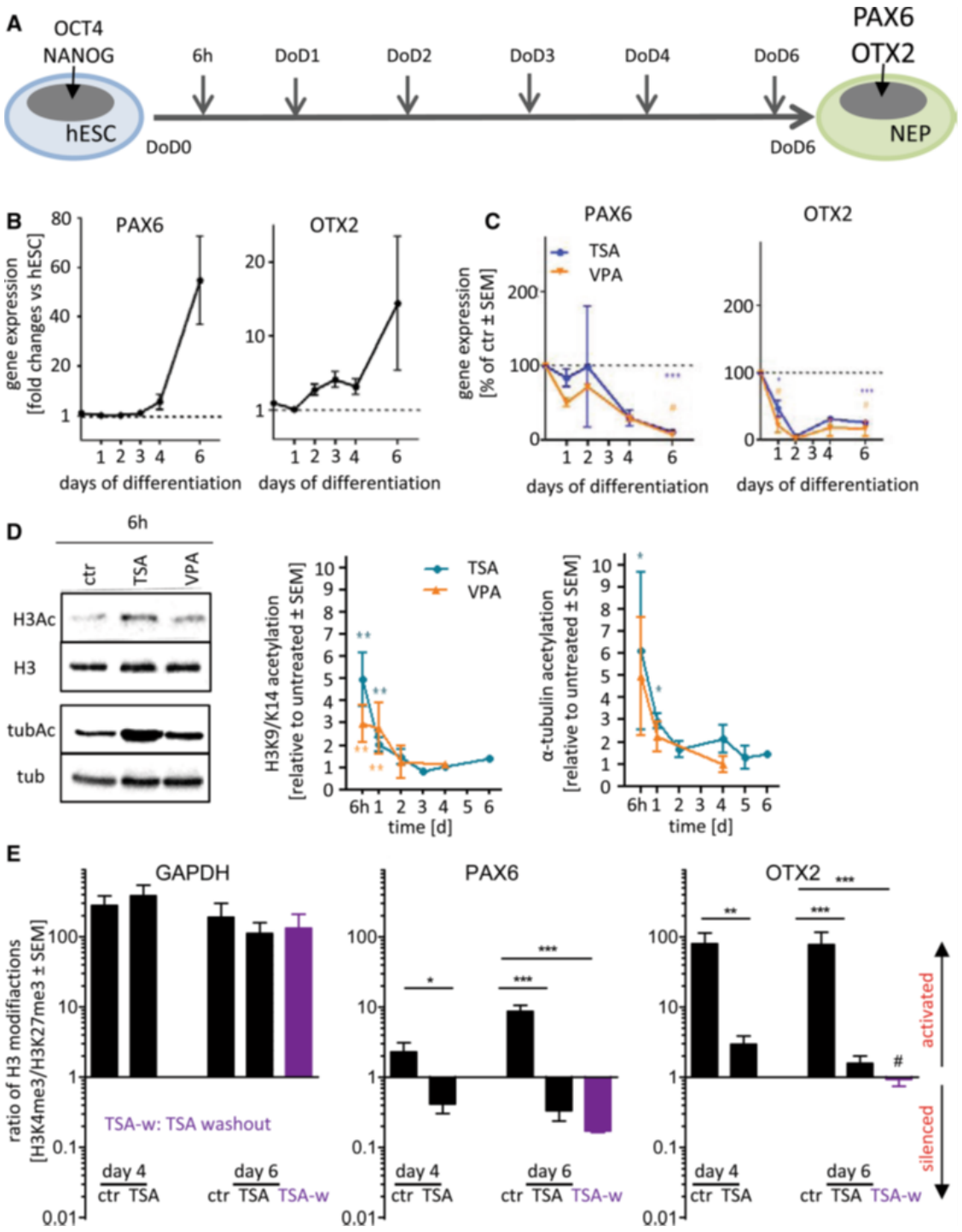

Fig. 5.1.1: Gene expression and histone methylation patterns of the neuroectodermal marker genes PAX6 and OTX2. (**A**) For all experiments, human embryonic stem cells (hESC) were differentiated to neuroepithelial precursor cells (NEP). Marker genes for hESC and NEP at the time points of analysis are indicated in the differentiation scheme. (**B**) Samples were taken at the indicated days of differentiation (DoD), and transcript levels of marker genes of neural differentiation were determined by RT-qPCR. Data (gene expression relative to hESC) are mean ± SEM of 3–5 experiments. (**C**) The differentiation was performed in the presence of non-cytotoxic concentrations of TSA (10 nM) or VPA (0.6 mM). At the indicated time points, transcript levels were determined by RT-qPCR. Data (expressed relative to control differentiated for the same time in the absence of drug) are mean ± SEM of 3–5 experiments. (**D**) Differentiating cells were treated with TSA or VPA for different time periods, and protein acetylation was analyzed by Western blots (WB) with antibodies specific for acetylated histone H3 (H3Ac) or acetylated α-tubulin (tubAc). WB against total histone 3 (H3) or

α-tubulin (tub) was performed for normalization. One representative blot for the 6-h time point is displayed. The graphs are based on densitometric analysis of WB from three independent experiments. The levels of acetylated protein are given relative to untreated controls differentiated for the same time period. Data are mean ± SEM of three experiments. (**E**) Differentiating cell was treated with TSA (10 nM) for 4 days (day 4), 6 days (day 6), and for 4 days followed by a 2-day washout of the drug (TSA-w, purple bars). Chromatin immunoprecipitation (ChIP) was performed with antibodies specific for H3K4me3 or H3K27me3. Samples were taken on day 4 of differentiation (day 4) or on day 6 of differentiation (day 6; TSA-w). The figure displays the ratio of the enrichment factors for H3K4me3 and H3K27me3 (individual values are found in supplemental files). A ratio >1 points to open chromatin (more H3K4me3) and a ratio <1 suggests a more silenced chromatin (more H3K27me3). Hash symbol indicates a bivalent state. Data are mean ± SEM of three experiments. *$p < 0.05$; **$p < 0.01$; ***$p < 0.01$

Time course of histone methylation changes triggered by HDACi during early neurogenesis

We had found earlier that a 6-day continued treatment with TSA resulted in alterations of histone methylation, but it remained unclear when such changes happened and how persistent they were. As a 4-day treatment with subsequent washout of the drug was sufficient to alter the expression of PAX6 (Chambers *et al.* 2009, Balmer *et al.* 2012, Krug *et al.* 2013), we investigated now in a first pilot experiment, whether the histone methylation pattern was already changed after 4 days and whether such changes would persist throughout a drug washout period. ChIP was performed with antibodies specific for the open/active chromatin mark trimethylated lysine 4 of histone 3 (H3K4me3) and with antibodies specific for the closed/inactive chromatin mark trimethylated lysine 27 of histone 3 (H3K27me3) (Fig. 5.1.S2). Ratios of H3K4me3 to H3K27me3 enrichment were calculated as a simple measure of the chromatin state [high ratio: open promoter and low ratio: rather silenced promoter (Burney *et al.* 2013)] (Fig. 5.1.1e). As expected, we found the methylation ratio of GAPDH, an actively described gene affected neither by TSA nor by differentiation, to be very high and to remain unchanged. We also confirmed our earlier finding that PAX6 and OTX2 have a high methylation ratio in normal NEP (DoD6) and that TSA strongly reduced this ratio ($p < 0.001$). Now, we found that this effect also held true for DoD4 cells. Moreover, the TSA-induced reduction in the methylation ratio was persistent, when the drug was washed out from DoD4 to DoD6 ($p < 0.001$) (Fig. 5.1.1e, Fig. 5.1.S2). Thus, altered histone methylation patterns correlated with drug effects on neurodifferentiation, and they may play a role in drug-induced developmental toxicity and persistent effects of HDACi.

Therefore, we examined the time course of histone methylations more closely. During normal development, H3K4me3 levels of PAX6 remained relatively constant, while promoter opening was indicated by a decrease in H3K27me3, especially between DoD4 and DoD6 (Fig. 5.1.2a). Treatment with TSA reduced this late decrease in the inactivating histone modification (thereby reducing PAX6 transcription) (Fig. 5.1.2b, Fig. 5.1.S3). Opening of the OTX2 promoter during neurodifferentiation was indicated by early (DoD1–2) increases in H3K4me3 and simultaneous decreases in H3K27me3 (Fig. 5.1.2a). Upon treatment with TSA, the methylation ratio at the OTX2 promoter was already slightly down-regulated at DoD1 and significantly down-regulated from DoD2 on ($p < 0.05$) (Fig. 5.1.2b, Fig. 5.1.S3). Thus, we found here that prolonged treatment with an HDACi can lead to an enrichment of inactivating histone modifications. This offers a mechanistic explanation for the down-regulation of important developmental genes (here PAX6 and OTX2) by TSA. These findings differ largely from those reported on short treatment (Nightingale *et al.* 2007, Jergil *et al.* 2011, Boudadi *et al.* 2013), which increases the amount of chromatin-opening histone modifications. On this basis, it became highly interesting to obtain more data on the persistence of altered histone methylations upon pulsed drug treatment.

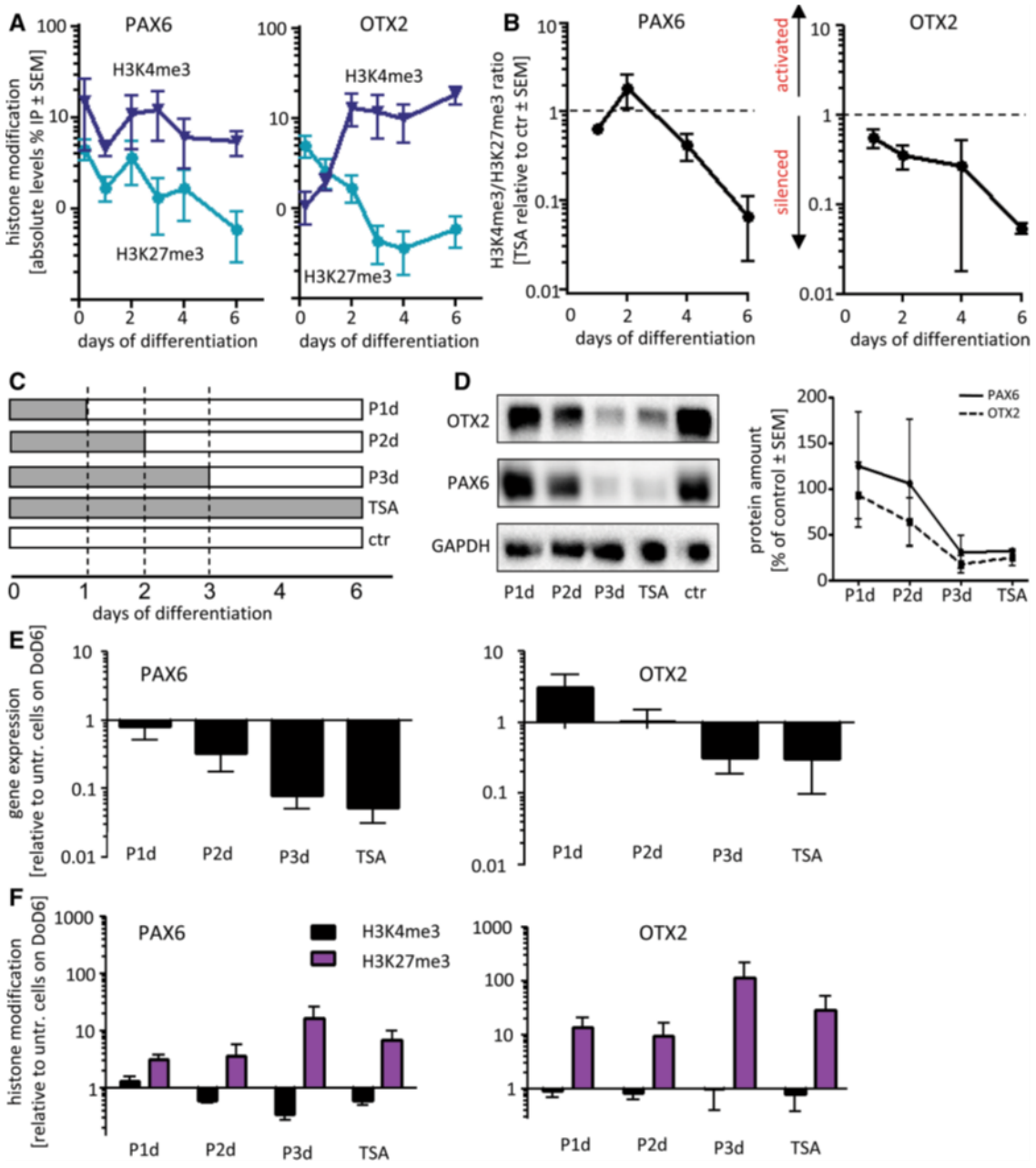

Fig. 5.1.2: Consequences of different drug washout periods for gene expression and histone methylation patterns. For all experiments, hESC were differentiated to NEP. (**A**) Samples for chromatin immunoprecipitation (ChIP) were prepared at the indicated days of differentiation. ChIP was performed with antibodies specific for H3K4me3 or H3K27me3 or control IgG. The enrichment factors of OTX2 and PAX6 promoter sequences are given as % input for H3K4me3 (dark blue) and H3K27me3 (light blue). Data are mean ± SEM of three independent cell preparations. (**B**) Differentiating cells were treated with TSA (10 nM) for the indicated time periods, and ChIP was performed with the same antibodies as described in **a**. The ratio of enrichment factors of H3K4me3 and H3K27me3 was calculated as measure of chromatin opening. Data are given relative to values of untreated control cells at the same time point (n = 3). (**C**) Scheme of experimental treatment and sampling for the following experiments. Gray bars indicate the period of drug exposure (e.g., P2d: pulsed drug treatment for 2 days) with 10 nM TSA, and white bars indicate medium without TSA. All samples were analyzed on day 6 of differentiation for each treatment scenario. (**D**) Protein levels of PAX6 or OTX2 were determined by Western blot, and relative (vs ctr.) protein levels (n = 3) were quantified. (**E**) Transcript levels of PAX6 and OTX2 were determined. They are expressed relative to untreated control on DoD6 (ctr). (**F**) ChIP was performed for

H3K27me3 (purple) or H3K4me3 (black) on promoter regions of PAX6 and OTX2, and enrichment factors were calculated relative to ChIP with control IgG. Then, these data were normalized to the values obtained for control cells (ctr). For instance, on day 6 of the differentiation, H3K27me3 was 15-fold higher in cells treated for 1 day with TSA and then left in control medium (P1d), compared to cells that were differentiated under control conditions. Data of **D-F** are mean ± SEM of 3–5 experiments.

Effects of pulsed drug treatment on histone methylation and NEP differentiation

After we had found that the increase in H3K27me3 as well as the down-regulation of PAX6 and OTX2 was persistent when the cells were treated for 4 days, followed by a 2-day wash out (Fig. 5.1.1e), we investigated the minimum treatment period required to induce this stable effects.

The cells were exposed to TSA for 1, 2, or 3 days, before the drug was removed, and differentiation was continued until DoD6. These pulsed treatments (P1d, P2d, and P3d) were compared to continuous exposure to TSA (Fig. 5.1.2c). As controls of the phenotypic effect of disturbed differentiation, we quantified the protein levels of PAX6 and OTX2. Short treatments of up to 2 days had no effect, while longer drug treatment resulted in strongly decreased levels of the phenotype markers of NEP (Fig. 5.1.2d). Thus, drug treatment of about 3 days was sufficient to cause developmental disturbances.

In parallel, we examined how the pulsed treatment affected the gene expression and promoter methylation of the NEP marker genes. As seen for the protein, 3-day treatment was sufficient to cause the same extent of down-regulation as continuous drug exposure (Fig. 5.1.2e). Examination of H3K4me3 and H3K27me3 marks showed that 3-day drug treatment, followed by 3-day washout triggered at least the same extent of change (i.e., increase in H3K27me3), as continuous drug treatment. In the case of OTX2, about 50 % of these changes were already triggered by 1–2-day treatment, while changes in the PAX6 promoter required up to 3 days of drug exposure (Fig. 5.1.2f). Under this set of experimental conditions, the developmental disturbance triggered by different drug exposures correlated well with altered methylation patterns. The data suggested that a 3–4-day exposure should definitely be sufficient to alter the differentiation track of the cells and to affect gene expression independent of the continued presence of drugs. However, an altered expression of only two NEP markers is not sufficient to answer the question, if we observe really a changed differentiation track. To explore this, we switched from the analysis of few stage-specific markers to full transcriptome analysis of the treated cells.

Transcriptome changes triggered by exposure to HDACi for various time periods

To obtain baseline information on the cell differentiation, the temporal alterations of the transcriptome were recorded first for undisturbed cells. Samples were taken after 6 h, DoD4, and DoD6, and they were related to the expression in hESC (Fig. 5.1.3a, C6h, C4d, C6d). Gene expression levels were measured on DNA microarrays for four complete and independent time course experiments. Principal component analysis (PCA) of the data sets showed that the differentiation model was robust, and large numbers of probe sets (PS) changed reproducibly over time (Fig. 5.1.S4). All PS significantly regulated at any time point relative to hESC (p value <0.01, fold change (FC) > 1.5 or FC < 0.67) were identified (Fig. 5.1.S4B, C, Tab. S1). Neuronal development and maturation were the most conspicuous themes within the up-regulated PS on DoD6 (Fig. 5.1.S4D). The overrepresented gene ontology terms (oGOs) in down-regulated PS gave mainly evidence of the known (Xu *et al.* 2013) metabolic changes related to mitochondrial and amino acid metabolism (Fig. 5.1.S4D). Altogether, these background data confirmed the large-scale changes, which the transcriptome has to undergo for correct lineage commitment, although only few PS (5 %) were found to be regulated at all time points (Fig. 5.1.S4B, C) ((Chambers *et al.* 2009, Coskun *et al.* 2012, Burney *et al.* 2013).

Having established baseline model behavior, the time dependent effects of TSA and VPA on transcriptome changes were examined (Fig. 5.1.3a, T6h, T4d, T6d). Early exposure for as little as 6 h (T6h) was sufficient to up-regulate >1,200 PS; but only about 150 PS were down-regulated. All these early regulations were reversed after a 6-day washout period (EP). Treatment for 4 days (T4d) resulted in similar numbers of up-/down-regulated PS (total: 1,342 PS for TSA, 2,760 PS for VPA). About 5,000–6,000 PS were regulated when cells were exposed for 6 days (T6d) (Fig. 5.1.3b, Tab. S2). Bootstrapping outlier analysis showed that the smaller number of PS at T4d (compared to day 6) was not due to a particularly high experimental variance of the samples (Fig. 5.1.S5).

TSA and VPA are HDACi with a >10,000-fold difference in potency and with little structural similarity. However, 62–74 % of the PS regulated by TSA were also altered by VPA (Fig. 5.1.3c). The high degree of overlap at all time points strongly suggests a common mode of action (HDAC inhibition) of both compounds. The analysis of potential transcription factor binding sites in the regulated PS for each compound showed >90 % overlap

(not shown) and further confirmed a similarity of the MoA. As TSA is the more specific drug, we focused further work strongly on this compound.

As we aimed to explore whether we indeed induce a wrong differentiation track with long treatments, but not with short treatments, we next compared the differentially expressed PS that are induced by short, medium, and long treatment with TSA. Comparison of the PS affected by different exposure periods of TSA showed that the overlap was only very small (1–13 %). An important implication of this is that the data obtained after 6 days of exposure did not reflect the initial/direct response to drug exposure (Fig. 5.1.3d, Fig. 5.1.S6). In addition, the data showed that the final outcome of such toxicogenomics experiments in a developing cell system depended to an astonishingly high degree on the time point of analysis (e.g., T4d vs T6d). To obtain an overview of the biological implications of the drug-induced transcriptome changes, we used two levels of data clustering. First, oGOs were determined among the up- and down-regulated PS. Then, the oGOs were binned according to related biological processes, such as 'apoptosis' or 'metabolism' (Waldmann *et al.* 2014). From this, a clear picture emerged: the down-regulated genes for T6d mainly reflect down-regulation of neuronal pathways and general development. This fully corroborated the neurodevelopmental toxicity character of the model. The up-regulated genes strongly indicated differentiation to non-neuronal lineages (Fig. 5.1.3e, Tab. S3). Therefore, we conclude that long- but not short-term treatment indeed changes the gene expression pattern toward a wrong (non neuronal) differentiation track.

The divergence from neuronal differentiation to non-neuronal lineages (according to oGOs) developed very strongly between T4d and T6d, i.e., during the time, when drug treatment was not important anymore for neurodevelopmental marker expression. From this and from our initial experiments (Figs. 5.1.1, 5.1.2), we concluded that overall transcriptome changes should be similar for T6d treatment and a medium drug pulse of 4-day exposure followed by a 2-day washout (MP).

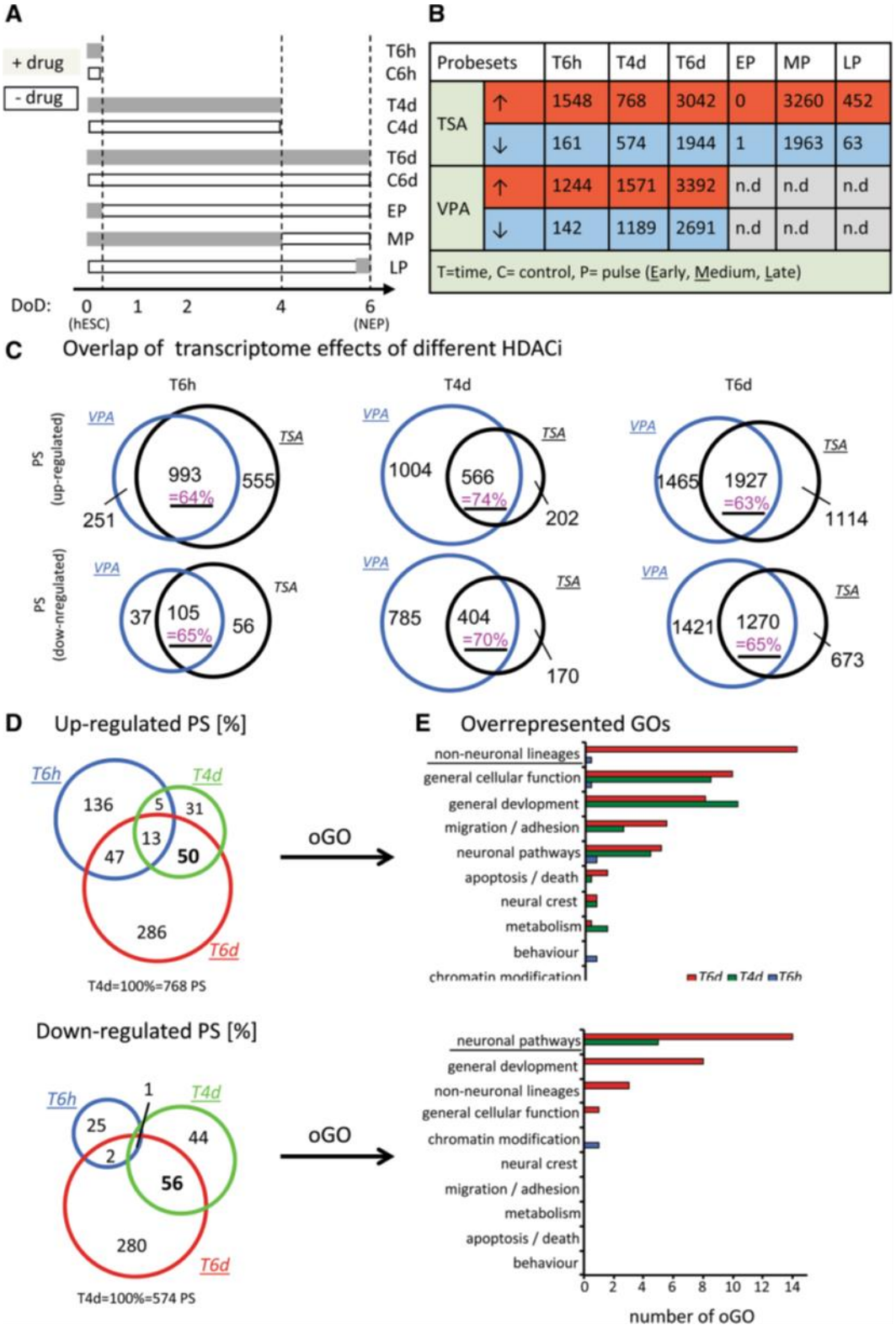

Fig. 5.1.3: Transcriptome analysis after different treatments with TSA and VPA. (**A**) Overview of the different exposure scenarios during differentiation. Bars indicate the duration of differentiation before samples were taken, and gray shading indicates the period of drug exposure within that time. (**B**) Differentiating cells were treated as indicated in **A**; mRNA was prepared and analyzed by Affymetric DNA microarrays. The numbers of probe sets (PS) regulated upwards (red) or downwards (blue) in the presence of TSA (10 nM) or VPA (600 µM) are given in the table. (**C**) Venn diagrams display absolute numbers of regulated PS ($p < 0.05$, FC > 1.5 or FC < 0.67) induced by TSA, VPA, or both during the indicated treatment periods. The percentage of overlap of the drug treatments is indicated in purple. (**D**) Venn diagrams display

PS altered by TSA treatment ($p < 0.05$, FC > 1.5 or FC < 0.67) for different time periods. The numbers in the sectors are given as percentages of the number at T4d (absolute numbers are in supplements). (**E**) Overrepresented gene ontology terms (oGOs) were determined from the regulated PS indicated in D. Individual oGOs were classified by their assigned to superordinate cell biological processes, and the number of oGO for each of these (e.g., migration or neuronal pathways) is displayed. Complete data sets on regulated PS, oGO, and superordinate biological processes are given in Tables S2 and S3

Transcriptome changes gain independence of drug presence after 4 days

We addressed the question of continued transcriptome effects in the absence of drugs by comparing T6d and MP (Tab. S2). The regulated PS showed a very high overlap of 80–87 % between MP and T6d (Fig. 5.1.4a, Fig. 5.1.S7). The oGOs among up-regulated PS pointed to the differentiation of several other cellular lineages (Fig. 5.1.4b, Tab. S4), such as the cardiovascular system, neural crest, skeletal system, and glands. Moreover, there was a high overlap of oGOs among T6d PS and the T6d/MP overlap PS (Fig. 5.1.4b). The higher GO enrichment among the latter set of genes was most likely due to the lower percentage of non-specific genes, eliminated through the overlap filter. The commonly down-regulated PS gave overwhelming evidence of disturbed neurodifferentiation (according to oGOs) (Fig. 5.1.4c, Tab. S4). We wondered whether the biological response to the drugs could have been predicted already on day 4. At this time (T4d), the majority [64 % (up)/55 % (down)] of TSA-regulated PS was the same as found after 6 days (Fig. 5.1.S7A). The PS of T4d that overlapped with T6d and MP pointed already to disturbed differentiation: the oGOs among these down-regulated PS indicated a defect in forebrain development (Fig. 5.1.S7B) and the up-regulated PS pointed again to an increase in unwanted differentiation tracks (Tab. S4). In summary, drug treatment for 4 days was sufficient to trigger the definite deviation from the normal differentiation path. From this point on, differentiation of wrong lineages most likely contributed to further increases in transcriptome changes (compared to control cells). This wrong differentiation track continued to deviate more and more from control cells, also in the absence of the drugs.

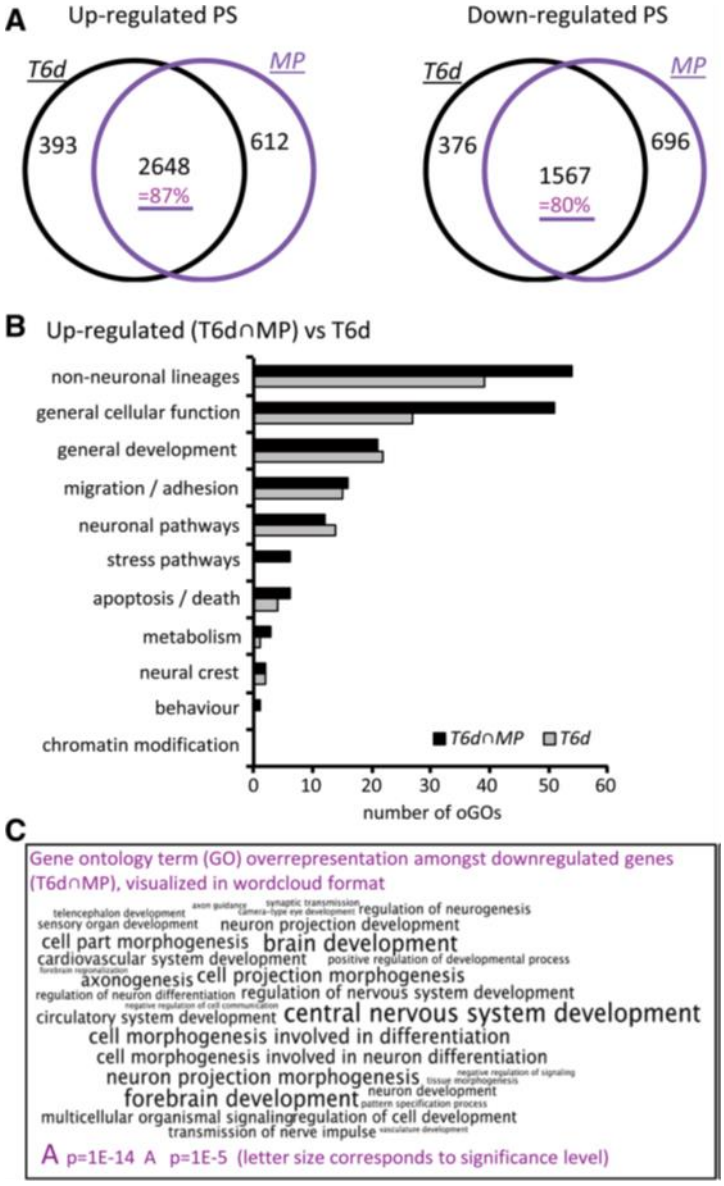

Fig. 5.1.4: Concordance of transcript changes after continued treatment or drug washout on DoD4. (**A**) Cells were differentiated in the presence of TSA for 6 days (T6d) or for 4 days followed by a drug washout period of 2 days (medium pulse, MP) and analyzed by Affymetrix DNA microarrays. The absolute numbers of up- and down-regulated PS are indicated in Venn diagrams. The percentage of overlap is indicated in purple. (**B**) The oGOs were determined from the up-regulated PS of T6D treatment as well as from the overlap of T6D with MP (T6d ∩ MP). The oGOs were further classified into superordinate cell biological processes, and the numbers in these categories are displayed. For full information on regulated PS, oGO, and superordinate biological processes, see Tables S2 and S4. (**C**) Significantly downregulated PS were determined for T6d ∩ MP. GOs overrepresented among the PS down-regulated are displayed as word cloud. The character size is scaled according to the *p* value of the corresponding GO

Comparison of continued drug exposure and short exposure of NEP

The independence of the transcriptome response from the presence of drugs suggested that the transcriptome changes did not inform on direct drug signaling. To address how the cells would react to short drug exposure, we generated NEP and exposed them to TSA

only during the last 6 or 24 h of the 6-day differentiation. This treatment caused a pronounced increase in histone acetylation and tubulin acetylation (about fivefold to eightfold, $p < 0.05$) (Fig. 5.1.5a). These results showed that HDACi could trigger the expected biochemical response (acetylation) in NEP acutely exposed to the drugs. This effect was similar in size as the one in cells pulsed with drug during the first 6 h of differentiation (Fig. 5.1.1d). A further similarity was that also the late drug pulse (LP) triggered a pronounced transcriptome response within 6 h. However, the regulated PS differed strongly from those of the T6d data set (Fig. 5.1.5b). Only 7 % of the up-regulated T6d PS and only 1 % of the down-regulated ones were contained in LP (Fig. 5.1.5b). It may be argued that T6d contains two types of regulated genes: PS altered because of an overall altered differentiation track and PS altered because of the continued presence of the drug. The latter set of genes may be termed 'affected by continued drug presence after long-term exposure.' To get information on this set of genes, we subtracted the MP (washout) PS from the T6d PS. This left 393 up-regulated PS and 376 down-regulated PS. Even this subset of genes (that should in theory be enriched for PS affected by the presence of TSA) overlapped only 8 % (up) or 1 % (down) with the LP PS (Fig. 5.1.5c). These findings only corroborated our earlier conclusion that the PS of T6d or MP hardly reflected any direct responses to drug exposure.

The direct drug response (LP), related to the change in acetylation, was further characterized by analysis of GO overrepresentation. This pointed to the biological processes of 'ion homeostasis' and 'phospholipase C signaling,' and they differed strongly from the long-term response (Fig. 5.1.5d, Tab. S3).

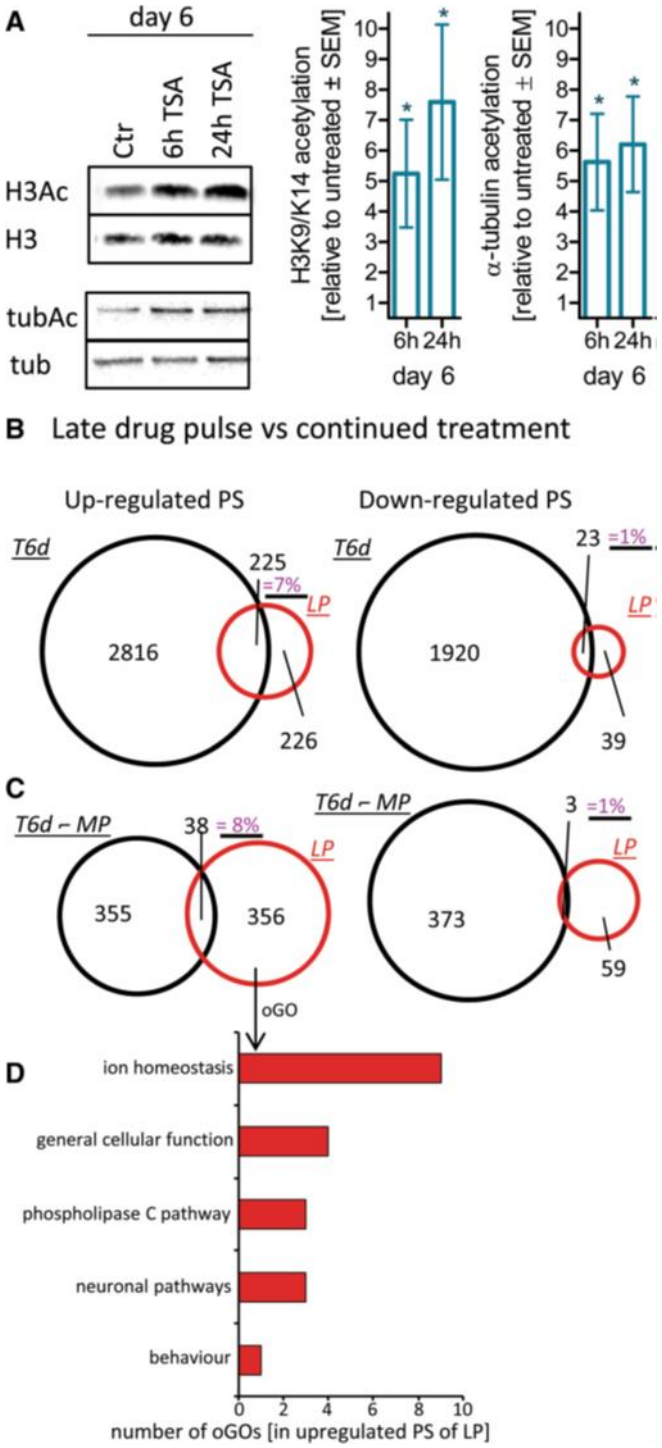

Fig. 5.1.5: Comparison of the acute and chronic (long-term treatment) effects of TSA. (**A**) Cells (hESC) were differentiated for 6 days to NEP, and TSA (10 nM) was added only during the last 6 h or 24 h. Then, protein acetylation was determined by Western blot as in Fig. 5.1.1. Data are mean ± SEM of three experiments. *p < 0.05. (**B**) Venn diagrams display the number of PS altered by drug treatment (p < 0.05, FC > 1.5 or FC < 0.67) after continuous (T6d, black circle) exposure, or after late, pulsed (LP) treatment (last 6 h of the 6-day differentiation, red circles). (**C**) Venn diagrams compare PS triggered by a late drug pulse (LP, red circles) with PS regulated by continuous drug exposure, but not found under MP washout conditions (T6d without—MP, black circles). The percentage of overlap is indicated in purple. (**D**) The GOs overrepresented among up-regulated PS of LP incubations were classified into superordinate cell biological processes (full information on regulated PS, oGO, and superordinate biological processes: Tables S2 and S4)

Differences and similarities of transcriptome changes associated with early direct drug response versus continued long exposure

We explored whether the immediate drug response to TSA at the beginning of the experiment (differentiating hESC exposed during the first 6 h = T6h) was sufficiently predicting T6d. Analysis of oGO among T6h up-regulated PS pointed to altered signaling/nerve activity, and developmental GOs were not overrepresented at all among up-regulated PS (in contrast to T6d). The PS down-regulated by TSA were indicative of one major underlying biological process: Six of the 13 oGOs were related to chromatin modification and 7 to acetylation (Fig. 5.1.6a, Tab. S3). A similar response was observed for VPA (Fig. 5.1.S8), and these findings are well consistent with major changes in histone acetylation. Both HDACi affected genes related to chromatin modification, such as ING5, KAT5 (histone acetylation), and several PHF genes (involved in chromatin remodeling and transcriptional regulation). Thus, one primary effect of VPA and TSA was alteration of genes involved in chromatin structure (Fig. 5.1.6a, Fig. 5.1.S8). Such epigenetic mechanisms triggered early by HDACi, and fixed by longer presence of the drugs, could initialize the massive changes observed later after prolonged drug treatment.

A direct comparison of the T6h and T6d transcriptome changes showed that 70 % of the PS up-regulated early were not up-regulated late (T6d) (Fig. 5.1.6b), and 90 % of PS down-regulated early were not down-regulated late. These findings were similar for TSA and VPA (Fig. 5.1.S9). Only 13 of 303 oGOs among up-regulated T6d genes ($p < 0.05$) overlapped with oGOs from up-regulated T6h genes (Fig. 5.1.S10). These data indicate very clearly that the early drug response predicted the overall outcome after 6 days only poorly, and vice versa the primary effects of TSA may not be identifiable from measurements at late time points.

However, there were at least some similarities of the responses: 463 PS overlapped for TSA responses after 6 h and 6 days (Fig. 5.1.6b). All oGOs among them pointed to altered signaling events, mainly related to phospholipase C (Fig. 5.1.6c, Tab. S4) as possibly common response feature. To narrow down the common drug responses to effects specific for HDACi, we extracted PS that were regulated by both TSA and VPA and at both time points (Fig. 5.1.S9A). Eleven GOs were overrepresented among these PS (Fig. 5.1.S9B), with 7 of them referring to phospholipase C regulation. They involved, e.g., EGFR, KIT, PDFGRA, and EDNRA. The other four oGOs referred either to neural crest (NC) or to their

guidance and migration (comprising TWIST1, SOX10, SNAI2, and SEMA3C) (Zimmer *et al.* 2012). Thus, the PS up-regulated by HDACi both early and late suggested that NC is one of the cell lineages that was erroneously generated in our model when differentiation was disturbed by drugs.

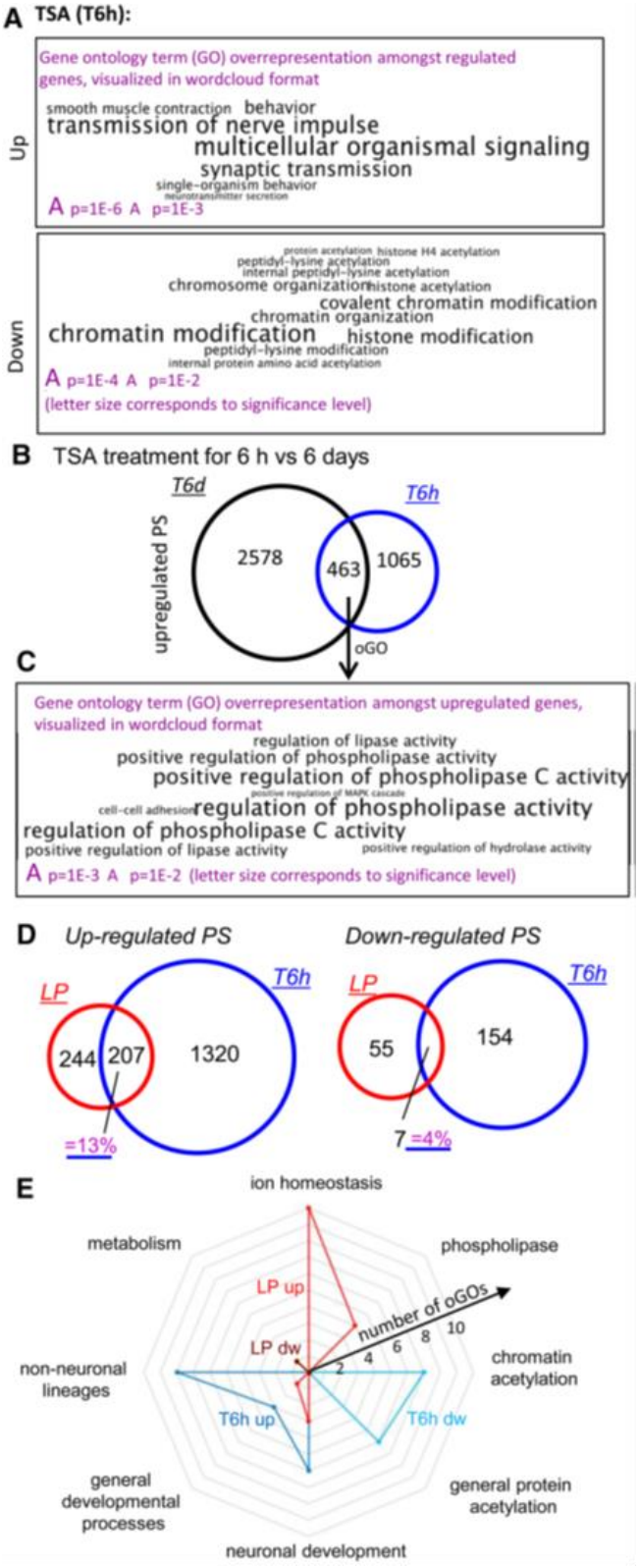

Fig. 5.1.6: Differences of acute effects of TSA either early or late during NEP differentiation. (**A**) Overrepresented GOs were determined from significantly up- (upper panel) and down-regulated (lower panel) PS from T6h samples. They were displayed as word clouds with character size scaling according to the p value of the corresponding GO. For full information, see Table S2 and S3. (**B**) Venn diagrams compare numbers of up-regulated PS of long-term (T6d, black circle) and early short-term (T6h, blue circle) treatment with TSA. (**C**) GOs overrepresented among the PS of the overlap shown in **B** are displayed as a word cloud. (**D**) Venn diagrams compare numbers of regulated PS of short-term TSA treatments at early (T6h, blue circle) and late (LP, red circle) time points. The percentage of overlap is displayed in purple (**E**) The oGOs determined from significantly up-regulated (blue) or down-regulated (red) PS of the LP and T6h incubations were assigned to superordinate cell biological processes. These were then used as axes on a radar plot, with the distance from the center indicating the number of oGO on each axis. For full information on regulated PS, oGO, and superordinate biological processes, see Tables S2 and S3

Dependence of immediate transcriptome responses to HDACi on the developmental stage

The above findings suggest that longer exposure is not suitable for defining the mode of action of drugs. Some literature data suggest that short drug pulses of few hours may be more suited (Jergil *et al.* 2011, Theunissen *et al.* 2012). However, this raises the question, when such short-term exposure should be performed. A developing biological system does not only consist of one defined cell type, but it rather reflects all biological stages between the starting point and the final population. On this basis, we hypothesized that the 'cellular' response, i.e., short-term transcriptome alterations would strongly depend on the time point of measurement, i.e., on the differentiation stage. To test this, we compared the responses to 6-h TSA treatment of cells at the early stage of differentiation (T6h) and at the final stage (LP). The down-regulated PS of the two conditions showed hardly any overlap at all. For the up-regulated PS, 13 % of the T6h PS were also found in LP and 46 % of the PS of LP were found in T6h (Fig. 5.1.6d). GOs overrepresented in commonly up-regulated PS referred only to regulation of phospholipase activity. Besides this hint toward signal transduction being affected in both cases, there was little further indication of common functional effects. On the contrary, the representation of superordinate biological processes by the oGOs was largely divergent between the two 6-h pulse experiments (Fig. 5.1.6e, Tab. S3). We conclude from this that typical HDACi target genes that inform on the mode of action do not exist as such. They depended to a very high degree on the experimental setup, the time point of measurement, as shown here, and they also depended to a high extent on the length of exposure, as shown in the above paragraphs.

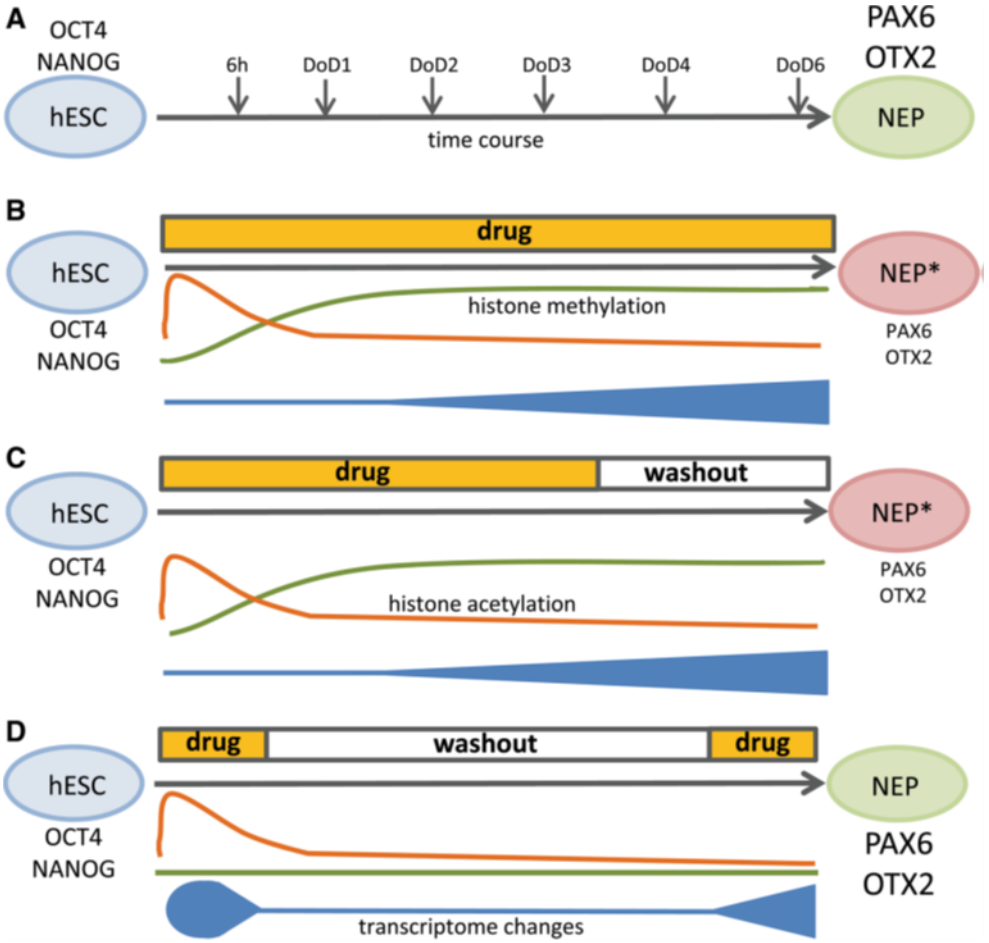

Fig. 5.1.7: Summary. (**A**) Neuroepithelial precursors (NEP) were generated from hESC within 6 days of differentiation (DoD). Main cell type markers are indicated. (**B**) Continuous drug treatment led to an altered NEP differentiation (NEP*) as indicated by transcriptome changes (blue), reduced marker expression (PAX6, OTX2), and permanent changes in histone methylation (after 2–3 days) at the promoters of the markers. Acetylation changes were only transient. (**C**) Drug exposure for 4 days resulted in the same disturbed NEP differentiation as continued drug exposure. The number of altered PS and the alterations of histone methylation were not affected by drug washout. (**D**) Short-term drug treatment induced a strong, but fully reversible change in gene expression. Methylation of marker promoters was not altered, and marker expression was normal. The transition of transient drug-induced gene expression and histone acetylation changes to a permanently altered transcriptome and NEP differentiation correlated with the permanence of promoter histone methylations.

4.1.5. Discussion

Transcriptomics studies have been instrumental for characterizing the development of model organisms, the human brain, or various stem cells (Kang *et al.* 2011, Mariani *et al.* 2012, Xie *et al.* 2013, Yang *et al.* 2013). Most available data refer to fixed time points, but some studies already showed the highly dynamic behavior of such systems (Zimmer *et al.* 2011, Theunissen *et al.* 2012). An additional layer of complexity is added, when experimental disturbances are studied in systems that change over time. A stressor that

switches a static system from one state to another one would be expected to shift such a dynamic system from one developmental track (dynamic series of changes) to another. Second and third levels of additional complexity are added, if the type and extent of such shifts depend on the length of exposure and on the time point of exposure relative to the normal differentiation track. Although the understanding of the temporal evolution of a developing biological model system under stress is essential in toxicology and pathophysiology, we are not aware of any study that has addressed this issue in a quantitative and systems-wide way. Three major conclusions from our study can form a basis for further exploration of this field:

First, it became clear that the usual (long-term exposure) toxicogenomics data recorded from developing stem cells describe to a large extent the cellular phenotypic changes and only to a small extent the direct drug action as such. Second, drug actions in a dynamic stem cell system can be fully reversible, even when the expression of hundreds of genes has been changed. However, at a certain point, permanent and persistent changes are triggered that can become independent of the continued presence of drug. We found that chromatin alterations in particular histone methylation could act as persistence detector or irreversibility switch. Third, even the short-term immediate effects on the transcriptome depended on the time point of drugs application. This apparently trivial finding, considering the dynamic behavior of a differentiation system, has important implications for future systems toxicology studies: Exposures at multiple times need to be performed in order to obtain data that sufficiently describe drug effects and responses of the cells.

Do transcriptomics data reveal the mechanisms by which a compound interferes with neural development? (Theunissen *et al.* 2012). Our data suggest unambiguously that final changes in the transcriptome at the end of the differentiation period mainly define the cellular phenotype. This is supported by the following six lines of evidence. (a) Primary drug responses to HDACi are dominated by up-regulated genes (Berger 2007). The chromatin opening due to acetylation may be enhanced and then stabilized by increased H3K4me3 (Nightingale *et al.* 2007). We find here equal numbers of up- and down-regulated PS for the T6d condition. This corroborates findings in the literature (Theunissen *et al.* 2012, Krug *et al.* 2013) and suggests that indirect responses play a large role after longer (>6 h) incubation periods. (b) The primary biochemical drug response (acetylation) was not detectable after prolonged exposure. Thus, it is unlikely that the transcriptome response at late time points was triggered by a direct response to HDACi. (c) The

long-term (T6d) response differed considerably from the acute response at the same time (LP). About 95 % of the T6d PS were not predicted by the LP direct drug response data. (d) The transcriptome response after a 2-day washout of the drugs (MP) was very similar to the response without washout (T6d). This makes it very unlikely that a direct drug response was measured at T6d. (e) Moreover, it should be assumed that the transcriptome response data should be to some degree independent of the experimental system, if they would characterize the MoA of drugs. However, we observed that closely related hESC-based systems showed very different responses to VPA (Krug *et al.* 2013) and apparent HDACi consensus genes (Jergil *et al.* 2009, Jergil *et al.* 2011) defined in murine cells by overlapping responses of different drugs were not regulated in our cells. In summary, this corroborates our hypothesis that transcriptome data from disturbed developmental systems reflect mainly an altered phenotype and that information on direct drug effects requires short drug treatments of up to 6 h. (f) When the overlap of drug-affected 'toxicant-response' genes (T-genes) and developmentally regulated gene (D-gene) clusters was examined, we found that 90 % of the genes regulated late during differentiation were affected by HDACi. This high percentage of overlap is hard to explain by primary drug action; in particular as TSA acted early, and the changes occurring between day 4 and day 6 did not even require the presence of the drug. Instead, the observation is plausible, if it is assumed that the drugs changed the overall development, and therefore nearly all later phase D-genes were affected. Thus, the apparently specific effects of HDACi on neurodevelopment may be mainly due to the fact that the system studied was based on neurodevelopment. One may then hypothesize that HDACi may preferentially target cardiac genes in a cardiac development model. Such findings have indeed been obtained from differentiating mESC. VPA affected their neural development upon neurodifferentiation and cardiac development upon cardiac differentiation (Theunissen *et al.* 2013).

The effects of a toxicant may depend not only on the time point of measurement, but also on the duration of exposure. Some developmental toxicity responses may require the activation of a 'persistence detector' to distinguish between short reversible interactions on the one hand and toxicity on the other hand (Lim *et al.* 2013). For instance, epigenetic changes have been suggested as persistence switches for ethanol sensitization (Qiang *et al.* 2011, Botia *et al.* 2012). An altered state of cells is also fixed by so-called 'gateway drugs.' These are compounds allowing the later action of other drugs, even when they

have been washed out for a long time. This is particularly important in the field of addiction, and the mode of action has also been explained by histone modifications (Levine *et al.* 2011).

Molecular persistence mechanisms are of high importance in the field of developmental toxicity, in which compounds might show effects years after the exposure has taken place (Kadereit *et al.* 2012). Evidence is emerging that altered behavior and late-onset disorders that are triggered early in life are associated with epigenetic alterations (Weaver *et al.* 2004, Rudenko *et al.* 2014). Early developmental exposure to toxicants could result in an accumulation of epigenetic changes that, when reaching a certain threshold, result in transcriptome alterations associated with adverse health effects. There are several examples for toxicants or stressors that can trigger diseases in later life when exposure takes place in utero or childhood or that can even trigger trans-generational effects (McGowan *et al.* 2009). Early exposure to lead has, for example, been associated with Alzheimer's disease (Wu *et al.* 2008).

The model system chosen here was based on the known neurodevelopmental disturbances of HDACi and the associated transcriptome responses (Fig. 5.1.7a, b). We used this as a test case to study time-dependent transcriptome responses. A short pulse of TSA (EP) triggered a strong transcriptional response that was fully reversible, while a longer exposure (MP) triggered a persistent effect, even after discontinuation of drug exposure. The transient response correlated well with acetylation. The persistent response did not correlate with histone acetylation, but rather with a shift of the histone methylation ratio (Fig. 5.1.7c, d). This shift required more time and was specific for the gene studied. For instance, OTX2 was affected earlier than PAX6, and the direction of methylation changes in the OCT4 promoter (Balmer *et al.* 2012) was opposite to the one described here for PAX6. Histone methylations are well suited for deciding on cell fate and long-term regulations, as they can favor transcription (H3K4me) or attenuate transcription (H3K27me), depending on the site of modification. Histone methylations do not usually change globally (i.e., their overall cellular level remains constant), but the pattern of the different methylases and demethylases can change dramatically during early neural differentiation (Weng *et al.* 2012), and individual promoters are affected in a highly specific manner. In particular, the ratio of promoter H3K4/ H3K27 trimethylation has been shown to reflect the phenotypic plasticity of stem cells during neural fate decision. Changes in this ratio at

promoters of genes associated with neural differentiation frequently precede the changes in gene expression (Burney *et al.* 2013).

If it is assumed that cells can react reversibly to short stimuli, as shown here, and that the duration of exposure plays a role for the overall outcome, then a mechanism functioning as drug persistence detector is required. The easiest way of imagining such a mechanism could be a superordinate regulator of a wrong pathway (e.g., a neural crest organizer) whose promoter chromatin structure functions as Boolean AND element being switched by acetylation *plus* a second alteration that takes more time in response to drug exposure. Short drug exposure would only trigger acetylation and thus not be sufficient for activation/ switching. Longer exposure would still allow for acetylation and now also for the second change. Together, they would lead to activation of the superordinate regulator, and the activation state would be fixed by the histone methylation pattern. At present, this is a speculative hypothesis just intended to give an idea how underlying regulations may be imagined; the model system chosen may be too complex to provide causal evidence for such a mechanism with the technology presently available. Further studies will require considerable technical optimizations. ChIP can easily be accommodated to a whole genome level by applying sequencing instead of PCR as endpoint. Yet, the real issue lies in the quantification across several independent experiments with human stem cells, and the handling of the type of information resulting from this. Quantitative detection of compound-induced histone changes requires a high level of robustness and sensitivity of the method, and this is much harder to achieve for ChIP than for methods such as PCR, DNA microarray, or Western blot. Already in the present study, considerable method optimization was required to obtain reproducible and statistically significant data on the chromatin changes taking place at few selected marker genes.

The acute responses to HDACi differed significantly from the response to continued treatment. More importantly, they differed also from one another. No matter whether the experiment was performed at the beginning or toward the end of differentiation, a vastly larger number of genes were up-regulated than down-regulated (as expected of HDACi). But different genes were affected. The 6-h time point has been found to be optimal in previous studies, e.g., on stem cells (Jergil *et al.* 2011) or a large number of human tumors (Cohen *et al.* 2011) to record direct drug effects. We conclude that the direct drug effect was different at distinct times of differentiation. This corroborates earlier findings of VPA acute cytotoxicity being highly dependent on the developmental stage (Fujiki *et al.* 2013).

Taken together, these findings imply that a potential mode of action of a developmental toxicant is not an intrinsic drug property, but it is a combined feature of the experimental system and the chemical used. In this respect, developmental toxicity may differ from other fields. Its testing may therefore require a battery of parallel tests and particularly complex systems toxicology approaches (Hermsen *et al.* 2013, Tonk *et al.* 2013) relative to more acute forms of toxicity. It needs to be established whether approaches, as in the ToxCast program (Sipes *et al.* 2011, Sipes *et al.* 2013), that rely mainly on hundreds of simple assays for biochemical/cellular targets can help to substitute or to complement the complex differentiation models used in a test battery (Piersma *et al.* 2013).

Our study has major implications for the design and interpretation of toxicogenomics data in development. We found that classical transcriptome data from a disturbed/ stressed differentiation model strongly reflect the altered phenotype. In the case of HDACi, the phenotype contribution is >90 %. This number may be smaller or larger for other stressors, but it will most likely always be sizeable. The question arises what this transcriptome information can be used for, if it does not inform on the mode of action of a chemical. We assume that different types of stressors result in different developmental disturbances and therefore also different transcriptome patterns ((Balmer *et al.* 2012, Krug *et al.* 2013). Thus, the information will be useful for compound classification, differentiation, and possibly potency ranking (Schulpen *et al.* 2014). Beyond this, there is a further dimension of information contained in the transcriptome data. If they are largely independent of direct compound effects, then they constitute a comprehensive phenotypic description of the culture state. In the classical toxicological literature, it has always been assumed that transcriptome endpoints require phenotypic anchoring to other types of endpoints (Paules 2003, Waters *et al.* 2004). Our data suggest now that the comprehensive transcriptome data can be a phenotypic anchor as such. Transcriptome data may be more comprehensive and robust than classical endpoints (such as immunostains). It appears worthwhile to develop quantification tools that indicate, on the basis of the transcriptome as phenotypic descriptor, how big a developmental insult is, and that allow the ranking of unknown drugs, or of different concentrations or exposure times of one given drug (Waldmann *et al.* 2014).

4.1.6. Acknowledgements

We thank M. Kapitza and B. Schimmelpfennig for excellent technical support. This work was supported by Grants from the German Research Foundation (RTG 1331, KoRS-CB), the BMBF SysDT and the European Commission's ESNATS project.

4.1.7. Conflict of interests

The authors declare that they have no conflict of interest.

4.1.8. Supplements

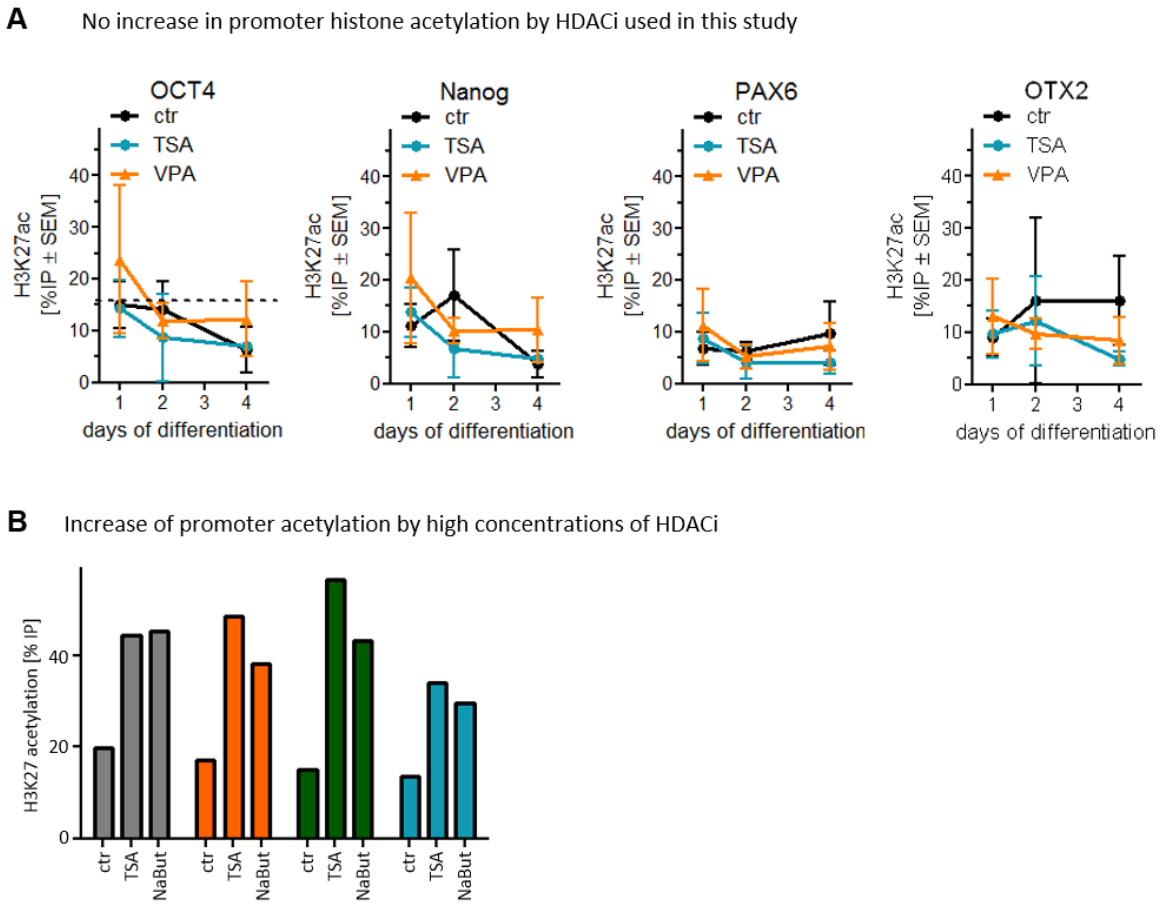

Fig. 5.1.S1: Experimental controls for histone acetylation analysis

Chromatin immunoprecipitation (ChIP) of H3K27 acetylation at marker gene promoters. (**A**) Histone acetylation at promoters of indicated marker genes for neural differentiation. ChIP was performed with antibodies specific for H3K27ac on samples differentiated in presence or absence of trichostatin A (TSA) and valproic acid (VPA) for indicated time periods. The amount of DNA from the promoter region of indicated genes was quantified by qPCR and compared to control precipitates to obtain enrichment factors (EF) of the chromatin mark which is displayed as % of IP from at least 3 independent experiments. (**B**) ChIP on samples treated for the first 6 h of differentiation with 50 nM TSA (normally

10 nM TSA were used), or a combination of 10 mM sodiumbutyrate and 10 mM nicotinamide and subsequently lysed. These samples are used as positive control for the antibody against H3K27ac, as the high concentrations of HDAC inhibitors should result in an increase of histone acetylation, which can also be seen compared to the control at every investigated promoter.

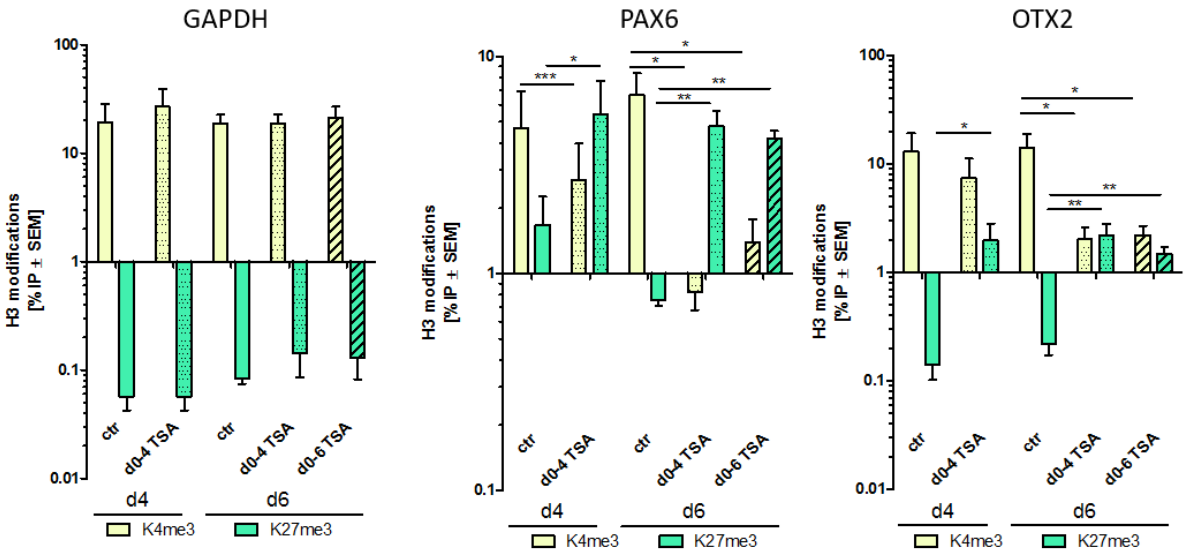

Fig. 5.1.S2: Details on histone methylation changes as basis for Fig. 5.1.1E

Chromatin immunoprecipitation (ChIP) was performed with antibodies specific for H3K4me3 or H3K27me3 on samples differentiated in presence or absence of TSA at indicated time periods. The amount of DNA from the promoter region of indicated genes was quantified by qPCR and compared to control precipitates to obtain enrichment factors (EF) given as % IP for the two histone marks. Data are means ± SEM of 3 experiments. Statistical analysis was done by repeated measured ANOVA followed by Tukey's multiple comparison test *p<0.05 **p<0.01 ***p<0.01 vs. control at respective days.

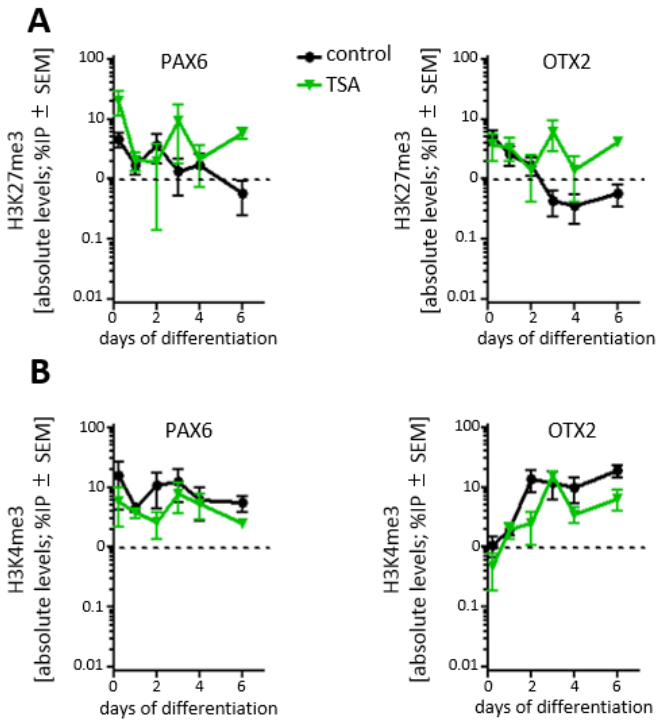

Fig. 5.1.S3: Details on histone methylation changes as basis for Fig. 5.1.2A
Chromatin immunoprecipitation (ChIP) was performed with antibodies specific for H3K4me3 or H3K27me3 on samples differentiated in presence or absence of TSA at indicated time periods. The amount of DNA from the promoter region of indicated genes was quantified by qPCR and compared to control precipitates to obtain enrichment factors (EF) given as % IP for the two histone marks. Data are means ± SEM of 3 experiments. Statistical analysis was done by repeated measured ANOVA followed by Tukey's multiple comparison test *p<0.05 **p<0.01 ***p<0.01 vs. control at respective days.

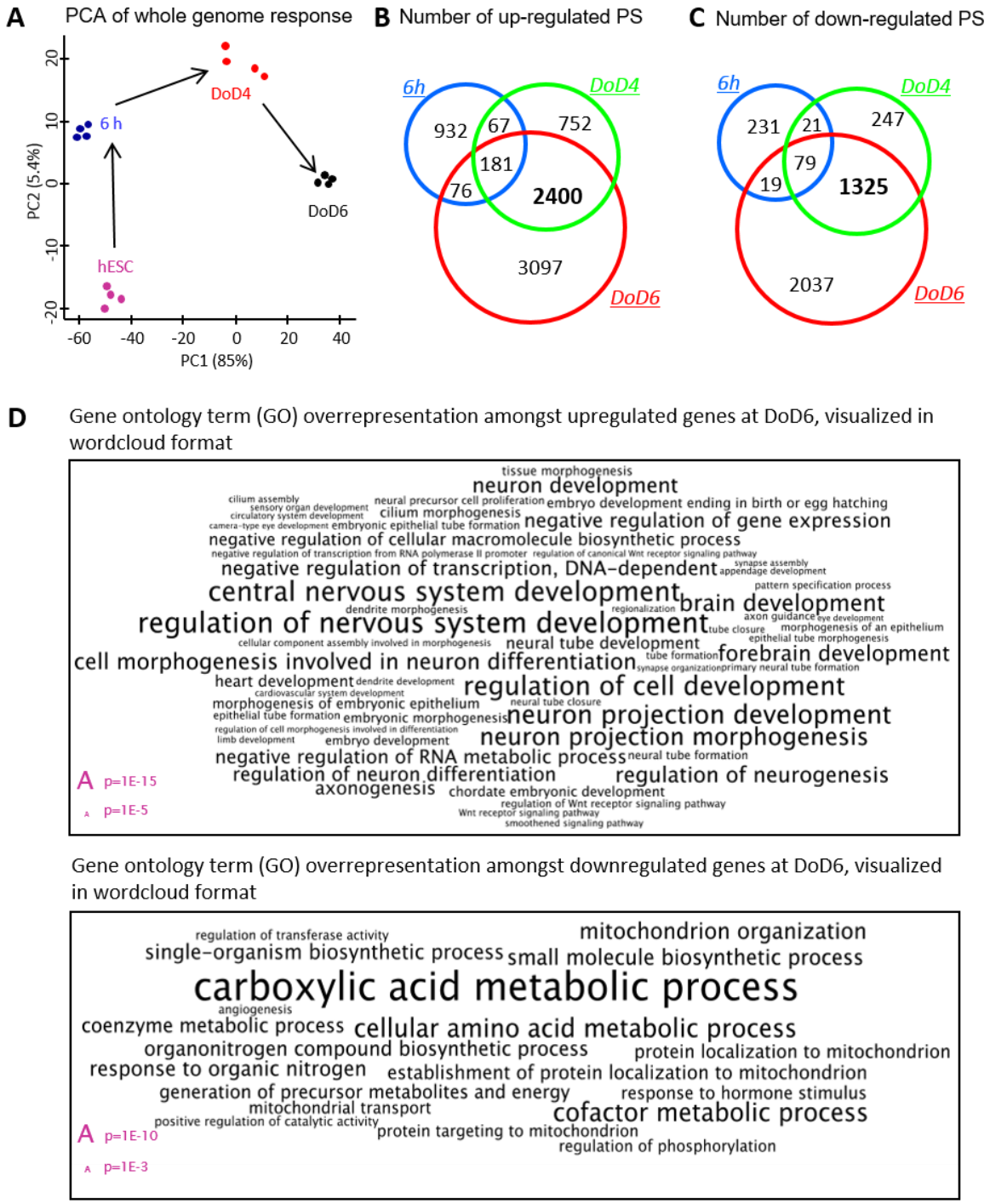

Fig. 5.1.S4: Transcriptome changes during early neuroectodermal differentiation

(**A**) Two-dimensional representation of principal component (PC) analysis of all data sets. (**B**) Comparison of expression changes of up-regulated PS over time. Venn diagrams were constructed for regulated PS (p<0.01, FC>1.5 or FC<0.67). The numbers in the sectors represent absolute numbers. (**C**) Comparison of expression changes of down-regulated PS over time. Venn diagrams were constructed for regulated PS (p<0.01, FC>1.5 or FC<0.67). The numbers in the sectors represent absolute numbers. (**D**) Overrepresented gene onthologies (GOs) amongst up- and down-regulated PS at DoD6. The character size in the word clouds is relative to the p-value of the corresponding GO (legends in purple).

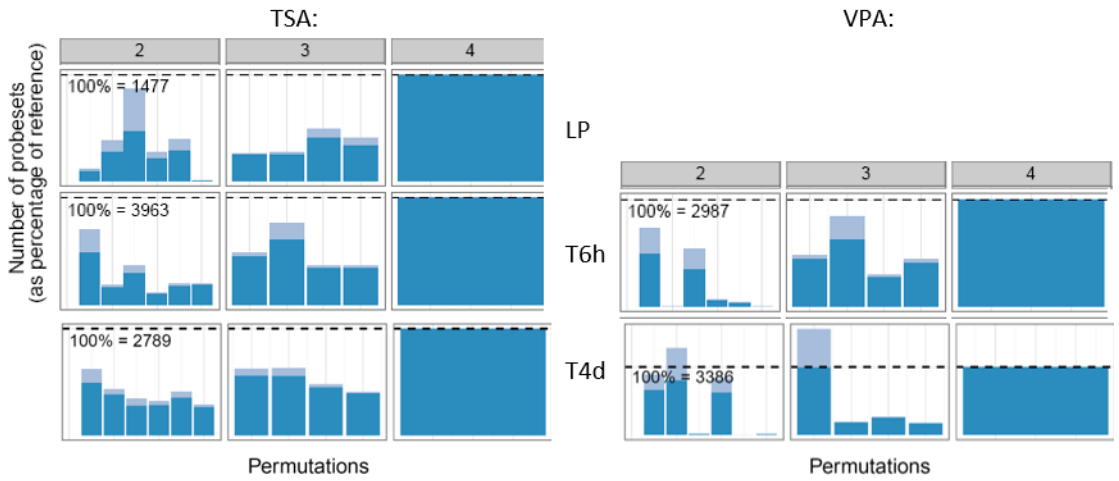

Fig. 5.1.S5: Quality controls of whole genome transcript profiles

Permutation analysis to control for potential outliers and microarray homogeneity. Permutation analysis of samples incubated for short time and possibly showing heterogeneity. The numbers of significantly altered PS given as 100% are higher than in our normal analysis (see Fig. 5.1.2) as no cut-off was set for fold change of regulation. Using all 4 arrays for analysis is set to 100% of significantly regulated PS. Panel 3 shows the number of regulated PS with all 3 possible combinations of leaving 1 array out. Panel 2 shows the number of regulated PS with all 6 possible combinations of leaving 2 arrays out. The analysis shows no outlier in these critical treatment periods.

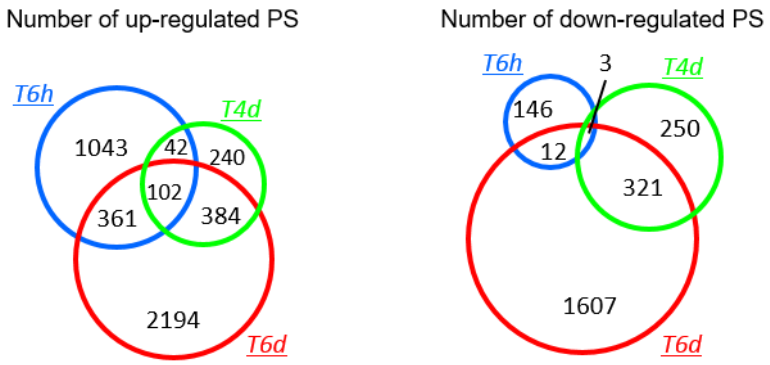

Fig. 5.1.S6: PS regulated by TSA treatment

Venn diagrams displaying actual numbers of PS corresponding to Fig. 5.1.3D. hESC were differentiated to NEP and treated and lysed with TSA for the indicated time periods and lysed at DoD6 (T6d), DoD4 (T4d) and after 6 h of induction of differentiation (T6h). The amount of commonly up- and down-regulated PS by TSA treatment performed on regulated PS at indicated time points are displayed as venn diagrams corresponding to Fig. 5.1.3D.

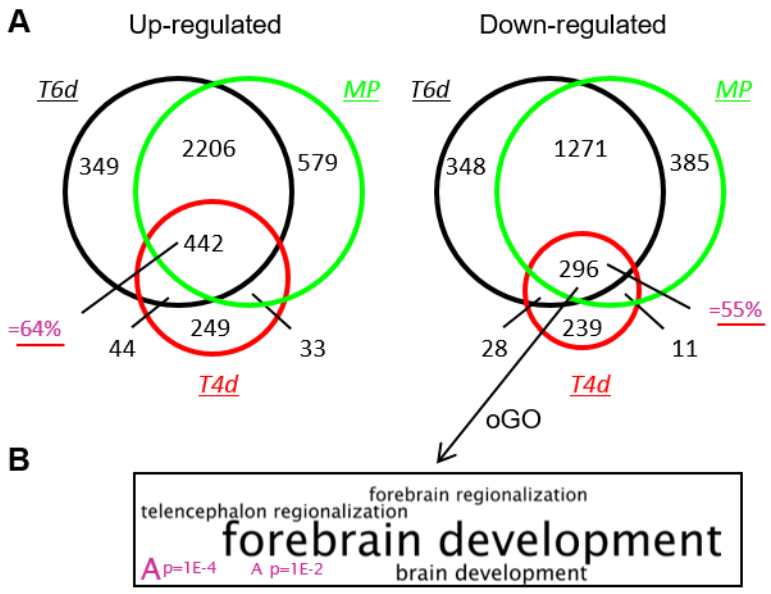

Fig. 5.1.S7: Overlap of 4 day (T4d) treatment and 6 day treatment with (MP) or without (T6d) washout

(**A**) Cells were differentiated in presence or absence of TSA for 6 days (T6d) or for 4 days followed by a period of 2 days in absence of the drug (MP) or for 4 days only (T4d). Cells were lysed and genome wide expression profiles were prepared at DoD6 (T6d and MP) or DoD4 (T4d). The numbers of up- regulated (left panel) or down-regulated (right panel) PS is given relative to untreated control. (**B**) Overrepresented gene ontology terms (GOs) of genes commonly down-regulated by T6d, MP and T4d are displayed as word clouds. The character size corresponds to the p-value. See Tab. S3 for GOs of PS up-regulated by T6d and MP.

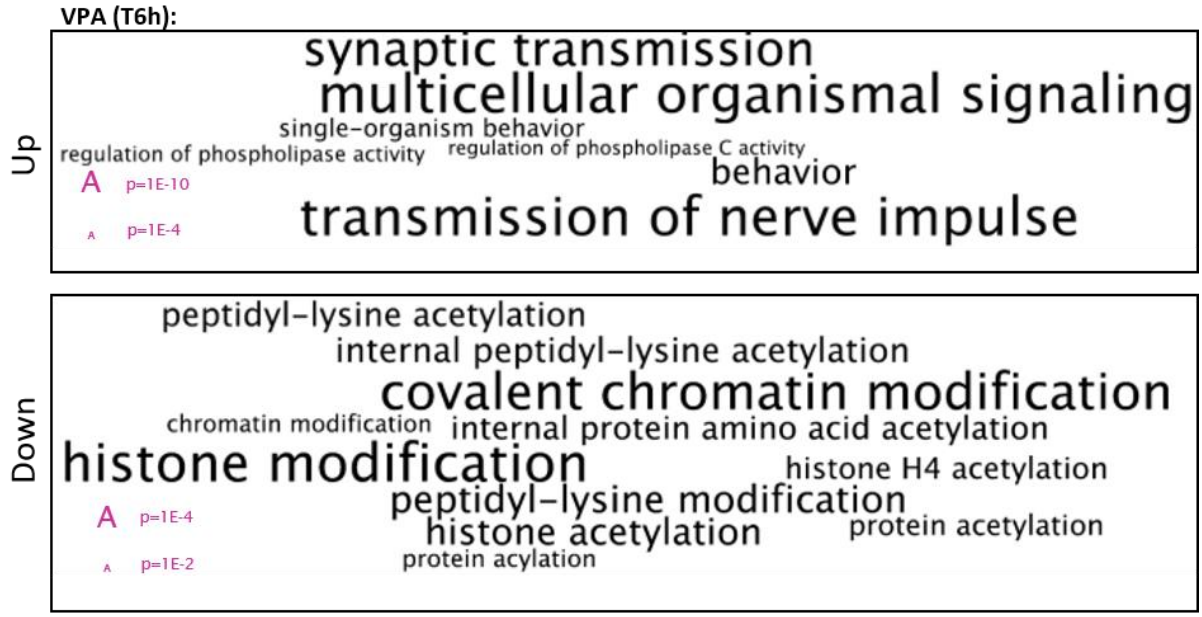

Fig. 5.1.S8: Word clouds of overrepresented GOs affected by 6 h exposure to VPA

The character size scaling relative to the p-value of the corresponding GO is shown in purple. The regulated PS (up or down) used as input data for the analysis correspond to the effect of TSA by short exposure displayed in Fig. 5.1.6A.

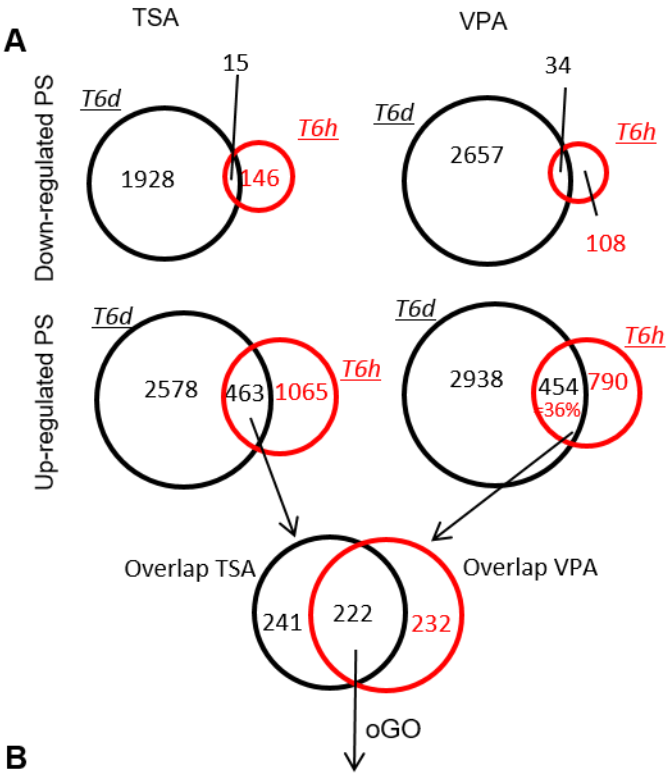

P-value	GO term	GO name
1.38e-05	GO:0010517	regulation of phospholipase activity
3.60e-05	GO:0010863	positive regulation of phospholipase C activity
4.06e-05	GO:1900274	regulation of phospholipase C activity
1.23e-04	GO:0010518	positive regulation of phospholipase activity
2.04e-04	GO:0060191	regulation of lipase activity
2.95e-04	GO:0060193	positive regulation of lipase activity
6.48e-03	GO:0014032	neural crest cell development
7.16e-03	GO:0007202	activation of phospholipase C activity
1.50e-02	GO:0014033	neural crest cell differentiation
2.46e-02	GO:0016337	cell-cell adhesion
4.22e-02	GO:0016477	cell migration

Fig. 5.1.S9: Distinct effects of short and prolonged exposure to HDACi

(**A**) Comparison of early short (T6h) vs prolonged (T6d) exposure to TSA or VPA. Cells were differentiated for indicated time periods in the presence or absence of TSA (left panel) or VPA (right panel). Differentially expressed PS were determined after long and short exposure to TSA and VPA. The number of regulated PS is given relative to untreated controls. The Venn diagrams display the overlap of up- or down- regulated PS at indicated exposure periods. Then, the PS commonly regulated by T6d and T6h were compared between TSA and VPA. (**B**) GO terms significantly overrepresented (oGO) amongst the consensus overlapping PS of VPA and TSA treatments.

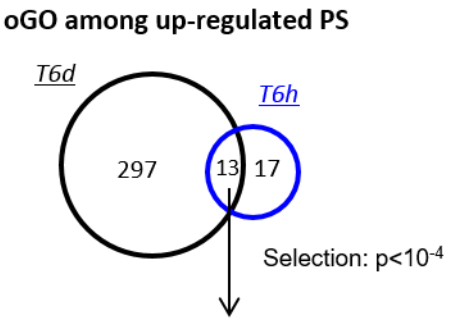

P-value (T6h)	P-value (T6d)	GO term	GO name
1.40e-08	8.93e-03	GO:0007610	behaviour
3.77e-03	1.69e-15	GO:0072359	circulatory system development *
3.77e-03	1.69e-15	GO:0072358	cardiovascular system development *
6.12e-03	2.46e-13	GO:0048514	blood vessel morphogenesis *
1.01e-02	5.50e-15	GO:0001568	blood vessel development *
1.55e-02	5.09e-15	GO:0001944	vasculature development *
2.14e-02	4.30e-09	GO:0001525	angiogenesis *
3.81e-02	6.77e-06	GO:0023056	positive regulation of signaling
7.00e-09	7.52e-03	GO:0035637	multicellular organismal signaling

Fig. 5.1.S10: Commonly oGOs of T6d and T6h among downregulated PS

Comparison of oGOs commonly down-regulated after long (T6d) and short treatment (T6h). (B) Table of oGOs overrepresented both in T6h and T6d.

Fig. 5.1.S11: Primers used for RT-qPCR and Chip

Name	Accession nr.	Forward sequence	Reverse sequence
Primers for gene expression analysis			
EMX2	NM_001165924.1	5'-CCAAGGGAACGACACTAGCC-3'	5'-CCATACTTTTACCTGAGTTTCCGTG-3'
NANOG	NM_024865.2	5'-GGTGAAGACCTGGTTCCAGAAC-3'	5'-CATCCCTGGTGGTAGGAAGAGTAAAG-3'
OCT4	NM_001173531.1	5'-GCAAAGCAGAAACCCTCGTGC-3	5'-ACACTCGGACCACATCCTTCTCG-3'
OTX2	NM_014562	5'-CAG CCC TCA CTC GCC ACA TC-3'	5'-GGA GGT GCA AAG TCG GCC CA-3'
PAX6	NM_000280	5'-CCGCCTATGCCCAGCTTCAC-3'	5'-AAGTGGTGCCCGAGGTGCCC-3'
RPL13A	NM_012423.2	5'-GGTATGCTGCCCCACAAAACC-3'	5'-CTGTCACTGCCTGGTACTTCCA-3'
ZIC3	NM_003413.3	5'-CTTTGCCCGTTCTGAGAAC-3'	5'-ATGTGCTTCTTACGGTCGCT-3'
TBP	NM_001172085.1	5'-GGGCACCACTCCACTGTATC-3'	5'-GCAGCAAACCGCTTGGGATTATATTCG-3'
Primers for ChIP analysis			
GAPDH	NT_009759.16	5'-TCGACAGTCAGCCGCATCT-3'	5'-CTAGCCTCCCGGGTTTCTCT-3'
OCT4	NT_113891.2	5'-GAGGATGGCAAGCTGAGAAA-3'	5'-CTCAATCCCCAGGACAGAAC-3'
OTX2	NT_026437.12	5'-CAG CAA ATC TCC CTG AGA GCG G-3'	5'-GAG GAA GGC GGC TAG AGT TCT AAA C-3'
PAX6	NT_009237.18	5'-AAGGGAACCGTGGCTCGG-3'	5'-ATTAGCGAAGCCTGACCTCTG-3'
NANOG	NT_009714.17	5'-GTTCTGTTGCTCGGTTTTCT-3'	5'-TCCCGTCTACCAGTCTCACC-3'

Fig. 5.1.S12: Antibodies used for Western blot and ChIP

Antigen	Antibody (supplier)	Catalogue number	Dilution	Species
Antibodies used for western blot				
H3Ac	Anti-acetyl-H3 (Millipore)	06-599	1:5000	rabbit
Pan-H3	anti-H3 (Abcam)	ab1791	1:5000	rabbit
α-tubulin	α-tubulin (Cell Signaling)	2125	1:10000	rabbit
α-tubulinAc	Acetyl-α-tubulin(Lys40) (Cell Signaling)	5335	1:10000	rabbit
PAX6	anti-Pax6 (Covance)	PRB-278P	1:1000	rabbit
OTX2	anti-Otx2 (Millipore)	ab9566	1:1000	rabbit
Rabbit IgG	Anti-rabbit-HRP (GE Healthcare)	NA934V	1:10000	donkey
Antibodies used for ChIP				
H3K4me3	anti-H3K4me3 (Millipore)	17-614		rabbit
H3K27me3	anti-H3K27me3 (Active Motif)	39535		rabbit
H3K27Ac	Anti-histone H3 (acetyl K27) (Abcam)	aT2729		rabbit

4.2. Paper 2: Examination of Microcystin Neurotoxicity using Central and Peripheral Human Neurons

published in *Altex* (2020)

Stefanie Klima[1,2], Ilinca Suciu[1,5], Lisa Hoelting[1], Simon Gutbier[1] Tanja Waldmann[1] ,Daniel Dietrich[2,3], Marcel Leist[1,4]

[1] In vitro Toxicology and Biomedicine, Dept inaugurated by the Doerenkamp-Zbinden foundation, University of Konstanz, Konstanz, Germany

[2] Cooperative doctorate college InViTe, University of Konstanz, Konstanz, Germany

[3] Human and Environmental Toxicology, University of Konstanz, Konstanz, Germany

[4] CAAT-Europe, University of Konstanz, Konstanz, Germany

[5] Konstanz Research School Chemical Biology (KoRS-CB), University of Konstanz, Konstanz, Germany

Key words: LUHMES, valinomycin, stem cell, ciguatoxin, Ca^{2+} signaling

4.2.1. Abstract

Microcystins (MC) are a group of cyanobacterial toxins that comprises MC-LF and other cyclic heptapeptides, best known as potent hepatotoxicants. Cell culture and epidemiological studies suggest that MC might also affect the nervous system, when there is systemic exposure e.g. via drinking water or food. We asked whether in vitro studies with human neurons could provide estimates on the neurotoxicity hazard of MC-LF. First, we used LUHMES neurons, a well-established test system for neurotoxicants and neuropathological processes. These central nervous system cells expressed OATP1A2, a presumed carrier of MC-LF, and we observed selective neurite toxicity in the µM range (EC20 = 3.3 µM ≈ 3.3 µg/ml). Toxicity paralleled transcriptome changes pointed towards attenuated cell maintenance and biosynthetic processes. Prolonged exposure for up to four days did not increase toxicity. As a second model, we used human dorsal root ganglia-like neurons. These peripheral nervous system cells represent parts of the nervous system not protected by the blood brain barrier in humans. Toxicity was observed in a similar concentration range (EC20 = 7.4 µM). We conclude that MC-LF poses a potential neurotoxic hazard in humans. The adverse effect concentrations observed here were orders of magnitude higher than those presumed to be encountered after normal nutritional or environmental exposure. However, the low µM concentrations found to be toxic are close to levels that may be reached after very excessive algae supplement intake.

4.2.2. Introduction

While microcystins (MCs) are widely known for their acute hepatotoxicity (Carmichael 1992) (Nishiwaki-Matsushima *et al.* 1992), their potentially adverse effects on other target organs, such as the nervous system, are less clear. MCs are small cyclic heptapeptides comprised of 5 D- and 2 L-amino acids (cyclo-d-Ala^{1}-X^{2}-d-MeAsp^{3}-Z^{4}-Adda^{5}-d-Glu^{6}-Mdha^{7}). Structural variation of side-chains has been encountered in all seven positions, but the most variable amino acids (X and Z) are the L-amino acids in positions 2 and 4 (Botes D.P. 1984) (Daneshian *et al.* 2013). These variable L-amino acid residues are used for naming of the MC congeners, of which more than 248 different congeners are known to date (Altaner *et al.* 2019) (Spoof *et al.* 2016). For example in MC-LF these amino acids

are L-leucine (L) and L-phenylalanine (F). A number of ubiquitously present cyanobacteria genera, e.g. *Microcystis*, *Planktothrix*, *Anabaena*, *Dolichospermum*, have been demonstrated to produce MC (Svirčev *et al.* 2019).

The main exposure route for humans is drinking water, albeit excessive exposure can occur when cyanobacterial supplements are voluntarily consumed (Heussner *et al.* 2012) (Dietrich *et al.* 2005). The World Health Organization (WHO) suggested a safe value of 1 µg/l (1 nM) for MC-LR into their guidance on cyanobacteria in drinking water (World Health Organization. Water *et al.* 2004). Based on the latter, the tolerable daily intake (TDI) for a human was calculated to be 0.04 µg MC-$LR_{equivalents}$/kg BW/day (≈ 40 pmol/kg BW/day) (World Health Organization. Water *et al.* 2004). In addition to the well-established hepatotoxicity, also renal- and neurotoxicity have been reported based on in vivo and in vitro experiments in rodents, fish and birds (Fischer *et al.* 2000) (Feurstein *et al.* 2009) (Feurstein *et al.* 2011) (Hu *et al.* 2016) (Herrera *et al.* 2018, Hinojosa *et al.* 2019).

There are several reported human exposures to MCs with an adverse outcome. In Caruaru (Jochimsen *et al.* 1998) (Pouria *et al.* 1998), patients at a haemodialysis clinic were accidentally exposed via dialysis water with an estimated MC concentration of 19.5 µg/l (20 nM) (Azevedo *et al.* 2002). The symptoms reported in the patients ranged from early visual disturbances to muscle weakness and nausea. Of the 126 - 131 patients, hundred developed acute liver toxicity and between 52 and 60 of them died within 10 months (Azevedo *et al.* 2002), (Pouria *et al.* 1998).

At lake Chaohu, China, fishermen were chronically exposed to MCs by drinking water and food. Concentrations of MC were 3.28 µg/l, which corresponds to 3.3 nM MC-$LR_{equivalents}$ in drinking water. The muscle of contaminated aquatic animals showed MC concentrations of 43 ng/g dry weight (DW) (43 pmol MC-$LR_{equivalent}$/g DW) which led to blood concentrations in fishermen ranging from 0.045 to 1.832 ng/ml (0.045 to 1.84 pM) (Chen *et al.* 2009). The blood samples showed increased levels of liver enzymes like alanine aminotransferase (ALT).

In the three gorges reservoir region of China, more than 1000 children were chronically exposed to MC. They showed elevated liver enzyme levels of ALT, compared to non-exposed children (Li *et al.* 2011). The average drinking water concentration of MC was 2.6 µg/l (2.6 nM), the mean concentration in fish was 0.22 µg/g DW (221.1 nmol/g DW).

MCs need to be actively transported into cells by organic anion transporting polypeptides (OATPs). Cells of the blood brain barrier as well as neurons express OATP1A2 (Hagenbuch *et al.* 2003) (Bronger *et al.* 2005). This suggests that MCs can cross the blood brain barrier, as OATP1A2 was demonstrated to transport MC-LR (Fischer *et al.* 2005). The best-documented mode of action of MC in mammalian cells (hepatocytes) is the inhibition of serine/threonine-specific protein phosphatase 1, 2A and 5 (MacKintosh *et al.* 1990, Buratti *et al.* 2017) (Chen *et al.* 2016, Valério *et al.* 2016) (Altaner *et al.* 2020). This results in a hyperphosphorylation of several protein kinase targets, which eventually leads to a widespread dysregulation of cellular processes (Yoshizawa *et al.* 1990) (MacKintosh *et al.* 1990) (Hinojosa *et al.* 2019).

As epidemiological and animal data from rodents, fish and birds suggest that MCs may not only induce hepatotoxicity, but also neurotoxicity, we explored the MC toxicity to human neurons. We used LUHMES cells, as representatives of central human neurons (Lotharius *et al.* 2005) (Scholz *et al.* 2011). These cells have a normal karyotype (Gutbier *et al.* 2018) and typical neuronal structure and electrophysiology (Scholz *et al.* 2011). They have been widely used as alternatives to animal testing and in neuropathology studies (Witt *et al.* 2017) (Lohren *et al.* 2015) (Delp *et al.* 2019) (Singh *et al.* 2018) (Scholz *et al.* 2018) (Delp *et al.* 2018) (Tong *et al.* 2018) (Höllerhage *et al.* 2017) (Devos *et al.* 2014) (Skirzewski *et al.* 2018). As second, complementary test system, we used human peripheral neurons. These were generated from pluripotent stem cells (Hoelting *et al.* 2016). They were established as a screening system for peripheral neurotoxicants (Delp *et al.* 2018). These models were used as *in vitro* approach to identify neurotoxic MC concentrations in order to compare them to serum concentrations reported in humans after exposure.

4.2.3. Material and methods

Material

Cisplatin, valinomycin, tubacin, microcystin-LF, microcystin-LR, PLO, fibronectin, glutamine, tetracycline, cAMP, apotransferrin, glucose, insulin, putrescine, selenium, progesterone and calcein-AM were purchased from Sigma, USA. AdvDMEM/F12, knockout serum replacement, DMEM/F12, N2 supplement, Glutamax, NEAA, ß-mercaptoethanol, Triton-X-100, PBS, H-33342, FBS, Trizol, Flou-4 DirectTM Calcium Assay Kit were pur-

chased from ThermoFisher Scientific, USA. FGF2, GDNF, noggin, BDNF and NGF were purchased from R&D systems, USA. Dorsomorphin, SB-431642 and SU5402 were purchased from Torcis, UK. Chir99021 was purchased from Axon Medchem, USA, DAPT was purchased from Merck Millipore, USA. Matrigel was purchased from Corning, USA, iScript and SsoFastTM EvaGreen® Supermix were purchased from BioRad, USA. pCTX isolated from a moray eel, was provided by the laboratory of Richard Lewis, University of Queensland, Brisbane, Australia. Chemical structures were drawn with ChemDraw (Version 16.0) from PerkinElmer.

LUHMES culture

LUHMES were used for modeling central human neurons and cultured as described earlier (Krug *et al.* 2013) (Lotharius *et al.* 2005) (Scholz *et al.* 2011). Briefly, cells were cultured on PLO/fibronectin (50 µg/ml poly-L-ornithine (PLO) and 1 µg/ml fibronectin) coated flasks and plates. Cells were maintained in proliferation medium (AdvDMEM/F12 supplemented with 2 mM glutamine, 1x N2 supplement and 40 ng/ml fibroblast growth factor-2 (FGF2)). Differentiation was started by seeding cells at a density of 100,000 cells/cm^2 in proliferation medium and changing the medium after 24 h to differentiation medium (AdvDMEM/F12 supplemented with 2 mM glutamine, 1x N2 supplement, 2.25 µM tetracycline, 1 mM dibutyryl 3',5'-cyclic adenosine monophosphate (cAMP) and 2 ng/ml recombinant human glial cell derived neurotrophic factor (GDNF)). Medium change was performed every 48 h after the differentiation was started.

Peripheral neurons

The stem cell line (WA09 line) was obtained from WiCell (Madison, WI, USA). The pluripotent stem cells were differentiated into immature dorsal root ganglia like neurons exactly according to the protocol of Hoelting et al. (Hoelting *et al.* 2016). Briefly, differentiation was started on day of differentiation (DoD) 0' by adding neural differentiation medium (KSR-S; knockout DMEM with 15% serum replacement, 1 x Glutamax, 1 x non-essential amino acids, and 50 µM ß-mercaptoethanol) and six small molecule pathway inhibitors (35 ng/ml noggin, 600 nM dorsomorphin, 10 µM SB-431642, 1.5 µM CHIR99021, 1.5 µM SU5402 and 5 µM DAPT). Starting from DoD4', medium was gradually replaced by N2-S medium (DMEM/F12, with 2 mM Glutamax, 0.1 mg/ml apotransferrin, 1.55 mg/ml glucose, 25 mg/ml insulin, 100 mM putrescine, 30 nM selenium, and 20 nM

progesterone). After eight days of differentiation, the neuronal precursors were cryopreserved. After thawing, cells were seeded at a density of 100,000 cells/cm^2 in 25% KSR-S and 75% N2-S supplemented with 1.5 µM CHIR99021, 1.5 µM SU5402 and 5 µM DAPT. On DoD1 and DoD2, 50% of the medium was changed. From DoD3 on cells received N2-S medium, supplemented with 10 ng/ml BNDF, 10 ng/ml GNDF and 25 ng/ml NGF for further differentiation and maturation, with medium changes every other day.

Ca^{2+} signaling

Peripheral neurons were seeded at a density of 100,000 cells/cm^2 and cultured according to Hoelting et al. (Hoelting *et al.* 2016). After 23 days of differentiation, the cells were loaded with Fluo4 AM-Calcium Assay Kit and Hoechst-33342 (H-33342) for 20 min at 37°C. Changes in the free intracellular Ca^{2+} concentration were monitored with VTI HCS microscope (Cellomics, USA) containing an incubation chamber providing an atmosphere with 5% CO_2 and 37°C. Substances (HBSS, 0.3% DMSO, 2.5 µM MC-LF, 30 mM KCl, 15 nM pCTX) were administered by an automated pipettor 10 s after the first image was taken. Images were taken as fast as possible for 45 s (approx. one image/second) and exported as .avi files. The files were analysed in CaFFEE software (Karreman *et al.* 2020).

Viability testing

LUHMES and peripheral neurons were seeded at a density of 100,000 cells/cm2, cultured and treated as indicated in the respective figure. One hour prior to analysis cells were stained with staining mix (1 µg/ml H-33342 and 1 µM calcein-AM), incubated one hour at 37°C and image acquisition was performed automatically with ArrayScan VTI HCS microscope (Cellomics, USA). Analysis of the pictures was performed as described earlier (Stiegler et al. 2011). Briefly, the neuronal area was identified by calcein stain and the somatic area was subtracted, which resulted in definition of neurite area. The viability was obtained from the same images. Cells with a double stain for H-33342 and calcein were counted as alive, whereas cells only positive for H-33342 were classified as dead.

Immunofluorescence and microscopy

Cells were grown on coated 96 well plates and fixed with 4% paraformaldehyde on day 6 (LUHMES) or DoD7 (peripheral neurons). Following permeabilisation in 0.3% Triton X-100, they were blocked 1 h in PBS containing 5% fetal bovine serum and 0.1% Triton X-100. Primary antibodies (Tuj1 (BioLegend Cat. No. 801202) 1:1000, OATP1A2 (Sigma-

Aldrich Cat. No. SAB4502814) 1:100, Peripherin (Santa Cruz Cat. No. sc-7604) 1:200) were added for 1 h at room temperature. After washing, secondary antibodies and H-33342 were incubated for 30 min. Images were taken at a Zeiss Axio Observer with ZEN 2 pro blue edition software and further processed with ImageJ (Version 1.52p).

RNA extraction, cDNA synthesis and real-time qPCR

Total RNA was extracted using TRIzol, according to the manufacture's protocol. Total RNA (1 µg) was reverse transcribed with iScript. Quantification of cDNA was performed using the SsoFast™ EvaGreen® Supermix. The threshold cycle (C_T) was determined for each sample, using the CFX data analysis software (Bio-Rad, USA). As reference gene RPL13A was used (forward: GGTATGCTGCCCCACAAAACC reverse: CTGTCACTGCCTGGTACTTCCA), mRNA levels of OATP1A2 (forward: TCCTGTGTGTGGAAACAATG reverse: AGCATCAAGGAACAGTCAGG) and OATP3A1 (forward: CTGGGCTCTTTCTGTACCAA reverse: GTGGAAACCCAAACATCAAG) were compared to reference gene using the ΔΔ method (Livak *et al.* 2001).

Transcriptome data generation and analysis

For the sample preparation, the medium was removed from each well and cells were immediately lysed in 25 µl of 1x Biospyder lysis buffer. Storage was done at -80ºC until samples were shipped to Bioclavis (BioSpyder Tech.) on dry ice. The assay used for the transcriptomics data is TempO-Seq, a targeted RNA-sequencing method developed by BioSpyder Technologies, Inc, described in detail in (House *et al.* 2017).

For the transcriptomics data analysis, the R package DESeq2 (v1.24.0) was employed (Love *et al.* 2014). The DESeq2 object was constructed from raw counts and its size factors were coerced to total sample counts per million (CPM). The analysis of differential gene expression in the treatment group (against the DMSO control group) was done with the Wald test. In order for a gene to be considered significantly deregulated, the threshold of Benjamini-Hochberg adjusted p-values ≤ 0.05 had to be satisfied. Overrepresentation analysis was based on Fisher's F-test as implemented in G-profiler software (Raudvere *et al.* 2019). PCA was generated with the online tool ClustVis (Metsalu *et al.* 2015).

Statistics

Experiments were performed at least on two (usually on three) cell preparations, with several (≥3) technical replicates for each cell batch. For statistical analysis GraphPad Prism 5 software (Version 5.03) was used. Data were evaluated by ANOVA with post-hoc testing (Dunnett's), or by t-test (two groups) as appropriate. P-values <0.05 were regarded as statistically significant. For curve fitting a four-parameter fit with top constrains set to 100% was used in GraphPad Prism 5 software (Version 5.03).

4.2.4. Results

Neurotoxicity of MC-LF, assessed on LUHMES neurons

LUHMES neurons, differentiated for 4-6 days are not only fully post-mitotic (Scholz *et al.* 2011), but also show many features of central nervous system cells (Tong *et al.* 2018) (Gutbier *et al.* 2018) (Matelski *et al.* 2020) (Weng *et al.* 2012) (Weng *et al.* 2014). The cells were also found here to be positive for OATP1A2, a transporter that accepts microcystins (MCs) as substrate (Fig. 5.2.1A) (Fischer *et al.* 2005) (Chen *et al.* 2016). When LUHMES cells were exposed to MC-LF (Fig. 5.2.1B) for 48 h, we observed a specific neurite degeneration at concentrations above about 2 µM (Fig. 5.2.1C, D). The number of viable cells (= cell bodies) was not affected at concentrations as high as 5 µM (Fig. 5.2.1C). Follow-up experiments showed that 24 h exposure was not sufficient to trigger neurite damage (Fig 5.2.S1A-C). Exposure of 24 h, followed by a 24 h washout period led to the same toxicity as 48 h continuous exposure (Fig. 5.2.S1D). This suggests that toxic effects were all triggered during the first 24 h, but manifestation of toxicity (neurite breakdown) took one day more to develop. We tested whether even longer times would allow for more potent toxicant effects. However, exposure for 48 h, followed by a 48 h washout (4 days in total) did not lead to more potent effects of MC-LF (Fig. 5.2.S1E). To further investigate effect specificity, we also investigated MC-LR (Fig. 5.2.S1F), known to be a less potent toxicant (Feurstein *et al.* 2011). Indeed, no toxicity was observed here at concentrations up to 5 µM (Fig. 5.2.S1G). To test for potentially more subtle effects of MC on neurons, serveral other endpoints were considered. Tau phosphorylation and activation of MAP kinases (ErK) were examined by Western blotting, but no changes were observed at ≤ 5 µM MC-LF (data not shown). For this series of experiments, we concluded that MC-LF can trigger neurotoxicity at high concentrations (> 2 µM). Our data based on established and sensitive endpoints of neurite toxicity suggest that lower concentrations of MC-LF are inactive in

the chosen experimental model of human neurons and with the exposure scenarios scrutinized here.

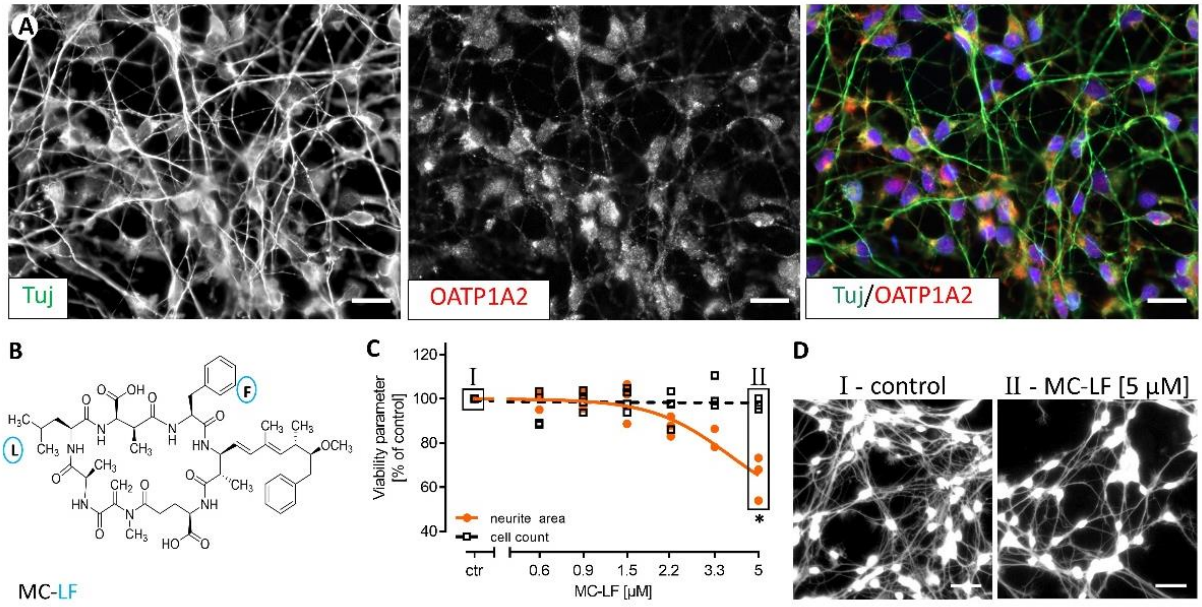

Fig. 5.2.1: Effect of MC-LF on LUHMES neurons

(**A**) LUHMES cells were differentiated on coverslips and fixed after six days. Double-immunofluorescence images were obtained for neurite structures (using an antibody against ß-III- tubulin, Tuj) and for OATP1A2. For maximum clarity the individual channels are shown in b/w, the composite image is shown with neurites in green and OATP1A2 in red. Scale bar is 20 µm. (**B**) Chemical structure of MC-LF. (**C**) Effect of MC-LF on neurite area (orange) and cell count (black), after 48 h treatment from d4 until d6. Data points are from three separate experiments, *p<0.05. (**D**) Exemplary pictures of calcein-stained cells treated with 5 µM MC-LF (II) or solvent (I), as described in C. Scale bar is 50 µm.

Transcriptome disturbances triggered by MC-LF

To broadly capture effects of MC on neurons, the transcriptional changes triggered by a 48 h treatment of 5 µM MC-LF were measured (Fig. 5.2.S2A). The PCA analysis clearly showed a separation between the MC treatment and the control (Fig. 5.2.S2B). The analysis identified 75 differentially expressed genes (DEGs) (Fig. 5.2.2B). The top downregulated DEGs were mainly related to differentiation and chromatin remodeling, such as EXO1, RAD54L or NCAPH and thus did not indicate specific pathways (Fig. 5.2.2C). The most upregulated DEGs include predominantly ribosomal genes like RRS27L, RPL13A, RPS13 and the anti proliferative factor BTG3. This pattern is consistent with a relatively unspecific cellular stress response. To get a better understanding of the DEGs, we performed a gene ontology overrepresentation analysis. The upregulated DEGs resulted in more than 20 overrepresented gene ontologies (oGO) (Fig. 5.2.S2C). Downregulated DEGs resulted in only eleven oGOs (Fig. 5.2.S2D). The gene PPP1R17 (protein phosphatase 1

regulatory subunit 17) is included in the oGOs “mRNA catabolic process”, “heterocycle catabolic process” (Fig. 5.2.S2E), “cellular nitrogen compound catabolic process” and “aromatic compound catabolic process”. Its gene product inhibits the phosphatase activities in protein phosphatase 1 (PP1) and protein phosphatase 2A (PP2A) complexes. The inhibition of PP1 and PP2A is also the best described direct mode of action of MCs (Altaner *et al.* 2020), (MacKintosh *et al.* 1990), (Chen *et al.* 2016), (Buratti *et al.* 2017), (Valério *et al.* 2016). It appears as if most of the downregulated DEGs are grouped into oGOs dealing with cell cycle (Fig. 5.2.S2D). But if investigated more precisely, the included genes in the respective oGOs are linked to cell cycle only very indirectly. Exemplarily, the DEGs included in the GO “mitotic nuclear division” are mainly genes related to (neuronal) differentiation status like EMX2, SNCA, and TCF4 (Fig. 5.2.S2F). To integrate the results of the downregulated DEGs and the GO analysis we assigned the oGOs to key biological processes according to Waldmann et al. (Waldmann *et al.* 2014) (Fig. 5.2.2D). Over 50% of the key biological processes of the downregulated oGOs can be assigned to genes involved in development and differentiation. The data of transcriptional changes after 48 h treatment with MC-LF point to an altered differentiation state of LUHMES, a typical generalized stress response in adult tissues (Desprez *et al.* 2019).

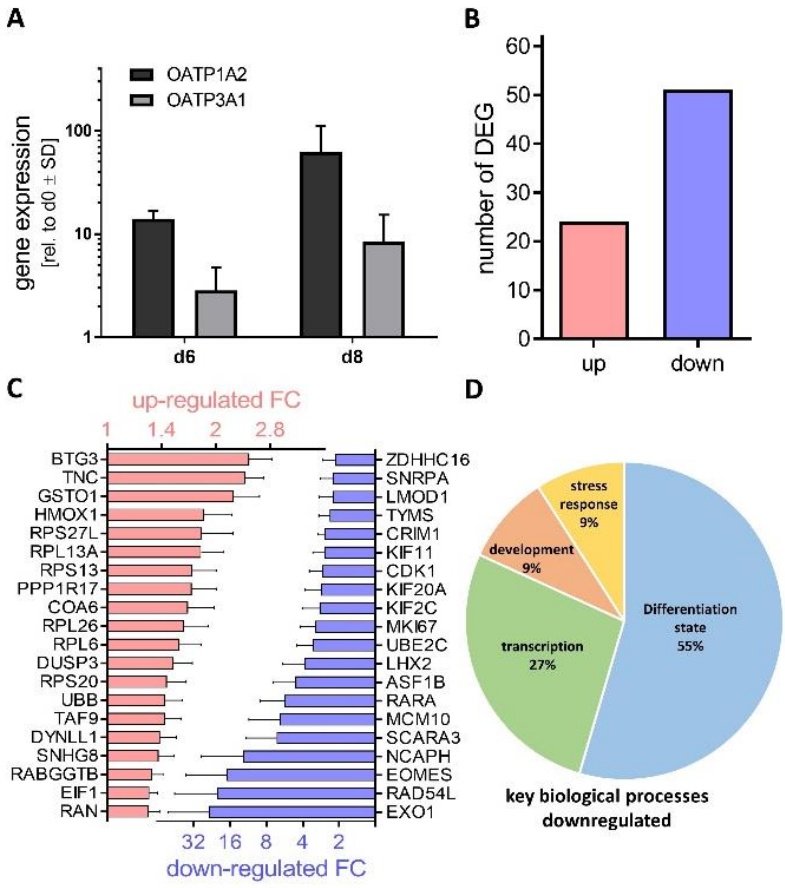

Fig. 5.2.2: Transcriptome analysis of MC-LF treated LUHMES

(**A**) OATP1A2 (black) and OATP3A1 (grey) expression levels of LUHMES on d6 and d8 relative to d0 determined with RT-qPCR. (n=2) (**B**) Samples were obtained at d6 from untreated LUHMES and LUHMES treated with 5 µM MC-LF for 48 h from d4 until d6 LUHMES, and RNA expression profiles were obtained. Number of differentially expressed genes (DEG) is shown for upregulations (red) and downregulations (blue) with an adjusted p-value ≤ 0.05. (**C**) Out of the DEGs in B the top 20 upregulated (red) and downregulated (blue) genes according to their fold change (FC) are shown. The error bars represent the standard deviation. (**D**) The gProfiler analysis tool was used to identify overrepresented GOs (oGOs) among the downregulated DEGs. These were then assigned to four different superordinate biological processes according to Waldmann et al. (Waldmann et al. 2014).

Toxicity of MC-LF to peripheral human neurons

As a second neuronal test system we used human pluripotent stem cell derived peripheral neurons (Fig. 5.2.S3A). The cells can be generated in big batches and thawed as required for testing (Fig. 5.2.S3B). They provide a suitable test system for mechanistic studies (Hoelting *et al.* 2016) and screening approach (Delp *et al.* 2018). At DoD7 after thawing, the cells express the transporter OATP1A2, which is known to transport also MCs (Fig. 5.2.S3C). As peripheral neurons are not protected by the blood brain barrier, they could be more susceptible to neurotoxicants than neurons from the central nervous system. We used the PeriTox assay in which more than 100 substances have been tested (Hoelting *et al.* 2016) (Delp *et al.* 2018), to investigate the effect of MC-LF on neurite outgrowth in peripheral neurons (Fig. 5.2.3A). As positive controls, valinomycin (Fig. 5.2.3B), a cyclic peptide, with L-amino acids, produced by *Streptomyces*, cisplatin, a chemotherapeutic drug, and tubacin, an HDAC inhibitor (Fig. 5.2.S3D), were used. Tubacin, as a specific HDAC6 inhibitor, catalyzes α-tubulin acetylation (Gao *et al.* 2007) and thereby interferes with neurite outgrowth. An often-observed side effect of chemotherapeutic drugs are peripheral neuropathies, which can be mimicked by cisplatin application. As no changes in viability or neurite area were observed after a 24 h MC-LF treatment, we investigated the effects after a longer treatment period. After 48 h MC-LF treatment with 10 µM, a reduction in cell count was observed (Fig. 5.2.3C). This was even more pronounced after 48 h of treatment, followed by 48 h of washout (Fig. 5.2.3D-F). Under these conditions, not only the cell count was reduced but also the neurites were completely broken down (Fig. 5.2.3F). In another approach, we tested whether a 24 h treatment at later time points, namely DoD 4-5, is also sufficient to see a reduction in cell count or neurite area. Therefore, we tested concentrations up to 5 µM MC-LF but we did not observe a reduction in either of the two parameters (Fig. 5.2.S3E). As alternative toxicity indicator, we considered acute signaling effects as measurable by intracellular calcium changes (Fig. 5.2.S4A).

As positive controls we used cell depolarization by an increase of potassium ions (30 mM) (Fig. 5.2.S4B) in the medium and exposure to ciguatoxin (15 nM) (Fig. 5.2.S4C), a polyether marine biotoxin specifically inhibiting voltage-gated Na^+ channels (Daneshian *et al.* 2013). In both cases, clear increases of intracellular free calcium were observed, while MC-LF (2.5 µM) had no effect at all (Fig. 5.2.S4A).

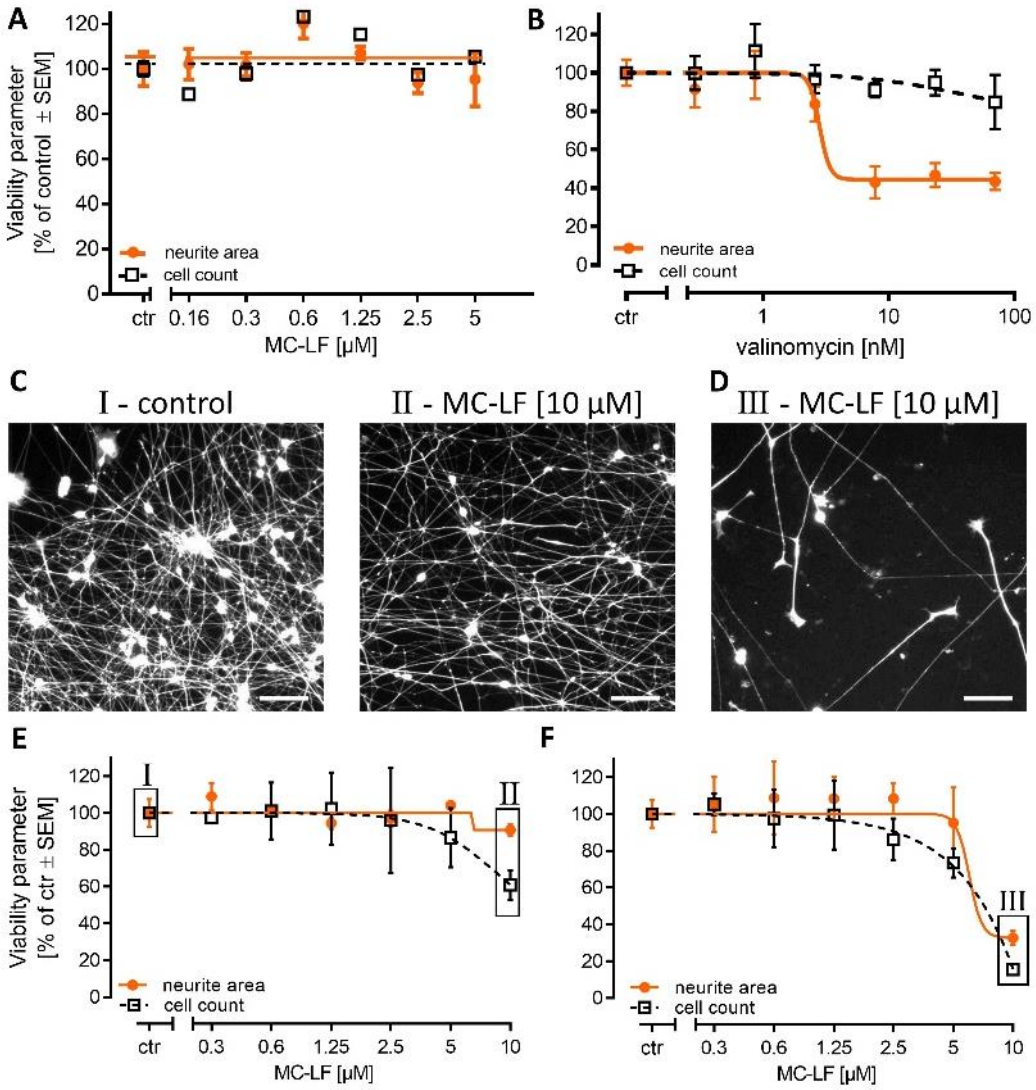

Fig. 5.2.3: Effect of MC-LF on peripheral neurons

Peripheral neurons were generated from human pluripotent stem cells according to an established protocol. After thawing, cells were immediately plated on 96-well plates and used for toxicity experiments. (**A**) Effect of MC-LF on neurite area (orange) and cell count (black) after a 24 h treatment from DoD0 until DoD1. Data are from three independent experiments. (**B**) Effect of the positive control valinomycin on neurite area (orange) and cell count (black) after treatment as in A. Data are from four independent experiments. (**C** and **D**) Exemplary pictures of calcein-stained cells treated with solvent (I) or 10 µM MC-LF for 48 h from DoD4 until DoD6 (II) or 10 µM MC-LF for 48 h from DoD4 until DoD6 followed by a 48 h washout period (III). Scale bar is 100 µm. (**E**) Effect of MC-LF on neurite area (orange) and cell count (black) after 48 h treatment from DoD4 until DoD6. Data are means ± SEM; n=3. (**F**) Effect of MC-LF on neurite area

(orange) and cell count (black) after 48 h treatment (from DoD4 until DoD6) followed by a 48 h washout period. Data are means ± SEM; n=3.

4.2.5. Conclusion and outlook

Both in vitro systems used in this study clearly showed, that low µM concentrations of MC lead to human neurotoxicity. Since one of the assays was representative of the peripheral nervous system, which is not protected by a blood-brain barrier, the concentration range identified here would with high likelihood trigger acute human neurotoxicity and may be used as point-of-departure for risk assessment of acute exposure settings. In standard nutritional exposure scenarios (including contaminated drinking water or food), human plasma concentrations are likely to be at least 100-1000 fold below this hazard threshold. It needs to be noted that this risk assessment statement does not account for parenteral exposure. It also does not allow conclusions on lower level exposures occurring over considerably longer times than tested here. A follow-up study on this would require cultures that can be exposed for several weeks, and it may use some of the regulated genes that were identified here as biomarkers of subtle effects.

4.2.6. Acknowledgement

This work was supported by the BMBF, INVITE, EFSA, the DK-EPA (MST-667-00205), and the University of Konstanz. It has received funding from the European Union's Horizon 2020 research and innovation programme under grant agreements No. 681002 (EU-ToxRisk) and No. 825759 (ENDpoiNTs), as well as from CHARM (BadenWürttemberg Wassernetzwerk). We are grateful to Viola Singer and Heidrun Leisner for invaluable experimental support.

4.2.7. Conflict of interest

The authors declare no conflict of interest.

4.2.8. Supplements

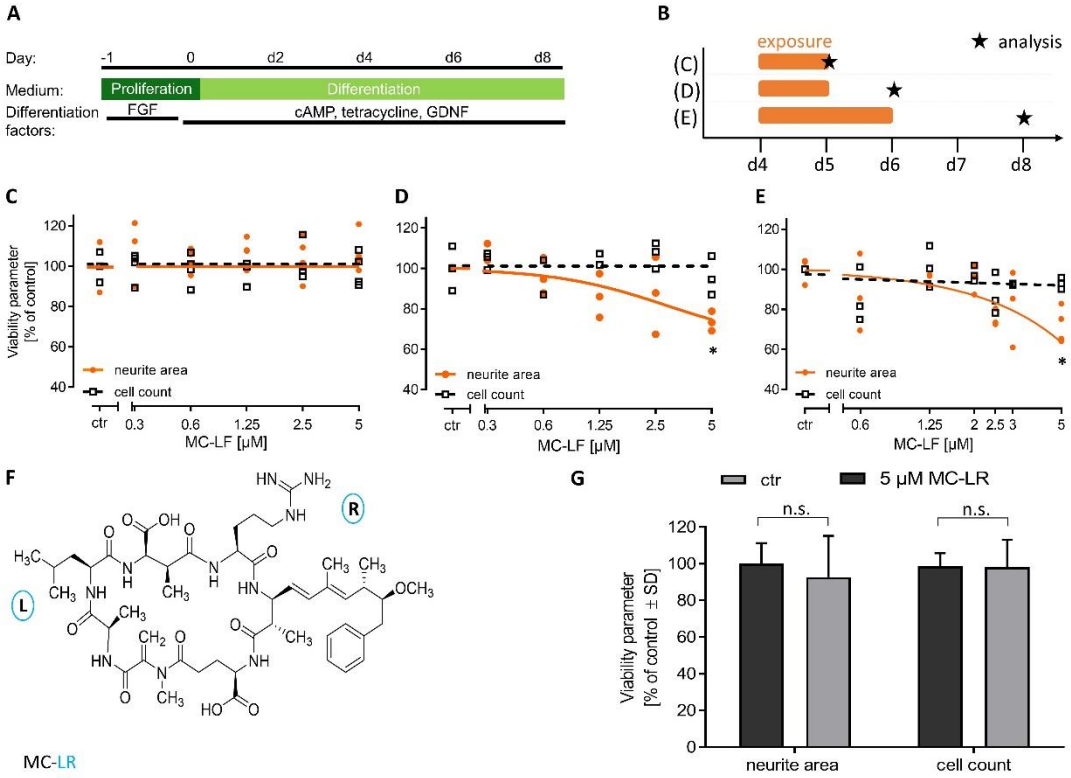

Fig. 5.2.S1: Time dependent effects of MC on LUHMES

LUHMES are a homogenous cell population that can be differentiated into postmitotic neurons within six days. They were used here as model system for central human neurons. (**A**) Schematic overview of LUHMES cultivation and differentiation. (**B**) Schematic depiction of MC-LF exposure scenarios and washout periods in LUHMES. (**C**) Effect of MC-LF on neurite area (orange) and cell count (black) after a 24 h treatment (d4 until d5) (**D**), a 24 h treatment (d4 until d5) followed by a 24 h washout period (**E**) or a 48 h treatment (d4 until d6) followed by a 48 h washout period. Data points are from three separate experiments, *p<0.05. (**F**) Chemical structure of MC-LR. (**G**) Effect of 5 µM MC-LR on neurite area and cell count after a 48 h treatment (d4 until d6) Data are means ± SD; n=3.

A

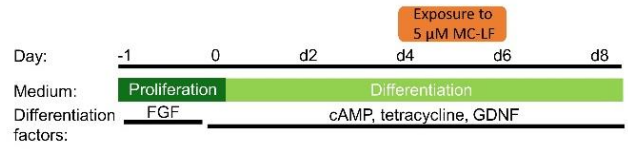

B

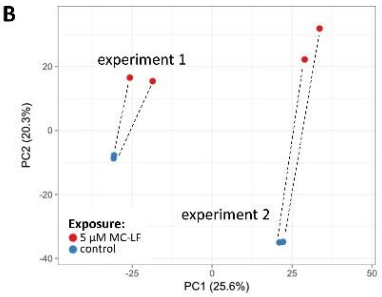

C

most upregulated GOs (biological process)	adjusted p-value
translational initiation	0.000006
nuclear-transcribed mRNA catabolic process nonsense-mediated decay	0.000014
ribonucleoprotein complex biogenesis	0.000110
SRP-dependent co-translational protein targeting to membrane	0.000217
Translation	0.000256
cotranslational protein targeting to membrane	0.000281
peptide biosynthetic process	0.000341
nuclear-transcribed mRNA catabolic process	0.000374
protein targeting to ER	0.000411
establishment of protein localization to endoplasmic reticulum	0.000493

D

downregulated GOs (biological process)	adjusted p-value
mitotic nuclear division	0.000007
mitotic cell cycle process	0.000237
DNA packaging	0.000256
nuclear division	0.000460
organelle fission	0.001165
DNA conformation change	0.006639
mitotic sister chromatid segregation	0.009819
telencephalon regionalization	0.012837
sister chromatid segregation	0.029134
DNA replication-independent nucleosome assembly	0.035066

E

DEGs of GO „heterocycle catabolic process“	Log2 fold change	Short explanation
RABGGTB	0.41	Rab Geranylgeranyltransferase
RPL6	0.67	Ribosomal protein
UBB	0.53	Ubiquitin
UCHL1	0.29	Ubiquitin hydrolase
GSTO1	1.16	Glutathione S-Transferase
PPP1R17	0.78	Inhibits phosphatase activities in PP1 and PP2A
RPL13A	0.86	Ribosomal protein
RPS27L	0.87	Ribosomal protein

F

DEGs of GO „mitotic nuclear division“	Log2 fold change	Short explanation
NCAN	-0.56	Neurocan
DUSP4	-0.64	Phosphatase, inactivating MAPK
EMX2	-0.87	Neurodevelopmental transcription factor
SNCA	-0.58	α-synuclein
SNRPA	-1.17	Small nuclear ribonucleoprotein (splicing)
TCF4	-1.08	Neurodevelopmental transcription factor
TYMS	-1.25	Thymidylate synthetase
HTATSF1	-0.57	transcription factor of transcriptional elongation
CENPK	-0.82	Subunit of the centromere complex
MRPS6	-0.51	Mitochondrial ribosomal protein

Fig. 5.2.S2: Overrepresented gene ontologies in MC-LF treated LUHMES

(**A**) Schematic overview of LUHMES cultivation and differentiation including the exposure period to 5 µM MC-LF for 48 h from d4 until d6. (**B**) Samples were obtained on d6 from untreated LUHMES (blue) and LUHMES treated with 5 µM MC-LF for 48 h from d4 until d6 and RNA expression profiles were obtained. The PCA was generated with the online tool ClustVis. The dotted lines connect the data points treated for 48 h with 5 µM MC-LF of two different biological replicates and its corresponding control. Data are from two independent biological experiments with each two technical replicates. (**C**) The gProfiler analysis tool was used to identify overrepresented GOs (oGOs) among the DEGs. The 10 most upregulated biological processes in this analysis are listed with their adjusted p-values. (**D**) The 10 most down-regulated biological processes in this analysis are listed with their adjusted p-values. All adjusted p-values included into the analysis are ≤ 0.05. (**E** and **F**) As examples for gene sets within oGO, those for “heterocycle catabolic process” and “mitotic nuclear division” are shown here. All tables indicate the gene symbol, the regulation (Log2 fold change) by MC-LF, and a short comment on the function or the gene name.

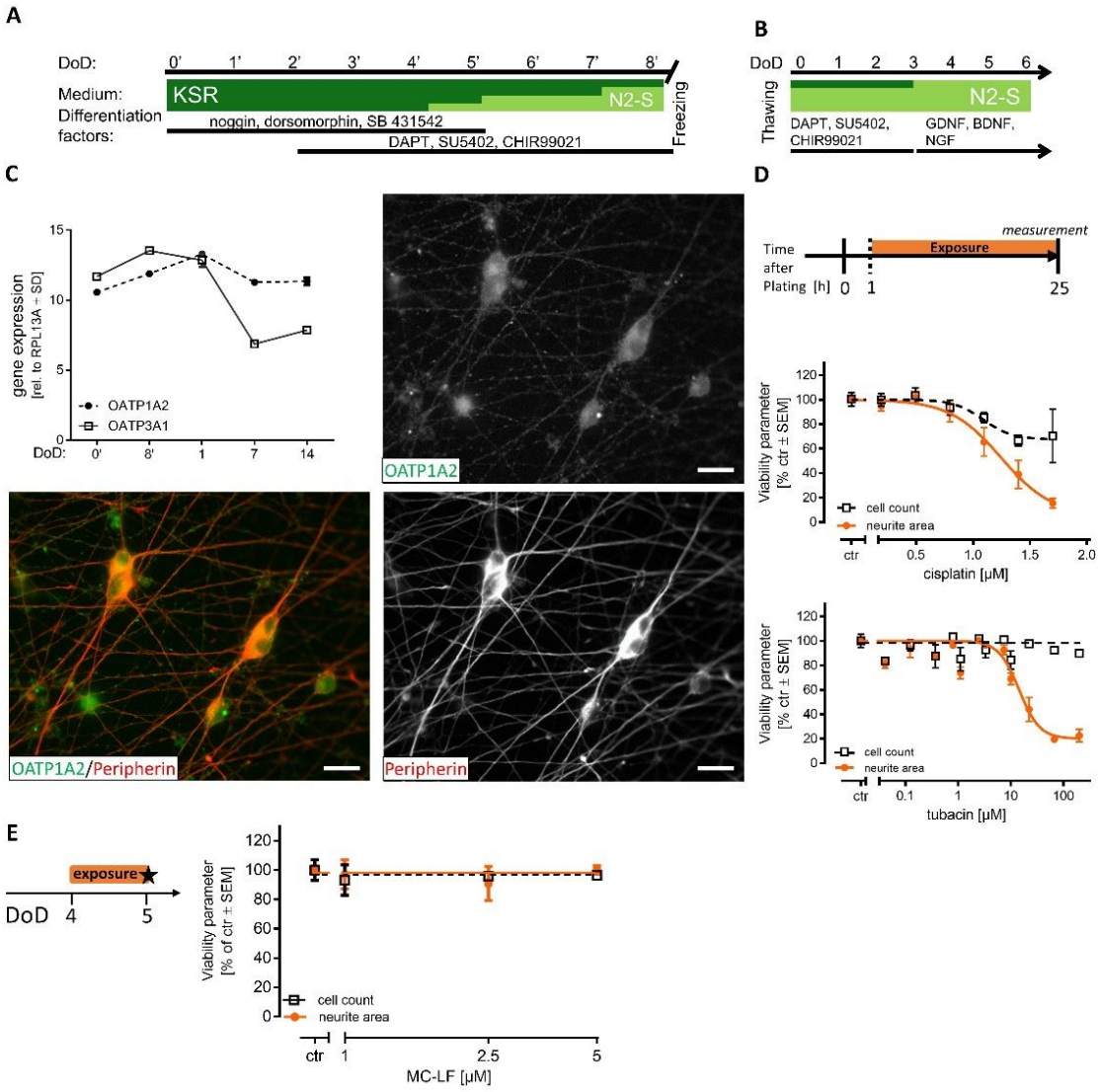

Fig. 5.2.S3: Characterization of peripheral neurons for toxicity evaluation

(A) Peripheral neurons are used as complementary test system and are generated from pluripotent stem cells according to an established protocol, which includes a freezing step, allowing the differentiation of large cell batches and thawing of cells for individual experiments. (B) After thawing, the cells are cultured and treated for various periods. (C) Time course of OATP1A2 (circle) and OATP3A1 (square) expression levels in peripheral neurons determined with RT-qPCR (n=2). Cells were differentiated on coverslips and fixed on DoD7. Double-immunofluorescence images were obtained for peripheral neurons (using an antibody against peripherin) and for OATP1A2. For maximum clarity the individual channels are shown in b/w, the composite image is shown with OATP1A2 in green and peripherin in red. Scale bar is 20 µm. (D) Schematic depiction of well-established PeriTox assay with a treatment of outgrowing neurites with various substances from DoD0 until DoD1. Effect of cisplatin and tubacin on neurite area (orange) and cell count (black) after a 24 h treatment from DoD0 until DoD1. Data are means ± SEM; n=3. (E) Effect of MC-LF on neurite area (orange) and cell count (black) after treatment for 24 h (DoD4 until DoD5) Data are means ± SEM; n=3.

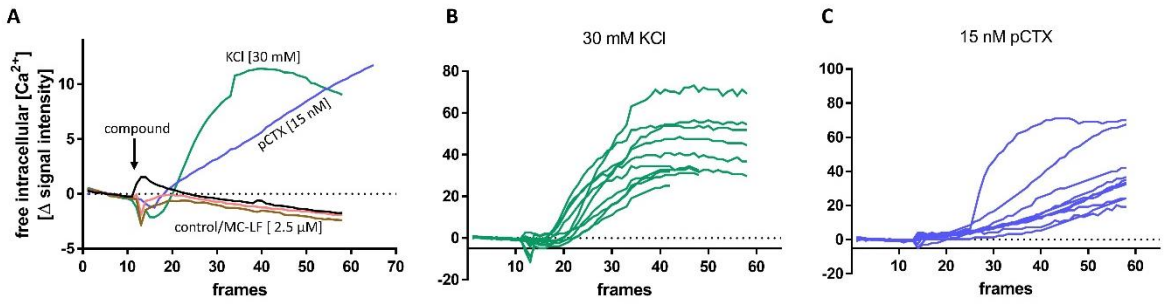

Fig. 5.2.S4: Ca^{2+} signaling as functional endpoint for toxicity evaluation

Peripheral neurons can be cultivated for longer time periods and are therefore suitable as a test system for electrically active neurons. Cells were cultured for 23 days and analysed on their ability for Ca^{2+} signaling. (A) Cells were treated with solvent control 0.3% DMSO (brown), buffer control (black), positive control 30 mM KCl (green), 15 nM pCTX (blue), or 2.5 µM MC-LF (red). The substance application was performed by a pipettor, images were taken by an automated microscope for 45 s, exported as .avi and analyzed by CaFFEE. The free intracellular Ca^{2+} is shown as the average Δ signal intensity tpeak - tbaseline. n=1 (B) The free intracellular Ca^{2+} of ten different cells is shown with their individual Δ signal intensity after the application of 30 mM KCl. (C) The free intracellular Ca^{2+} of ten different cells is shown with their individual Δ signal intensity after the application of 15 nM pCTX.

4.3. Paper 3: A human stem cell-derived test system for agents modifying neuronal N-methyl-D-aspartate-type glutamate receptor Ca^{2+}-signaling

published in *Arch Toxicol* (2021)

Stefanie Klima[1,2], Markus Brüll[1], Anna-Sophie Spreng[1,3], Ilinca Suciu[1,3], Tjalda Falt[1], Jens C Schwamborn[4], Tanja Waldmann[1], Christiaan Karreman[1], Marcel Leist[1,5]

[1] In vitro Toxicology and Biomedicine, Dept inaugurated by the Doerenkamp-Zbinden foundation, University of Konstanz, Konstanz, Germany

[2] Cooperative doctorate college InViTe, University of Konstanz, Konstanz, Germany

[3] Konstanz Research School Chemical Biology (KoRS-CB), University of Konstanz, Konstanz, Germany

[4] Developmental and Cellular Biology, Luxembourg Centre for Systems Biomedicine (LCSB), University of Luxembourg, 7, avenue des Hauts-Fourneaux, 4362 Esch-sur-Alzette, Luxembourg.

[5] CAAT-Europe, University of Konstanz, Konstanz, Germany

Key words: ketamine, MEA, phencyclidine, dextromethorphan, domoic acid, neurotoxicity, ibotenic acid

4.3.1. Abstract

Methods to assess neuronal receptor functions are needed in toxicology and for drug development. Human-based test systems that allow studies on glutamate signaling are still scarce. To address this issue, we developed and characterized pluripotent stem cell (PSC)-based neural cultures capable of forming a functional network. Starting from a stably proliferating neuroepithelial stem cell (NESC) population, we generate "mixed cortical cultures" (MCC) within 24 days. Characterization by immunocytochemistry, gene expression profiling and functional tests (multi-electrode arrays) showed that MCC contain various functional neurotransmitter receptors, and in particular the N-methyl-D-aspartate subtype of ionotropic glutamate receptors (NMDA-R). As this important receptor is found neither on conventional neural cell lines nor on most stem cell-derived neurons, we focused here on the characterization of rapid glutamate-triggered Ca^{2+} signaling. Changes of the intracellular free calcium ion concentration ($[Ca^{2+}]_i$) were measured by fluorescent imaging as main endpoint, and a method to evaluate and quantify signals in hundreds of cells at the same time was developed. We observed responses to glutamate in the low µM range. MCC responded to kainate and α-amino-3-hydroxy-5-methyl-4-isoxazolepropionic acid (AMPA), and a subpopulation of 50% had functional NMDA-R. The receptor was modulated by Mg^{2+}, Zn^{2+} and Pb^{2+} in the expected ways, and various toxicologically-relevant agonists (quinolinic acid, ibotenic acid, domoic acid) triggered $[Ca^{2+}]_i$ responses in MCC. Antagonists, such as phencyclidine, ketamine and dextromethorphan were also readily identified. Thus, the MCC developed here may fill an important gap in the panel of test systems available to characterize effects of chemicals on neurotransmitter receptors.

4.3.2. Introduction

Identification of compounds that interfere with ionotropic glutamate receptor signaling is important for the safety evaluation of drugs and environmental chemicals. Such information is of utmost toxicological relevance, as L-glutamate is the main excitatory neurotransmitter in the brain (Maycox *et al.* 1988, Fukaya *et al.* 2003). Therefore, modulation of glutamate signaling may lead to many adverse effects. The many receptors of this acidic amino acid can be divided into metabotropic receptors and ionotropic receptors. The latter group can be further subdivided into N-methyl-D-aspartate (NMDA) receptors and non-NMDA receptors (kainate and AMPA subtypes) (Traynelis *et al.* 2010).

The NMDA receptor (NMDA-R) plays a critical role in synaptic plasticity in the hippocampus, i.e. for memory and learning (Malenka *et al.* 1993, Morris 2013). Disturbed signaling of the receptor is assumed to contribute to neurodegenerative diseases (Alzheimer's disease, Huntington's disease) (DiFiglia 1990, Liu *et al.* 2019), neurological disorders like epilepsy and stroke (Lipton 1999, EpiPM 2015), and neuropsychiatric disorders like schizophrenia (Cohen *et al.* 2015). Therefore, several agonists, antagonist and modulators of the NMDA-R have been developed as drug candidates or pharmacological tools: NMDA has been identified as a specific agonist for the NMDA-R; the NMDA-R antagonist ketamine is used clinically as anesthetic (Sinner *et al.* 2008); the receptor blocker memantine is an approved medication for Alzheimer's disease (Witt *et al.* 2004); and some NMDA-R antagonists, e.g., phencyclidine (PCP) and dextromethorphan (DXM) produce hallucinogenic and dissociative symptoms, they are used as illicit recreational drugs (Williams *et al.* 2019).

Biochemically, the NMDA-R is a heterotetramer consisting of two different subunit classes, namely the glycin-binding NR1 (gene: *GRIN1*) and the glutamate-binding NR2 (Ulbrich *et al.* 2008). The latter has the different isoforms NR2A, NR2B, NR2C and NR2D (genes: *GRIN2A-D*) with distinct spatial and temporal expression patterns (Cull-Candy *et al.* 2001). Specifically, the subunit composition of the NMDA-R changes during the development of the CNS. Most changes occur prenatally. In human cortex and hippocampus, *GRIN2B* is expressed at relatively constant levels, while *GRIN2A* expression levels increase during brain development and early postnatal life (Bar-Shira *et al.* 2015). The heteromeric GRIN1/GRIN2B receptor is more prevalent amongst extrasynaptic NMDA-R than e.g. the GRIN1/GRIN2A complex (Tovar *et al.* 1999).

For receptor activation, sufficient occupancy of both the agonist (Glu) and the co-agonist sites (glycine or D-serine) needs to be reached (Johnson *et al.* 1987). In addition, the postsynaptic membrane has to be depolarized so that the physiological Mg^{2+} block is relieved (Cull-Candy *et al.* 2001). When the NMDA-R channel opens, Na^{+} and Ca^{2+} can enter the cell (Balu 2016). The influx of Ca^{2+} into the postsynaptic neuron triggers many specific signaling pathways (Papadia *et al.* 2007). The activity of the receptor as an ion channel can be inhibited with general antagonists of the glutamate site (e.g. AP5 (Hansen *et al.* 2018)), antagonists of the glycine site (e.g. kynurenic acid (Zhou *et al.* 2012)), specific antagonists against NR2 isoforms (e.g. traxoprodil selective for NR2B (Chenard *et al.* 1995))

or universal channel blockers, (MK801, memantine, PCP, DXM, ketamine (Hansen *et al.* 2018)).

As the NMDA-R is involved in many diseases and toxicological AOPs (Wang *et al.* 2017, Liu *et al.* 2019, Sachana *et al.* 2019, Tschudi-Monnet *et al.* 2019, Chen *et al.* 2020), agents interfering with its function are a major health concern and need to be identified. An *in vitro* test method for this purpose would ideally employ human cells and measure a physiological change directly linked to ionotropic glutamate receptors. There is a range of possibilities to establish test methods for glutamate receptor interactions. One extreme end of the spectrum are typical pharmacological binding assays, as used for advanced drug candidates (Berger *et al.* 2012, Pottel *et al.* 2020). The disadvantages of these assays are the uncoupling from the natural physiological environment, and that adversity is hard to define. On the other end of the spectrum are traditional animal studies. Besides issues of species correlation and ethical aspects, these models have disadvantages concerning the exact target definition and the throughput. In between, there are many cellular and tissue-based models (Hondebrink *et al.* 2016, Yamazaki *et al.* 2016, Nehme *et al.* 2018, Meijer *et al.* 2019). Some of them allow both measurements of very early events (in the sense of initial key events of an AOP), but also more complex downstream disturbances, as proxy for an adverse outcome.

Modeling the human brain for toxicity studies is challenging, as test systems should include the various cell types the human brain is composed of. This may be achieved by the generation of mixed neuronal cultures from pluripotent stem cells (Heikkilä *et al.* 2009, Russo *et al.* 2018, Sasaki *et al.* 2019). Such a test system should include excitatory and inhibitory neurons, to be able to form self-regulating neuronal networks that also can be modulated. Another important cell type are astrocytes, as they are important modulators of neuronal signaling (Ishii *et al.* 2017, Tukker *et al.* 2018). The *conditio sine qua non* is that (i) at least some of the cells express ionotropic glutamate receptors, in particular NMDA-R, that (ii) they react to known pharmacological agonists, and (iii) that this response can be quantified.

One commonly used method to investigate neurotransmitter activity is to measure their effect on the free intracellular Ca^{2+} concentration ($[Ca^{2+}]_i$) (Leist *et al.* 1998, Nicotera *et al.* 1999). To this end, cells are stained with a Ca^{2+}-sensitive dye and to record its fluorescence changes (Leist *et al.* 1997, Miyawaki *et al.* 1997, Volbracht *et al.* 2006, Karreman

et al. 2020). Another method is to culture cells on microelectrode arrays (MEA). These arrays record the extracellular field potential of cultured neurons and thereby give a comprehensive overview of the electric activity of cultured neuronal networks (Hogberg *et al.* 2011, Hofrichter *et al.* 2017, Vassallo *et al.* 2017, Strickland *et al.* 2018, Shafer 2019, Nimtz *et al.* 2020).

In the past, it has been notoriously difficult to set up cell-based test systems for NMDA-R, as the activity of this receptor can lead to cell death by excitotoxicity (Leist *et al.* 1998, Nicotera *et al.* 1999). Assays used in the past maintained the cells in the presence of antagonists that were washed out before testing (Bettini *et al.* 2010, Feuerbach *et al.* 2010, Guo *et al.* 2017). Repeated testing or follow-up of downstream effects is not possible in such systems. We therefore developed a novel mixed neuronal culture, in which NMDA-R expressing cells can survive. We set out to characterize this test system and to establish Ca^{2+} imaging as quantitative endpoint. Potential applications were demonstrated by assessment of agonists and by profiling of toxicologically relevant inhibitors.

4.3.3. Material and methods

Materials

L-glutamine, cAMP, apotransferrin, glucose, insulin, putrescine, selenium, progesterone, ascorbic acid, AP5, domoic acid, ketamine, quinolinic acid, traxoprodil, nicotine, dextromethorphan (DXM), MK801, and bicuculline were purchased from Sigma (St. Louis, USA). DMEM/F12, knockout serum replacement, Neurobasal, N2 supplement, B27 without ascorbic acid supplement, Glutamax, NEAA, ß-mercaptoethanol, HBSS, Triton-X-100, PBS, H-33342, FBS, Trizol, Fluo-4 Direct™ Calcium Assay Kit were purchased from ThermoFisher Scientific (Waltham, USA). GDNF, noggin, BDNF and NGF were purchased from R&D systems (Minneapolis, USA). Dorsomorphin, SB-431642, SU5402, ibotenic acid, NMDA, S-AMPA, phencyclidine (PCP), and kainate were purchased from Tocris (Bristol, UK). Chir99021 was purchased from Axon Medchem (Groningen, Netherlands); DAPT was purchased from Merck Millipore (Billerica, USA). Matrigel was purchased from Corning (Corning, USA); iScript and SsoFast™ EvaGreen® Supermix were purchased from BioRad (Hercules, USA). EdU click Kit was purchased from baseclick (Neuried, Germany). Purmorphamine (PMA) was purchased from Enzo (Farmingdale, USA). Veratridine was purchased from alomone labs (Jerusalem, Israel). TGFß was purchased from Peprotech (Rocky Hill, USA).

Differentiation and maintenance of NESC

The pluripotent stem cell line WA09 line (H9) (Thomson et al. 1998, Balmer et al. 2014, Dreser et al. 2020) was obtained from WiCell (Madison, WI, USA) and the line iPSC EPITHELIAL-1 (= Sigma 0028) was obtained from Sigma. The pluripotent stem cells were differentiated with a protocol adapted from Reinhardt et al. (Reinhardt et al. 2013) into neuroepithelial stem cells (NESCs) via embryoid body (EB) formation. To distinguish the differentiation protocols here, we used "days of differentiation prime" (DoD') for the generation of NESC from PSC, and "days of differentiation" (DoD) for the protocol leading from NESC to MCC. On DoD0' colonies of PSC were detached with accutase and transferred to non-coated dishes to spontaneously form EBs in EB medium (KnockOut DMEM, 25 % serum replacement, 2.5 mM L-glutamine, 1 x nonessential amino acids, and 100 µM µM ß-mercaptoethanol) supplemented with 10 µM SB-431542, 1 µM dorsomorphin, 3 µM CHIR99021, and 0.5 µM purmorphamine. On DoD2', medium was changed to differentiation medium (N2B27 medium: 50% Dulbecco's modified Eagle's medium/F12 [DMEM/F12], 50% Neurobasal medium, 2 mM L-glutamine, 1x B27 without vitamin A, and 1x N2 (all purchased from Gibco, Carlsbad, USA)) supplemented with 10 µM SB-431542, 1 µM dorsomorphin, 3 µM CHIR99021, and 0.5 µM purmorphamine. On DoD4' medium was changed to NESC maintance medium (N2B27 medium supplemented with 150 µM ascorbic acid, 3 µM CHIR99021, and 0.5 µM purmorphamine). At DoD6', EBs were disaggregated, transferred to matrigel coated 6-well plates in a 1:6 dilution, and cultured for seven days with a medium change (NESC maintance medium) every other day. After seven days, cells were detached with accutase and split in a 1:5 ratio. Cells were always split when reaching a confluency of 80%. After three passages, NESCs were cryopreserved in NESC maintenance medium containing 10 % DMSO without serum addition. This allowed the production of working stocks of the same NESCs. For maintaining a NESC population, cells were thawed and cultured in NESC maintenance medium with medium changes every other day. Cells were split when a confluency of about 75% was reached. Cells were used for differentiation into MCCs between passage 4 and 20.

Differentiation of MCCs from NESCs

A single-cell suspension of NESC was seeded at a density of 28,000 cells/cm^2 on Matrigel-coated plates in NESC maintenance medium. After two days, defined here as day of differentiation 0 (DoD0) the medium was replaced by neuronal differentiation medium (N2B27 supplemented with 10 ng/ml BDNF, 10 ng/ml GDNF, 1µM TGFß3, 500 µM cAMP, 200 µM ascorbic acid). Under these conditions, cells were left to differentiate into MCCs for > 20 days. On DoD2, DoD4, DoD7, half of the medium was changed. After this time, half of the medium was changed twice a week.

Differentiation of peripheral neurons

The iPSCs were differentiated into immature dorsal root ganglia neurons according to Hoelting *et al.* (Hoelting *et al.* 2016) with the following minor changes. Cells were seeded at a density of 90,000 cells/cm^2 on Matrigel. The differentiation was started by addition of neural differentiation medium (KSR-S; Dulbecco's modified Eagle's medium [DMEM/F12] with 15% knockout serum replacement, 1 x Glutamax, 1 x nonessential amino acids, and 50 µM ß-mercaptoethanol) supplemented with 17.5 ng/ml noggin, 10 µM SB-431642 from DoD0 to DoD5. From DoD2 on, the three small molecules CHIR99021 (1.5 µM), SU5402 (5 µM) and DAPT (5 µM) were added. Starting at DoD4', medium was gradually replaced by N2-S medium (DMEM/F12, with 2 mM Glutamax, 0.1 mg/ml apo-transferrin, 1.55 mg/ml glucose, 25 mg/ml insulin, 100 mM putrescine, 30 nM selenium, and 20 nM progesterone). After differentiating for nine days, the cells were cryo-preserved. The cells were thawed and subsequently seeded at a density of 100,000 cells/cm^2 in 25% KSR-S and 75% N2-S supplemented with 1.5 µM CHIR99021, 5 µM SU5402 and 5 µM DAPT. On DoD1 and DoD2, 50% of the medium was changed. On DoD3 and DoD4 cells received N2-S medium, supplemented with 25 ng/ml BNDF, 25 ng/ml GNDF and 25 ng/ml NGF and 2 µM AraC for further differentiation and maturation, with medium changes every three days.

Measurement of changes in intracellular Ca^{2+} concentrations

MCCs or peripheral neuron precursors were seeded in 96-well plates and differentiated as described above. Before measuring the changes in the concentration of intracellular free Ca^{2+} ($[Ca^{2+}]_i$), differentiation medium was changed to artificial cerebrospinal fluid (aCSF): NaCl [140 mM], KCl [3 mM], $CaCl_2$ [2.5 mM], $MgCl_2$ [1 mM], Na_2HPO_4 [1.2 mM], pH 7.4 and the cells were loaded with Fluo-4 Direct™ Calcium Assay Kit and H-33342 for 30

min at 37°C. For experiments requiring a pre-incubation phase, loading with Fluo-4 was performed in parallel. The changes in $[Ca^{2+}]_i$ were monitored with a VTI HCS microscope (ThermoFisher Scientific, Pittsburgh, USA) equipped with an incubation chamber providing an atmosphere with 5% CO_2 at 37°C. Test compounds were administered by an automated pipettor at 10 s after the first picture was taken. Images were taken as fast as possible for 45 s (approx. one image/second) and exported as .avi video files. The video files were afterwards analysed with the CaFFEE software (Karreman *et al.* 2020) to obtain single cell time-course information on $[Ca^{2+}]_i$.

Microelectrode array recordings

NESCs were seeded at a density of 25,000 cells/7 µl drop on Matrigel-coated 24-well CytoView MEA plates (16 electrodes per well). After 1 h, the well was filled up with 500 µl medium. The cells were then allowed to differentiate as described above. For time course experiments, the same plates were measured on different days. All plates were equilibrated for 10 min prior to recording (Maestro Edge, Axion Biosystems, Atlanta, USA), followed by 30 minutes of baseline recording. After the baseline recording agonists/antagonists were added and recording was continued for another 30 minutes. All compounds were applied in 250 µl of neuronal differentiation medium. All recordings were captured using the Axion Integrated Studio Navigator (Axion Biosystems, Atlanta, USA) with a recording chamber at 37°C and 5% CO_2. For raw data acquisition, signals from all electrodes were recorded simultaneously with a sampling frequency of 12.5 kHz/channel. The recorded raw files were converted offline from voltage traces into various time-dependent data sets, such as spiking frequency, etc. The threshold spike detector was set to 5.5x of the noise level (signal SD) on each electrode, using adaptive threshold crossing for spike detection. Bursts were detected by setting inter-spike intervals (ISI) to ≤ 100 ms and requiring minimum 5 spikes per second. Network bursts were defined by the same ISI of 100 ms, a minimum of 50 spikes per second and at least 60% of active electrodes involved in bursting. To analyze the acute effects of agonists and antagonist, the number of spikes was binned (bin size = 0.1 s) and shown over time in comparison to baseline.

Immunofluorescence staining and microscopy

Cells were grown on Matrigel-coated coverslips and fixed with 4% paraformaldehyde. Then, they were permeabilised in 0.3% Triton X-100 and blocked for 1 h in PBS containing 5% fetal bovine serum and 0.1% Triton X-100. Primary antibodies (see Tab. 5.3.S2) were

administered for 1 h at room temperature, followed by washing and incubation with secondary antibodies and Hoechst H-33342 for 30 min. Images were taken at a Zeiss Axio Observer with ZEN 2 pro blue edition software or a Zeiss LSM 880 and further processes with ImageJ (Version 1.52p).

RNA extraction, cDNA synthesis and real-time qPCR

The extraction of total RNA was performed with TRIzol, according to the manufacture's protocol, followed by the reverse transcription of 1 µg total RNA with iScript. cDNA was quantified using the SsoFast™ EvaGreen® Supermix. The threshold cycle (C_T) was determined for each sample, using the CFX data analysis software (Bio-Rad, USA). Reference genes were used and mRNA levels of different genes of interest were compared to them at different time points of the differentiation using the ΔΔ method (Livak *et al.* 2001). For a detailed list of primers used in this study see Tab. 5.3.S3.

Transcriptome data generation and analysis

Sample preparation was performed by removing the medium from each well and lysing the cells immediately in 25 µl of 1x Biospyder lysis buffer (BioSpyder Tech., Glasgow, UK). Samples were stored at -80ºC until shipment to Bioclavis (BioSpyder Tech., Glasgow, UK) on dry ice. Transcriptomics data were determined by TempO-Seq technology (BioSpyder Tech., Glasgow, UK), a targeted RNA-sequencing method developed by BioSpyder Technologies, Inc. (House *et al.* 2017). The set of genes analyzed, and the read data are detailed in supplement file 2, organized as Excel workbook, including labelling and clear explanations.

For the data analysis, the R package DESeq2 (v1.24.0) was employed (Love *et al.* 2014). The DESeq2 object was constructed from raw counts of mRNA species and its size factors were normalized to total sample counts per million (CPM). The statistical analysis of differential gene expression in the treatment group (against the DMSO control group) was done with the Wald test. In order for a gene to be considered significantly deregulated, the threshold of Benjamini-Hochberg adjusted p-values was set to ≤ 0.05. A cutoff for fold changes (FC) was not introduced. Over-representation analysis of gene ontology terms (GO) was based on Fisher's F-test as implemented in g:profiler software (Raudvere *et al.* 2019).

Statistics

Experiments were performed at least on three cell preparations, with several technical replicates for each cell batch. Descriptive statistics, transparent display of the data structure and experimental variability was included in display figures and supplementary information. For significance testing, GraphPad Prism 5 software (Version 7.04, Graphpad Software, Inc, San Diego, USA) was used. Data were evaluated by Fisher's exact test or by t-test (when two groups were compared). P-values <0.05 were regarded as statistically significant.

4.3.4. Results

Generation and phenotyping of mixed cortical cultures (MCCs)

To generate mixed cortical cultures (MCCs) expressing neurotransmitter receptors, we used a two-step protocol. First, pluripotent stem cells (pSCs) were differentiated into a proliferating neuroepithelial stem cell population (NESC) (Fig. 5.3.S1) (Reinhardt *et al.* 2013). These cells did not express the pluripotency markers NANOG and OCT4 and could be cultivated for up to 20 passages (Fig. 5.3.S1B). During this time, the expression of typical NESC markers HES5, PAX6, and DCX was stable (Fig. 5.3.S1C), while PAX3 and NES even increased expression levels (Fig. 5.3.S1D). The activity of cell cycle genes (CDK1, CDK2, CCND1, and CCND2) remained constant (Fig. 5.3.S1E). Immunostaining confirmed the presence of Sox1, Pax3, Pax6, doublecortin, and nestin protein, as well as of the proliferation marker Ki67 (Fig. 5.3.S1F).

In the next step, NESCs were differentiated for >20 days by addition of the five differentiation factors: BDNF, GDNF, cAMP, TGFß3 and ascorbic acid (Fig. 5.3.1A). During the time course of differentiation, the cells acquired following features of mature neurons: (i) they formed a neuronal network with a complex and extensive neurite structure (Fig. 5.3.S2A); (ii) the typical marker of post-mitotic neurons, RBFOX3 (Fig. 5.3.1B), and synaptic markers, like SLC17A6, SYN, DLG4 (Fig. 5.3.1C) were upregulated. This was paralleled by the protein expression of NeuN (the product of the RBFOX3 gene), Map2, ßIII-tubulin, and synaptophysin (Fig. 5.3.S2B,C). The MCCs also included glial cells, as indicated by the gene expression of GFAP and S100ß (Fig. 5.3.1D) and immunopositivity for S100ß (Fig. 5.3.S2D); (iii) subunits of the NMDA-R (GRIN1, GRIN2A, and GRIN2B) increased their expression levels over differentiation time (Fig. 5.3.1E). The vesicular glutamate transporter 1 (vGlut1), a marker of glutamatergic neurons (Ito *et al.* 2015), was

strongly expressed in MCCs (Fig. 5.3.1F); (iv) MCCs contained only 1 % of dividing cells (Fig. 5.3.1G), while 40 % of NESC incorporated EdU within the same labelling period. (Fig. 5.3.S2D). Thus, the cells were mostly postmitotic, which is a defined feature of neurons.

The most important functional features of mature neurons are their individual electrical activity and the formation of functional networks (Hogberg *et al.* 2011, Strickland *et al.* 2018). To examine this, MCCs were cultured on MEA, and their spontaneous electrical activity was recorded on different DoDs. Network bursts were observed from about DoD18 on. The frequency increased until DoD24 and then remained stable until DoD32. The number of spikes included in a burst increased slightly from DoD18 until DoD32. The same was observed for the synchronicity coefficient, a measure of coordination between different areas of the network (Fig. 5.3.1H). These data show that MCCs were electrically active, and that their network properties required at least three weeks to develop. To test whether the spontaneous network activity could be modified by pharmacological intervention, DoD24 MCCs were treated with the $GABA_A$ antagonist bicuculline (BIC). The application of 1 µM BIC resulted in a massive increase in spike frequency as acute response (Fig. 5.3.1I). This period of pronounced electrical activity was followed by a short period of anergy (approx. 550 s) and then established a new steady state that showed higher activity than the untreated control cultures (Fig. 5.3.1E). All these features show that MCCs represent a mature neuronal culture, comprising various types of neurons (e.g. glutamatergic and GABAergic).

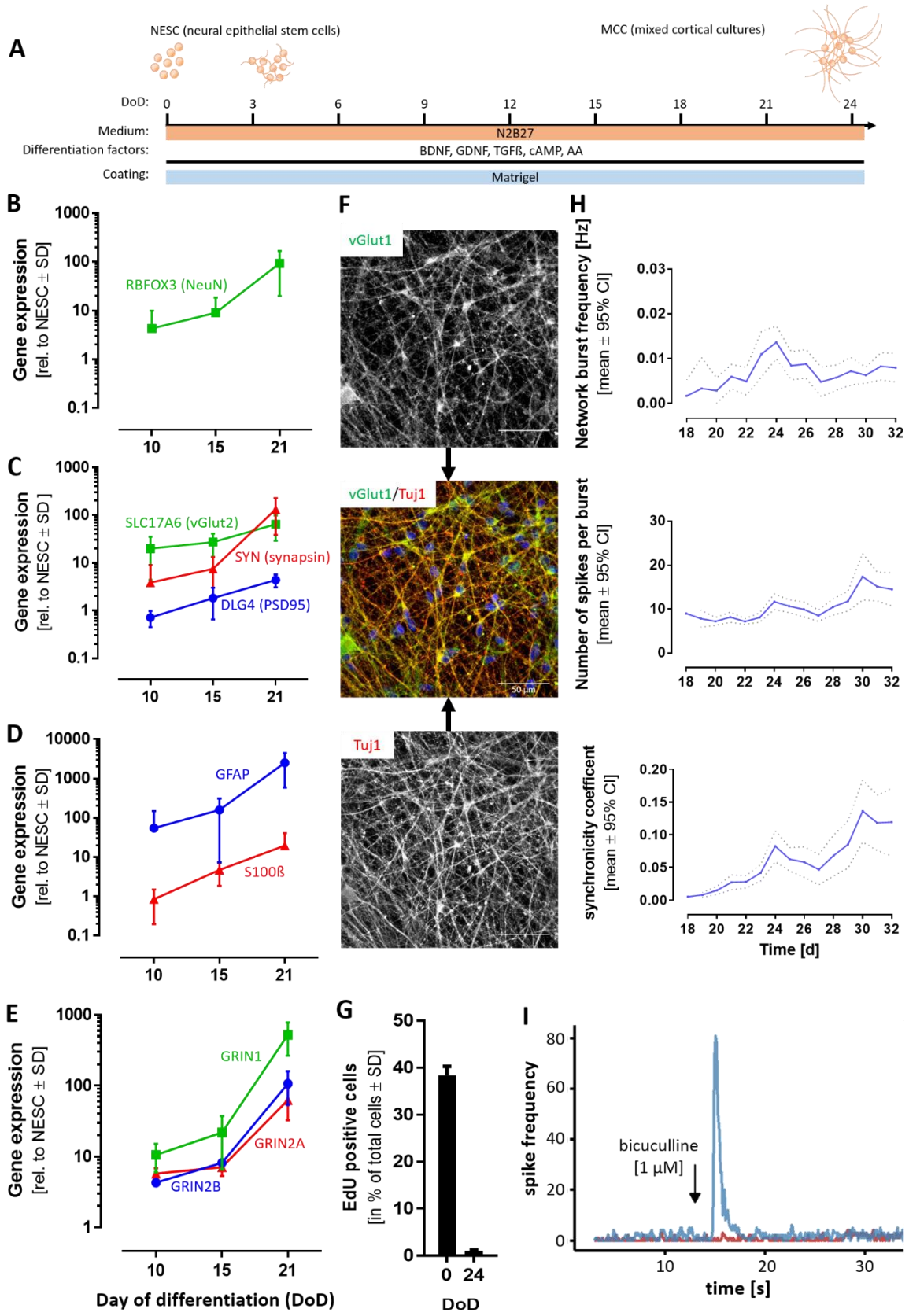

Fig. 5.3.1: Characterization of mixed cortical cultures (MCCs)

Mixed cortical cultures (MCCs) were generated from NESCs according to Reinhardt et al. (Reinhardt *et al.* 2013), by differentiating them for > 20 days on Matrigel in neuronal differentiation medium. (**A**) Schematic display of MCC differentiation (BDNF – brain-derived neurotrophic factor, GDNF – glia cell-derived neurotrophic factor, TGFß – transforming

growth factor beta, cAMP - cyclic adenosine monophosphate, AA – ascorbic acid). (**B**) Gene expression profile of the neuronal marker RBFOX3. Gene expression was quantified by real-time PCR. Data are given relative to the NESC starting population (=DoD0) for the DoD10, DoD15 and DoD21; (**C**) Gene expression of synaptic markers. Gene expression (**D**) of glial markers and of (**E**) NMDA receptor sub-units NR1 (*GRIN1*), NR2A (*GRIN2A*) and NR2B (*GRIN2B*). All data are means ± SD of 3 biological replicates. (**F**) Immunofluorescence image of MCCs on DoD24 using antibodies against the neuron-specific cytoskeletal marker beta-III-tubulin (Tuj1) and the vesicular glutamate transporter 1 (vGlut1). The composite images also includes the nuclei stained with H33342 (blue) Scale bar: 50 µm. (**G**) Cells on DoD0 and DoD24 were allowed to incorporate the nucleotide analog EdU, to visualize mitotic activity. EdU-positive cells were counted and are shown as percentage of total cell number ± SD. (**H**) MCCs were differentiated on MEA plates. Spontaneous spikes of electrical activity were recorded on various days of differentiation for the same cells. Form these activity measurements (30 min each day), the parameters "network burst frequency", "number of spikes per burst", and "synchronicity coefficient" were calculated and plotted over time. (**I**) On DoD24 MCCs on MEAs were treated with the $GABA_A$ receptor antagonist bicuculline [1 µM] (blue, addition is indicated by the black arrow, baseline in red). The generation of spikes was recorded directly before and after administration, the number of spikes was binned (bin size 0.1 s) and a representative example of the acute response is shown. A full set of data over an extended time span is presented in Fig. 5.3.*S*2.

Gene expression profiling of MCCs

Throughout this work, two cell lines were used. They behaved phenotypically in a similar way. Here, transcriptome data were used to further explore their similarity. A first overview of the data structure was obtained by a principle component analysis (PCA) (Fig. 5.3.2A). NESC and MCC differed clearly from pluripotent source cells. The differentiation process moved NESC of both lineages in a similar way along the first principal component axis (PC1). NESC of the two cell lines showed some differences, but the final MCC populations were overlapping in their profiles. This analysis also showed that the differentiation was highly reproducible, as 16 samples from two cell lines yielded highly similar MCC populations.

To get a closer insight into neuronal characteristics of MCCs, absolute expression values for genes related to neuronal lineages, neurotransmitters, and non-neuronal lineages were compared. This analysis showed that pan-neuronal markers (like NEFL, MAPT, and MAP2) had a higher expression in MCCs than in NESC. Genes related to glutamate receptors (like GRIA, GRIK, GRIN and SLC17A6/7) were hardly expressed in NESC but were highly expressed in MCCs. Also, genes coding for GABA receptors (GABR) or synaptic markers were higher expressed in MCCs than in NESC. Furthermore, some genes related to the astrocyte lineage (SLC1A2/3, S100ß, MAOB) were upregulated. In contrast to this, the expression of neural crest genes and stem cell genes remained low and unchanged.

Importantly, genes coding for proteins from other tissues, like liver (CYPs), were not expressed in MCCs (Fig. 5.3.2B).

To allow a first overview of relative regulations, the ratios of NESC vs MCC expression were calculated. This confirmed the general picture evident from an overview of the absolute levels. These regulation data provided additional evidence of the robustness of the differentiation protocol, and revealed some minor differences between the cell lines. For instance, Sigma 0028 derived cells seemed to produce more mature astrocytes (AQP4, GFAP expression). This was however not followed up here, as the focus of our study was on neuronal (excitatory) signaling. In summary, this gene expression pattern was well in line with a mixed culture of neurons, with a machinery in place for excitatory (glutamate) and inhibitory (GABA) neurotransmission. To investigate the similarity of the two cell lines used here (Sigma 0028 and H9) in more detail, their differentially expressed genes (DEGs) were plotted against each other. This scatter plot showed a high correlation (Fig. 5.3.S3A), and a clustering analysis of the various cell populations confirmed that MCCs from both lineages clustered together, while they separated well from their precursors (Fig. 5.3.S3B). As the variation between the two lines was not larger than variations between individual preparations of one line, we did not distinguish cell lines in the further course of our studies.

Besides looking at preselected neural and non-neural genes, we also took an unbiased approach to gene expression analysis: The overall number of DEGs from the 3257 analyzed genes were determined (about 600 DEGs) (Fig. 5.3.2C), and the genes that were most upregulated or downregulated (on a fold change basis) were compiled (Fig. 5.3.2D). Among the 20 most upregulated DEGs were the neurotransmitter receptors and channels SLC17A6, SCN2A, GABRA2, GRIN1, GRIA2, and GRIN2B. The most upregulated (about 300-fold) gene was CNTN1, a glycoprotein specific for neurons. Among the 20 most downregulated DEGs were genes involved in the Wnt/beta-catenin pathway (like FZD10), as well as GLI1, TERT, LEF1, HES3 which are involved in stem cell/precursor cell biology. Also HOXB1, a regulator for neural crest cells was strongly downregulated when NESCs were differentiated to MCCs. Genes generally involved in the cell cycle (E2F2, INHBE, FOXM1) were also amongst the most downregulated (Fig. 5.3.2D).

We also performed a gene ontology overrepresentation analysis. This resulted in over 400 overrepresented gene ontologies (oGOs) amongst upregulated DEGs. We assigned the

50 oGOs with lowest p-value to the four key biological processes (KBPs) “neurodevelopment”, “neuronal subtypes (glutamate)”, “synapse”, and “neurotransmitter” according to Waldmann *et al.* (Waldmann *et al.* 2014) (Fig. 5.3.S3C). Following our interest in a test system that may be used to assess glutamate signaling, we looked for the genes common to the four KBPs. This resulted in a set of 14 genes (Fig. 5.3.S3D). Most of them were subunits of glutamate receptors or were involved in synapse function or formation (Fig. 5.3.2E). Five genes were in the KBP “neuronal subtypes (glutamate)” but not the all other KBPs (Fig. 5.3.S3E). For completeness, we also examined the 20 oGOs with the lowest p-value for downregulation. They all dealt with regulation of cell cycle (supplement 2), which confirms the conversion of a proliferating precursor population (NESC) to (postmitotic) neurons (MCC).

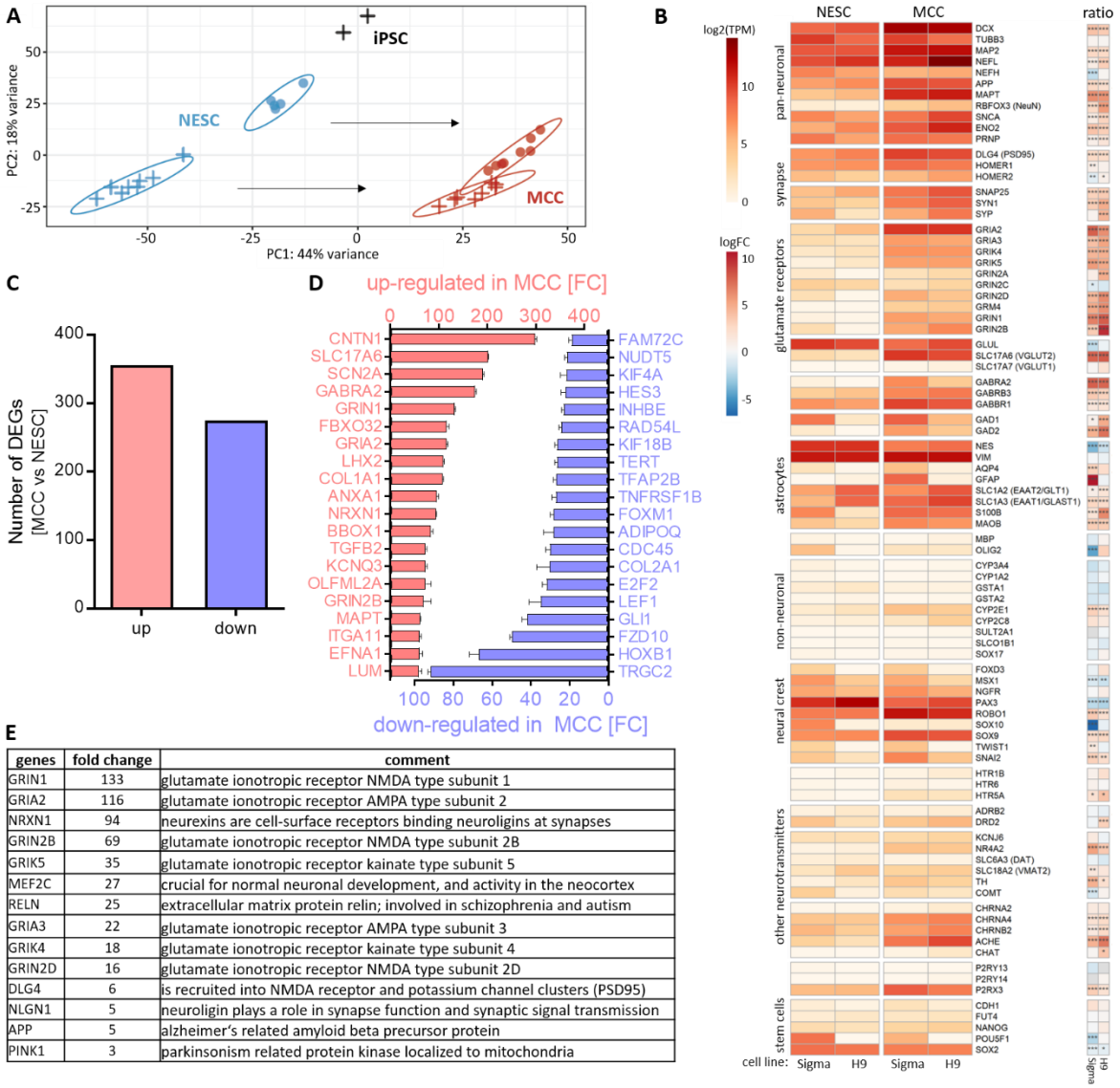

E

genes	fold change	comment
GRIN1	133	glutamate ionotropic receptor NMDA type subunit 1
GRIA2	116	glutamate ionotropic receptor AMPA type subunit 2
NRXN1	94	neurexins are cell-surface receptors binding neuroligins at synapses
GRIN2B	69	glutamate ionotropic receptor NMDA type subunit 2B
GRIK5	35	glutamate ionotropic receptor kainate type subunit 5
MEF2C	27	crucial for normal neuronal development, and activity in the neocortex
RELN	25	extracellular matrix protein relin; involved in schizophrenia and autism
GRIA3	22	glutamate ionotropic receptor AMPA type subunit 3
GRIK4	18	glutamate ionotropic receptor kainate type subunit 4
GRIN2D	16	glutamate ionotropic receptor NMDA type subunit 2D
DLG4	6	is recruited into NMDA receptor and potassium channel clusters (PSD95)
NLGN1	5	neuroligin plays a role in synapse function and synaptic signal transmission
APP	5	alzheimer’s related amyloid beta precursor protein
PINK1	3	parkinsonism related protein kinase localized to mitochondria

Fig. 5.3.2: Transcriptome analysis of NESC and MCCs

Neuroepithelial stem cells (NESCs) from two pluripotent stem cell lines (H9 and Sigma iPSC) were differentiated into mixed cortical cultures (MCCs), and mRNA was prepared for transcriptome analysis. A set of about 3500 genes was used for targeted RNAseq analysis (TempOSeq method), and expression levels were obtained for four independent cell preparations (some with two samples per cell preparation). (**A**) A PCA was obtained for the three developmental stages, iPSC (n=2), NESCs (n=4), and MCCs (n=4).The H9-derived cells are indicated by a filled circle. A cross indicates Sigma hiPSC-derived cells. The axes are scaled according to the variance covered and the black arrows indicate the main differentiation effect in the 2-dimensional PCA space. (**B**) The heatmap shows the expression of selected neuronal, non-neuronal and stem cell markers for two cell lines (H9, and Sigma iPSC). Data to the left are given as absolute expression values in transcripts per kilobase million (TPM). In the small heatmap to the right data are given on a $\log_2$ fold change (FC) scale with MCC relative to NESC where red colours indicate increased expression in MCC. * = padj < 0.05, ** = padj < 0.01, *** = padj < 0.001. (**C**) Number of differentially expressed genes (DEGs) from the overlap of H9-derived cells and iPSC-derived cells is shown for upregulations (red) and downregulations (blue) with an adjusted p-value ≤ 0.05. (**D**) Out of the DEGs in C, the top 20 up-regulated and down-regulated genes according to their fold change (FC) are shown. The error bars represent the standard deviation. (**E**) All upregulated DEGs with an adjusted p-value ≤ 0.05 and log2FC >1 were analyzed for over-represented gene ontology (GO) terms (Raudvere *et al.* 2019). GO terms with a size between 4 and 1000 genes were included in further analysis. The first (lowest p-value) 50 GOs of the category biological process were further assigned to the four key biological processes "neurodevelopment", "synapse", "neurotransmitter", and "neuronal subtype (glutamate)". The 14 genes relating to the glutamate system, and being involved in the other three key biological processes are listed with their respective fold change and a short description for each gene. More data are displayed in Fig. 5.3.S3.

Establishment of Ca^{2+} measurements as test endpoint

The hallmark of mature neurons is their communication by neurotransmitters. As excitatory neurotransmission is associated with a change in the intracellular free Ca^{2+} concentration ($[Ca^{2+}]_i$) (Leist *et al.* 1998), this process can be investigated by Ca^{2+} imaging (Tsien *et al.* 1990). Therefore, we set out to establish Ca^{2+} imaging as endpoint in the MCC test system. Initially, we used standard approaches to depolarize cells, such as an increase of K^+ ions in the medium, or the opening of Na^+ channels by the alkaloid veratridine (Scholz *et al.* 2011, Hoelting *et al.* 2016). The application of KCl [30 mM] (Fig. 5.3.3A) or veratridine [100 µM] (Fig. 5.3.3B) triggered a fast and strong increase in $[Ca^{2+}]_i$ in all individual cells. As data, obtained from a large number of cells over time, requires further processing to allow quantification, we took two steps into this direction. First, a dedicated software (Karreman *et al.* 2020) identified the peak time point. Then fluorescence data were obtained for the ground state (F_0) of each cell and for the peak time point (F_1). Second, we compared the different approaches of the scientific literature (F_1-F_0; F_1/F_0; F_1/F_0-1) to calculate the fluorescence offset (Fig. 5.3.3C, D, E). A simple subtraction of F_0 from F_1 ($\Delta F = F_1$-F_0) was found to give the best separation of stimulated cells (KCl, veratridine) and cells

exposed only to buffer (HBSS) (Fig. 5.3.3C, D, E). This way, Ca^{2+} imaging allowed capturing signal changes in the complex MCC cultures.

In order to determine for an individual cell, whether it reacted to a stimulus, or not, we took a statistical approach to define an activation threshold. For this purpose, the Δ signal intensity values of >2600 cells treated with HBSS were collected, and the data distribution, including average and the standard deviation of this data set, was determined (Fig. 5.3.S4A). A range of three standard deviations was defined as the noise band on top of the data means. Based on this, the upper noise level was a $\Delta F = 9$ (Fig. 5.3.S4B). Every cell with a Δ signal intensity value ≥9 was defined as a reactive cell. According to this approach, our endpoint had a false positive rate of 3.6% (Fig. 5.3.S4C). When typical traces of cells treated with HBSS were followed over time (instead of peak time measurements), they did not cross the threshold of 9 at any time point (Fig. 5.3.S4D). Based on the above procedure and findings, we used the signal threshold of 9 for further experiments to define reactive cells.

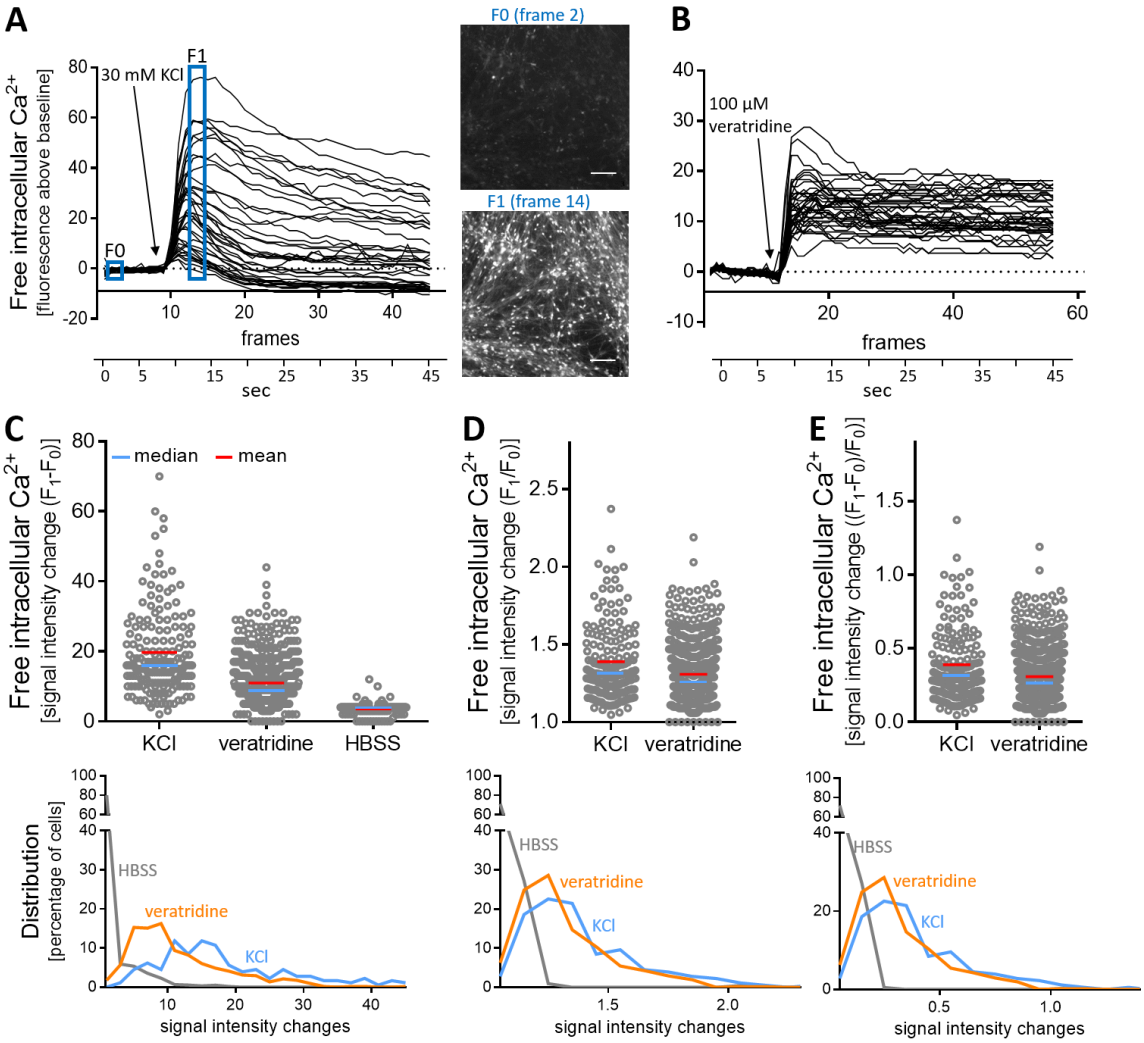

Fig. 5.3.3: Quantification of Ca2+ imaging signals of control stimuli in MCCs

MCCs were used after a 24 day differentiation period for Ca^{2+} imaging. (**A**) Cells were depolarized with KCl [30 mM] and the fluorescence of the intracellular Ca^{2+} indicator was recorded over time. Raw data were processed by an imaging software that automatically identified cell bodies and produced fluorescence-time traces for every cell of the image field. These time traces were then aligned for baseline fluorescence (non-stimulated state), which was set to "zero". This way, traces of absolute fluorescence changes (Δ signal intensity traces of 40 randomly selected cells are shown) due to the stimulus are displayed. To give an impression of the non-normalized data structure, fluorescence images at time point F_0 and F_1 are shown. Scale bar: 100 µm. (**B**) MCCs were treated with veratridine [100 µM] and data were processed as in A. (C-E) To quantify the data, Δ signal intensity values were calculated from the baseline (F_0) and peak (F_1) data with three different methods: (**C**) F_1-F_0, (**D**) F_1/F_0, and (**E**) (F_1-F_0)/ F_0. The upper row shows the data distribution on a "per cell" basis. The lower row shows how signal intensity changes (bins of 3 fluorescence units) were distributed over the cell population.

Quantification of excitatory neurotransmitter response in MCCs

MCCs were exposed to low concentrations of glutamate on DoD24, and ≥ 5 µM glutamate led to a significant increase in the amount of reacting cells. At a concentration of 10 µM glutamate, 78% of cells were reactive (Fig. 5.3.4A). To confirm the specific response to

glutamate by another well-established method, we measured the spike frequency on MEA after exposure of MCCs on DoD24 to glutamate [10 µM]. A clearly positive response was observed. (Fig. 5.3.4B). For a selective stimulation of NMDA-R, we administered increasing concentrations of NMDA to MCCs. This resulted in a significant number of reactive cells at concentrations of ≥ 10 µM. At 50 µM NMDA, half of all cells were reactive (Fig. 5.3.4C). Moreover, the addition of NMDA [50 µM] was followed by a strong increase of the spike frequency on MEA (Fig. 5.3.4D). From the above data, we conclude that approx. 80% of MCCs express functional ionotropic glutamate receptors, and about 50% of the cells had a sufficient NMDA receptor expression to allow $[Ca^{2+}]_i$ responses. We pre-incubated MCCs with 10 µM glycine or 10 µM D-serine followed by glutamate [10 µM] or NMDA [50 µM] administration. The percentage of reactive cells did not change when cells were pre-incubated with the co-agonists (data not shown). Thus, exogenously added glycine or D-serine had no influence on the above-described effects of glutamate and NMDA.

In the next set of experiments, we selected potential negative controls to ensure the specificity of the NMDA response in MCCs. For this purpose, a strong activator of non-glutamate ionotropic receptors was used. We chose nicotine, as a nAChR ligand. Concentrations up to 50 µM (50x the known EC_{50}) did not trigger a $[Ca^{2+}]_i$ response (Fig. 5.3.S5A). In another approach, we used human peripheral neurons. The positive control KCl [10 mM] triggered a pronounced increase in $[Ca^{2+}]_i$. No response was observed after the administration of NMDA [50 µM] (Fig. 5.3.S5B). Taken together these data show that MCCs contain a population of neurons that express functional NMDA-R, and react to an NMDA stimulus, but not e.g. to nicotine. A strong immediate reaction to NMDA is not observed in many stem cell-derived cultures, as also shown here for otherwise well-developed peripheral neurons.

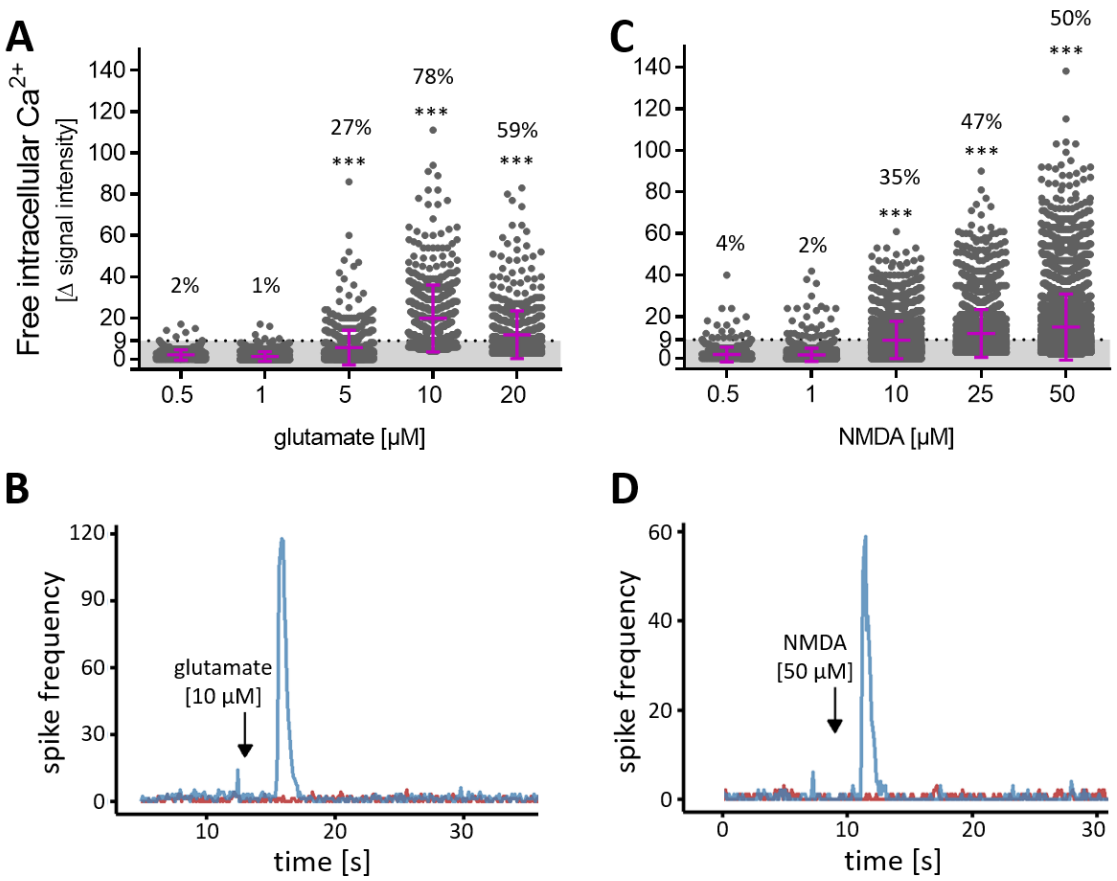

Fig. 5.3.4: Concentration-dependent response of MCCs towards glutamate and NMDA

MCCs were differentiated for 24 days and subsequently used for Ca^{2+} imaging. (**A**) The changes of Ca^{2+} indicator fluorescence (= delta signal intensity) of each individual cell treated with glutamate is shown as a dot. The mean ± SD is shown in purple. The threshold of Δ signal intensity (≥ 9) is shown as dotted line the number above each bar indicates the percentage of cells with a Δ signal intensity above the threshold (=defined as reactive cell). Significance was tested with Fisher's exact test; *** = p-value < 0.001 relative to the lowest concentration. (**B**) On DoD24 MCCs on MEAs were treated with glutamate [10 µM] (blue, addition is indicated by the black arrow; baseline in red). The generation of spikes was recorded directly before and after administration and the number of spikes was binned (bin size 0.1 s). A respective example of the acute response is shown. (**C**) The changes of Ca^{2+} indicator fluorescence (= delta signal intensity) of each individual cell treated with NMDA is shown as a circle. The mean ± SD is shown in purple and the number above each bar indicates the percentage of cells that are activated. Significance was tested with Fisher's exact test; *** = p-value < 0.001 relative to the lowest concentration. (**D**) On DoD24 MCCs on MEAs were treated with NMDA [50 µM] (blue, addition is indicated by the black arrow; baseline in red). The generation of spikes was recorded directly before and after administration and the number of spikes was binned (bin size 0.1 s). A respective example of the acute response is shown.

Investigation of ionotropic glutamate receptors in MCC cultures

For further investigation of the functionality of the NMDA-R in MCCs, we used different receptor agonists and antagonists that have been often used in pharmacology and toxicology for system characterization. For instance, ketamine binds to the dizocilpine site of the

NMDA-R (Sinner *et al.* 2008) and thereby inhibits the ion influx of Na^+ and Ca^{2+} into the post-synaptic neuron in a voltage-dependent manner (MacDonald *et al.* 1987). Ketamine is also used as a tool compound in schizophrenia research, as it models several disease symptoms. As NMDA-R dysfunction is considered an important basis of schizophrenia (Balu 2016), a system showing clear effects of such drugs can benefit this research. MCCs pre-incubated with ketamine [50 µM] had a completely blunted $[Ca^{2+}]_i$ response after NMDA [50 µM] application (Fig. 5.3.5A, B). To further control these data, we performed quantifications over the entire time course of several differentiations. This fully confirmed our findings for the peak time. For cells reactive to NMDA [50 µM] there was a fast increase in Δ signal intensity and a slower decline. In the presence of ketamine, we did not observe a signal, also after a considerable delay (Fig. 5.3.5C). The defined pharmacological responses to NMDA with/without its antagonist (ketamine) were used to confirm and refine our quantification approach for pharmaco-toxicological studies: Single-cell fluorescence quantification showed that not all cells reacted to the same extent. MCCs treated with NMDA [50 µM] showed a wide spread of Δ signal intensity, and about half of the cells remained below the activation threshold (Fig. 5.3.5D). MCCs most likely contain cells (e.g. glia or immature neurons) that do not react to NMDA. The quantification should ideally focus on the subpopulation of neurons with functional glutamate receptors. Therefore, we defined here the pool of absolutely non-reactive cells to be 20%, as this percentage did not react to glutamate [10 µM] (Fig. 5.3.4A). It was considered unlikely that cells would react to NMDA, but not to glutamate. Based on this assumption, the non-reactive population baseline (corresponding to 20% of all cells in a field) was removed from the analysis. This correction step had no visible effect on the apparent distribution and average signal intensity of cells treated with HBSS. For cells exposed to NMDA [50 µM] the average signal slightly increased and the lower boundary of the signal intensities was slightly higher. Cells pre-incubated with ketamine [50 µM] prior to NMDA [50 µM] behaved similar to those exposed to solvent (HBSS) (Fig. 5.3.5E). The frequency distribution of reactive cells showed that only after exposure to NMDA, there were Ca^{2+} signals above the threshold. For HBSS and ketamine pre-incubation, more than 95% of cells had a signal intensity change value below the baseline (≤ 9) (Fig. 5.3.5F). When the baseline-subtracted data set was used to calculate the percentage of reacting cells, an excellent signal separation (NMDA vs NMDA + ketamine) was obtained (Fig. 5.3.5G).

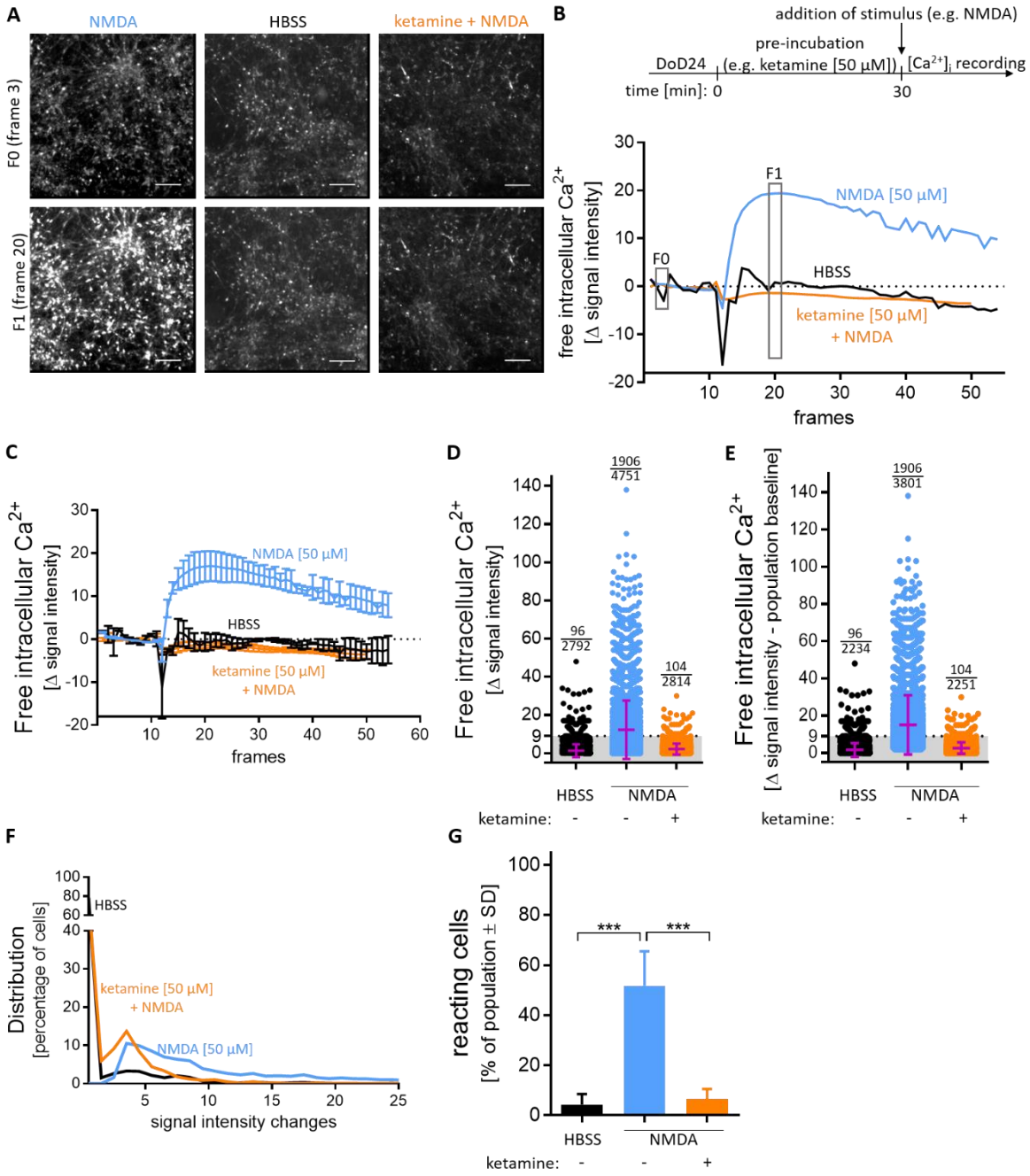

Fig. 5.3.5: Different possibilities of analysis and depiction of Δ signal intensities

MCCs were differentiated for 24 days and subsequently used for Ca^{2+} imaging. (**A**) Images from cells treated with negative control HBSS, NMDA [50 µM], pre-incubated with ketamine [50 µM] for 30 min before addition of NMDA [50 µM], before stimuli addition (F0 (frame 3)), or after (F1 (frame 20)). Scale bar: 100 µm. (**B**) A schematic overview of Ca^{2+} imaging. Traces from wells shown in A. (**C**) Averaged traces of three individual wells treated with negative control HBSS or NMDA [50 µM], pre-incubated or not with ketamine [50 µM]. Data are means ± SD; n=3. (**D**) The changes of Ca^{2+} indicator fluorescence (= delta signal intensity) of each individual cell treated with HBSS or NMDA [50 µM], pretreated or not with ketamine [50 µM], is shown as a circle. The mean ± SD is shown in purple. The threshold of Δ signal intensity (≥ 9) is shown as dotted line. The number above each column represents the number of reactive cells and the number of total cells analyzed. (**E**) The Δ signal intensity of the population baseline was subtracted from the Δ signal intensity of each individual cell treated with HBSS or NMDA [50 µM], pretreated or not with ketamine [50 µM], and is shown as a circle. The mean ± SD is shown in purple. The threshold of Δ signal intensity (≥ 9) is shown as dotted line. The number

above each column represents the number of reactive cells and the number of total cells analyzed. (**F**) The data distribution of E is shown. (**G**) The percentage of cells with a Δ signal intensity ≥9 of the whole population was calculated for HBSS, NMDA [50 µM] pretreated or not with ketamine [50 µM]. Data are means ± SD; n=3; *** = p-value < 0.001

To further characterize ionotropic glutamate receptors, using this optimized quantification protocol, cells were treated with glutamate [10 µM], KCl [30 mM], and NMDA [50 µM]. The positive responses of the positive control were confirmed. The negative control nicotine showed the expected (non)-response (Fig. 5.3.6A). In this broader test panel we also included AMPA [10 µM], a stimulus of a subgroup of non-NMDA glutamate receptors (Hollmann *et al.* 1994). The Δ signal intensity values indicated a clear response of MCC (Fig. 5.3.6A). This was confirmed using MEA technology where the addition of AMPA led to an immediate, transient increase in spike frequency (Fig. 5.3.6B). We also used kainate [10 µM], a seizurogenic compound triggering another subgroup of glutamate receptors (Hollmann *et al.* 1994). The reaction to this agonist was slightly less intense but still MCCs showed Δ signal intensity values significantly above the threshold (Fig. 5.3.6A), and MEA recordings confirmed the reactivity of the MCC network to kainate (Fig. 5.3.6C). A quantitative comparison of the percentage of reacting cells showed that glutamate was the most effective agonist, but still about half of MCCs reacted to each of the receptor subfamily agonists NMDA, AMPA and kainate (Fig. 5.3.6D). The heterogeneity of MCCs reflects the multiple cell types with their individual receptor patterns, as is also common in human brains. The broad spectrum of glutamate responses allows for studies of activated or disturbed neuronal signaling not possible in frequently used human cell based test systems, such as LUHMES cells (Lotharius *et al.* 2005, Scholz *et al.* 2011, Gutbier *et al.* 2018) or SH-SY5Y cells (Krebs *et al.* 2020).

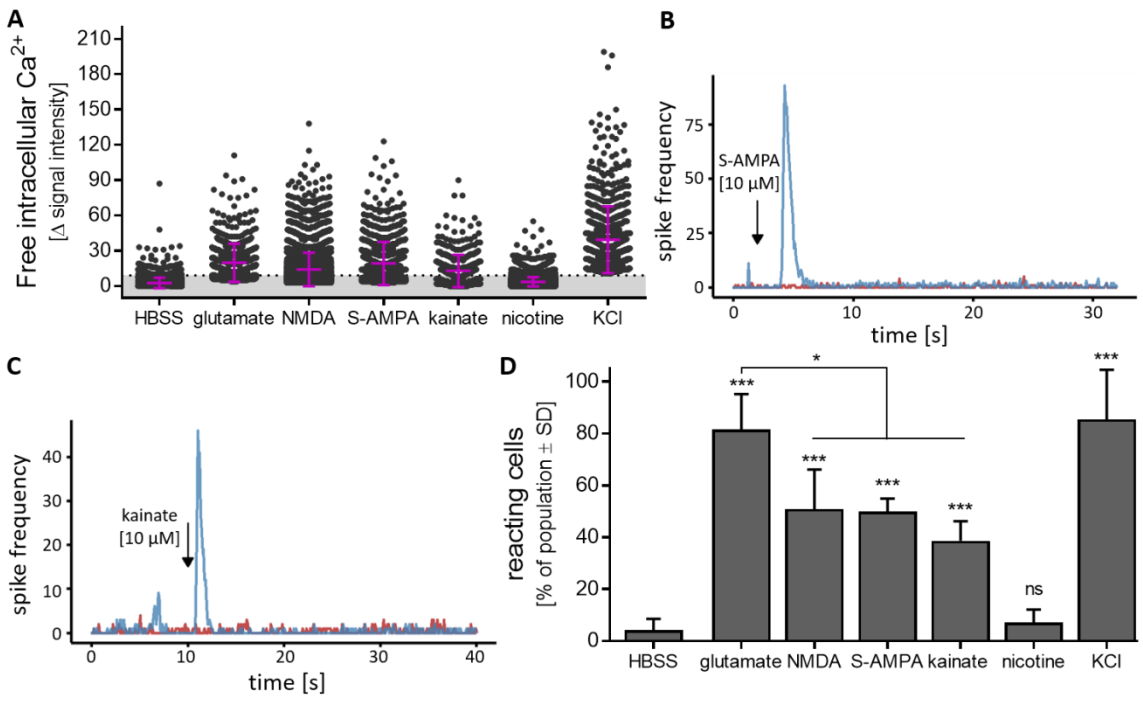

Fig. 5.3.6: Characterization of different ionotropic glutamate receptors in MCCs

MCCs were differentiated for 24 days and subsequently used for Ca^{2+} signaling or MEA analysis. Agonists of different ionotropic glutamate receptors were applied. (**A**) The changes of Ca^{2+} indicator fluorescence (= delta signal intensity) of each individual cell treated with the negative control HBSS, nicotine [50 µM], the glutamate receptor agonists glutamate [10 µM], NMDA [50 µM], S-AMPA [10 µM], kainate [10 µM] or KCl [30 mM] is shown as a dot. The mean and SD is shown in purple. The threshold of Δ signal intensity ≥ 9 (=defined as reactive cell) is shown as dotted line. On DoD24 MCCs on MEAs were treated with (**B**) S-AMPA [10 µM], (**C**) kainate [10 µM] (blue, addition is indicated by the black arrow; baseline in red). The generation of spikes was recorded directly before and after administration and the number of spikes was binned (bin size 0.1 s). A respective example of the acute response is shown. (**D**) The data from (A) are shown as percentage of reactive cells from the whole population. *** = p-value <0.001, ns = not significant.

Toxicants acting on the glutamate signaling in MCC

The MCC system was established to measure glutamate responses in human neurons, and preferentially those mediated by the NMDA-R. Therefore, further agonists of the NMDA-R were investigated, and the percentage of reacting cells was determined: Quinolinic acid is an endogenous NMDA-R agonist produced by microglia and macrophages in the kynurenine pathway of liver and brain. It is involved in many neurological diseases (Myint 2012). About 45% of MCCs reacted after quinolinic acid [500 µM] application (Fig. 5.3.7A). The same percentage of cells could be activated by the addition of ibotenic acid [50 µM] (Fig. 5.3.7A). This NMDA-R agonist, typically produced by e.g. *Amanita muscaria* mushrooms, is often used for toxic lesioning models in rodents, and as template to design

new drugs (Winn *et al.* 1984, Krogsgaard-Larsen *et al.* 1996). From this set of experiments, we conclude that neurotoxicants acting by NMDA-R agonism can be detected in MCCs.

As a further well studied neurotoxicant, we chose domoic acid. This compound is produced by algae, and it accumulates in the marine food chain (Doucette *et al.* 2016). It is notorious for causing serious shellfish poisoning, and extensive pharmacological studies have identified it as kainate receptor agonist (Larm *et al.* 1997). The percentage of reacting cells after administration was about 20% (Fig. 5.3.7A). It was striking, that the shape of Ca^{2+} imaging traces differed between the neurotoxins. The positive control NMDA [50 µM] showed a fast and steep increase in Δ signal intensity and a slow decrease after reaching the maximum. In contrast, the $[Ca^{2+}]_i$ response of ibotenic acid, domoic acid, and quinolinic acid increased slower but then remained at its highest level for at least 45 s. (Fig. 5.3.7B and Fig. 5.3.S6A,B). This kinetic may be further explored in the future. While some of the observed differences may be related to receptor binding (off-rates) properties of the toxicants, they may also be caused by differential signaling (involvement of different Ca^{2+} pools, different secondary regulations, different desensitization of involved receptors). The later phase of the recorded Ca^{2+} kinetics may also involve intercellular processes, such as the activation of neighboring cells to release neurotransmitters, which affect $[Ca^{2+}]_i$.

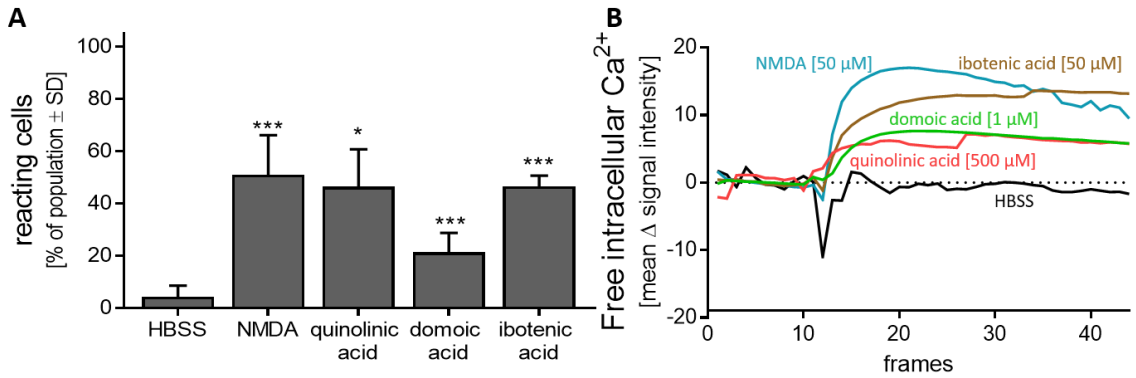

Fig. 5.3.7: Characterisation of NMDA receptor with agonists

DoD24 MCCs were used for Ca^{2+} imaging and were stimulated with different agonists of the NMDA receptor. (**A**) Percentage of cells reacting to HBSS, NMDA [50 µM], quinolinic acid [500 µM] (an endogenous NMDA-R agonist), domoic acid [1 µM] (a neurotoxin produced by algae, kainate- and AMPA-recptor agonist), or ibotenic acid [50 µM] (a fungal neurotoxin acting as NMDA-R agonist) compared to the whole cell population is shown. Data are means of three biological replicates ± SD. * = p-value < 0.05, *** = p-value < 0.001; (**B**) Averaged traces from Ca^{2+} signaling of (A) are shown. The full set of data with standard deviations is displayed in Fig. 5.3.S6.

Toxicity by glutamate receptor antagonism

We explored a panel of antagonists of the NDMA-R. First, we used apparently simple Mg^{2+} ions. As they block the NMDA-R pore channel, they can act as potent and efficient antagonists in cell culture experiments (Volbracht *et al.* 2006). When MCCs were pre-incubated with $MgCl_2$ [5 mM] the response to NMDA [50 µM] was completely blocked (Fig. 5.3.8A). The antagonist MK801 (=dizocilpine) also acts on the channel pore and thereby blocks the NMDA-R (Scatton 1993). Indeed, no stimulation with NMDA [50 µM] was possible after pre-incubation with MK801 [6 µM] (Fig. 5.3.8A). When we used a classical competitive antagonist of the glutamate binding site, e.g. AP5, the NMDA response was attenuated by about 80% (Fig. 5.3.8A). As further antagonist, we used traxoprodil [5 µM]. This compound specifically inhibits the NR2B subtype of NMDA-Rs. Like AP5 it reduced the NMDA response by about 80% (Fig. 5.3.8A). Traxoprodil was developed as neuroprotective agent to prevent brain damage after stroke (Wang *et al.* 2005). Recently it has been considered as potential antidepressant (Preskorn *et al.* 2008).

After showing that well-established NMDA-R antagonists may be detected by our system, we investigated whether lead ions showed any effect. This is interesting as lead is a well-known developmental neurotoxicant, which changes synaptogenesis and NMDA-R behavior (Toscano *et al.* 2005). Older reports have suggested lead to be an antagonist or a negative allosteric modulator of the NMDA-R (Guilarte *et al.* 1995, Schulte *et al.* 1995). MCCs were pre-incubated with Pb(II)acetate [50 µM] prior to NMDA [50 µM] administration. The percentage of reacting cells was not significantly changed in the presence of lead (Fig. 5.3.8A). As positive control, cells were pre-incubated with Zn^{2+} [10 µM], a well-established negative regulator of the NMDA-R (Jalali-Yazdi *et al.* 2018). Indeed, we found that the NMDA-R could not be stimulated by NMDA anymore (Fig. 5.3.8A, B and Fig. 5.3.S6D) when Zn^{2+} was present. The different effects of Pb^{2+} vs Zn^{2+} were fully confirmed when the entire traces generated by Ca^{2+} imaging were considered (Fig. 5.3.8B and Fig. 5.3.S6C). These effects agree well with more recent literature on lead: It has become clear that the neurodevelopmental toxicity of lead is due to this metal ion interfering with synaptogenesis. A direct inhibition of the NMDA-R could not be confirmed. It is now rather assumed that Pb^{2+} affects synaptic signaling indirectly by attenuating BDNF transcription (Sachana *et al.* 2018). When lead affects BDNF in the developing CNS, synapses cannot form properly. Therefore, the vulnerability to lead exposure is higher in earlier developmental stages (Guilarte *et al.* 1992). Chronic Pb^{2+} exposure during development results in

decreased levels of NR2A (Zhang *et al.* 2002). Although, lead is a well-known DNT compound with severe effects on the nervous system, these are not acute effects and need time to establish. Here, the lead exposure was only 30 minutes and we only investigated direct effects on Ca^{2+} signaling. Thus, the absence of an inhibitory effect is fully consistent with the available literature.

The last group of compounds we explored here are drugs, which may be used recreationally (illicitly) because of their psychedelic effects. We chose phencyclidine (PCP) and dextromethorphan (DXM) to investigate their effect on the NMDA-R in MCCs. Both showed a strong antagonistic effect, and they fully abolished the Ca^{2+} response after stimulation with either NMDA [50 µM] (Fig. 5.3.8C) or ibotenic acid [50 µM] (Fig. 5.3.8D). The cough suppressant DXM binds like ketamine and PCP to the dizocilpine site of the NMDA-R. All three substances are abused as illicit drugs and induce psychoses (Jodo 2013, Powers *et al.* 2015, Martinak *et al.* 2017), and symptoms of schizophrenia (Jodo 2013, Frohlich *et al.* 2014). These symptoms are associated with the NMDA-R antagonistic effects of the compounds. Our MCC-based test system may be used to identify such compounds from various sources (drugs, environmental toxicants, and natural occurring neurotoxins).

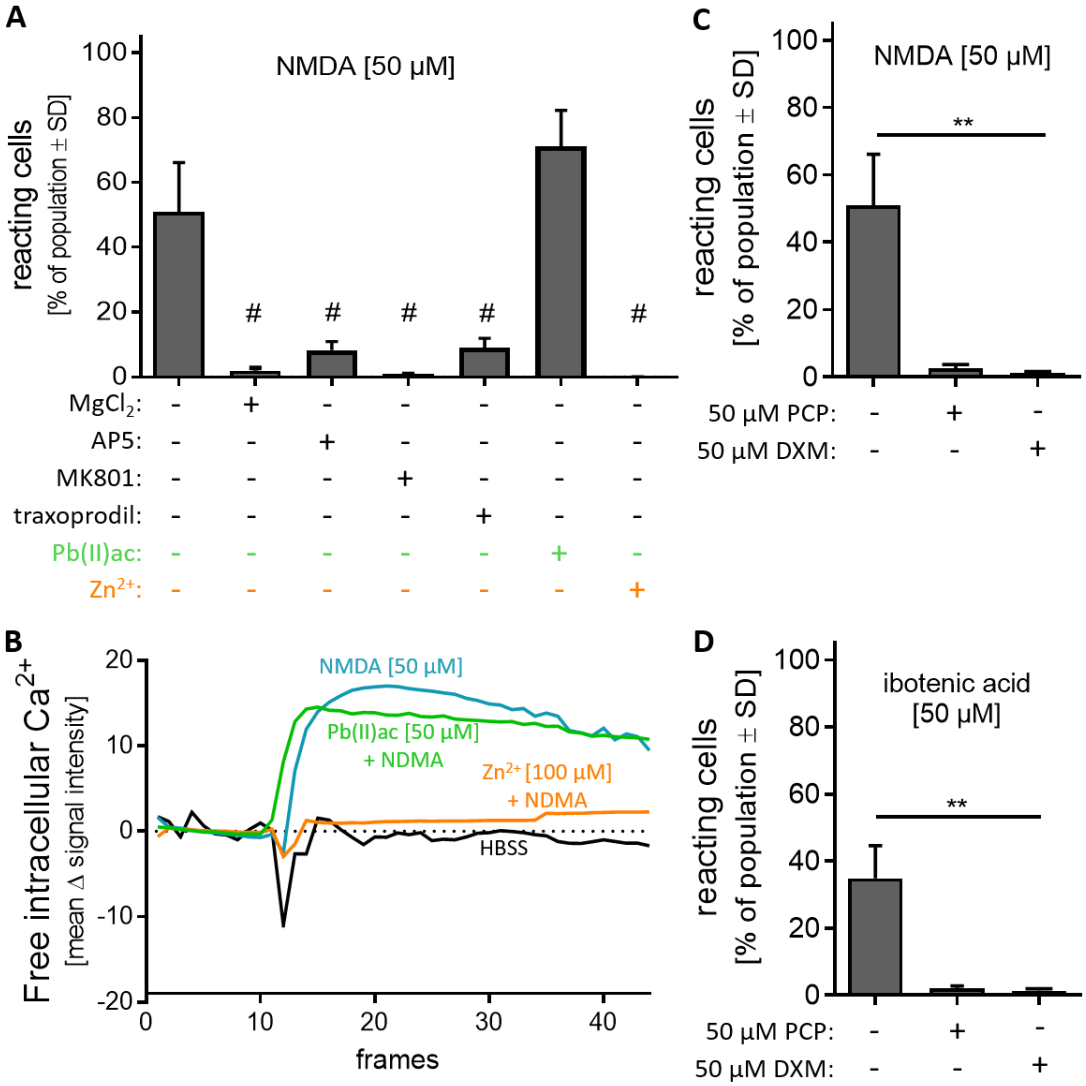

Fig. 5.3.8: Characterization of NMDA receptor with antagonists

DoD24 MCCs were used for Ca^{2+} imaging and were preincubated with different antagonists of the NMDA receptor. (**A**) MCCs were pre-incubated for 30 minutes with different antagonists of the NMDA-R: $MgCl_2$ [5 mM], AP5 [50 µM], MK801 [6 µM], traxoprodil [5 µM], Pb(II)ac [50 µM], or Zn^{2+} [10 µM] followed by addition of 50 µM NMDA. The percentage of reacting cells from the whole cell population is shown. Data are means of three biological replicates ± SD, # = p-value < 0.05 (reaction vs NMDA alone). (**B**) Averaged traces from Ca^{2+} signaling of (A). The full set of data with standard deviations is displayed in Fig. S. 6. (**C**) MCCs were pre-incubated for 30 min with phencyclidine [50 µM] (PCP) or dextromethorphan [50 µM] (DXM) followed by the addition of NMDA [50 µM]. The percentage of reacting cells compared to the whole cell population is shown. Data are means of three biological replicates ± SD. ** = p-value <0.01. (**D**) MCCs were pre-incubated for 30 min with phencyclidine [50 µM] (PCP) or dextromethorphan [50 µM] (DXM) followed by the addition of ibotenic acid [50 µM]. The percentage of reacting cells compared to the whole cell population is shown. Data are means of three biological replicates ± SD; ** = p-value <0.01.

4.3.5. Conclusion and outlook

In this study, we presented a test system comprised of excitatory and inhibitory neurons as well as glia cells. We showed that $[Ca^{2+}]_i$ imaging can be used as quantitative readout, despite the heterogeneity of cell types present in MCC. The functional glutamate receptors were further characterized as belonging to the subclasses of NMDA-R, AMPA receptors, and kainate receptors. We focused on NMDA-R responses by applying various agonists and antagonists.

As NMDA-R have such a particularly high physiological, pathological and pharmacological importance, several other differentiation protocols for neurons containing functional NMDA-R have been developed in the past (Heikkilä *et al.* 2009, Yamazaki *et al.* 2016, Pruunsild *et al.* 2017, Nehme *et al.* 2018, Meijer *et al.* 2019). The objective of these studies was to study the role of NMDA-R for biological functions (gene expression, synaptic transmission and plasticity, modulation by astrocytes). They were not focused on toxicological testing and usually provided little information on endpoint quantification. To our knowledge neither a response profiling by agonists and antagonists, nor a clear description of test system responses on the population level is available elsewhere.

Most cell systems developed for neurotoxicity testing have until recently been based on rodent primary cultures (Suñol *et al.* 2008, Hogberg *et al.* 2011, Zurich *et al.* 2013, Alépée *et al.* 2014, Hondebrink *et al.* 2016, Kreir *et al.* 2018, Strickland *et al.* 2018, Zwartsen *et al.* 2018, Kosnik *et al.* 2020). The human iPSCs based systems that have undergone first evaluations rely on commercially available cells with costs that prevent their routine use in academic laboratories. Moreover, the first data from such systems did not provide strong evidence for a robust NMDA-R response. However, compounds acting on other glutamate receptors like domoic acid, have shown clear responses (Nimtz *et al.* 2020, Tukker *et al.* 2020). As MCCs can be generated relatively fast, and Ca^{2+} imaging is performed in 96-well format, our system allows a sufficient throughput for small screens and relatively extensive follow-up characterizations.

During system evaluation, we also considered another important pathological process related to NMDA-R: excitotoxicity (Olney *et al.* 1978, Choi *et al.* 1989, Leist *et al.* 1997, Leist *et al.* 1998). However, we did not observe cell death responses after exposure to

glutamate or NMDA for up to 24 h. However, this may be related to the medium composition or other culture factors that are modifiable, and the issue deserves further investigation in the future.

One of the most comprehensive approaches to identify potential functional neurotoxicity is the use of neuronal networks on MEA (Vassallo *et al.* 2017, Strickland *et al.* 2018, Kosnik *et al.* 2020). The hitherto most robust MEA data have been generated with rat primary neurons. More recently, murine and human-stem cell-derived neurons have been demonstrated to be principally suitable for the analysis of network signaling on MEA (Pagan-Diaz *et al.* 2020, Tukker *et al.* 2020). However, the production of cultures at reasonable price, time effort and robustness has proven challenging. Under such conditions, the presence of both, excitatory and inhibitory neurons is important to obtain stable networks (Tukker *et al.* 2018, Zou *et al.* 2020). We have shown for MCC that they may be used for such MEA analysis. They develop a functional neuronal network within 24 days. This is relatively fast compared to other differentiation protocols based on PSC (Cao *et al.* 2017, Nehme *et al.* 2018, Russo *et al.* 2018, Klapper *et al.* 2019, Meijer *et al.* 2019). Our initial MEA data (NMDA / bicuculline exposure) suggest that both excitatory and inhibitory neurons are present. Additionally, MCCs contain glia cells, which are essential for synaptogenesis and maturation of a functional neuronal network (Ishii *et al.* 2017, Klapper *et al.* 2019). As MEA analysis was not the focus of the current work, mostly qualitative and descriptive data have been presented, but the speed of differentiation and the strength of the responses observed seem promising for further adaptation of MCC to MEA.

We focused here on toxicological applications, as neurotoxicity is one of the major reasons for drugs failure (Cook *et al.* 2014). However, MCC may be interesting also for general biomedical research. As many types of receptors are expressed, it may be possible to use the system to investigate multiple complex network responses, such as seizurogenic activity or circuitry disturbances related to schizophrenia.

4.3.6. Acknowledgements

This work was supported by the Land-BW (INVITE), the DK-EPA (MST-667-00205), EFSA, the University of Konstanz and the projects from the European Union's Horizon 2020 research and innovation program EU-ToxRisk (grant agreement No 681002) and END-poiNTs (grant agreement No 825759). The Bioimaging Center of the University of Konstanz is acknowledged for providing excellent support and the confocal microscopy instrumentation. We are grateful to Marion Kapitza and Alice Wiedmann for providing great experimental support.

4.3.7. Conflict of interest

The authors declare no conflict of interest.

4.3.8. Supplements

Tab. 5.3.S1: Overview of compounds used in this study

Compound	Solvent	Concentration [µM]	Supplier	Catalogue number
AP5	water	50	Sigma	A8054
bicuculline	DMSO	1	Sigma	B-9130
dextromethorphan (DXM)	water	50	Sigma	D2531
domoic acid	water	1	Sigma	D6152
glutamate	water	0.5-20	Sigma	G1626
ibotenic acid	water	50	Tocris	0285
kainate	water	10	Tocris	0222
KCl	water	10000, 30000	Sigma	P9541
ketamine	water	50	Sigma	K2753
$MgCl_2$	water	5000	Merck	105833
MK801	DMSO	6	Sigma	M107
nicotine	DMSO	50	Sigma	36733
NMDA	water	0.5-50	Tocris	0114
Pb(II)ac	water	50	Sigma	316512
phencyclidine (PCP)	water	50	Tocris	2557
quinolinic acid	DMSO	500	Sigma	P63204
S-AMPA	water	10	Tocris	0254
traxoprodil	DMSO	5	Sigma	SML0053
veratridine	DMSO	100	alomone labs	V-110
Zn^{2+}	water	100	Sigma	Z0152

Tab. 5.3.S2: Primary antibodies used in this study

Target	Isotype	Dilution	Supplier	Catalogue number	Lot number
TUBB3	mouse IgG2a	1:1000	Covance	MMS-435P	D13AF00117
Nestin	mouse IgG1	1:100	R&D	MAB1259	HSG0213091
Ki67 (PE)	mouse IgG1	1:600	BD Pharmingen	556027	03428
DCX	goat	1:100	Santa Cruz	sc-8067	L1008
PAX6	rabbit	1:200	Covance	PRB-278-P	D14BF00330
PAX3	mouse IgG2a	1:200	Ch. O. Ordahl, San Francisco		
SOX1	goat	1:200	R&D Systems	AF3369	XUV0213111
MAP2	mouse IgG1	1:1000	Sigma	M4403	063M4802
NeuN	mouse IgG1	1:200	Merck Millipore	MAB377	2159655
Gad65/67	rabbit	1:200	Bioworld	BS1400	360803
Synaptophysin	mouse IgG1	1:200	Synaptic Systems	101011	1-51
S100ß	mouse IgG1	1:500	Sigma	S2532	023M4828
vGlut1	rabbit	1:500	Synaptic-Systems	AB5905	LV1439669

Tab. 5.3.S3: Primers antibodies used in this study

Target	Sequence (For)	Sequence (Rev)
CDK1	AGAGCTTTGGGCACTCCCAA	TGCCAGAAATTCGTTTGGCTG
CDK2	GAATCTCCAGGGAATAGGCC	TACACCCATGAGGTGGTGAC
CYCLIN D1	CTCACACGCTTCCTCTCCA	CACCTCCTCCTCCTCCTCTT
CYCLIN D2	ATGTTCCTGGCCTCCAAAC	GCCAGGTTCCACTTCAACTT
DCX	GCGAAATTTTTCAGGACCAC	CACAGAAGCCATCAAACTGG
GAPDH	ATGGAGAAGGCTGGGGCTCA	AGTGATGGCATGGACTGTGGTCAT
GFAP	CGAGATCGCCACCTACAGGAAGC	CCTTAATGACCTCTCCATCCCGC
HES5	TTGGAGTTGGGCTGGTG	CCCAAAGAGAAAAACCGA
MAP2	CGGATGACCTAAAGCGATTC	TCTGGAGCATTGTCATTTGC
NANOG	GGTGAAGACCTGGTTCCAGAAC	CATCCCTGGTGGTAGGAAGAGTAAAG
NESTIN	GCACCTCAAGATGTCCCTCAGC	GGGAAGTTGGGCTCAGGACTG
NEUN	AGCCCGGGAGAAGCTGAATG	GTGCCGGTGGTGGGGTAGGG
NR1	GTCCACCAGACTGAAGATTGTGAC	CTCCTCCTTGCATGTCCCA
NR2A	GCTCTTCTCCATCAGCAGGG	GGATCCCGTCAGATTGAAGTCT
NR2B	GGTCTTCTCCATCAGCAGAGG	TGTTGTTCATGGTTGCGGT
OCT4	GCAAAGCAGAAACCCTCGTGC	ACACTCGGACCACATCCTTCTCG
PAX3	GACTGGCTCCATACGTCCTGGTGC	CGGCTGATGGAACTCACTGACGG
PAX6	CCGCCTATGCCCAGCTTCAC	AAGTGGTGCCCGAGGTGCCC
PSD95	CACTCCTCACAGTGCTGCAT	TGTCTTCATCTTGGTAGCGG
RPL13A	GGTATGCTGCCCCACAAAACC	CTGTCACTGCCTGGTACTTCCA
S100ß	CTTAGAGGAAATCAAAGAGCAGGAGGT	CATGTTCAAAGAACTCGTGGCAGG
SLC17A6	GCGGCCTGGGCTTCTGCATC	AGCCGAGACGCGATGTAGCC
SOX1	CCGGGATAAGGGCCTCCCCA	ACACAGGGGAGCACAGGGGC
SYNAPSIN	TCAGACCTTCTACCCCAATCA	GTCCTGGAAGTCATGCTGGT
TBP	GGGCACCACTCCACTGTATC	GCAGCAAACCGCTTGGGATTATATTCG
TUBB3	AACTACGTGGGCGACTCGGA	GTTGTTGCCGGCCCCACTCT

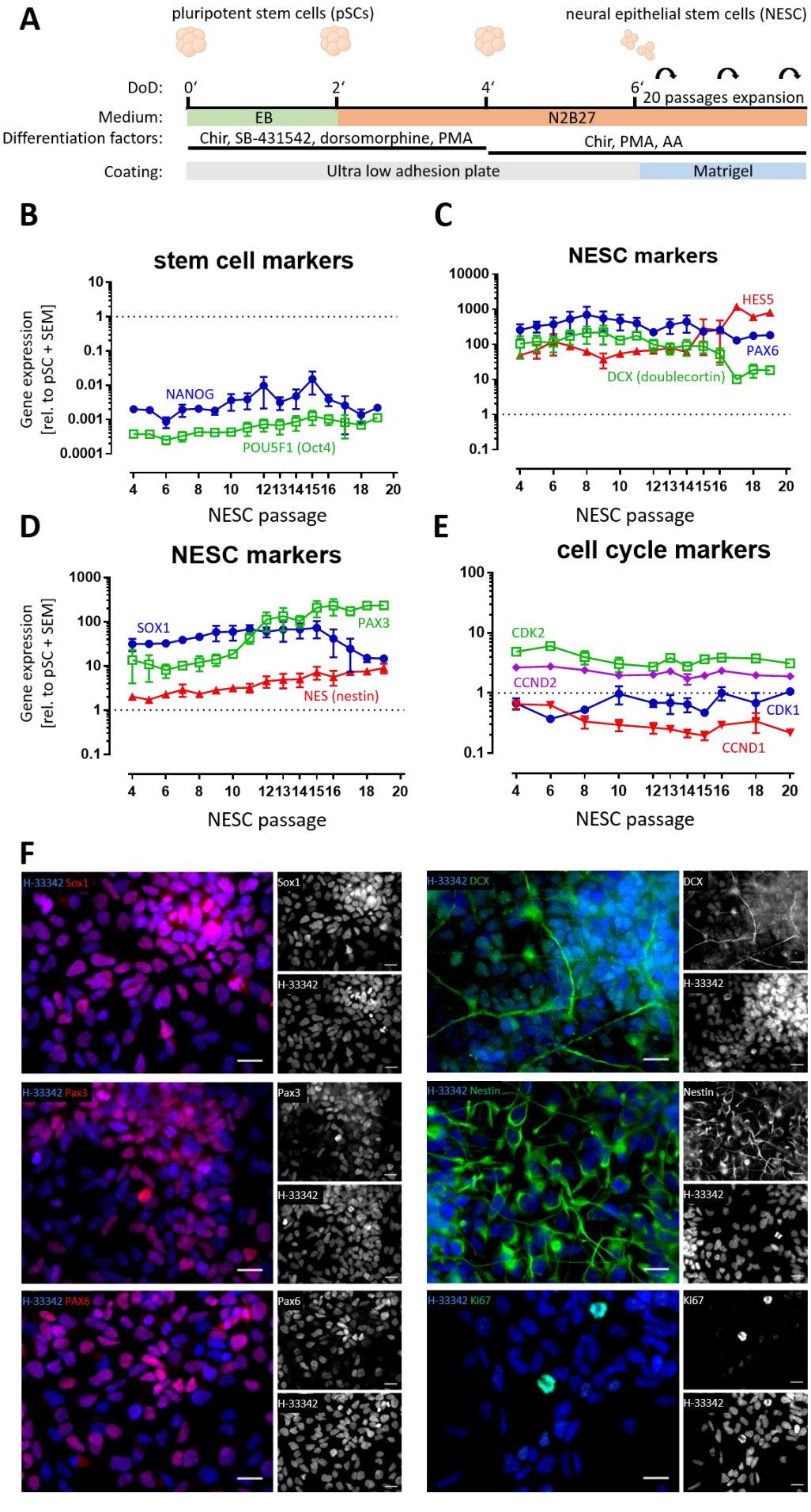
A
pluripotent stem cells (pSCs)
neural epithelial stem cells (NESC)
DoD:
0‘
2‘
4‘
6‘
20 passages expansion
Medium:
EB
N2B27
Differentiation factors:
Chir, SB-431542, dorsomorphine, PMA
Chir, PMA, AA
Coating:
Ultra low adhesion plate
Matrigel
B
stem cell markers
Gene expression [rel. to pSC + SEM]
NANOG
POU5F1 (Oct4)
NESC passage
C
NESC markers
HES5
PAX6
DCX (doublecortin)
NESC passage
D
NESC markers
SOX1
PAX3
NES (nestin)
NESC passage
E
cell cycle markers
CDK2
CCND2
CDK1
CCND1
NESC passage
F
H-33342 Sox1
Sox1
H-33342
H-33342 DCX
DCX
H-33342
H-33342 Pax3
Pax3
H-33342
H-33342 Nestin
Nestin
H-33342
H-33342 PAX6
Pax6
H-33342
H-33342 Ki67
Ki67
H-33342

Fig. 5.3.S1: Characterization of NESC

Neuroepithelial stem cells (NESC) were generated from pluripotent stem cells (pSCs) according to Reinhardt *et al.* (Reinhardt *et al.* 2013) by differentiating for 6 days in 3D spheres, followed by an expansion and maintenance phase of up to 20 passages. (**A**) Schematic display of NESC differentiation and expansion (Chir – Chir99021, PMA – purmorphamine, AA – ascorbic acid). (**B**) Gene expression profiles of the stem cell markers NANOG, POU5F1. Gene expression was quantified by real-time PCR. Data are shown relative to pSCs. (**C** and **D**) Gene expression of NESC markers PAX6, DCX, HES5, SOX1, PAX3, NES. (**E**) Gene expression of the cell cycle markers cyclin dependent kinase CDK1, CDK2, CCND1, and CCND2. All data are means ± SEM of 2-3 biological replicates and cover NESC passage 4 until NESC passage 20. (**F**) Immunofluorescence images of NESC at passage 13 using antibodies against the neural progenitor markers Sox1, Pax3, Pax6, doublecortin (DCX), nestin, and the proliferation marker Ki67 (green). Nuclei were counterstained with Hoechst H-33342. Scale bars: 50 μm.

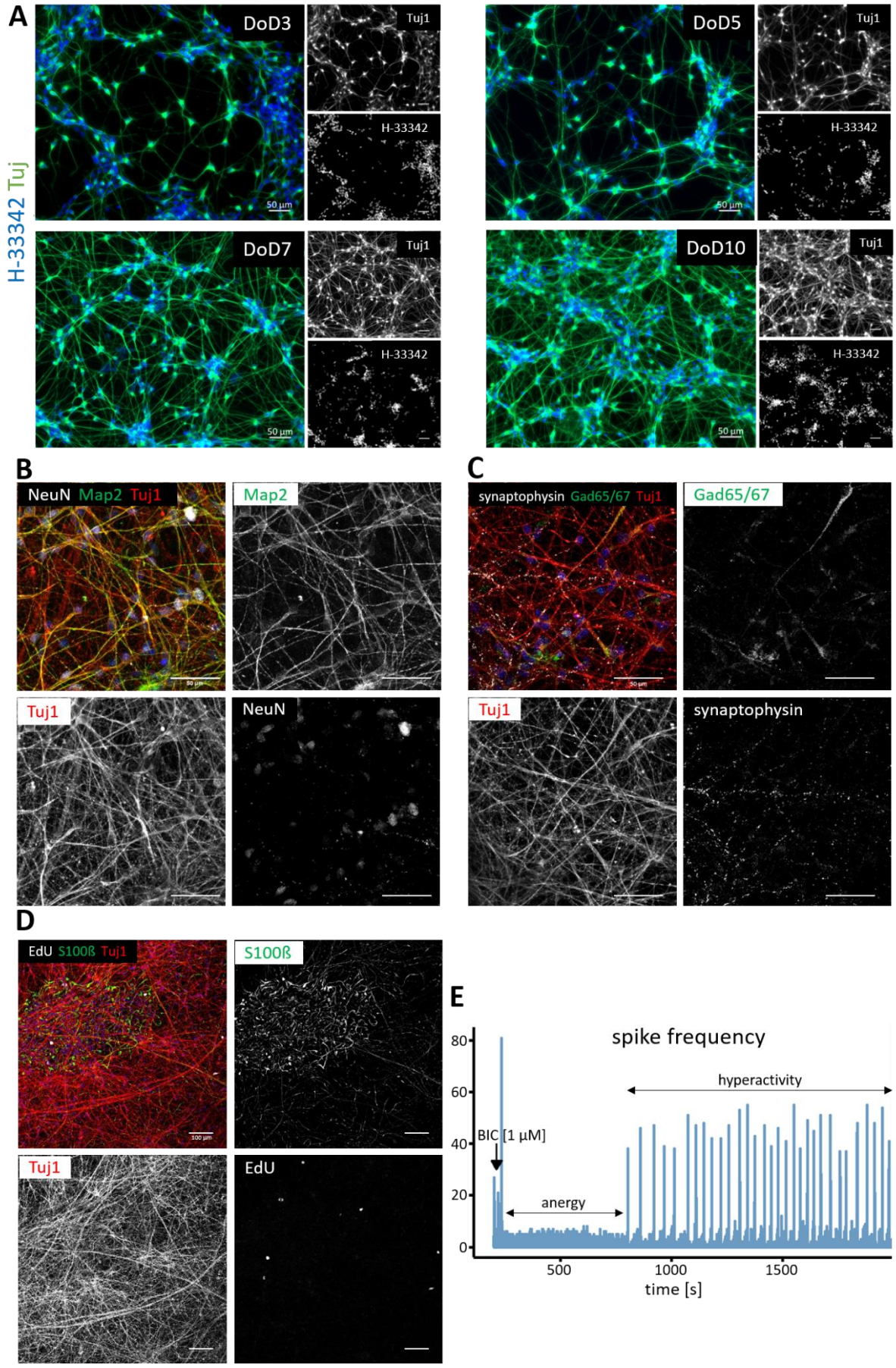
A
H-33342 Tuj
DoD3
Tuj1
H-33342
DoD5
Tuj1
H-33342
DoD7
Tuj1
H-33342
DoD10
Tuj1
H-33342
50 µm
B
NeuN Map2 Tuj1
Map2
Tuj1
NeuN
C
synaptophysin Gad65/67 Tuj1
Gad65/67
Tuj1
synaptophysin
D
EdU S100ß Tuj1
S100ß
Tuj1
EdU
100 µm
E
spike frequency
hyperactivity
BIC [1 µM]
anergy
80
60
40
20
0
500
1000
1500
time [s]

Fig. 5.3.S2: Characterization of MCCs at different developmental stages

MCCs were differentiated on glass coverslips for 3, 5, 7, 10, or 24 days and fixed for immunostaining on the respective day. (**A**) Time course of neuronal network formation: cells stained on DoD3, DoD5, DoD7, and DoD10 with an antibody against the neuron specific cytoskeletal marker beta-III-tubulin (Tuj1). (**B**) Neurons were differentiated for 24 days and stained with markers of mature neurons like NeuN, Map2, and the neuronal marker Tuj1. (**C**) Immunostaining of the presynaptic marker synaptophysin, Gad65/67, the enzyme catalyzing the decarboxylation of glutamate to γ-aminobutyric acid (GABA), and the neuronal marker Tuj1 on DoD24. (**D**) Replicating cells on DoD24 were visualized by the nucleotide analog 5-ethynyl-2'-deoxyuridine (EdU), cells were counterstained against the glial cell marker S100ß, and the neuronal marker Tuj1. Scale bars: 50 µm. (**E**) MCCs were differentiated on MEA plates. Spontaneous spikes of electrical activity were recorded. On DoD24 MCCs on MEAs were treated with the $GABA_A$ receptor antagonist [1 µM] bicuculline (addition is indicated by the black arrow). The generation of spikes was recorded directly before and after administration, the number of spikes was binned (bin size 0.1 s) and a representative example of the response is shown.

A

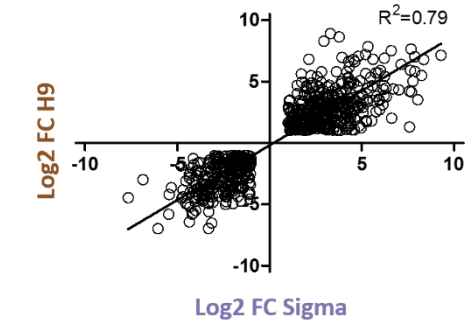

B

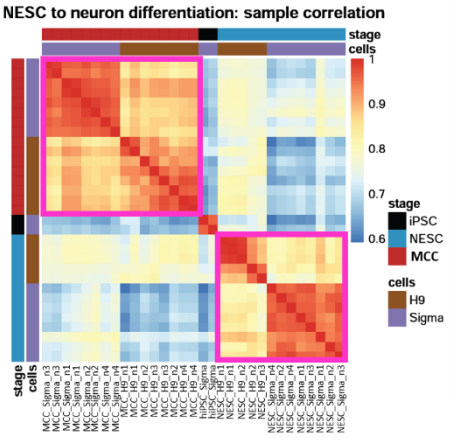

C

key biological process	term name	term id
neurodevelopment	regulation of nervous system development	GO:0051960
	cell morphogenesis involved in neuron differentiation	GO:0048667
	regulation of membrane potential	GO:0042391
	axon development	GO:0061564
	regulation of neurogenesis	GO:0050767
	axonogenesis	GO:0007409
	regulation of neuron differentiation	GO:0045664
	positive regulation of nervous system development	GO:0051962
	negative regulation of nervous system development	GO:0051961
	regulation of neuron projection development	GO:0010975
	negative regulation of neurogenesis	GO:0050768
	positive regulation of neurogenesis	GO:0050769
	positive regulation of neuron differentiation	GO:0045666
	regulation of axonogenesis	GO:0050770
neuronal subtype (glutamate)	regulation of NMDA receptor activity	GO:2000310
	glutamate receptor signaling pathway	GO:0007215
	regulation of glutamate receptor signaling pathway	GO:1900449
synapse	regulation of trans-synaptic signaling	GO:0099177
	synaptic signaling	GO:0099536
	trans-synaptic signaling	GO:0099537
	anterograde trans-synaptic signaling	GO:0098916
	neuron projection morphogenesis	GO:0048812
	regulation of postsynaptic membrane potential	GO:0060078
	positive regulation of synaptic transmission	GO:0050806
	regulation of synaptic plasticity	GO:0048167
	chemical synaptic transmission, postsynaptic	GO:0099565
neurotransmitter	modulation of chemical synaptic transmission	GO:0050804
	chemical synaptic transmission	GO:0007268
	neurotransmitter transport	GO:0006836
	regulation of neurotransmitter levels	GO:0001505
	regulation of neurotransmitter receptor activity	GO:0099601

D

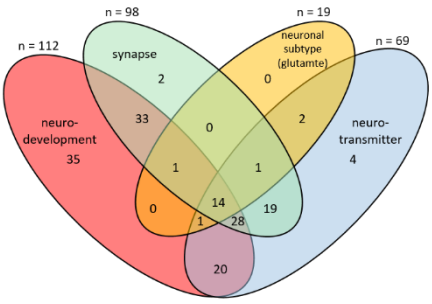

E

genes	fold change	comment
CCL2	43	not neurodevelopment; CCL2 inhibits glutamate-induced neuronal cell death
PPARGC1A	11	overlaps with neurotransmitter; interacts and regulated with CREB
KLHL24	9	overlaps with neurotransmitter; involved in regulation of kainate receptors
ACTN2	6	not in synapse; actinin alpha 2 belongs to the spectrin superfamily
GNAQ	2	not in neurotransmitter; G-protein subunit alpha Q

Fig. 5.3.S3: Comparison between transcriptome analysis of ESC-derived and PSC-derived MCCs

Neuroepithelial stem cells (NESCs) from two pluripotent stem cell lines (H9 and Sigma iPSC) were differentiated into mixed cortical cultures (MCCs), and mRNA was prepared for transcriptome analysis. A set of about 3500 genes was used for targeted RNAseq analysis (TempOSeq method), and expression levels were obtained for four cell preparations (some with two samples per cell preparation). For both cell types differentially expressed genes (DEGs) between NESC and MCC were identified, for further analysis only DEGs present in both H9-derived and iPSC-derived cells were used. (**A**) Log2FC of DEGs from H9-derived and iPSC-derived cells were plotted against each other and the R^2 of the correlation was determined. (**B**) A correlogram describing the distance of samples and thereby showing their similarity was prepared. Samples were allowed to cluster in an unsupervised way. (**C**) All upregulated DEGs with an adjusted p-value <0.05 and log2FC >1 were analyzed for over-represented gene ontology (GO) terms (Raudvere *et al.* 2019). GO terms with a size between 4 and 1000 genes were included in further analysis. The first (lowest p-value) 50 GOs of the category biological process were further assigned to the four key biological processes "neurodevelopment", "synapse", "neurotransmitter", and "neuronal subtype (glutamate)". In the table all GOs included in a key biological process are listed with their term name and their corresponding term id. (**D**) As one gene can be present in different GOs, multiple entries of the same gene in one key biological process are possible. Genes with multientries were counted only once per key biological process. The genes included in the four key biological processes were compared and overlays were performed. (**E**) The table shows the five genes from the key biological process "neuronal subtype (glutamate)" which are only included in this term and not in one of the other three biological processes, the fold change and a short comment on the respective gene is given.

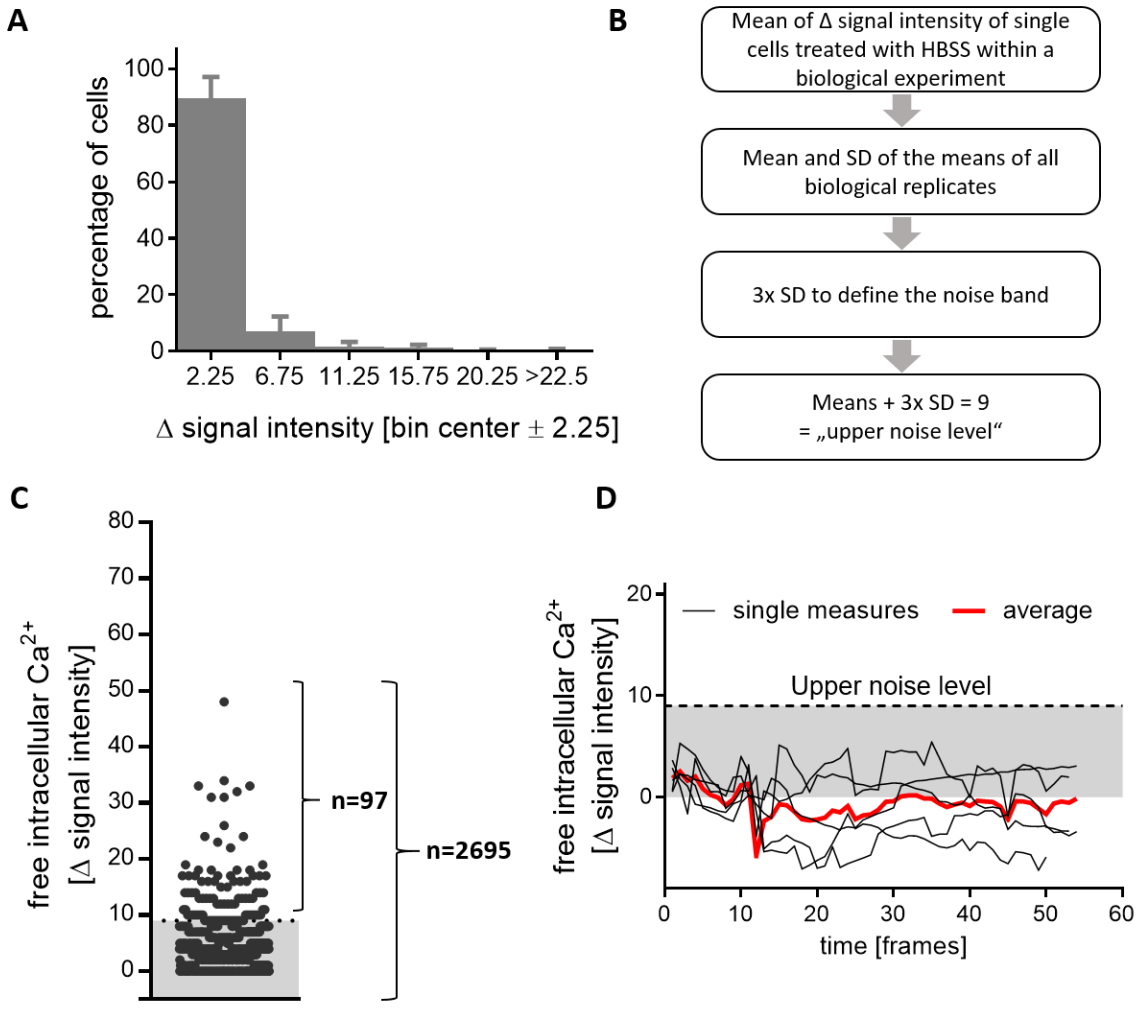

Fig 5.3.S4: Determination of reactivity thresholds

MCCs were differentiated for 24 days and subsequently used for Ca^{2+} imaging. Stimulation with the negative control Hank's balanced salt solution (HBSS) was performed to determine the background noise and the threshold of reactivity. (**A**) Changes of Ca^{2+} indicator fluorescence (=delta signal intensity values) of cells treated with HBSS were binned (bin size 4.5), and data are shown as percentage of total cells analyzed. Data are means ± SD; n=6 (**B**) Workflow to determine the noise band of HBSS and of the threshold of Δ signal intensity to discriminate negative and positive responses. (**C**) Delta signal intensity of each individual cell treated with HBSS on DoD24. The grey area under the dotted line represents the noise band. All values above the threshold of 9 are counted as reactive cells. Measurements for 2695 individual cells from six biological replicates are shown. False positive were 3.6%. (**D**) Ca^{2+} signaling traces of five different measurements are shown in black, the red trace represents the average of all single measurements. The grey area under the dotted line represents the noise band.

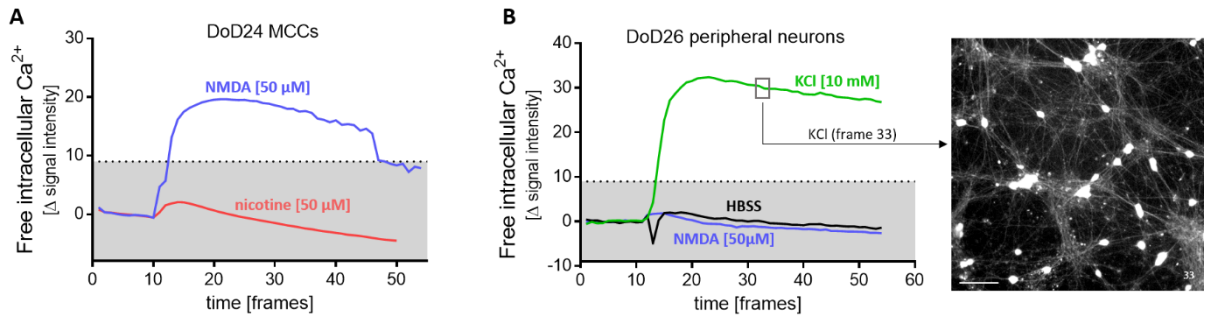

Fig. 5.3.S5: Specificity controls of Ca^{2+} signaling in MCCs and peripheral neurons

(**A**) MCCs were differentiated for 24 days and subsequently used for Ca^{2+} imaging. To test for specificity, NMDA [50 µM] or nicotine [50 µM] were administered and free intracellular Ca^{2+} was measured. Traces of the mean Δ signal intensity from >20 cells are shown. (**B**) Peripheral neurons were differentiated for 26 days according to Hoelting *et al.* (Hoelting *et al.* 2016) and also used for Ca^{2+} imaging. Changes in free intracellular Ca^{2+} were measured after the administration of KCl [10 mM], NMDA [50 µM] and HBSS. An image of cells after the treatment with KCl [10 mM] illustrates the neuronal phenotype the cells have on DoD26. Data are averages from >50 cells.

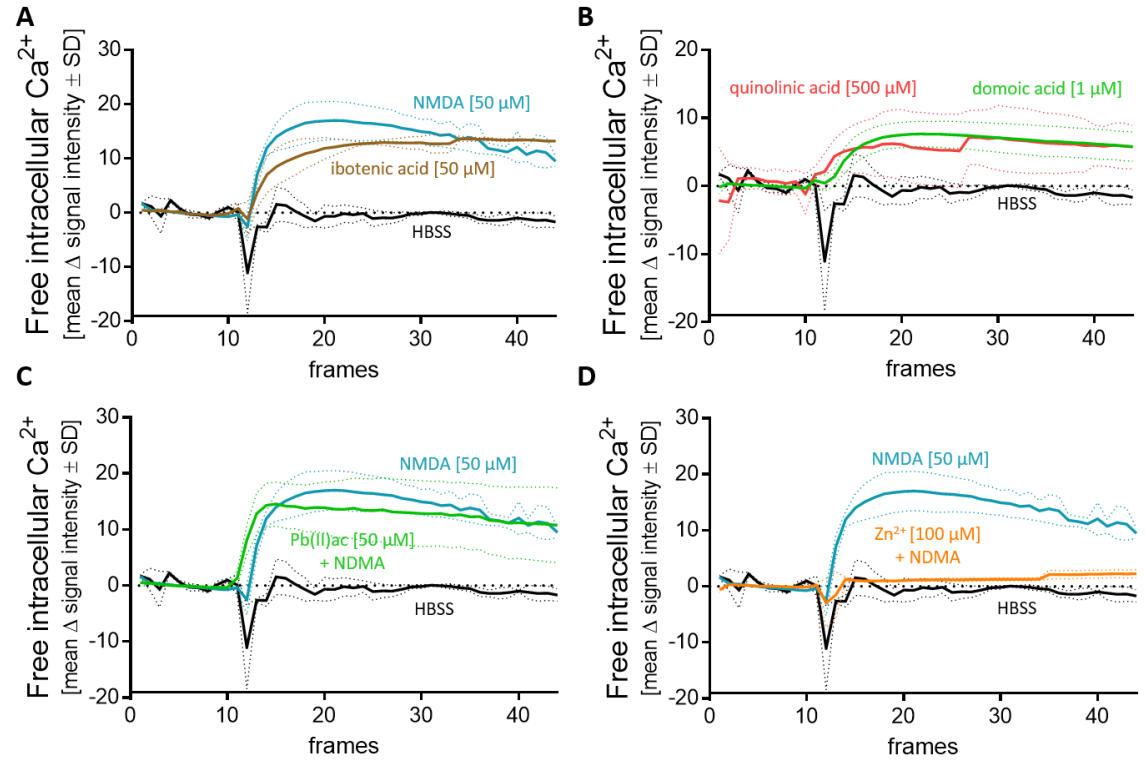

Fig. 5.3.S6: Ca^{2+} traces of MCCs to characterize their NMDA receptor

MCCs were differentiated until DoD24 and subsequently Ca^{2+} imaging was performed. Changes in free intracellular Ca^{2+} were measured after the administration of the different NMDA receptor agonist: (**A**) NMDA [50 µM], ibotenic acid [50 µM], (**B**) quinolinic acid [500 µM], and domoic acid [1 µM]. Cells were pre-incubated for 30 minutes with (**C**) Pb(II)ac [50 µM] and (**D**) with Zn^{2+} [100 µM] a known NMDA receptor antagonist and subsequently stimulated with NMDA [50 µM]. Data are averages from 2-4 biological replicates, the dotted lines represent the SD.

5. Concluding discussion and perspectives

In this thesis, four *in vitro* test methods and cell systems were used to investigate the influence of various compounds on human neurodevelopment. The different cellular systems recapitulate various stages and cover several developmental processes important for neurodevelopment. Dependent on their purpose, these systems have different endpoints, throughput and vary strongly in their readiness for regulatory acceptance. However, they can be combined in one test battery covering several developmental processes thereby promoting the paradigm shift towards a mechanism and knowledge based toxicology.

5.1. Interplay of epigenetics and transcriptional changes in early development

Epigenetics and transcriptional changes are closely related and influence each other strongly. In the first paper of this thesis, it was investigated whether transcriptional changes in the UKN1 test system evoked by drug exposure are accompanied by epigenetic changes. Furthermore, it was investigated if these epigenetic changes can function as an indicator for altered differentiation. Additionally, this was one of the first studies to explore transcriptomics as an endpoint for DNT. It was of special interest whether the data obtained by transcriptomics can provide information about the MoA and/or about an altered differentiation track.

5.1.1. Epigenetic marks manifest switch between transient and persistent transcriptome changes

As described in paper 1 of this thesis, only transient transcriptional changes were observed in the UKN1 test system following short exposure (up to 24 h) to histone deacetylase inhibitors (HDACi). These transient transcriptional changes were accompanied by transient changes in histone acetylation (acute effect). When the cells were exposed to the HDACi for a longer time period (minimum 3 to 4 days), the transcriptional changes became persistent and were still detectable on DoD6. This was even true, if the HDACi was not present anymore. On an epigenetic level, these permanent transcriptional changes

were reflected in a changed histone methylation ratio (H3K4me3/H3K27me3). This indicates that a drug effect can be fully reversible on a transcriptional level until a particular point in time. After this point in time, drug effects are permanent with or without prolonged drug exposure. As it seems that histone methylation plays a critical role in this change between reversibility and manifestation it could serve as a marker for permanent changes. Also in the field of addiction, epigenetics are discussed as a crucial player in stabilizing changes after drug exposure (reviewed inWalker *et al.* 2018, Hamilton *et al.* 2019).

If epigenetic changes are used as an endpoint to figure out the MoA, the exposure time point can be chosen relatively flexible, as the increased histone acetylation (acute effect of HDACi) is always found shortly after drug exposure independent of the exposure time point. If epigenetic marks are used to assess changes in the differentiation of a developing systems histone methylation should be used as marks. Therefore, epigenetic changes are suitable to distinguish between acute, reversible and permanent changes. Furthermore, changes in epigenetic modifier genes are found to be differently regulated between cell lineages like brain and liver cells (Weng *et al.* 2014) and also between different neural lineages (Weng *et al.* 2012) pointing to their potential use in identifying changes in lineage commitment. Thus, they could be used as lineage markers.

5.1.2. Transcriptomics reflect MoA and altered differentiation

Beside the epigenetic changes following HDACi exposure, transcriptomic changes were assessed in parallel in order to test their usefulness for measuring acute compound effects, identifying pathways of toxicity, and revealing alterations in differentiation. It returned out that transcriptomics are capable to detect both. To identify the mode of action (MoA) of a compound, short term exposures are appropriate and to detect phenotypic changes long term exposures are needed. Yet, not only is the duration of an exposure critical but also its timing. Therefore, the exposure time point needs to be critically considered, if transcriptomics are used to identify a compound's MoA.

At the same time, transcriptome analysis after long term exposures can be considered itself as an endpoint in this test system. The evaluation of these transcriptome changes can be categorized and thereby help to identify classes of DNToxicants. Therefore, the UKN1 test system was exposed to six different HADCi and six "mercurials". Transcriptome

changes were analyzed and a classifier was developed. As a consequence, the classifier could predict, whether the cells were exposed to an HDACi or a mercurial allowing to mechanistically group compounds and predict toxicants (Rempel *et al.* 2015). The grouping of chemicals according to their transcriptional changes was also performed in other *in vitro* test systems (Dreser *et al.* 2015, Pallocca *et al.* 2016, Shinde *et al.* 2017). Furthermore, transcriptomics data were used to extrapolate biomarkers that are predictive for the respective test system and thereby anticipate toxicity in a less expensive fashion (Pallocca *et al.* 2016, Dreser *et al.* 2020).

Meanwhile, the UKN1 test system has been expanded and a functional endpoint has been included. The transcriptome endpoint has been combined with the phenotypic endpoint of rosette formation (Dreser *et al.* 2020). Rosette formation is the neural tube closure equivalent in *in vitro* assays (Conti *et al.* 2010) providing the opportunity to directly link the transcriptome changes to a physiological endpoint. Combining these two endpoints yields comprehensive information about compounds interfering with very early neural precursor differentiation which is utilizable for regulatory toxicology.

5.1.3. Challenges in transcriptomics in developing systems

Transcriptomics are a powerful tool to examine DNT. However, in a developing test system, the generated data have several levels of complexity. (i) Even without compound-induced disturbances the baseline changes in a differentiating test system. Therefore, not every transcriptional change indicates an adverse effect. (ii) As in every toxicological test system, the exposure time is important to consider and has drastic influences on the results obtained. (iii) Based on the changing baseline, the time point of exposure has also severe effects on the results. (iv) The changes of developmental track increase the complexity of the transcriptomics in developing test systems. (v) Often, as in paper 1 of this thesis, only one compound concentration is applied in toxicogenomics. However, dose response experiments for transcriptomic data are highly desirable to get a better understanding of the complex, multilayered effects and to delineate adaptational from toxic effects. To address this in more detail, the UKN1 test system was exposed to increasing concentrations of VPA (Waldmann *et al.* 2014) and methyl mercury (Waldmann *et al.* 2017). These studies identified groups of concentrations that could be categorized (tolerated, functional adaption, cytotoxic) and most changes could be already found in the "functional adaption" range. With respect to these challenges, experiments have to be

planned very precisely, in order to assure the experimental setup is suitable to answer the question addressed in the study.

5.2. Implementation of new approach methods (NAM) in risk assessment

In the second paper of this thesis, neuronal integrity was used as an endpoint to investigate the effect MC-LF has on mature neurons. It has been found, that low µM concentrations of MC-LF were neurotoxic. Yet, testing MC-LF in adequate test systems is not sufficient to assess the risk for humans. Instead, it is necessary to compare the effective *in vitro* concentrations to concentrations known to induce toxicity in humans. Optimally, these data are obtained in epidemiological studies where human were exposed to MC. Such a comparison was performed in paper 2 indicating that the concentrations needed to induce neurotoxicity in the test systems where higher than human *in vivo* blood concentrations after normal MC intake.

However, to conduct a comprehensive risk assessment, it is also necessary to include information like hazard identification, dose response assessment, exposure assessment, mixtures, and a uncertainty analysis (Krewski *et al.* 2014). Some of these requirements were fulfilled, though it was never intended to conduct a complete risk assessment in the second paper of this thesis. Nevertheless, the information obtained could contribute to risk assessment in the frame of an IATA or next generation risk science as proposed by the NextGen project initiated by the US-EPA (Krewski *et al.* 2014). These new approaches for risk assessment include also data obtained with NAM. Strategies for "dose and species extrapolation" are compared for exemplification. The traditional approach is to translate doses obtained in animal testing to humans. This is implemented by adding certain security factors to the tested doses and thereby obtain tolerable human exposure levels. The new approach, includes cellular assays which directly measure disturbances of PoT in human *in vitro* test methods and makes use of in vitro in vivo extrapolation (IVIVE) (Krewski *et al.* 2014). This approach is similar to IATA, as it also includes information from NAMs to make use of all available information. Still, when data from NAM are integrated into risk assessment or prioritization, it is crucial to precisely control the settings the NAM data are obtained from, e.g. with respect to exposure scheme. In the study presented here, only conclusions can be drawn about short term exposures. For information on long term exposure or possible accumulation of MC, other test systems are needed.

5.3. Human mixed cortical cultures (MCC), an essential building block for *in vitro* test batteries

For the third paper of this thesis, a differentiation protocol for mixed cortical culture (MMC), expressing ionotropic glutamate receptors, with special emphasis on the NMDA-R has been established. The incorporation of a test system with a functional neuronal network into a test battery has many benefits. One of the most important features of neurons is their ability to transfer, transduce and integrate signals in functional neuronal networks. These unique properties make neurons particularly vulnerable, as they have e.g. a high energy demand, a high surface to plasma ratio, special receptors and various tightly regulated processes (Mattson *et al.* 2006). To study this feature also *in vitro* the models must possess neuronal networks. The need of these test systems becomes even more obvious, when classical DNT compounds are considered. Many of these are compounds like cocaine, domoic acid, ethanol, heroine, ketamine, MDMA, and nicotine (an extended list is available inAschner *et al.* 2017). A lot of these compounds interfere with neuronal signaling, network formation or directly with neuronal receptors. Thus, they all have a similar MoA.

Most *in vitro* test systems included in DNT test batteries have functional endpoints based on morphological changes instead of neuronal function. These test systems are very suitable to recognize compounds interfering e.g. with the cytoskeleton and thereby inhibit neurite outgrowth, or with cell-cell contact and thereby prevent neural crest migration. However, there are also known DNT compounds that interfere with neural signal transmission causing disturbances of neuronal circuits. To test a compounds ability to interfere with neuronal signaling, test systems with a functional network are needed. Yet, currently only few cell systems are available containing human neuronal networks and thus with the ability to detect changes in neuronal signaling or network formation (Nimtz *et al.* 2020, Tukker *et al.* 2020). Most of the used test systems are based on primary rat neurons (Alépée *et al.* 2014, Strickland *et al.* 2018, Zwartsen *et al.* 2018) and therefore struggling with the problem of interspecies extrapolation.

How close a neuronal network resembles the human *in vivo* situation depends amongst others on the complexity of the cells involved in network formation. On the lower end of complexity there are very simple systems which are suitable to investigate the signaling of single synapses (Meijer *et al.* 2019). On the other end there are very complex 3D

systems that resemble the human brain at time points close to birth (Luo *et al.* 2016). Both cell systems have their advantages for different scientific questions, however for (D)NT testing none of these systems is suitable. When developing a test method, a cell system needs to exhibit as much complexity as necessary to model the critical step (in this case neuronal signaling) at the same time the method should be as simple as possible. Here, MCC provide a well suited cell system. Their differentiation, is relatively fast and very robust. Furthermore, large batches can be easily generated. Therefore, MCC are suitable to investigate neuronal signaling with special emphasis on ionotropic glutamate and NMDA signaling.

In paper 3 of this thesis, a cell model with mixed cortical cultures, expressing NMDA-R and other ionotropic glutamate receptors, was established. With this cell system it was possible to detect toxic effects of compounds such as ketamine that could not be found with other test systems (Masjosthusmann *et al.* 2020). In a screen initiated by EFSA, around 160 compounds were screened. 29 compounds were applied to all eleven *in vitro* test methods included in the test battery. In none of the initially included test methods ketamine was detected as a hit. At the same time, domoic acid was only identified as a hit, when data from a rat neural network formation assay (Strickland *et al.* 2018) were added to the original data set. In contrast, MCCs could identify ketamine and domoic acid as compounds interfering with the normal signaling of the cells. This example highlights the importance of human test systems capable of identifying neuronal network disturbances. While the cell system presented here constitutes a promising basis further development is needed until it can be considered as ready to use test system and eventually get regulatory approval.

5.4. Technical progress of the applied test systems towards regulatory acceptance

In order to implement NAMs in regulatory toxicity it is necessary to assemble different test methods into a test battery covering the whole range of neurodevelopment including neurobehavioral endpoints. Four different systems were used in this thesis, UKN1, LUHMES, peripheral neurons and MCC. To obtain confidence in the data from every test method it is essential to have exact knowledge about their characteristics, such as cell

stage, applicability domain, throughput, performance and acceptance criteria. Therefore, the systems have been examined with respect to different important characteristics.

5.4.1. Neurodevelopmental stages covered by the applied test systems

As already mentioned above, the used test systems recapitulate different developmental stages as depicted in Fig. 6.1: the differentiation of NEP in very early neurodevelopment is modelled by UKN1; LUHMES can be used as a test systems for neurite outgrowth and for mature neurons of the CNS; peripheral neurons also represent a test system for neurite outgrowth of PNS neurons, but can also be differentiated into mature peripheral neurons; MCCs represent a culture of mixed cortical neurons, composed of neurons expressing various ionotropic glutamate receptors and glia cells and therefore mimic later stages of neurodevelopment as neural network formation and signaling.

Since NEP are the major precursors of many different cells of the later nervous system, their correct differentiation is key to neurodevelopment. It is not only important that enough NEP are generated, they also need to show the correct gene expression profile to ensure the correct differentiation track, as already minor changes in precursors can have major effects on their differentiation potential. Furthermore, the process of neural tube closure can be mimicked with NEP (Dreser *et al.* 2020). This is also a critical step in early neurodevelopment and disturbances thereof may result in severe birth defects like spina bifida (Nikolopoulou *et al.* 2017). All these early neurodevelopmental processes can be modeled with the original UKN1 test system and its additional endpoints. Also neurite outgrowth covers an important process of neurodevelopment. If this process is interrupted and neurites are too short or too long, they do not exactly meet other neurons and are not able to form neuronal networks. This is why, neurite outgrowth needs to be covered in a test battery for DNT. The degeneration of a neuronal network has also major effects on its functionality, therefore the integrity of a neuronal network is important to assess. The process of neurite outgrowth occurs mainly in the differentiation phase of neurodevelopment. Even if a network is morphologically intact, still the signaling in this network may be disturbed, which is why a test system testing for disturbances in receptor signaling is needed. The network formation and signaling occur later in neurodevelopment and therefore represent a later phase. The test systems applied in this thesis cover a lot of important neurodevelopmental processes and thereby provide the opportunity for comprehensive (D)NT testing.

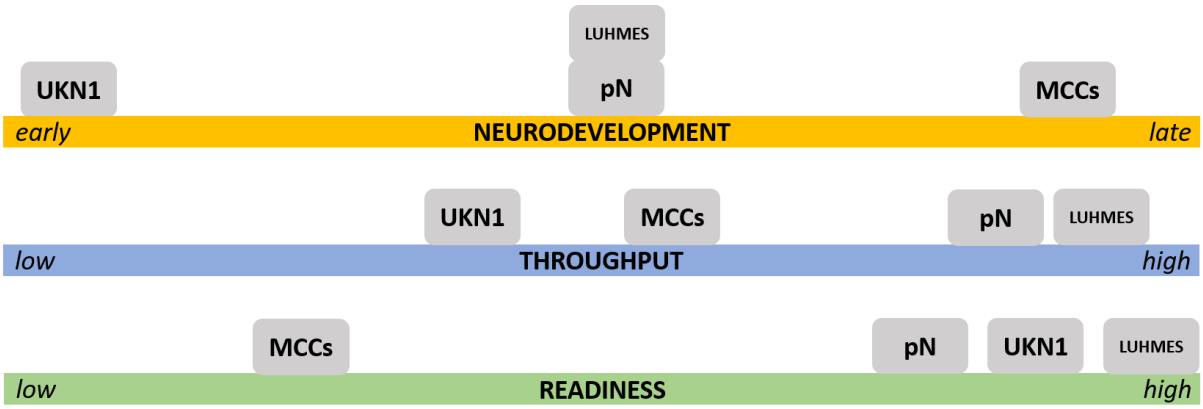

Fig. 6.1: Neurodevelopmental stage, throughput, and readiness of the applied test systems
The test system UKN1 was used in the first paper and mimics the differentiation of PSC to NEP and thereby serves as a test system for very early neurodevelopment. LUHMES and peripheral neurons (pN) were used in the second paper to investigate neurite outgrowth and neuronal integrity. The differentiation of mixed cortical cultures (MCCs) and their use to identify agonists and antagonists of the NMDA receptor were examined in the third manuscript. All test systems were evaluated concerning the neurodevelopmental stage they mimic (yellow), their throughput (blue) and their readiness (green).

5.4.2. Throughput of the applied test systems

Another important aspect to judge a test method is its throughput which depends on the differentiation time and effort of a test system, the assay well format of the endpoint, the automatization of the endpoint and the time and effort needed for data evaluation. With respect to these aspects the throughput of the presented methods has been evaluated. In an academic environment, UKN1 has a medium throughput (about 20 compounds can be screened per month), as the endpoint of epigenetic modifications is labor-intensive and the data evaluation of transcriptomics time consuming and complicated. In return the data outcome is very comprehensive and a lot of new information can be generated. The throughput of MCC is slightly higher (about 30 compounds can be screened per month). The cells differentiate for more than 20 days to establish the functional neuronal network. Furthermore, the data evaluation of Ca^{2+} imaging and MEA data is time consuming, but also rich in information. Nevertheless, experiments can be performed in 96 well plates, and data evaluation could be partly automated in the future. In contrast, the differentiation of peripheral neurons and LUHMES is relatively short and the endpoints of neurite outgrowth and neurite integrity are easy to measure and evaluate (Hoelting *et al.* 2016, Delp *et al.* 2018). Hence, they have the highest throughput among the test systems applied here (about 100 substances can be screened per month) (Fig. 6.1).

5.4.3. Compound selection

Also the spectrum of compounds already tested in a test system is of importance. In peripheral neurons and LUHMES already a broad spectrum of compounds has been tested (Hoelting *et al.* 2016, Delp *et al.* 2018, Masjosthusmann *et al.* 2020) whereas in UKN1 mainly HDACi and mercurials have been tested (Rempel *et al.* 2015, Shinde *et al.* 2017, Dreser *et al.* 2020). The scope of tested compounds should be widened in the future. Possible candidates of compound classes would be retinoids or compounds interfering with SHH signaling. However, for MCC the lack of diverse compound selection is most striking. At the moment only known agonists and antagonists for the NMDA receptor have been applied, which is common for cell systems in their early phase of development. In the future it would be interesting, to also apply compounds from the group of pesticides, addictive drugs, or pharmaceuticals with seizurogenic potential. To test the seizure ability of the cell system, also the implementation of MEA as a routinely applied endpoint has to be optimized. However, the preconditions of the cell system (comprising of excitatory and inhibitory neurons and glia cells) constitute a very good starting point to investigate many of these exiting questions. Also disturbances triggered by compounds not directly interfering with the NMDA receptor would be interesting to investigate with MCC. Here, it could be imaginable to investigate sensitizing effects.

5.4.4. Readiness of the applied test systems

A recent publication of Bal-Price *et al.* defined criteria to assess the readiness of published test systems for regulatory acceptance. The publication also included some of the test systems presented in this thesis. Here, the readiness of all test systems presented in this thesis is evaluated, based on the criteria defined by Bal-Price *et al.* 2018.

In their study, Bal-Price *et al.* have introduced a semi-quantitative measure to evaluate the readiness in a comprehensive way. For this purpose, the criteria were clustered in 13 groups e.g. test system, endpoints, prediction model, applicability domain, each group had various sub-groups. Main groups were sorted in three phases: phase I deals with the basic features of a test method, e.g. biological plausibility of a test methods and its controls; phase II addresses the implementation of the test method for practical use, here e.g. testing strategy, robustness and prediction model are evaluated; phase III is optional and

considers screening hits. Each phase is scored and graded independently, and results in an overall rank from A ("close to ready or ready") to D ("not ready at all") (Bal-Price *et al.* 2018). LUHMES, peripheral neurons and UKN1 have already been assessed on their readiness. According to this approach, LUHMES were graded with "A-A-A" resulting in an overall "A" grading ("ready"). Peripheral neurons were graded with "A-B-A" resulting in an overall "A-" grading ("close to ready"). UKN1 achieved a "B" rank and minor improvements were suggested to achieve readiness. Meanwhile, the test method was improved and issues missing in the initial readiness ranking were addressed. In detail, the assay was transferred into another laboratory, a prediction model was set up and confirmed, and a borderline range was defined (Dreser *et al.* 2020), and an AOP was set up (AOP 2020). Now, the UKN1 test system also has an "A" rank and can be assumed as ready. MCC are not a fully developed test method and are therefore not ready yet (Fig. 6.1). Several issues have to be addressed, like a prediction model, cytotoxicity and the evaluation of more unknown compounds. Until now, mainly tool compounds were tested, which are known to act as agonists or antagonist of the NMDA receptor. The Ca^{2+} signaling needs to be routinely multiplexed with a cytotoxicity endpoint after 24 hours, to distinguish changes in receptor signaling from cytotoxicity but also to detect excitotoxicity. Furthermore, it would be beneficial to investigate the cell composition of MCC in more detail. Therefore, single cell sequencing is ideal to reveal the transcriptional fingerprint of the different cell types present in the mixed culture. When these issues are adapted, also criteria that require more historical data, as long term reproducibility, can be evaluated and a inter lab transfer could be considered. Nevertheless, the MCC cell system constitutes a good basis to build up a valuable test system, closing a gap in existing test batteries.

5.5. Future perspectives

In this thesis it has been shown, that differentiation of pluripotent stem cells into various cell types of the human nervous system provide a substantial advantage for DNT testing. Instead of traditional animal experiments, they can reveal the underlying mechanisms inducing toxicity. Thereby they support the attempts of a comprehensive understanding of PoT, a new risk assessment, and chemical prioritization in accordance with IATA. In order to augment the value of NAMs and implement them better in regulatory toxicity, it is worth to conduct appropriate *in vivo* to *in vitro* extrapolation (IVIVE) approaches. In some cases, human based models do not perfectly predict old data generated in animal models.

This is also not to be expected, as animal data do also not perfectly reflect the human situation. The goal should be to predict human toxicity with all available methods. Therefore, it would be interesting to apply IVIVE to the used NAMs.

LUHMES and peripheral neurons can be implemented in test batteries and were already in use in screenings organized by the EFSA (Masjosthusmann *et al.* 2020). UKN1 is also ready for screening and is implemented in a project initiated by the OECD. It would be beneficial to increase the throughput of this test method. This could be achieved by differentiation in a smaller well format allowing to test more compounds per differentiation. The addition of the functional endpoint also allows a higher throughput, especially in combination with a freezing step that enables the production of bigger cell batches. As discussed before, MCC are at the beginning of its test method development and need improvements in many regards.

Although the test methods used in this thesis cover already a lot of very important neurodevelopmental processes, other NAMs are needed to construct a complete test battery for developmental neurotoxicity. For example the essential process of neural crest cell migration was not covered at all in this thesis. However, a ready to use test method is available (Nyffeler *et al.* 2017), which has already been used i.a. in a test battery of a screening with about 120 substances (Masjosthusmann *et al.* 2020). Another crucial, area of neurodevelopment is radial glia migration. Radial glia cells are the main class of neural stem cells in the developing brain (Dimou *et al.* 2014) and therefore are important to assess. They also provide the scaffold for neuronal migration in the later cortex. When the migration and subsequent scaffold formation is disturbed, e.g. by methylmercury, this could lead to disturbed cortex development (Choi 1989). Furthermore, neuronal migration and astrocyte differentiation, as well as oligodendrocyte differentiation are covered by the test systems used in this thesis. However, there are test systems available for these neurodevelopmental processes (see Fig. 6.1). As mentioned before, the whole area of synaptogenesis and neuronal network formation and signaling is mainly covered by test systems with rat primary cells. With respect to inter species differences, it would be favorable to develop more test systems based on human cells in the later stages of neurodevelopment.

Even, when a comprehensive test battery is assembled, it is important to think about an efficient test strategy. Therefore, all test systems could be either used in a paralleled

approach where all compounds are tested in all systems at the same time. Subsequently the most sensitive test system is evaluated and thereby also information about the most sensitive neurodevelopmental process is obtained. As some test systems, like LUHMES or peripheral neurons are very fast and easy to conduct, and others, like UKN1 and MCC are slightly more complicated, but also provide more mechanistic understanding of the induced toxicity, one could think about a tiered testing strategy. In a tiered testing strategy fast and easy test systems could be used first, while more complicated ones with a lower throughput follow. To this end, all compounds would be tested in the first tier and only negative compounds would be tested in the more elaborated test system. This testing strategy could speed up the screening process, but it would be accompanied by a loss in information, as not all possible neurodevelopmental processes would be covered for all substances. Hence, no statement about all possible disturbed neurodevelopmental processes could be given but for the first tier test systems these information could be provided. A more guided testing strategy could include a compound grouping with *in silico* methods like QSAR prior to testing. Therefore, the compounds would be assessed with respect to their possible MoA and the test system that best covers this MoA would be chosen as a first tier. Also combinations of these testing strategies could be considered, e.g. all compounds are tested in high throughput test systems as first tier. Subsequently, negative compounds plus compounds with an interesting MoA for a specific test system are tested in the respective test systems as a seconds tier.

A comprehensive test battery paired with a well-planned test strategy will be essential for future chemical testing and prioritization in regulatory toxicology.

6. Danksagung

Diese Dissertation wäre ohne die Hilfe vieler Menschen nicht möglich gewesen.

Zuerst möchte ich meinem Erstbetreuer Marcel Leist herzlich für sein Vertrauen, seinen kritischen Rat und seine Unterstützung über all die Jahre danken. Weiter möchte ich mich bei Alexander Bürkle für hilfreiche Diskussionen bei InViTe Retreats und die Übernahme des Zweitgutachtens bedanken. Außerdem möchte ich meinem Zweitbetreuer Dan Dietrich für seine vielen Ideen und seinen Rat zum Thema Microcystin danken.

Wichtig sind und waren auch meine Kollegen in der AG Leist. Sie waren immer für mich da, um mich aufzumuntern und mit mir Ideen zu entwickeln, wenn ich nicht weiter kam, aber auch, um sich mit mir über Erfolge zu freuen. Auch außerhalb der professionellen Zusammenarbeit gab es viele schöne Momente. Ich denke da zum Beispiel an gemeinsames Fußball-WM-Schauen, Fasnacht, grillen, Weihnachtsfeiern, diverse Bouldersessions, PhD-Abende, Laborausflüge, Kindergeburtstage, spontane Wiedersehensfeiern und vieles mehr. Ich erinnere mich sehr gerne zurück und bin dankbar für die gemeinsame Zeit und die entstandenen Freundschaften. Ein besonderer Dank geht auch an meine Bürokollegen Nadine, Tanja, Matze, Anna, Sophie, Jonny und Markus für die vielen gemeinsamen Stunden, gefüllt mit Arbeit, Spaß, Gelächter und angeregten Diskussionen. Ein ganz herzlicher Dank geht auch an Marion, dafür dass sie immer mit Rat und Tat zur Seite steht, sei es beruflich oder persönlich.

Ganz besonders möchte ich Xenia danken, die mir immer ein Dach über dem Kopf gewährt hat und einige lange und lustige Abende mit mir verbracht hat. Danke Nadine, Simon und Tanja für das kritische Korrekturlesen dieser Dissertation und ihre Anmerkungen.

Danken möchte ich auch meiner Familie, die mir mein Studium ermöglicht und mich immer unterstützt hat. Zuletzt möchte ich meinem Partner Axel dafür danken, dass er immer für mich da ist und es schafft mir Gelassenheit zu geben und mich zum Lachen zu bringen.

7. Author's contribution

For the paper "From transient transcriptome responses to disturbed neurodevelopment: Role of histone acetylation and methylation as epigenetic switch between reversible and irreversible drug effects." Nina V. Balmer and I performed most of the laboratory work. Affymetrix samples were measured in Cologne by Margit Henry, Kesavan Meganathan, and Agapios Sachinidis. The statistical analysis of the transcriptome data was performed by Michael R. Berthold, Violetta N. Ivanova, Raivo Kolde, Jörg Rahnenführer, and Eugen Rempel. Matthias K. Weng performed some of the ChiP experiments. Jan G. Hengstler was involved in project design. I was supervised by Tanja Waldmann und Marcel Leist. The paper was written by Nina V. Balmer, Marcel Leist, Tanja Waldmann and me.

For the paper "Examination of microcystin neurotoxicity using central and peripheral human neurons" the majority of the laboratory work was performed by myself. My co-authors contributed as follows: The initial analysis of the transcriptomic data was done by Ilinca Suciu. Some qPCR data were obtained by Lisa Hoelting. Simon Gutbier and Tanja Waldmann performed parts of the LUHMES cell culture. I was supervised by Tanja Waldmann, Daniel R. Dietrich and Marcel Leist. The paper was written by Marcel Leist and me.

For the paper "A human stem cell-derived test system for agents modifying neuronal N-methyl-D-aspartate-type glutamate receptor Ca^{2+} signaling" the majority of the laboratory work was performed by myself. My co-authors contributed as follows: The transcriptomic data were analyzed and evaluated by Markus Brüll, Ilinca Suciu and me. Sophie Spreng performed the characterization of NESC. MEA data were obtained by Tjalda Falt. The program CaFFEE was developed by Christiaan Karreman. I learned the differentiation protocol from Reinhardt *et al.* in the laboratory of Jens C. Schwamborn. I was supervised by Tanja Waldmann, Christiaan Karreman and Marcel Leist. The paper was written by Marcel Leist and me.

8. References

Abranches E, Silva M, Pradier L, Schulz H, Hummel O, Henrique D, Bekman E (2009) Neural differentiation of embryonic stem cells in vitro: a road map to neurogenesis in the embryo *PLoS One* 4, e6286.

Agirman G, Broix L, Nguyen L (2017) Cerebral cortex development: an outside-in perspective *FEBS Letters* 591, 3978-3992.

Alépée N, Bahinski A, Daneshian M, De Wever B, Fritsche E, Goldberg A, Hansmann J, Hartung T, Haycock J, Hogberg H, Hoelting L, Kelm JM, Kadereit S, McVey E, Landsiedel R, Leist M, Lübberstedt M, Noor F, Pellevoisin C, Petersohn D, Pfannenbecker U, Reisinger K, Ramirez T, Rothen-Rutishauser B, Schäfer-Korting M, Zeilinger K, Zurich MG (2014) State-of-the-art of 3D cultures (organs-on-a-chip) in safety testing and pathophysiology *Altex* 31, 441-477.

Allen NJ, Lyons DA (2018) Glia as architects of central nervous system formation and function *Science* 362, 181.

Allis C, Jenuwein T, Reinberg D (2007) Epigenetics New York Cold Spring Harbor Laboratory Press.

Altaner S, Jaeger S, Fotler R, Zemskov I, Wittmann V, Schreiber F, Dietrich DR (2020) Machine learning prediction of cyanobacterial toxin (microcystin) toxicodynamics in humans *Altex* 37, 24-36.

Altaner S, Puddick J, Fessard V, Feurstein D, Zemskov I, Wittmann V, Dietrich DR (2019) Simultaneous Detection of 14 Microcystin Congeners from Tissue Samples Using UPLC- ESI-MS/MS and Two Different Deuterated Synthetic Microcystins as Internal Standards *Toxins* 11, 388.

Andersen ME, Krewski D (2010) The vision of toxicity testing in the 21st century: moving from discussion to action *Toxicol Sci* 117, 17-24.

Ankley GT, Bennett RS, Erickson RJ, Hoff DJ, Hornung MW, Johnson RD, Mount DR, Nichols JW, Russom CL, Schmieder PK, Serrrano JA, Tietge JE, Villeneuve DL (2010) Adverse outcome pathways: a conceptual framework to support ecotoxicology research and risk assessment *Environ Toxicol Chem* 29, 730-741.

AOP W (2020). Retrieved 2020/11/22, from https://aopwiki.org/aops/275.

Aschner M, Ceccatelli S, Daneshian M, Fritsche E, Hasiwa N, Hartung T, Hogberg HT, Leist M, Li A, Mundi WR, Padilla S, Piersma AH, Bal-Price A, Seiler A, Westerink RH, Zimmer B, Lein PJ (2017) Reference compounds for alternative test methods to indicate developmental neurotoxicity (DNT) potential of chemicals: example lists and criteria for their selection and use *Altex* 34, 49-74.

Avila AM, Bebenek I, Bonzo JA, Bourcier T, Davis Bruno KL, Carlson DB, Dubinion J, Elayan I, Harrouk W, Lee SL, Mendrick DL, Merrill JC, Peretz J, Place E, Saulnier M, Wange RL, Yao J, Zhao D, Brown PC (2020) An FDA/CDER perspective on nonclinical testing strategies: Classical toxicology approaches and new approach methodologies (NAMs) *Regul Toxicol Pharmacol* 114, 104662.

Azevedo SMFO, Carmichael WW, Jochimsen EM, Rinehart KL, Lau S, Shaw GR, Eaglesham GK (2002) Human intoxication by microcystins during renal dialysis treatment in Caruaru-Brazil *Toxicology* 181-182, 441-446.

Bal-Price A, Fritsche E (2018) Editorial: Developmental neurotoxicity *Toxicol Appl Pharmacol* 354, 1-2.

Bal-Price A, Hogberg HT, Crofton KM, Daneshian M, FitzGerald RE, Fritsche E, Heinonen T, Hougaard Bennekou S, Klima S, Piersma AH, Sachana M, Shafer TJ, Terron A, Monnet-Tschudi F, Viviani B, Waldmann T, Westerink RHS, Wilks MF, Witters H, Zurich MG, Leist M (2018) Recommendation on test readiness criteria for new approach methods in toxicology: Exemplified for developmental neurotoxicity *Altex* 35, 306-352.

Bal-Price A, Lein PJ, Keil KP, Sethi S, Shafer T, Barenys M, Fritsche E, Sachana M, Meek MEB (2017) Developing and applying the adverse outcome pathway concept for understanding and predicting neurotoxicity *Neurotoxicology* 59, 240-255.

Bal-Price A, Meek MEB (2017) Adverse outcome pathways: Application to enhance mechanistic understanding of neurotoxicity *Pharmacol Ther* 179, 84-95.

Balmer NV, Klima S, Rempel E, Ivanova VN, Kolde R, Weng MK, Meganathan K, Henry M, Sachinidis A, Berthold MR, Hengstler JG, Rahnenführer J, Waldmann T, Leist M (2014) From transient transcriptome responses to disturbed neurodevelopment: role of histone acetylation and methylation as epigenetic switch between reversible and irreversible drug effects *Arch Toxicol* 88, 1451-1468.

Balmer NV, Weng MK, Zimmer B, Ivanova VN, Chambers SM, Nikolaeva E, Jagtap S, Sachinidis A, Hescheler J, Waldmann T, Leist M (2012) Epigenetic changes and disturbed neural development in a human embryonic stem cell-based model relating to the fetal valproate syndrome *Hum Mol Genet* 21, 4104-4114.

Balu DT (2016) The NMDA Receptor and Schizophrenia: From Pathophysiology to Treatment *Adv Pharmacol* 76, 351-382.

Bannister AJ, Kouzarides T (2011) Regulation of chromatin by histone modifications *Cell Res* 21, 381-395.

Bar-Shira O, Maor R, Chechik G (2015) Gene Expression Switching of Receptor Subunits in Human Brain Development *PLoS Comput Biol* 11, e1004559.

Baumann J, Barenys M, Gassmann K, Fritsche E (2014) Comparative human and rat "neurosphere assay" for developmental neurotoxicity testing *Curr Protoc Toxicol* 59, 12.21.11-24.

Benjamini Y, Hochberg Y (1995) Controlling the false discovery rate: a practical and powerful approach to multiple testing *Journal of the Royal statistical society: series B (Methodological)* 57, 289-300.

Berger ML, Palangsuntikul R, Rebernik P, Wolschann P, Berner H (2012) Screening of 64 tryptamines at NMDA, 5-HT1A, and 5-HT2A receptors: a comparative binding and modeling study *Curr Med Chem* 19, 3044-3057.

Berger SL (2007) The complex language of chromatin regulation during transcription *Nature* 447, 407-412.

Beronius A, Johansson N, Rudén C, Hanberg A (2013) The influence of study design and sex-differences on results from developmental neurotoxicity studies of bisphenol A: implications for toxicity testing *Toxicology* 311, 13-26.

Berthold MR, Cebron N, Dill F, Gabriel TR, Kötter T, Meinl T, Ohl P, Sieb C, Thiel K, Wiswedel B (2008). Data analysis, machine learning and applications. Proceedings of the 31st Annual Conference of the Gesellschaft für Klassifikation eV (Studies in classification, data analysis, and knowledge organization). Springer, Berlin.

Bettini E, Sava A, Griffante C, Carignani C, Buson A, Capelli AM, Negri M, Andreetta F, Senar-Sancho SA, Guiral L, Cardullo F (2010) Identification and Characterization of Novel NMDA Receptor Antagonists Selective for NR2A- over NR2B-Containing Receptors *J Pharmacol Exp Therap* 335, 636-644.

Bihaqi SW, Zawia NH (2012) Alzheimer's disease biomarkers and epigenetic intermediates following exposure to Pb in vitro *Curr Alzheimer Res* 9, 555-562.

Bondy SC, Campbell A (2005) Developmental neurotoxicology *J Neurosci Res* 81, 605-612.

Bose R, Onishchenko N, Edoff K, Janson Lang AM, Ceccatelli S (2012) Inherited effects of low-dose exposure to methylmercury in neural stem cells *Toxicol Sci* 130, 383-390.

Botes D.P. TAA, Wessels P.L., Viljoen C.C., Kruger H., Williams D.H., Santikarn S., Smith R.J. Hammond S.J. (1984) The structure of cyanoginosin-LA, a cyclic heptapeptide toxin from the cyanobacterium Microcystis aeruginos. *J. Chem. Soc. Perkin Trans.* I, 2311-2318.

Botia B, Legastelois R, Alaux-Cantin S, Naassila M (2012) Expression of ethanol-induced behavioral sensitization is associated with alteration of chromatin remodeling in mice *PLoS One* 7, e47527.

Boudadi E, Stower H, Halsall JA, Rutledge CE, Leeb M, Wutz A, O'Neill LP, Nightingale KP, Turner BM (2013) The histone deacetylase inhibitor sodium valproate causes limited transcriptional change in mouse embryonic stem cells but selectively overrides Polycomb-mediated Hoxb silencing *Epigenetics Chromatin* 6, 11.

Bronger H, König J, Kopplow K, Steiner H-H, Ahmadi R, Herold-Mende C, Keppler D, Nies AT (2005) ABCC drug efflux pumps and organic anion uptake transporters in human gliomas and the blood-tumor barrier *Cancer research* 65, 11419-11428.

Buratti FM, Manganelli M, Vichi S, Stefanelli M, Scardala S, Testai E, Funari E (2017) Cyanotoxins: producing organisms, occurrence, toxicity, mechanism of action and human health toxicological risk evaluation *Arch Toxicol* 91, 1049-1130.

Burney MJ, Johnston C, Wong KY, Teng SW, Beglopoulos V, Stanton LW, Williams BP, Bithell A, Buckley NJ (2013) An epigenetic signature of developmental potential in neural stem cells and early neurons *Stem Cells* 31, 1868-1880.

Cao SY, Hu Y, Chen C, Yuan F, Xu M, Li Q, Fang KH, Chen Y, Liu Y (2017) Enhanced derivation of human pluripotent stem cell-derived cortical glutamatergic neurons by a small molecule *Sci Rep* 7, 3282.

Carmichael WW (1992) Cyanobacteria secondary metabolites--the cyanotoxins *J Appl Bacteriol* 72, 445-459.

Casati S (2018) Integrated Approaches to Testing and Assessment *Basic Clin Pharmacol Toxicol* 123 Suppl 5, 51-55.

Chambers SM, Fasano CA, Papapetrou EP, Tomishima M, Sadelain M, Studer L (2009) Highly efficient neural conversion of human ES and iPS cells by dual inhibition of SMAD signaling *Nat Biotechnol* 27, 275-280.

Chazaud C, Yamanaka Y, Pawson T, Rossant J (2006) Early lineage segregation between epiblast and primitive endoderm in mouse blastocysts through the Grb2-MAPK pathway *Dev Cell* 10, 615-624.

Chen J, Xie P, Li L, Xu J (2009) First identification of the hepatotoxic microcystins in the serum of a chronically exposed human population together with indication of hepatocellular damage *Toxicol Sci* 108, 81-89.

Chen K, Yang LN, Lai C, Liu D, Zhu LQ (2020) Role of GRINA/NMDARA1 in Central Nervous System Diseases *Curr Neuropharmacol*.

Chen L, Xie P (2016) Mechanisms of Microcystin-induced Cytotoxicity and Apoptosis *Mini Rev Med Chem* 16, 1018-1031.

Chenard BL, Bordner J, Butler TW, Chambers LK, Collins MA, De Costa DL, Ducat MF, Dumont ML, Fox CB (1995) (1S,2S)-1-(4-Hydroxyphenyl)-2-(4-hydroxy-4-phenylpiperidino)-1-propanol: A Potent New Neuroprotectant Which Blocks N-Methyl-D-Aspartate Responses *J Med Chem* 38, 3138-3145.

Choi BH (1989) The effects of methylmercury on the developing brain *Prog Neurobiol* 32, 447-470.

Choi DW, Viseskul V, Amirthanayagam M, Monyer H (1989) Aspartate neurotoxicity on cultured cortical neurons *J Neurosci Res* 23, 116-121.

Cohen AL, Soldi R, Zhang H, Gustafson AM, Wilcox R, Welm BE, Chang JT, Johnson E, Spira A, Jeffrey SS, Bild AH (2011) A pharmacogenomic method for individualized prediction of drug sensitivity *Mol Syst Biol* 7, 513.

Cohen SM, Tsien RW, Goff DC, Halassa MM (2015) The impact of NMDA receptor hypofunction on GABAergic neurons in the pathophysiology of schizophrenia *Schizophr Res* 167, 98-107.

Colleoni S, Galli C, Gaspar JA, Meganathan K, Jagtap S, Hescheler J, Sachinidis A, Lazzari G (2011) Development of a neural teratogenicity test based on human embryonic stem cells: response to retinoic acid exposure *Toxicol Sci* 124, 370-377.

Collins FS, Gray GM, Bucher JR (2008) Toxicology. Transforming environmental health protection *Science* 319, 906-907.

Conti L, Cattaneo E (2010) Neural stem cell systems: physiological players or in vitro entities? *Nat Rev Neurosci* 11, 176-187.

Cook D, Brown D, Alexander R, March R, Morgan P, Satterthwaite G, Pangalos MN (2014) Lessons learned from the fate of AstraZeneca's drug pipeline: a five-dimensional framework *Nat Rev Drug Discov* 13, 419-431.

Coskun V, Tsoa R, Sun YE (2012) Epigenetic regulation of stem cells differentiating along the neural lineage *Curr Opin Neurobiol* 22, 762-767.

Crofton KM, Mundy WR, Shafer TJ (2012) Developmental neurotoxicity testing: a path forward *Congenit Anom* 52, 140-146.

Cull-Candy S, Brickley S, Farrant M (2001) NMDA receptor subunits: diversity, development and disease *Curr Opin Neurobiol* 11, 327-335.

Daneshian M, Botana LM, Dechraoui Bottein M-Y, Buckland G, Campàs M, Dennison N, Dickey RW, Diogène J, Fessard V, Hartung T, Humpage A, Leist M, Molgó J, Quilliam MA, Rovida C, Suarez-Isla BA, Tubaro A, Wagner K, Zoller O, Dietrich D (2013) A roadmap for hazard monitoring and risk assessment of marine biotoxins on the basis of chemical and biological test systems *Altex* 30, 487-545.

de Leeuw VC, Hessel EVS, Pennings JLA, Hodemaekers HM, Wackers PFK, van Oostrom CTM, Piersma AH (2020) Differential effects of fluoxetine and venlafaxine in the neural embryonic stem cell test (ESTn) revealed by a cell lineage map *Neurotoxicology* 76, 1-9.

Delp J, Funke M, Rudolf F, Cediel A, Bennekou SH, van der Stel W, Carta G, Jennings P, Toma C, Gardner I, van de Water B, Forsby A, Leist M (2019) Development of a neurotoxicity assay that is tuned to detect mitochondrial toxicants *Arch Toxicol* 93, 1585-1608.

Delp J, Gutbier S, Klima S, Hoelting L, Pinto-Gil K, Hsieh J-H, Aichem M, Klein K, Schreiber F, Tice RR, Pastor M, Behl M, Leist M (2018) A high-throughput approach to identify specific neurotoxicants/ developmental toxicants in human neuronal cell function assays *Altex* 35, 235-253.

Desprez B, Birk B, Blaauboer B, Boobis A, Carmichael P, Cronin MTD, Curie R, Daston G, Hubesch B, Jennings P, Klaric M, Kroese D, Mahony C, Ouédraogo G, Piersma A, Richarz A-N, Schwarz M, van Benthem J, van de Water B, Vinken M (2019) A mode-of-action ontology model for safety evaluation of chemicals: Outcome of a series of workshops on repeated dose toxicity *Toxicology in vitro* 59, 44-50.

Devos D, Moreau C, Devedjian JC, Kluza J, Petrault M, Laloux C, Jonneaux A, Ryckewaert G, Garçon G, Rouaix N, Duhamel A, Jissendi P, Dujardin K, Auger F, Ravasi L, Hopes L, Grolez G, Firdaus W, Sablonnière B, Strubi-Vuillaume I, Zahr N, Destée A, Corvol J-C, Pöltl D, Leist M, Rose C, Defebvre L, Marchetti P, Cabantchik ZI, Bordet R (2014) Targeting chelatable iron as a therapeutic modality in Parkinson's disease *Antioxi Redox signal* 21, 195-210.

Dietrich D, Hoeger S (2005) Guidance values for microcystins in water and cyanobacterial supplement products (blue-green algal supplements): a reasonable or misguided approach? *Toxicol Appl Pharmacol* 203, 273-289.

DiFiglia M (1990) Excitotoxic injury of the neostriatum: a model for Huntington's disease *Trends Neurosci* 13, 286-289.

Dimou L, Götz M (2014) Glial cells as progenitors and stem cells: new roles in the healthy and diseased brain *Physiol Rev* 94, 709-737.

Doucette TA, Tasker RA (2016) Perinatal Domoic Acid as a Neuroteratogen *Curr Top Behav Neurosci* 29, 87-110.

Dreser N, Madjar K, Holzer AK, Kapitza M, Scholz C, Kranaster P, Gutbier S, Klima S, Kolb D, Dietz C, Trefzer T, Meisig J, van Thriel C, Henry M, Berthold MR, Blüthgen N, Sachinidis A, Rahnenführer J, Hengstler JG, Waldmann T, Leist M (2020) Development of a neural rosette formation assay (RoFA) to identify neurodevelopmental toxicants and to characterize their transcriptome disturbances *Arch Toxicol* 94, 151-171.

Dreser N, Zimmer B, Dietz C, Sügis E, Pallocca G, Nyffeler J, Meisig J, Blüthgen N, Berthold MR, Waldmann T, Leist M (2015) Grouping of histone deacetylase inhibitors and other toxicants disturbing neural crest migration by transcriptional profiling *Neurotoxicology* 50, 56-70.

Dufour-Rainfray D, Vourc'h P, Le Guisquet AM, Garreau L, Ternant D, Bodard S, Jaumain E, Gulhan Z, Belzung C, Andres CR, Chalon S, Guilloteau D (2010) Behavior and serotonergic disorders in rats exposed prenatally to valproate: a model for autism *Neurosci Lett* 470, 55-59.

Dulac C (2010) Brain function and chromatin plasticity *Nature* 465, 728-735.

ECHA (2016) New Approach Methodologies in Regulatory ScienceProceedings of a scientific workshopHelsinki, 19–20 April 2016.

Elshazzly M, Lopez MJ, Reddy V, Caban O (2020) Embryology, Central Nervous System StatPearls Publishing LLC.

EpiPM (2015) A roadmap for precision medicine in the epilepsies *Lancet Neurol* 14, 1219-1228.

Escher SE, Kamp H, Bennekou SH, Bitsch A, Fisher C, Graepel R, Hengstler JG, Herzler M, Knight D, Leist M, Norinder U, Ouédraogo G, Pastor M, Stuard S, White A, Zdrazil B, van de Water B, Kroese D (2019) Towards grouping concepts based on new approach methodologies in chemical hazard assessment: the read-across approach of the EU-ToxRisk project *Arch Toxicol* 93, 3643-3667.

Fass DM, Shah R, Ghosh B, Hennig K, Norton S, Zhao WN, Reis SA, Klein PS, Mazitschek R, Maglathlin RL, Lewis TA, Haggarty SJ (2010) Effect of Inhibiting Histone Deacetylase with Short-Chain Carboxylic Acids and Their Hydroxamic Acid Analogs on Vertebrate Development and Neuronal Chromatin *ACS Med Chem Lett* 2, 39-42.

Feuerbach D, Loetscher E, Neurdin S, Koller M (2010) Comparative pharmacology of the human NMDA-receptor subtypes R1-2A, R1-2B, R1-2C and R1-2D using an inducible expression system *Eur J Pharmacol* 637, 46-54.

Feurstein D, Holst K, Fischer A, Dietrich DR (2009) Oatp-associated uptake and toxicity of microcystins in primary murine whole brain cells *Toxicol Appl Pharmacol* 234, 247-255.

Feurstein D, Stemmer K, Kleinteich J, Speicher T, Dietrich DR (2011) Microcystin congener- and concentration-dependent induction of murine neuron apoptosis and neurite degeneration *Toxicol Sci* 124, 424-431.

Fischer I, Milton C, Wallace H (2020) Toxicity testing is evolving! *Toxicol Res (Camb)* 9, 67-80.

Fischer WJ, Altheimer S, Cattori V, Meier PJ, Dietrich DR, Hagenbuch B (2005) Organic anion transporting polypeptides expressed in liver and brain mediate uptake of microcystin *Toxicol Appl Pharmacol* 203, 257-263.

Fischer WJ, Dietrich DR (2000) Pathological and biochemical characterization of microcystin-induced hepatopancreas and kidney damage in carp (Cyprinus carpio) *Toxicol Appl Pharmacol* 164, 73-81.

Fritsche E, Crofton KM, Hernandez AF, Hougaard Bennekou S, Leist M, Bal-Price A, Reaves E, Wilks MF, Terron A, Solecki R, Sachana M, Gourmelon A (2017) OECD/EFSA workshop on developmental neurotoxicity (DNT): The use of non-animal test methods for regulatory purposes *Altex* 34, 311-315.

Frohlich J, Van Horn JD (2014) Reviewing the ketamine model for schizophrenia *J Psychopharmacol* 28, 287-302.

Fujiki R, Sato A, Fujitani M, Yamashita T (2013) A proapoptotic effect of valproic acid on progenitors of embryonic stem cell-derived glutamatergic neurons *Cell Death Dis* 4, e677.

Fukaya M, Kato A, Lovett C, Tonegawa S, Watanabe M (2003) Retention of NMDA receptor NR2 subunits in the lumen of endoplasmic reticulum in targeted NR1 knockout mice *Proceedings of the National Academy of Sciences* 100, 4855-4860.

Gammill LS, Bronner-Fraser M (2003) Neural crest specification: migrating into genomics *Nat Rev Neurosci* 4, 795-805.

Gao Y-s, Hubbert CC, Lu J, Lee Y-S, Lee J-Y, Yao T-P (2007) Histone deacetylase 6 regulates growth factor-induced actin remodeling and endocytosis *Mol Cell Biol* 27, 8637-8647.

Gautier L, Cope L, Bolstad BM, Irizarry RA (2004) affy--analysis of Affymetrix GeneChip data at the probe level *Bioinformatics* 20, 307-315.

Gentleman RC, Carey VJ, Bates DM, Bolstad B, Dettling M, Dudoit S, Ellis B, Gautier L, Ge Y, Gentry J, Hornik K, Hothorn T, Huber W, Iacus S, Irizarry R, Leisch F, Li C, Maechler M, Rossini AJ, Sawitzki G, Smith C, Smyth G, Tierney L, Yang JY, Zhang J (2004) Bioconductor: open software development for computational biology and bioinformatics *Genome Biol* 5, R80.

Göttlicher M, Minucci S, Zhu P, Krämer OH, Schimpf A, Giavara S, Sleeman JP, Lo Coco F, Nervi C, Pelicci PG, Heinzel T (2001) Valproic acid defines a novel class of HDAC inhibitors inducing differentiation of transformed cells *Embo J* 20, 6969-6978.

Gräff J, Rei D, Guan JS, Wang WY, Seo J, Hennig KM, Nieland TJ, Fass DM, Kao PF, Kahn M, Su SC, Samiei A, Joseph N, Haggarty SJ, Delalle I, Tsai LH (2012) An epigenetic blockade of cognitive functions in the neurodegenerating brain *Nature* 483, 222-226.

Grandjean P, Landrigan PJ (2006) Developmental neurotoxicity of industrial chemicals *Lancet* 368, 2167-2178.

Grandjean P, Landrigan PJ (2014) Neurobehavioural effects of developmental toxicity *Lancet Neurol* 13, 330-338.

Greene ND, Copp AJ (2014) Neural tube defects *Annu Rev Neurosci* 37, 221-242.

Guilarte TR, Miceli RC (1992) Age-dependent effects of lead on [3H]MK-801 binding to the NMDA receptor-gated ionophore: in vitro and in vivo studies *Neurosci Lett* 148, 27-30.

Guilarte TR, Miceli RC, Jett DA (1995) Biochemical evidence of an interaction of lead at the zinc allosteric sites of the NMDA receptor complex: effects of neuronal development *Neurotoxicology* 16, 63-71.

Guo F, Sun Y, Wang X, Wang H, Wang J, Gong T, Chen X, Zhang P, Su L, Fu G, Su J, Yang S, Lai R, Jiang C, Liang P (2019) Patient-Specific and Gene-Corrected Induced Pluripotent Stem Cell-Derived Cardiomyocytes Elucidate Single-Cell Phenotype of Short QT Syndrome *Circ Res* 124, 66-78.

Guo H, Camargo LM, Yeboah F, Digan ME, Niu H, Pan Y, Reiling S, Soler-Llavina G, Weihofen WA, Wang HR, Shanker YG, Stams T, Bill A (2017) A NMDA-receptor calcium influx assay sensitive to stimulation by glutamate and glycine/D-serine *Sci Rep* 7, 11608.

Gutbier S, May P, Berthelot S, Krishna A, Trefzer T, Behbehani M, Efremova L, Delp J, Gstraunthaler G, Waldmann T, Leist M (2018) Major changes of cell function and toxicant sensitivity in cultured cells undergoing mild, quasi-natural genetic drift *Arch Toxicol* 92, 3487-3503.

Gutbier S, Spreng A-S, Delp J, Schildknecht S, Karreman C, Suciu I, Brunner T, Groettrup M, Leist M (2018) Prevention of neuronal apoptosis by astrocytes through thiol-mediated stress response modulation and accelerated recovery from proteotoxic stress *Cell Death Differ* 25, 2101-2117.

Hagenbuch B, Meier PJ (2003) The superfamily of organic anion transporting polypeptides *Biochimica et biophysica acta* 1609, 1-18.

Hamilton PJ, Nestler EJ (2019) Epigenetics and addiction *Curr Opin Neurobiol* 59, 128-136.

Hansen KB, Yi F, Perszyk RE, Furukawa H, Wollmuth LP, Gibb AJ, Traynelis SF (2018) Structure, function, and allosteric modulation of NMDA receptors *J Gen Physiol* 150, 1081-1105.

Harrill J, Shah I, Setzer RW, Haggard D, Auerbach S, Judson R, Thomas RS (2019) Considerations for Strategic Use of High-Throughput Transcriptomics Chemical Screening Data in Regulatory Decisions *Curr Opin Toxicol* 15, 64-75.

Harrill JA, Freudenrich TM, Machacek DW, Stice SL, Mundy WR (2010) Quantitative assessment of neurite outgrowth in human embryonic stem cell-derived hN2™ cells using automated high-content image analysis *Neurotoxicology* 31, 277-290.

Hartung T (2008) Food for thought... on animal tests *Altex* 25, 3-16.

Hartung T, van Vliet E, Jaworska J, Bonilla L, Skinner N, Thomas R (2012) Systems toxicology *Altex* 29, 119-128.

Hass U (2006) The need for developmental neurotoxicity studies in risk assessment for developmental toxicity *Reprod Toxicol* 22, 148-156.

Heikkilä TJ, Ylä-Outinen L, Tanskanen JM, Lappalainen RS, Skottman H, Suuronen R, Mikkonen JE, Hyttinen JA, Narkilahti S (2009) Human embryonic stem cell-derived neuronal cells form spontaneously active neuronal networks in vitro *Exp Neurol* 218, 109-116.

Hermsen SA, Pronk TE, van den Brandhof EJ, van der Ven LT, Piersma AH (2013) Transcriptomic analysis in the developing zebrafish embryo after compound exposure: individual gene expression and pathway regulation *Toxicol Appl Pharmacol* 272, 161-171.

Herrera N, Herrera C, Ortíz I, Orozco L, Robledo S, Agudelo D, Echeverri F (2018) Genotoxicity and cytotoxicity of three microcystin-LR containing cyanobacterial samples from Antioquia, Colombia *Toxicon* 154, 50-59.

Heussner AH, Mazija L, Fastner J, Dietrich DR (2012) Toxin content and cytotoxicity of algal dietary supplements *Toxicol Appl Pharmacol* 265, 263-271.

Hezroni H, Sailaja BS, Meshorer E (2011) Pluripotency-related, valproic acid (VPA)-induced genome-wide histone H3 lysine 9 (H3K9) acetylation patterns in embryonic stem cells *J Biol Chem* 286, 35977-35988.

Hinojosa MG, Gutiérrez-Praena D, Prieto AI, Guzmán-Guillén R, Jos A, Cameán AM (2019) Neurotoxicity induced by microcystins and cylindrospermopsin: A review *Sci Total Environ* 668, 547-565.

Hoelting L, Klima S, Karreman C, Grinberg M, Meisig J, Henry M, Rotshteyn T, Rahnenfuhrer J, Bluthgen N, Sachinidis A, Waldmann T, Leist M (2016) Stem Cell-Derived Immature Human Dorsal Root Ganglia Neurons to Identify Peripheral Neurotoxicants *Stem Cells Transl Med* 5, 476-487.

Hofrichter M, Nimtz L, Tigges J, Kabiri Y, Schröter F, Royer-Pokora B, Hildebrandt B, Schmuck M, Epanchintsev A, Theiss S, Adjaye J, Egly JM, Krutmann J, Fritsche E (2017) Comparative performance analysis of human iPSC-derived and primary neural progenitor cells (NPC) grown as neurospheres in vitro *Stem Cell Res* 25, 72-82.

Hogberg HT, Sobanski T, Novellino A, Whelan M, Weiss DG, Bal-Price AK (2011) Application of micro-electrode arrays (MEAs) as an emerging technology for developmental neurotoxicity: evaluation of domoic acid-induced effects in primary cultures of rat cortical neurons *Neurotoxicology* 32, 158-168.

Höllerhage M, Moebius C, Melms J, Chiu W-H, Goebel JN, Chakroun T, Koeglsperger T, Oertel WH, Rösler TW, Bickle M, Höglinger GU (2017) Protective efficacy of phosphodiesterase-1 inhibition against alpha-synuclein toxicity revealed by compound screening in LUHMES cells *Scientific reports* 7, 11469-11469.

Hollmann M, Heinemann S (1994) Cloned Glutamate Receptors *Annu Rev Neurosci* 17, 31-108.

Hondebrink L, Verboven AHA, Drega WS, Schmeink S, de Groot M, van Kleef R, Wijnolts FMJ, de Groot A, Meulenbelt J, Westerink RHS (2016) Neurotoxicity screening of (illicit) drugs using novel methods for analysis of microelectrode array (MEA) recordings *Neurotoxicology* 55, 1-9.

Houghton FD (2006) Energy metabolism of the inner cell mass and trophectoderm of the mouse blastocyst *Differentiation* 74, 11-18.

House JS, Grimm FA, Jima DD, Zhou YH, Rusyn I, Wright FA (2017) A Pipeline for High-Throughput Concentration Response Modeling of Gene Expression for Toxicogenomics *Front Genet* 8, 168.

Hu Y, Chen J, Fan H, Xie P, He J (2016) A review of neurotoxicity of microcystins *Environ Sci Pollut Res Int* 23, 7211-7219.

ICCVAM ICCotVoAM (2018) A Strategic Roadmap for Establishing New Approaches to Evaluate the Safety of Chemicals and Medical Products in the United States

Ishii MN, Yamamoto K, Shoji M, Asami A, Kawamata Y (2017) Human induced pluripotent stem cell (hiPSC)-derived neurons respond to convulsant drugs when co-cultured with hiPSC-derived astrocytes *Toxicology* 389, 130-138.

Ito T, Inoue K, Takada M (2015) Distribution of glutamatergic, GABAergic, and glycinergic neurons in the auditory pathways of macaque monkeys *Neuroscience* 310, 128-151.

Jalali-Yazdi F, Chowdhury S, Yoshioka C, Gouaux E (2018) Mechanisms for Zinc and Proton Inhibition of the GluN1/GluN2A NMDA Receptor *Cell* 175, 1520-1532.e1515.

Jentink J, Loane MA, Dolk H, Barisic I, Garne E, Morris JK, de Jong-van den Berg LT (2010) Valproic acid monotherapy in pregnancy and major congenital malformations *N Engl J Med* 362, 2185-2193.

Jeong S (2017) Molecular and Cellular Basis of Neurodegeneration in Alzheimer's Disease *Mol Cells* 40, 613-620.

Jergil M, Forsberg M, Salter H, Stockling K, Gustafson AL, Dencker L, Stigson M (2011) Short-time gene expression response to valproic acid and valproic acid analogs in mouse embryonic stem cells *Toxicol Sci* 121, 328-342.

Jergil M, Kultima K, Gustafson AL, Dencker L, Stigson M (2009) Valproic acid-induced deregulation in vitro of genes associated in vivo with neural tube defects *Toxicol Sci* 108, 132-148.

Jessell TM (2000) Neuronal specification in the spinal cord: inductive signals and transcriptional codes *Nat Rev Genet* 1, 20-29.

Jochimsen EM, Carmichael WW, An JS, Cardo DM, Cookson ST, Holmes CE, Antunes MB, de Melo Filho DA, Lyra TM, Barreto VS, Azevedo SM, Jarvis WR (1998) Liver failure and death after exposure to microcystins at a hemodialysis center in Brazil *N Engl J Med* 338, 873-878.

Jodo E (2013) The role of the hippocampo-prefrontal cortex system in phencyclidine-induced psychosis: a model for schizophrenia *J Physiol Paris* 107, 434-440.

Johnson JW, Ascher P (1987) Glycine potentiates the NMDA response in cultured mouse brain neurons *Nature* 325, 529-531.

Kadereit S, Zimmer B, van Thriel C, Hengstler JG, Leist M (2012) Compound selection for in vitro modeling of developmental neurotoxicity *Front Biosci* 17, 2442-2460.

Kamieniarz K, Izzo A, Dundr M, Tropberger P, Ozretic L, Kirfel J, Scheer E, Tropel P, Wisniewski JR, Tora L, Viville S, Buettner R, Schneider R (2012) A dual role of linker histone H1.4 Lys 34 acetylation in transcriptional activation *Genes Dev* 26, 797-802.

Kandel ER, Mack S, Jessell TM, J.M. S, S.A. S, A.J. H (2013) Principles of Neural Science, Fifth Edition.

Kang HJ, Kawasawa YI, Cheng F, Zhu Y, Xu X, Li M, Sousa AM, Pletikos M, Meyer KA, Sedmak G, Guennel T, Shin Y, Johnson MB, Krsnik Z, Mayer S, Fertuzinhos S, Umlauf S, Lisgo SN, Vortmeyer A, Weinberger DR, Mane S, Hyde TM, Huttner A, Reimers M, Kleinman JE, Sestan N (2011) Spatio-temporal transcriptome of the human brain *Nature* 478, 483-489.

Karreman C, Klima S, Holzer AK, Leist M (2020) CaFFEE: A program for evaluating time courses of Ca2+ dependent signal changes of complex cells loaded with fluorescent indicator dyes *Altex* 37, 332-336.

Kataoka S, Takuma K, Hara Y, Maeda Y, Ago Y, Matsuda T (2013) Autism-like behaviours with transient histone hyperacetylation in mice treated prenatally with valproic acid *Int J Neuropsychopharmacol* 16, 91-103.

Kessaris N, Fogarty M, Iannarelli P, Grist M, Wegner M, Richardson WD (2006) Competing waves of oligodendrocytes in the forebrain and postnatal elimination of an embryonic lineage *Nature neurosci* 9, 173-179.

Khan N, Jeffers M, Kumar S, Hackett C, Boldog F, Khramtsov N, Qian X, Mills E, Berghs SC, Carey N, Finn PW, Collins LS, Tumber A, Ritchie JW, Jensen PB, Lichenstein HS, Sehested M (2008) Determination of the class and isoform selectivity of small-molecule histone deacetylase inhibitors *Biochem J* 409, 581-589.

Kiernan MC, Vucic S, Cheah BC, Turner MR, Eisen A, Hardiman O, Burrell JR, Zoing MC (2011) Amyotrophic lateral sclerosis *Lancet* 377, 942-955.

Klapper SD, Garg P, Dagar S, Lenk K, Gottmann K, Nieweg K (2019) Astrocyte lineage cells are essential for functional neuronal differentiation and synapse maturation in human iPSC-derived neural networks *Glia* 67, 1893-1909.

Kleensang A, Maertens A, Rosenberg M, Fitzpatrick S, Lamb J, Auerbach S, Brennan R, Crofton KM, Gordon B, Fornace AJ, Jr., Gaido K, Gerhold D, Haw R, Henney A, Ma'ayan A, McBride M, Monti S, Ochs MF, Pandey A, Sharan R, Stierum R, Tugendreich S, Willett C, Wittwehr C, Xia J, Patton GW, Arvidson K, Bouhifd M, Hogberg HT, Luechtefeld T, Smirnova L, Zhao L, Adeleye Y, Kanehisa M, Carmichael P, Andersen ME, Hartung T (2014) Pathways of Toxicity *Altex* 31, 53-61.

Kosnik MB, Strickland JD, Marvel SW, Wallis DJ, Wallace K, Richard AM, Reif DM, Shafer TJ (2020) Concentration-response evaluation of ToxCast compounds for multivariate activity patterns of neural network function *Arch Toxicol* 94, 469-484.

Krebs A, van Vugt-Lussenburg BMA, Waldmann T, Albrecht W, Boei J, Ter Braak B, Brajnik M, Braunbeck T, Brecklinghaus T, Busquet F, Dinnyes A, Dokler J, Dolde X, Exner TE, Fisher C, Fluri D, Forsby A, Hengstler JG, Holzer AK, Janstova Z, Jennings P, Kisitu J, Kobolak J, Kumar M, Limonciel A, Lundqvist J, Mihalik B, Moritz W, Pallocca G, Ulloa APC, Pastor M, Rovida C, Sarkans U, Schimming JP, Schmidt BZ, Stöber R, Strassfeld T, van de Water B, Wilmes A, van der Burg B, Verfaillie CM, von Hellfeld R, Vrieling H, Vrijenhoek NG, Leist M (2020) The EU-ToxRisk method documentation, data processing and chemical testing pipeline for the regulatory use of new approach methods *Arch Toxicol* 94, 2435-2461.

Kreir M, Van Deuren B, Versweyveld S, De Bondt A, Van den Wyngaert I, Van der Linde H, Lu HR, Teuns G, Gallacher DJ (2018) Do in vitro assays in rat primary neurons predict drug-induced seizure liability in humans? *Toxicol Appl Pharmacol* 346, 45-57.

Krewski D, Westphal M, Andersen ME, Paoli GM, Chiu WA, Al-Zoughool M, Croteau MC, Burgoon LD, Cote I (2014) A framework for the next generation of risk science *Environ Health Perspect* 122, 796-805.

Kriegstein A, Alvarez-Buylla A (2009) The glial nature of embryonic and adult neural stem cells *Annu Rev Neurosci* 32, 149-184.

Krogsgaard-Larsen P, Ebert B, Lund TM, Bräuner-Osborne H, Sløk FA, Johansen TN, Brehm L, Madsen U (1996) Design of excitatory amino acid receptor agonists, partial agonists and antagonists: ibotenic acid as a key lead structure *Eur J Med Chem* 31, 515-537.

Krug AK, Balmer NV, Matt F, Schönenberger F, Merhof D, Leist M (2013) Evaluation of a human neurite growth assay as specific screen for developmental neurotoxicants *Arch Toxicol* 87, 2215-2231.

Krug AK, Kolde R, Gaspar JA, Rempel E, Balmer NV, Meganathan K, Vojnits K, Baquié M, Waldmann T, Ensenat-Waser R, Jagtap S, Evans RM, Julien S, Peterson H, Zagoura D, Kadereit S, Gerhard D, Sotiriadou I, Heke M, Natarajan K, Henry M, Winkler J, Marchan R, Stoppini L, Bosgra S, Westerhout J, Verwei M, Vilo J, Kortenkamp A, Hescheler J, Hothorn L, Bremer S, van Thriel C, Krause KH, Hengstler JG, Rahnenführer J, Leist M, Sachinidis A (2013) Human embryonic stem cell-derived test systems for developmental neurotoxicity: a transcriptomics approach *Arch Toxicol* 87, 123-143.

Kuegler PB, Zimmer B, Waldmann T, Baudis B, Ilmjärv S, Hescheler J, Gaughwin P, Brundin P, Mundy W, Bal-Price AK, Schrattenholz A, Krause KH, van Thriel C, Rao MS, Kadereit S, Leist M (2010) Markers of murine embryonic and neural stem cells, neurons and astrocytes: reference points for developmental neurotoxicity testing *Altex* 27, 17-42.

Landowski LM, Dyck PJ, Engelstad J, Taylor BV (2016) Axonopathy in peripheral neuropathies: Mechanisms and therapeutic approaches for regeneration *J Chem Neuroanat* 76, 19-27.

Landrigan PJ, Kimmel CA, Correa A, Eskenazi B (2004) Children's health and the environment: public health issues and challenges for risk assessment *Environ Health Perspect* 112, 257-265.

Landrigan PJ, Sonawane B, Butler RN, Trasande L, Callan R, Droller D (2005) Early environmental origins of neurodegenerative disease in later life *Environ Health Perspect* 113, 1230-1233.

Larm JA, Beart PM, Cheung NS (1997) Neurotoxin domoic acid produces cytotoxicity via kainate- and AMPA-sensitive receptors in cultured cortical neurones *Neurochem Int* 31, 677-682.

Leist M, Fava E, Montecucco C, Nicotera P (1997) Peroxynitrite and nitric oxide donors induce neuronal apoptosis by eliciting autocrine excitotoxicity *Eur J Neurosci* 9, 1488-1498.

Leist M, Ghallab A, Graepel R, Marchan R, Hassan R, Bennekou SH, Limonciel A, Vinken M, Schildknecht S, Waldmann T, Danen E, van Ravenzwaay B, Kamp H, Gardner I, Godoy P, Bois FY, Braeuning A, Reif R, Oesch F, Drasdo D, Höhme S, Schwarz M, Hartung T, Braunbeck T, Beltman J, Vrieling H, Sanz F, Forsby A, Gadaleta D, Fisher C, Kelm J, Fluri D, Ecker G, Zdrazil B, Terron A, Jennings P, van der Burg B, Dooley S, Meijer AH, Willighagen E, Martens M, Evelo C, Mombelli E, Taboureau O, Mantovani A, Hardy B, Koch B, Escher S, van Thriel C, Cadenas C, Kroese D, van de Water B, Hengstler JG (2017) Adverse outcome pathways: opportunities, limitations and open questions *Arch Toxicol* 91, 3477-3505.

Leist M, Hartung T, Nicotera P (2008) The dawning of a new age of toxicology *Altex* 25, 103-114.

Leist M, Lidbury BA, Yang C, Hayden PJ, Kelm JM, Ringeissen S, Detroyer A, Meunier JR, Rathman JF, Jackson GR, Jr., Stolper G, Hasiwa N (2012) Novel technologies and an overall strategy to allow hazard assessment and risk prediction of chemicals, cosmetics, and drugs with animal-free methods *Altex* 29, 373-388.

Leist M, Nicotera P (1998) Apoptosis, excitotoxicity, and neuropathology *Exp Cell Res* 239, 183-201.

Leist M, Nicotera P (1998) Calcium and neuronal death Reviews of Physiology Biochemistry and Pharmacology, Volume 132 Berlin, Heidelberg Springer Berlin Heidelberg, 79-125.

Leist M, Nicotera P (1998) Calcium and neuronal death *Rev Physiol Biochem Pharmacol* 132, 79-125.

Leist M, Volbracht C, Fava E, Nicotera P (1998) 1-Methyl-4-phenylpyridinium induces autocrine excitotoxicity, protease activation, and neuronal apoptosis *Mol Pharmacol* 54, 789-801.

Leist M, Volbracht C, Kühnle S, Fava E, Ferrando-May E, Nicotera P (1997) Caspase-mediated apoptosis in neuronal excitotoxicity triggered by nitric oxide *Mol Med* 3, 750-764.

Lemoine MD, Mannhardt I, Breckwoldt K, Prondzynski M, Flenner F, Ulmer B, Hirt MN, Neuber C, Horváth A, Kloth B, Reichenspurner H, Willems S, Hansen A, Eschenhagen T, Christ T (2017) Human iPSC-derived cardiomyocytes cultured in 3D engineered heart tissue show physiological upstroke velocity and sodium current density *Sci Rep* 7, 5464.

Levine A, Huang Y, Drisaldi B, Griffin EA, Jr., Pollak DD, Xu S, Yin D, Schaffran C, Kandel DB, Kandel ER (2011) Molecular mechanism for a gateway drug: epigenetic changes initiated by nicotine prime gene expression by cocaine *Sci Transl Med* 3, 107ra109.

Li Y, Chen J-a, Zhao Q, Pu C, Qiu Z, Zhang R, Shu W (2011) A cross-sectional investigation of chronic exposure to microcystin in relationship to childhood liver damage in the Three Gorges Reservoir Region, China *Environ Health Perspect* 119, 1483-1488.

Lim WA, Lee CM, Tang C (2013) Design principles of regulatory networks: searching for the molecular algorithms of the cell *Mol Cell* 49, 202-212.

Lipton P (1999) Ischemic Cell Death in Brain Neurons *Physiol Rev* 79, 1431-1568.

Liu J, Chang L, Song Y, Li H, Wu Y (2019) The Role of NMDA Receptors in Alzheimer's Disease *Front Neurosci* 13, 43-43.

Livak KJ, Schmittgen TD (2001) Analysis of relative gene expression data using real-time quantitative PCR and the 2(-Delta Delta C(T)) Method *Methods* 25, 402-408.

Lohren H, Blagojevic L, Fitkau R, Ebert F, Schildknecht S, Leist M, Schwerdtle T (2015) Toxicity of organic and inorganic mercury species in differentiated human neurons and human astrocytes *J Trace Elem Med Biol* 32, 200-208.

Lotharius J, Falsig J, van Beek J, Payne S, Dringen R, Brundin P, Leist M (2005) Progressive degeneration of human mesencephalic neuron-derived cells triggered by dopamine-dependent oxidative stress is dependent on the mixed-lineage kinase pathway *J Neurosci* 25, 6329-6342.

Love MI, Huber W, Anders S (2014) Moderated estimation of fold change and dispersion for RNA-seq data with DESeq2 *Genome Biol* 15, 550.

Luo C, Lancaster MA, Castanon R, Nery JR, Knoblich JA, Ecker JR (2016) Cerebral Organoids Recapitulate Epigenomic Signatures of the Human Fetal Brain *Cell Rep* 17, 3369-3384.

MacDonald JF, Miljkovic Z, Pennefather P (1987) Use-dependent block of excitatory amino acid currents in cultured neurons by ketamine *J Neurophysiol* 58, 251-266.

MacKintosh C, Beattie KA, Klumpp S, Cohen P, Codd GA (1990) Cyanobacterial microcystin-LR is a potent and specific inhibitor of protein phosphatases 1 and 2A from both mammals and higher plants *FEBS letters* 264, 187-192.

Makris SL, Raffaele K, Allen S, Bowers WJ, Hass U, Alleva E, Calamandrei G, Sheets L, Amcoff P, Delrue N, Crofton KM (2009) A retrospective performance assessment of the developmental neurotoxicity study in support of OECD test guideline 426 *Environ Health Perspect* 117, 17-25.

Malenka RC, Nicoll RA (1993) NMDA-receptor-dependent synaptic plasticity: multiple forms and mechanisms *Trends Neurosci* 16, 521-527.

Mariani J, Simonini MV, Palejev D, Tomasini L, Coppola G, Szekely AM, Horvath TL, Vaccarino FM (2012) Modeling human cortical development in vitro using induced pluripotent stem cells *Proc Natl Acad Sci U S A* 109, 12770-12775.

Marinova Z, Leng Y, Leeds P, Chuang DM (2011) Histone deacetylase inhibition alters histone methylation associated with heat shock protein 70 promoter modifications in astrocytes and neurons *Neuropharmacology* 60, 1109-1115.

Martinak B, Bolis RA, Black JR, Fargason RE, Birur B (2017) Dextromethorphan in Cough Syrup: The Poor Man's Psychosis *Psychopharmacol Bull* 47, 59-63.

Masjosthusmann S, Blum J, Bartmann K, Dolde X, Holzer A-K, Stürzl L-C, Keßel EH, Förster N, Dönmez A, Klose J, Pahl M, Waldmann T, Bendt F, Kisitu J, Suciu I, Hübenthal U, Mosig A, Leist M, Fritsche E (2020) Establishment of an a priori protocol for the implementation and interpretation of an in-vitro testing battery for the assessment of developmental neurotoxicity *EFSA Supporting Publications* 17, 1938E.

Matelski L, Morgan RK, Grodzki AC, Van de Water J, Lein PJ (2020) Effects of cytokines on nuclear factor-kappa B, cell viability, and synaptic connectivity in a human neuronal cell line *Mol Psychiatry*, 10.1038/s41380-41020-40647-41382.

Mattson MP, Magnus T (2006) Ageing and neuronal vulnerability *Nat Rev Neurosci* 7, 278-294.

Maycox PR, Deckwerth T, Hell JW, Jahn R (1988) Glutamate uptake by brain synaptic vesicles. Energy dependence of transport and functional reconstitution in proteoliposomes *J Biol Chem* 263, 15423-15428.

McGowan PO, Sasaki A, D'Alessio AC, Dymov S, Labonté B, Szyf M, Turecki G, Meaney MJ (2009) Epigenetic regulation of the glucocorticoid receptor in human brain associates with childhood abuse *Nat Neurosci* 12, 342-348.

Meador KJ, Baker GA, Browning N, Clayton-Smith J, Combs-Cantrell DT, Cohen M, Kalayjian LA, Kanner A, Liporace JD, Pennell PB, Privitera M, Loring DW (2009) Cognitive function at 3 years of age after fetal exposure to antiepileptic drugs *N Engl J Med* 360, 1597-1605.

Meijer M, Rehbach K, Brunner JW, Classen JA, Lammertse HCA, van Linge LA, Schut D, Krutenko T, Hebisch M, Cornelisse LN, Sullivan PF, Peitz M, Toonen RF, Brüstle O, Verhage M (2019) A Single-Cell Model for Synaptic Transmission and Plasticity in Human iPSC-Derived Neurons *Cell Rep* 27, 2199-2211.e2196.

Menegola E, Cappelletti G, Di Renzo F (2012) Epigenetic approaches and methods in developmental toxicology: role of HDAC inhibition in teratogenic events *Methods Mol Biol* 889, 373-383.

Metsalu T, Vilo J (2015) ClustVis: a web tool for visualizing clustering of multivariate data using Principal Component Analysis and heatmap *Nucleic Acids Res* 43, W566-W570.

Miyawaki A, Llopis J, Heim R, McCaffery JM, Adams JA, Ikura M, Tsien RY (1997) Fluorescent indicators for Ca2+ based on green fluorescent proteins and calmodulin *Nature* 388, 882-887.

Moné MJ, Pallocca G, Escher SE, Exner T, Herzler M, Bennekou SH, Kamp H, Kroese ED, Leist M, Steger-Hartmann T, van de Water B (2020) Setting the stage for next-generation risk assessment with non-animal approaches: the EU-ToxRisk project experience *Arch Toxicol* 94, 3581-3592.

Morris RGM (2013) NMDA receptors and memory encoding *Neuropharmacology* 74, 32-40.

Myint AM (2012) Kynurenines: from the perspective of major psychiatric disorders *FEBS J* 279, 1375-1385.

Nagoshi N, Okano H (2018) iPSC-derived neural precursor cells: potential for cell transplantation therapy in spinal cord injury *Cell Mol Life Sci* 75, 989-1000.

Nehme R, Zuccaro E, Ghosh SD, Li C, Sherwood JL, Pietilainen O, Barrett LE, Limone F, Worringer KA, Kommineni S, Zang Y, Cacchiarelli D, Meissner A, Adolfsson R, Haggarty S, Madison J, Muller M, Arlotta P, Fu Z, Feng G, Eggan K (2018) Combining NGN2 Programming with Developmental Patterning Generates Human Excitatory Neurons with NMDAR-Mediated Synaptic Transmission *Cell Rep* 23, 2509-2523.

Nicotera P, Leist M, Manzo L (1999) Neuronal cell death: a demise with different shapes *Trends Pharmacol Sci* 20, 46-51.

Nightingale KP, Gendreizig S, White DA, Bradbury C, Hollfelder F, Turner BM (2007) Cross-talk between histone modifications in response to histone deacetylase inhibitors: MLL4 links histone H3 acetylation and histone H3K4 methylation *J Biol Chem* 282, 4408-4416.

Nikolopoulou E, Galea GL, Rolo A, Greene NDE, Copp AJ (2017) Neural tube closure: cellular, molecular and biomechanical mechanisms *Development* 144, 552.

Nimtz L, Hartmann J, Tigges J, Masjosthusmann S, Schmuck M, Keßel E, Theiss S, Köhrer K, Petzsch P, Adjaye J, Wigmann C, Wieczorek D, Hildebrandt B, Bendt F, Hübenthal U, Brockerhoff G, Fritsche E (2020) Characterization and application of electrically active neuronal networks established from human induced pluripotent stem cell-derived neural progenitor cells for neurotoxicity evaluation *Stem Cell Res* 45, 101761.

Nishiwaki-Matsushima R, Ohta T, Nishiwaki S, Suganuma M, Kohyama K, Ishikawa T, Carmichael WW, Fujiki H (1992) Liver tumor promotion by the cyanobacterial cyclic peptide toxin microcystin-LR *J Cancer Res Clin Oncol* 118, 420-424.

NRC (2007) Toxicity testing in the 21st century: a vision and a strategy. Washington National Academies press.

Nyffeler J, Dolde X, Krebs A, Pinto-Gil K, Pastor M, Behl M, Waldmann T, Leist M (2017) Combination of multiple neural crest migration assays to identify environmental toxicants from a proof-of-concept chemical library *Arch Toxicol* 91, 3613-3632.

Nyffeler J, Karreman C, Leisner H, Kim YJ, Lee G, Waldmann T, Leist M (2017) Design of a high-throughput human neural crest cell migration assay to indicate potential developmental toxicants *Altex* 34, 75-94.

OECD (2017) Guidance Document for the Use of Adverse Outcome Pathways in Developing Integrated Approaches to Testing and Assessment (IATA).

OECD (2017) Guidance Document on the Reporting of Defined Approaches to be Used Within Integrated Approaches to Testing and Assessment.

Oksanen M, Petersen AJ, Naumenko N, Puttonen K, Lehtonen Š, Gubert Olivé M, Shakirzyanova A, Leskelä S, Sarajärvi T, Viitanen M, Rinne JO, Hiltunen M, Haapasalo A, Giniatullin R, Tavi P, Zhang SC, Kanninen KM, Hämäläinen RH, Koistinaho J (2017) PSEN1 Mutant iPSC-Derived Model Reveals Severe Astrocyte Pathology in Alzheimer's Disease *Stem Cell Reports* 9, 1885-1897.

Olney JW, de Gubareff T (1978) Glutamate neurotoxicity and Huntington's chorea *Nature* 271, 557-559.

Onishchenko N, Tamm C, Vahter M, Hökfelt T, Johnson JA, Johnson DA, Ceccatelli S (2007) Developmental exposure to methylmercury alters learning and induces depression-like behavior in male mice *Toxicol Sci* 97, 428-437.

Osmond C, Barker DJ (2000) Fetal, infant, and childhood growth are predictors of coronary heart disease, diabetes, and hypertension in adult men and women *Environ Health Perspect* 108 Suppl 3, 545-553.

Pagan-Diaz GJ, Drnevich J, Ramos-Cruz KP, Sam R, Sengupta P, Bashir R (2020) Modulating electrophysiology of motor neural networks via optogenetic stimulation during neurogenesis and synaptogenesis *Sci Rep* 10, 12460.

Pallocca G, Grinberg M, Henry M, Frickey T, Hengstler JG, Waldmann T, Sachinidis A, Rahnenführer J, Leist M (2016) Identification of transcriptome signatures and biomarkers specific for potential developmental toxicants inhibiting human neural crest cell migration *Arch Toxicol* 90, 159-180.

Pamies D, Barreras P, Block K, Makri G, Kumar A, Wiersma D, Smirnova L, Zang C, Bressler J, Christian KM, Harris G, Ming GL, Berlinicke CJ, Kyro K, Song H, Pardo CA, Hartung T, Hogberg HT (2017) A human brain microphysiological system derived from induced pluripotent stem cells to study neurological diseases and toxicity *Altex* 34, 362-376.

Papadia S, Hardingham GE (2007) The dichotomy of NMDA receptor signaling *Neuroscientist* 13, 572-579.

Paules R (2003) Phenotypic anchoring: linking cause and effect *Environ Health Perspect* 111, A338-339.

Petanjek Z, Judaš M, Šimić G, Rašin MR, Uylings HBM, Rakic P, Kostović I (2011) Extraordinary neoteny of synaptic spines in the human prefrontal cortex *Proceedings of the National Academy of Sciences* 108, 13281.

Piersma AH, Bosgra S, van Duursen MB, Hermsen SA, Jonker LR, Kroese ED, van der Linden SC, Man H, Roelofs MJ, Schulpen SH, Schwarz M, Uibel F, van Vugt-Lussenburg BM, Westerhout J, Wolterbeek AP, van der Burg B (2013) Evaluation of an alternative in vitro test battery for detecting reproductive toxicants *Reprod Toxicol* 38, 53-64.

Pottel J, Armstrong D, Zou L, Fekete A, Huang XP, Torosyan H, Bednarczyk D, Whitebread S, Bhhatarai B, Liang G, Jin H, Ghaemi SN, Slocum S, Lukacs KV, Irwin JJ, Berg EL, Giacomini KM, Roth BL, Shoichet BK, Urban L (2020) The activities of drug inactive ingredients on biological targets *Science* 369, 403-413.

Pouria S, de Andrade A, Barbosa J, Cavalcanti RL, Barreto VT, Ward CJ, Preiser W, Poon GK, Neild GH, Codd GA (1998) Fatal microcystin intoxication in haemodialysis unit in Caruaru, Brazil *Lancet* 352, 21-26.

Powers AR, 3rd, Gancsos MG, Finn ES, Morgan PT, Corlett PR (2015) Ketamine-Induced Hallucinations *Psychopathology* 48, 376-385.

Preskorn SH, Baker B, Kolluri S, Menniti FS, Krams M, Landen JW (2008) An innovative design to establish proof of concept of the antidepressant effects of the NR2B subunit selective N-methyl-D-aspartate antagonist, CP-101,606, in patients with treatment-refractory major depressive disorder *J Clin Psychopharmacol* 28, 631-637.

Pruunsild P, Bengtson CP, Bading H (2017) Networks of Cultured iPSC-Derived Neurons Reveal the Human Synaptic Activity-Regulated Adaptive Gene Program *Cell Rep* 18, 122-135.

Qiang M, Denny A, Lieu M, Carreon S, Li J (2011) Histone H3K9 modifications are a local chromatin event involved in ethanol-induced neuroadaptation of the NR2B gene *Epigenetics* 6, 1095-1104.

Raffaele KC, Rowland J, May B, Makris SL, Schumacher K, Scarano LJ (2010) The use of developmental neurotoxicity data in pesticide risk assessments *Neurotoxicol Teratol* 32, 563-572.

Raudvere U, Kolberg L, Kuzmin I, Arak T, Adler P, Peterson H, Vilo J (2019) g:Profiler: a web server for functional enrichment analysis and conversions of gene lists (2019 update) *Nucleic Acids Res* 47, W191-w198.

Reimand J, Arak T, Vilo J (2011) g:Profiler--a web server for functional interpretation of gene lists (2011 update) *Nucleic Acids Res* 39, W307-315.

Reinhardt P, Glatza M, Hemmer K, Tsytsyura Y, Thiel CS, Höing S, Moritz S, Parga JA, Wagner L, Bruder JM, Wu G, Schmid B, Röpke A, Klingauf J, Schwamborn JC, Gasser T, Schöler HR, Sterneckert J (2013) Derivation and expansion using only small molecules of human neural progenitors for neurodegenerative disease modeling *PLoS One* 8, e59252.

Rempel E, Hoelting L, Waldmann T, Balmer NV, Schildknecht S, Grinberg M, Das Gaspar JA, Shinde V, Stöber R, Marchan R, van Thriel C, Liebing J, Meisig J, Blüthgen N, Sachinidis A, Rahnenführer J, Hengstler JG, Leist M (2015) A transcriptome-based classifier to identify developmental toxicants by stem cell testing: design, validation and optimization for histone deacetylase inhibitors *Arch Toxicol* 89, 1599-1618.

Ribes V, Briscoe J (2009) Establishing and interpreting graded Sonic Hedgehog signaling during vertebrate neural tube patterning: the role of negative feedback *Cold Spring Harb Perspect Biol* 1, a002014.

Rice D, Barone S, Jr. (2000) Critical periods of vulnerability for the developing nervous system: evidence from humans and animal models *Environ Health Perspect* 108 Suppl 3, 511-533.

Richardson JR, Fitsanakis V, Westerink RHS, Kanthasamy AG (2019) Neurotoxicity of pesticides *Acta Neuropathol* 138, 343-362.

Robinson JF, Pennings JL, Piersma AH (2012) A review of toxicogenomic approaches in developmental toxicology *Methods Mol Biol* 889, 347-371.

Robinson JF, Piersma AH (2013) Toxicogenomic approaches in developmental toxicology testing *Methods Mol Biol* 947, 451-473.

Robinson JF, Verhoef A, Pennings JL, Pronk TE, Piersma AH (2012) A comparison of gene expression responses in rat whole embryo culture and in vivo: time-dependent retinoic acid-induced teratogenic response *Toxicol Sci* 126, 242-254.

Rodier PM (1995) Developing brain as a target of toxicity *Environ Health Perspect* 103 Suppl 6, 73-76.

Rotroff DM, Wetmore BA, Dix DJ, Ferguson SS, Clewell HJ, Houck KA, Lecluyse EL, Andersen ME, Judson RS, Smith CM, Sochaski MA, Kavlock RJ, Boellmann F, Martin MT, Reif DM, Wambaugh JF, Thomas RS (2010) Incorporating human dosimetry and exposure into high-throughput in vitro toxicity screening *Toxicol Sci* 117, 348-358.

Rudenko A, Tsai LH (2014) Epigenetic regulation in memory and cognitive disorders *Neuroscience* 264, 51-63.

Russell W, Burch R (1959) The principles of humane experimental technique London London Methuen.

Russo FB, Freitas BC, Pignatari GC, Fernandes IR, Sebat J, Muotri AR, Beltrão-Braga PCB (2018) Modeling the Interplay Between Neurons and Astrocytes in Autism Using Human Induced Pluripotent Stem Cells *Biol Psychiatry* 83, 569-578.

Ryan KR, Sirenko O, Parham F, Hsieh JH, Cromwell EF, Tice RR, Behl M (2016) Neurite outgrowth in human induced pluripotent stem cell-derived neurons as a high-throughput screen for developmental neurotoxicity or neurotoxicity *Neurotoxicology* 53, 271-281.

Sachana M, Bal-Price A, Crofton KM, Bennekou SH, Shafer TJ, Behl M, Terron A (2019) International Regulatory and Scientific Effort for Improved Developmental Neurotoxicity Testing *Toxicol Sci* 167, 45-57.

Sachana M, Munn S, Bal-Price A (2019). "Chronic binding of antagonist to N-methyl-D-aspartate receptors (NMDARs) during brain development induces impairment of learning and memory abilities." Retrieved October 23, 2020, from https://aopwiki.org/aops/13.

Sachana M, Rolaki A, Bal-Price A (2018) Development of the Adverse Outcome Pathway (AOP): Chronic binding of antagonist to N-methyl-d-aspartate receptors (NMDARs) during brain development induces impairment of learning and memory abilities of children *Toxicol Appl Pharmacol* 354, 153-175.

Sánchez-Serrano SL, Cruz SL, Lamas M (2011) Repeated toluene exposure modifies the acetylation pattern of histones H3 and H4 in the rat brain *Neurosci Lett* 489, 142-147.

Sasaki T, Suzuki I, Yokoi R, Sato K, Ikegaya Y (2019) Synchronous spike patterns in differently mixed cultures of human iPSC-derived glutamatergic and GABAergic neurons *Biochem Biophys Res Commun* 513, 300-305.

Scatton B (1993) The NMDA receptor complex *Fundam Clin Pharmacol* 7, 389-400.

Scholz D, Chernyshova Y, Ückert A-K, Leist M (2018) Reduced Aβ secretion by human neurons under conditions of strongly increased BACE activity *J Neurochem* 147, 256-274.

Scholz D, Pöltl D, Genewsky A, Weng M, Waldmann T, Schildknecht S, Leist M (2011) Rapid, complete and large-scale generation of post-mitotic neurons from the human LUHMES cell line *J Neurochem* 119, 957-971.

Schulpen SH, Pennings JL, Tonk EC, Piersma AH (2014) A statistical approach towards the derivation of predictive gene sets for potency ranking of chemicals in the mouse embryonic stem cell test *Toxicol Lett* 225, 342-349.

Schulte S, Müller W, Friedberg K (1995) In vitro and in vivo effects of lead on specific 3H-MK-801 binding to NMDA-receptors in the brain of mice *Neurotoxicology* 16, 309-317.

Senut MC, Cingolani P, Sen A, Kruger A, Shaik A, Hirsch H, Suhr ST, Ruden D (2012) Epigenetics of early-life lead exposure and effects on brain development *Epigenomics* 4, 665-674.

Seok J, Warren HS, Cuenca AG, Mindrinos MN, Baker HV, Xu W, Richards DR, McDonald-Smith GP, Gao H, Hennessy L, Finnerty CC, López CM, Honari S, Moore EE, Minei JP, Cuschieri J, Bankey PE, Johnson JL, Sperry J, Nathens AB, Billiar TR, West MA, Jeschke MG, Klein MB, Gamelli RL, Gibran NS, Brownstein BH, Miller-Graziano C, Calvano SE, Mason PH,

Cobb JP, Rahme LG, Lowry SF, Maier RV, Moldawer LL, Herndon DN, Davis RW, Xiao W, Tompkins RG (2013) Genomic responses in mouse models poorly mimic human inflammatory diseases *Proc Natl Acad Sci U S A* 110, 3507-3512.

Shafer TJ (2019) Application of Microelectrode Array Approaches to Neurotoxicity Testing and Screening *Adv Neurobiol* 22, 275-297.

Sheng M, Kim E (2011) The postsynaptic organization of synapses *Perspect Biol* 3.

Shinde V, Hoelting L, Srinivasan SP, Meisig J, Meganathan K, Jagtap S, Grinberg M, Liebing J, Bluethgen N, Rahnenführer J, Rempel E, Stoeber R, Schildknecht S, Förster S, Godoy P, van Thriel C, Gaspar JA, Hescheler J, Waldmann T, Hengstler JG, Leist M, Sachinidis A (2017) Definition of transcriptome-based indices for quantitative characterization of chemically disturbed stem cell development: introduction of the STOP-Tox(ukn) and STOP-Tox(ukk) tests *Arch Toxicol* 91, 839-864.

Singh N, Lawana V, Luo J, Phong P, Abdalla A, Palanisamy B, Rokad D, Sarkar S, Jin H, Anantharam V, Kanthasamy AG, Kanthasamy A (2018) Organophosphate pesticide chlorpyrifos impairs STAT1 signaling to induce dopaminergic neurotoxicity: Implications for mitochondria mediated oxidative stress signaling events *Neurobiol Dis* 117, 82-113.

Sinner B, Graf BM (2008) Ketamine Modern Anesthetics Schüttler J ,Schwilden H Berlin, Heidelberg Springer Berlin Heidelberg, 313-333.

Sipes NS, Martin MT, Kothiya P, Reif DM, Judson RS, Richard AM, Houck KA, Dix DJ, Kavlock RJ, Knudsen TB (2013) Profiling 976 ToxCast chemicals across 331 enzymatic and receptor signaling assays *Chem Res Toxicol* 26, 878-895.

Sipes NS, Martin MT, Reif DM, Kleinstreuer NC, Judson RS, Singh AV, Chandler KJ, Dix DJ, Kavlock RJ, Knudsen TB (2011) Predictive models of prenatal developmental toxicity from ToxCast high-throughput screening data *Toxicol Sci* 124, 109-127.

Skirzewski M, Karavanova I, Shamir A, Erben L, Garcia-Olivares J, Shin JH, Vullhorst D, Alvarez VA, Amara SG, Buonanno A (2018) ErbB4 signaling in dopaminergic axonal projections increases extracellular dopamine levels and regulates spatial/working memory behaviors *Mol Psychiatry* 23, 2227-2237.

Smirnova L, Hogberg HT, Leist M, Hartung T (2014) Developmental neurotoxicity - challenges in the 21st century and in vitro opportunities *Altex* 31, 129-156.

Smirnova L, Sittka A, Luch A (2012) On the role of low-dose effects and epigenetics in toxicology *Exp Suppl* 101, 499-550.

Smyth GK (2005) Limma: linear models for microarray data Bioinformatics and computational biology solutions using R and Bioconductor Springer, 397-420.

Spoof L, Catherine A (2016) Appendix 3: Tables of Microcystins and Nodularins.

Stiegler NV, Krug AK, Matt F, Leist M (2011) Assessment of chemical-induced impairment of human neurite outgrowth by multiparametric live cell imaging in high-density cultures *Toxicol Sci* 121, 73-87.

Strickland JD, Martin MT, Richard AM, Houck KA, Shafer TJ (2018) Screening the ToxCast phase II libraries for alterations in network function using cortical neurons grown on multi-well microelectrode array (mwMEA) plates *Arch Toxicol* 92, 487-500.

Südhof TC (2012) The Presynaptic Active Zone *Neuron* 75, 11-25.

Südhof TC (2018) Towards an Understanding of Synapse Formation *Neuron* 100, 276-293.

Suñol C, Babot Z, Fonfría E, Galofré M, García D, Herrera N, Iraola S, Vendrell I (2008) Studies with neuronal cells: From basic studies of mechanisms of neurotoxicity to the prediction of chemical toxicity *Toxicology in Vitro* 22, 1350-1355.

Svirčev Z, Lalić D, Bojadžija Savić G, Tokodi N, Drobac Backović D, Chen L, Meriluoto J, Codd GA (2019) Global geographical and historical overview of cyanotoxin distribution and cyanobacterial poisonings *Arch Toxicol* 93, 2429-2481.

Takahashi K, Tanabe K, Ohnuki M, Narita M, Ichisaka T, Tomoda K, Yamanaka S (2007) Induction of pluripotent stem cells from adult human fibroblasts by defined factors *Cell* 131, 861-872.

Terron A, Bennekou SH (2018) Towards a regulatory use of alternative developmental neurotoxicity testing (DNT) *Toxicol Appl Pharmacol* 354, 19-23.

Theunissen PT, Pennings JL, van Dartel DA, Robinson JF, Kleinjans JC, Piersma AH (2013) Complementary detection of embryotoxic properties of substances in the neural and cardiac embryonic stem cell tests *Toxicol Sci* 132, 118-130.

Theunissen PT, Robinson JF, Pennings JL, de Jong E, Claessen SM, Kleinjans JC, Piersma AH (2012) Transcriptomic concentration-response evaluation of valproic acid, cyproconazole, and hexaconazole in the neural embryonic stem cell test (ESTn) *Toxicol Sci* 125, 430-438.

Thomson JA, Itskovitz-Eldor J, Shapiro SS, Waknitz MA, Swiergiel JJ, Marshall VS, Jones JM (1998) Embryonic stem cell lines derived from human blastocysts *Science* 282, 1145-1147.

Tong Z-B, Huang R, Wang Y, Klumpp-Thomas CA, Braisted JC, Itkin Z, Shinn P, Xia M, Simeonov A, Gerhold DL (2018) The Toxmatrix: Chemo-Genomic Profiling Identifies Interactions That Reveal Mechanisms of Toxicity *Chem Res Toxicol* 31, 127-136.

Tonk EC, Robinson JF, Verhoef A, Theunissen PT, Pennings JL, Piersma AH (2013) Valproic acid-induced gene expression responses in rat whole embryo culture and comparison across in vitro developmental and non-developmental models *Reprod Toxicol* 41, 57-66.

Toscano CD, Guilarte TR (2005) Lead neurotoxicity: from exposure to molecular effects *Brain Res Brain Res Rev* 49, 529-554.

Tovar KR, Westbrook GL (1999) The incorporation of NMDA receptors with a distinct subunit composition at nascent hippocampal synapses in vitro *J Neurosci* 19, 4180-4188.

Traynelis SF, Wollmuth LP, McBain CJ, Menniti FS, Vance KM, Ogden KK, Hansen KB, Yuan H, Myers SJ, Dingledine R (2010) Glutamate receptor ion channels: structure, regulation, and function *Pharmacol Rev* 62, 405-496.

Tschudi-Monnet F, FitzGerald R (2019). "Chronic binding of antagonist to N-methyl-D-aspartate receptors (NMDARs) during brain development leads to neurodegeneration with impairment in learning and memory in aging." Retrieved October 23, 2020, from https://aopwiki.org/aops/12.

Tsien RW, Tsien RY (1990) Calcium channels, stores, and oscillations *Annu Rev Cell Biol* 6, 715-760.

Tsuji R, Crofton KM (2012) Developmental neurotoxicity guideline study: Issues with methodology, evaluation and regulation *Congenit Anom (Kyoto)* 52, 122-128.

Tukker AM, Wijnolts FMJ, de Groot A, Westerink RHS (2018) Human iPSC-derived neuronal models for in vitro neurotoxicity assessment *Neurotoxicology* 67, 215-225.

Tukker AM, Wijnolts FMJ, de Groot A, Westerink RHS (2020) Applicability of hiPSC-derived neuronal co-cultures and rodent primary cortical cultures for in vitro seizure liability assessment *Toxicol Sci*.

Tung EW, Winn LM (2010) Epigenetic modifications in valproic acid-induced teratogenesis *Toxicol Appl Pharmacol* 248, 201-209.

Ulbrich MH, Isacoff EY (2008) Rules of engagement for NMDA receptor subunits *Proceedings of the National Academy of Sciences* 105, 14163-14168.

Umlauf D, Goto Y, Feil R (2004) Site-specific analysis of histone methylation and acetylation *Methods Mol Biol* 287, 99-120.

USEPA (2018) Strategic Plan to Promote the Development and Implementation of Alternative Test Methods Within the TSCA Program.

Valério E, Vasconcelos V, Campos A (2016) New Insights on the Mode of Action of Microcystins in Animal Cells - A Review *Mini Rev Med Chem* 16, 1032-1041.

van Dartel DA, Zeijen NJ, de la Fonteyne LJ, van Schooten FJ, Piersma AH (2009) Disentangling cellular proliferation and differentiation in the embryonic stem cell test, and its impact on the experimental protocol *Reprod Toxicol* 28, 254-261.

van Thriel C, Westerink RH, Beste C, Bale AS, Lein PJ, Leist M (2012) Translating neurobehavioural endpoints of developmental neurotoxicity tests into in vitro assays and readouts *Neurotoxicology* 33, 911-924.

Vassallo A, Chiappalone M, De Camargos Lopes R, Scelfo B, Novellino A, Defranchi E, Palosaari T, Weisschu T, Ramirez T, Martinoia S, Johnstone AFM, Mack CM, Landsiedel R, Whelan M, Bal-Price A, Shafer TJ (2017) A multi-laboratory evaluation of microelectrode array-based measurements of neural network activity for acute neurotoxicity testing *Neurotoxicology* 60, 280-292.

Villeneuve DL, Crump D, Garcia-Reyero N, Hecker M, Hutchinson TH, LaLone CA, Landesmann B, Lettieri T, Munn S, Nepelska M, Ottinger MA, Vergauwen L, Whelan M (2014) Adverse outcome pathway (AOP) development I: strategies and principles *Toxicol Sci* 142, 312-320.

Vojnits K, Ensenat-Waser R, Gaspar JA, Meganathan K, Jagtap S, Hescheler J, Sachinidis A, Bremer-Hoffmann S (2012) A tanscriptomics study to elucidate the toxicological mechanism of methylmercury chloride in a human stem cell based in vitro test *Curr Med Chem* 19, 6224-6232.

Volbracht C, van Beek J, Zhu C, Blomgren K, Leist M (2006) Neuroprotective properties of memantine in different in vitro and in vivo models of excitotoxicity *Eur J Neurosci* 23, 2611-2622.

Waldmann T, Grinberg M, König A, Rempel E, Schildknecht S, Henry M, Holzer AK, Dreser N, Shinde V, Sachinidis A, Rahnenführer J, Hengstler JG, Leist M (2017) Stem Cell Transcriptome Responses and Corresponding Biomarkers That Indicate the Transition from Adaptive Responses to Cytotoxicity *Chem Res Toxicol* 30, 905-922.

Waldmann T, Rempel E, Balmer NV, König A, Kolde R, Gaspar JA, Henry M, Hescheler J, Sachinidis A, Rahnenführer J, Hengstler JG, Leist M (2014) Design principles of concentration-dependent transcriptome deviations in drug-exposed differentiating stem cells *Chem Res Toxicol* 27, 408-420.

Waldmann T, Schneider R (2013) Targeting histone modifications-epigenetics in cancer *Curr Opin Cell Biol* 25, 184-189.

Walker DM, Nestler EJ (2018) Neuroepigenetics and addiction *Handbook of clinical neurology* 148, 747-765.

Wang CX, Shuaib A (2005) NMDA/NR2B selective antagonists in the treatment of ischemic brain injury *Curr Drug Targets CNS Neurol Disord* 4, 143-151.

Wang R, Reddy PH (2017) Role of Glutamate and NMDA Receptors in Alzheimer's Disease *J Alzheimers Dis* 57, 1041-1048.

Wang S, Bates J, Li X, Schanz S, Chandler-Militello D, Levine C, Maherali N, Studer L, Hochedlinger K, Windrem M, Goldman SA (2013) Human iPSC-derived oligodendrocyte progenitor cells can myelinate and rescue a mouse model of congenital hypomyelination *Cell Stem Cell* 12, 252-264.

Waters MD, Fostel JM (2004) Toxicogenomics and systems toxicology: aims and prospects *Nat Rev Genet* 5, 936-948.

Weaver IC, Cervoni N, Champagne FA, D'Alessio AC, Sharma S, Seckl JR, Dymov S, Szyf M, Meaney MJ (2004) Epigenetic programming by maternal behavior *Nat Neurosci* 7, 847-854.

Weng MK, Natarajan K, Scholz D, Ivanova VN, Sachinidis A, Hengstler JG, Waldmann T, Leist M (2014) Lineage-specific regulation of epigenetic modifier genes in human liver and brain *PLoS One* 9, e102035.

Weng MK, Zimmer B, Pöltl D, Broeg MP, Ivanova V, Gaspar JA, Sachinidis A, Wüllner U, Waldmann T, Leist M (2012) Extensive transcriptional regulation of chromatin modifiers during human neurodevelopment *PLoS One* 7, e36708.

Wetmore BA, Wambaugh JF, Ferguson SS, Sochaski MA, Rotroff DM, Freeman K, Clewell HJ, 3rd, Dix DJ, Andersen ME, Houck KA, Allen B, Judson RS, Singh R, Kavlock RJ, Richard AM, Thomas RS (2012) Integration of dosimetry, exposure, and high-throughput screening data in chemical toxicity assessment *Toxicol Sci* 125, 157-174.

Whelan M, Andersen ME (2013) Toxicity Pathways –from concepts to application in chemical safety assessment.

Williams JF, Lundahl LH (2019) Focus on Adolescent Use of Club Drugs and "Other" Substances *Pediatr Clin North Am* 66, 1121-1134.

Winn P, Tarbuck A, Dunnett SB (1984) Ibotenic acid lesions of the lateral hypothalamus: comparison with the electrolytic lesion syndrome *Neuroscience* 12, 225-240.

Witt A, Macdonald N, Kirkpatrick P (2004) Memantine hydrochloride *Nat Rev Drug Discov* 3, 109-110.

Witt B, Meyer S, Ebert F, Francesconi KA, Schwerdtle T (2017) Toxicity of two classes of arsenolipids and their water-soluble metabolites in human differentiated neurons *Arch Toxicol* 91, 3121-3134.

Wobus AM, Löser P (2011) Present state and future perspectives of using pluripotent stem cells in toxicology research *Arch Toxicol* 85, 79-117.

World Health Organization. Water S, Health T (2004) Guidelines for drinking-water quality. Vol. 1, Recommendations Geneva World Health Organization.

Wu J, Basha MR, Brock B, Cox DP, Cardozo-Pelaez F, McPherson CA, Harry J, Rice DC, Maloney B, Chen D, Lahiri DK, Zawia NH (2008) Alzheimer's disease (AD)-like pathology in aged monkeys after infantile exposure to environmental metal lead (Pb): evidence for a developmental origin and environmental link for AD *J Neurosci* 28, 3-9.

Xie W, Schultz MD, Lister R, Hou Z, Rajagopal N, Ray P, Whitaker JW, Tian S, Hawkins RD, Leung D, Yang H, Wang T, Lee AY, Swanson SA, Zhang J, Zhu Y, Kim A, Nery JR, Urich MA, Kuan S, Yen CA, Klugman S, Yu P, Suknuntha K, Propson NE, Chen H, Edsall LE, Wagner U, Li Y, Ye Z, Kulkarni A, Xuan Z, Chung WY, Chi NC, Antosiewicz-Bourget JE,

Slukvin I, Stewart R, Zhang MQ, Wang W, Thomson JA, Ecker JR, Ren B (2013) Epigenomic analysis of multilineage differentiation of human embryonic stem cells *Cell* 153, 1134-1148.

Xu X, Duan S, Yi F, Ocampo A, Liu GH, Izpisua Belmonte JC (2013) Mitochondrial regulation in pluripotent stem cells *Cell Metab* 18, 325-332.

Yamazaki K, Fukushima K, Sugawara M, Tabata Y, Imaizumi Y, Ishihara Y, Ito M, Tsukahara K, Kohyama J, Okano H (2016) Functional Comparison of Neuronal Cells Differentiated from Human Induced Pluripotent Stem Cell-Derived Neural Stem Cells under Different Oxygen and Medium Conditions *J Biomol Screen* 21, 1054-1064.

Yang H, Zhou Y, Gu J, Xie S, Xu Y, Zhu G, Wang L, Huang J, Ma H, Yao J (2013) Deep mRNA sequencing analysis to capture the transcriptome landscape of zebrafish embryos and larvae *PLoS One* 8, e64058.

Yoshizawa S, Matsushima R, Watanabe MF, Harada K, Ichihara A, Carmichael WW, Fujiki H (1990) Inhibition of protein phosphatases by microcystins and nodularin associated with hepatotoxicity *J Cancer Res Clin Oncol* 116, 609-614.

Zhang XY, Liu AP, Ruan DY, Liu J (2002) Effect of developmental lead exposure on the expression of specific NMDA receptor subunit mRNAs in the hippocampus of neonatal rats by digoxigenin-labeled in situ hybridization histochemistry *Neurotoxicol Teratol* 24, 149-160.

Zhao X, Bhattacharyya A (2018) Human Models Are Needed for Studying Human Neurodevelopmental Disorders *Am J Hum Genet* 103, 829-857.

Zhou SJ, Xue LF, Wang XY, Jiang WG, Xue YX, Liu JF, He YY, Luo YX, Lu L (2012) NMDA receptor glycine modulatory site in the ventral tegmental area regulates the acquisition, retrieval, and reconsolidation of cocaine reward memory *Psychopharmacology (Berl)* 221, 79-89.

Zimmer B, Ewaleifoh O, Harschnitz O, Lee YS, Peneau C, McAlpine JL, Liu B, Tchieu J, Steinbeck JA, Lafaille F, Volpi S, Notarangelo LD, Casanova JL, Zhang SY, Smith GA, Studer L (2018) Human iPSC-derived trigeminal neurons lack constitutive TLR3-dependent immunity that protects cortical neurons from HSV-1 infection *Proc Natl Acad Sci U S A* 115, E8775-e8782.

Zimmer B, Kuegler PB, Baudis B, Genewsky A, Tanavde V, Koh W, Tan B, Waldmann T, Kadereit S, Leist M (2011) Coordinated waves of gene expression during neuronal differentiation of embryonic stem cells as basis for novel approaches to developmental neurotoxicity testing *Cell Death Differ* 18, 383-395.

Zimmer B, Lee G, Balmer NV, Meganathan K, Sachinidis A, Studer L, Leist M (2012) Evaluation of developmental toxicants and signaling pathways in a functional test based on the migration of human neural crest cells *Environ Health Perspect* 120, 1116-1122.

Zou R-X, Gu X, Ding J-J, Wang T, Bi N, Niu K, Ge M, Chen X-T, Wang H-L (2020) Pb exposure induces an imbalance of excitatory and inhibitory synaptic transmission in cultured rat hippocampal neurons *Toxicology in Vitro* 63, 104742.

Zurich M-G, Stanzel S, Kopp-Schneider A, Prieto P, Honegger P (2013) Evaluation of aggregating brain cell cultures for the detection of acute organ-specific toxicity *Toxicology in Vitro* 27, 1416-1424.

Zwartsen A, Hondebrink L, Westerink RH (2018) Neurotoxicity screening of new psychoactive substances (NPS): Effects on neuronal activity in rat cortical cultures using microelectrode arrays (MEA) *Neurotoxicology* 66, 87-97.